Lithium-ion 18650 cylindrical Battery Thermal Management: Multi-level CFD Simulations utilising Phase Change Materials for Enhanced Performance

---

By

Renaldo Antonio Nicholls

Thesis submitted in partial fulfilment of the requirements for the degree of

Doctor of Philosophy

School of Digital, Technologies, and Arts

Staffordshire University

Principal Supervisor:
Dr. Mohammad Moghimi Ardekani

January 2024

ABSTRACT

This thesis undertakes a comprehensive exploration of Battery Thermal Management Systems (BTMS), with a specific emphasis on improving cylindrical 18650 batteries' performance, through the integration of passive cooling techniques via multi-level Computational Fluid Dynamics (CFD) simulations. The research was meticulously designed to enhance the thermal performance and lifespan of lithium-ion (Li-ion) batteries, pivotal components of Electric Vehicles (EVs) and Hybrid Electric Vehicles (HEVs). The investigation commenced with an extensive literature review delving into Thermal Energy Storage (TES), focusing on Latent Heat Storage (LHS) and Phase Change Materials (PCMs). The study encompassed types, designs, and applications, including their integration with Electrical Energy Storage (EES) devices such as Li-ion batteries. The primary goal was to implement thermal renewable energy systems in EVs and HEVs, with a particular interest in passive cooling methods and their impact on battery performance from the cellular to the module level. Given the high energy density of Li-ion batteries, their safe operation under diverse temperature conditions poses a challenge, necessitating an effective BTMS. The literature review scrutinised thermal and electrochemical battery modelling, heat transfer mechanisms, BTMS developments, and CFD analysis methods. Different BTMS technologies were evaluated based on criteria like cost, efficiency, safety, and adaptability to various cooling and heating techniques. A specific focus on PCMs within the BTMS domain explored various types, including pure, composite, and hybrid-based systems, analysing the behaviour of cells and modules upon PCM integration. This multidimensional exploration aimed to contribute essential insights for advancing BTMS, which is crucial for EVs' widespread adoption and sustainability.

In terms of LHS, a proposed horizontal concentric double-pipe heat exchanger with N-eicosane PCM for Latent Heat Storage (LHS) was studied. It focused on the impact of fin type and orientation on charging (melting PCM) and discharging (solidifying PCM). Various cases were considered including fin orientation (longitudinal and transversal) and fin types (corrugated and flat), which were simulated for optimal thermal and heat transfer performance when compared with and without the addition of the fins. The results showed that natural convection enhanced melting while conduction dominated during discharging. Fins significantly reduced charging and discharging times, influenced by orientation and type. Higher fin surface area (corrugated) and transversal position exhibit a 27 % improvement in heat transfer. For melting, transversal corrugated fins outperform, achieving over 88 % reduction in melting time. The transversal corrugated fin design excelled in both processes, with the shortest overall processing time. Notably, longitudinal flat-finned arrangements were 1.2x faster, and transversal flat-finned arrangements were 8.7x faster than the unfinned case.

Additionally, a numerical study examined EV battery cell performance using a Latent Heat (LH) jacket for passive cooling. The battery cell was coupled with PCM and assessed through continuous cycles. Validation against literature values for a Panasonic 18650PF Li-ion cell displayed less than 1 % deviation. Thermal and electrical parameters were analysed under various climatic conditions. Passive cooling, especially with a 3 mm jacketed PCM, resulted in a significant 340 % thermal performance improvement at ambient weather (25 °C). Higher temperatures (40 °C and 55 °C) displayed improvements of up to 275 % and 440 %, respectively. At lower temperatures (-20 °C and 0 °C), passive cooling maintains stability with improvements of 162 % and 160 %, respectively. The study concluded that efficient passive cooling enhances EES safety and performance in EVs and HEVs.

Moreover, the efficacy of passive cooling with PCMs in BTMS was further explored. The study focused on a single cylindrical Panasonic 18650 battery cell with a circumferential LH jacket under real-world drive cycles when compared without. The challenge was understanding the diverse driving behaviours' impact on battery performance and thermal stability with passive cooling. Using conjugated thermo-chemical and electrical models based on simulated real-world scenarios, the study indicated that significant battery performance enhancement was achieved with LH jackets, improving over 50 % in most cycles. Particularly, in aggressive drive cycles, the battery life extended from 2.2x to 2.4x. LH jackets maintain thermal stability and result in more than 45 % thermal performance improvement and over 200 % life extension across all cycles. This approach enhanced understanding and improved BTMS in real-world scenarios, especially in passive cooling through LH jackets.

Furthermore, another study investigated passive cooling's impact on BTMS by analysing various module configurations under ideal continuous cycling and real-world drive cycles. Using numerical CFD, the study focused on circumferential PCM jackets for each cell in 3 dimensional (3D) modules consisting of 24 battery cells. Modules, arranged in different configurations, were simulated with and without LH/PCM jackets. Evaluation criteria included battery module temperature, PCM liquid fraction, state of charge (SOC), and passive zone potentials. Findings emphasised passive cooling, which stabilised the system and cell temperatures under normal and harsh conditions. The results indicated a stable and uniform temperature, with an average 20 °C module temperature reduction and less than 5 °C difference. There was over 200 % improvement in battery module life across all assessed drive cycles, regardless of module arrangements.

PUBLICATIONS

The following research studies were published/under review during the PhD thus far:

Journal Articles

1. **Nicholls**, R.A, Moghimi, M.A., and Griffiths, A.L., Impact of fin type and orientation on performance of phase change material-based double pipe thermal energy storage, *Journal of Energy Storage*, 50, 2022, pp 104671. https://doi.org/10.1016/j.est.2022.104671.

2. Yang, M., **Nicholls**, R.A, Moghimi, M.A., and Griffiths, A.L., Performance management of EV battery coupled with latent heat jacket at cell level, *Journal of Power Sources*, 558, 2023, pp 232618. https://doi.org/10.1016/j.jpowsour.2022.232618.

3. **Nicholls**, R.A, Moghimi, M.A., and Griffiths, A.L., Influence of latent heat based passive cooling on the performance of EV battery under automotive drive cycles, *Journal of Energy Storage,* 77, 2024, pp. 109924 https://doi.org/10.1016/j.est.2023.109924.

4. **Nicholls**, R.A, Cash, A., Moghimi, M.A., and Griffiths, A.L, Thermal performance review of electric vehicles/hybrid electric vehicles battery modelling using latent heat cooling-based management system, *Renewable and Sustainable Energy Reviews*, manuscript number (RSER-D-23-04839) submitted and awaiting review.

5. **Nicholls**, R.A, Moghimi, M.A., and S. Sehhat, Thermal performance analysis of battery modules with passive cooling under different cycling loads in electric vehicles, *Journal of Energy Storage,* 94, 2024, pp. 112349 https://doi.org/10.1016/j.est.2024.112349.

6. Igweh, P.C., **Nicholls**, R.A, Moghimi, M.A., and Griffiths, A.L, Investigative study on the impact of reduction of thermal conductivity with the introduction of longitudinal air pockets, under review for possible *Journal of Power Sources/Energy Conversion and Management/Journal of Energy Storage* submission.

7. **Nicholls**, R.A., Moghimi, M.A., and Bourne, F., Investigation into the thermal response of internal short-circuit treatment of a cylindrical battery cell jacketed with passive cooling, under

review for possible *Journal of Power Sources/Energy Conversion and Management/Journal of Energy Storage* submission.

8. Nwaobia, K., **Nicholls**, R.A., and Moghimi, M.A., Numerical investigation of the impact of the axial length of a passive cooling jacket on the performance of Lithium-ion battery under variable Operating conditions, under review for possible *Journal of Power Sources/Energy Conversion and Management/Journal of Energy Storage* submission.

9. **Nicholls**, R.A., Moghimi, M.A., and Igweh, P.C., Reduction of phase change material thermal conductivity with the introduction of transversal air pockets for effective thermal management of lithium-ion battery cell, under review for possible *Journal of Power Sources/Energy Conversion and Management/Journal of Energy Storage* submission.

Conference Articles

1. **Nicholls**, R.A, Moghimi, M.A., and Griffiths, A.L., Can passive cooling be a practical solution for the thermal management of battery in electric vehicles, *Proceedings of the 16th International Conference on Heat Transfer, Fluid Mechanics and Thermodynamics and Editorial Board of Applied Thermal Engineering*, Amsterdam, Netherlands, Accepted, August 2022.

2. **Nicholls**, R.A, Moghimi, M.A., and Griffiths, A.L., A comparative study of corrugated fins during melting of phase change material in a double pipe heat exchanger, *Proceedings of the 17th UK International Heat Transfer Conference*, Manchester, United Kingdom, Paper number 116, April 2022. http://cfd.mace.manchester.ac.uk/ukhtc21-proc/papers/O-12-5.pdf.

ACKNOWLEDGEMENTS

As I stand on the threshold of submitting this doctoral thesis, I am compelled to express my deepest gratitude to the myriad of individuals and entities who have not only been instrumental in shaping my academic journey over the past three years but as ever standing in support for which, I actively seek.

First and foremost, my heartfelt appreciation to **God** for blessing me with the opportunity to undertake this challenging yet rewarding PhD research. The strength, determination, and resilience that have brought me to this juncture are undoubtedly a manifestation of divine guidance.

To my cherished family, I extend boundless thanks. My mother, **Bernadette Nicholls**, whose unwavering support has been my pillar of strength; my grandmother, **Meatrice Lavia**, whose wisdom has been a guiding light; my aunt, **Calastra Issac** whose, words of encouragement and belief in my capabilities and my start of Master's degree, and my sisters, **Rosanna**, **Christina**, and **Shaquilla**, your encouragement and understanding has been my constant motivation.

I reserve a special place in my gratitude for my esteemed main supervisor, **Dr. Mohammad Moghimi Ardekani**. His mentorship has been nothing short of remarkable – his insights, advice, and unwavering support have been a compass steering me through the complexities of research. Countless conversations and guidance have left an undeniable mark on my professional and personal growth. It is by this approach, that I receive countless statements of gratitude from students under my supervision, new researchers and colleagues for my insights and knowledge, all of which have been developed and moulded through my passion and motivation under his supervision.

I extend profound thanks to my second supervisor, **Dr. Alison Griffiths**. Her presence, comments and intuitive ideas have been instrumental in refining my thought process, particularly in the presentations through written and recorded video work. Her intellectual guidance has been a catalyst for improving the quality of my research.

A heartfelt acknowledgement is also due to the **Staffordshire Advanced Manufacturing and Innovation Demonstrator (SAMPID)**, its officers, technical support team, and board. Their sponsorship of this research and the wealth of technical experience provided and gained in support of student projects sought by companies have significantly enriched my academic pursuit.

In closing, I express my deepest gratitude to everyone who has played a role, whether big or small, in this academic odyssey. Your contributions have not only shaped this thesis but have profoundly impacted my growth as a researcher and an individual. This journey has been a collective effort, and for that, I am sincerely thankful.

TABLE OF CONTENTS

LIST OF FIGURES

LIST OF TABLES

NOMENCLATURE

A_{mush}	mushy zone constant ($kg/m^3 s$)
C_p	specific heat (J/kgK)
D_i	inner diameter
D_o	outer diameter
f	friction factor
F_o	Fourier Number
g	gravity acceleration (m/s^2)
h	Sensible enthalpy (J/kg)
h_{ref}	reference enthalpy (J/kg)
H	total enthalpy (J/kg)
k	thermal conductivity (W/mK)
L	Latent heat (J/kg)
P	Pressure Pa
S	source term
t	time (s)
T	temperature K
$T_{liquidous}$	Liquid temperature K
T_0	operation temperature K
T_s	inner surface temperature K
$T_{solidus}$	solid temperature
T_{ref}	reference temperature K
$\vec{v}$	fluid velocity

Greek symbols

α	thermal diffusivity
β	expansion coefficient ($1/K$)
μ	dynamic viscosity ($Pa\ s$)
ε	small number
ρ	density (kg/m^3)
ρ_0	constant density (kg/m^3)
∇	non-dimensional term

CHAPTER 1: INTRODUCTION

1.1 Background and Motivation

Developing energy challenges as a direct consequence of the consistent advancement of humanity to improve the role of advanced industrial processes and products that enhance our day-to-day lives, have affected our immediate natural environment both domestically and globally. The sharp upsurge in energy levels post-industrial development markedly corresponds to additional heat generation and an increase in worldwide temperature levels from fossil fuel exploitation including greenhouse gas emissions and carbon emissions. Human activity has caused considerable effects on our climate affecting all life, the economy, and the natural environment as devastating as the extinction of individual species and the melting of the polar ice caps. Post-industrial levels show rising planet temperatures causing heat waves, major flooding, and wildfires across the globe. In this regard, there is a need to shift towards alternative forms of energy crucial to sustainability and to reduce contribution to climate change for the betterment of current and future generations.

A revolution towards renewable energy sources particularly in the application of zero-emission vehicles and green transport as outlined by governmental initiatives to reduce carbon emissions, and the implementation of stricter regulations, has shifted attention towards Hybrid Electric Vehicles (HEV) and Electric Vehicles (EVs). Research and applications into Thermal Energy Storage (TES) seek to contribute to the UK and a larger extent, the world, for green energy initiatives and decarbonisation for all sectors according to the NetZero Strategy: Build Back Greener, for net zero carbon emissions by 2050 published October 2021 and recommended by the Climate Change Committee (CCC). The plan centres around improving renewable energy resources to reduce carbon emissions, implementation of nuclear power, shift to zero-emission vehicles and green transport and construction as well as carbon capture, usage and storage and investments to innovation and protection of the natural environment. Unfortunately, these forms of energy e.g., solar, wind and thermal are intermittent. Effective energy storage becomes crucial in which case Latent Heat Storage (LHS) and Phase Change Materials (PCMs) for their thermophysical properties including constant temperature during material phase change, are becoming widely acceptable.

These EVs and HEVs use battery technology where the lithium-ion (Li-ion) battery has been seen to be consistent and outperform competitors for high energy density, voltage, and low self-discharge rate to name a few. However, during loading such as charging and discharging, the operating temperature has a direct impact on the battery cells' performance. These optimum operating temperatures usually lie between 20-40 degrees (°C) based on the type and so outside of these, the battery's electrical performance is reduced significantly, as some Battery Thermal Management System

(BTMS) is usually employed using air or liquid cooling or some combination of both with the drawback being complicated designs and added weight to the vehicles.

Published on 26th November 2023, the UK battery strategy has further propelled the need for this research and the topics conducted within this thesis directly align with the objectives and new commitments by the UK government to improve the Battery sector. In this regard, batteries are poised to be a pivotal force in our journey towards a sustainable energy future and fulfil the NetZero plan published in 2021. With their indispensable role in various devices, transportation modes, and the evolving landscape of energy generation, high energy capacity and rechargeable batteries are at the forefront. According to the recently published battery strategy, the government plans to commit billions of investments into critical areas such as research and development within the automotive sector. Looking ahead five years, a vision which fosters economic prosperity and the facilitation of transition to a net-zero environment would see the implementation of battery supply chains including design and production for a vibrant ecosystem of battery innovation.

This research explores the viability of incorporating passive cooling mechanisms to prolong the maintenance of EV battery temperatures. The overarching aim is to enhance battery efficiency and performance across diverse loading and climatic conditions. The literature and research study chapters within this thesis revolve around the outcomes stemming from the integration of two storage techniques: LHS and Electrical Energy Storage (EES). The study zeroes in on the cellular level, incorporating modular-level research into this thesis. Additionally, within the study chapters, a post-processing analysis of the results is conducted, culminating in a comprehensive conclusion. The thesis not only encapsulates the current state of affairs but also casts a forward-looking gaze into the prospects for recommendations for future work. It emphasises TES utilising PCMs and their combination with Li-ion batteries. The enhancement focus spans from single-cell configurations to module-level setups, all directed toward enhancing thermal performance.

1.2 Statement of the Problem

Batteries are the cornerstone of modern applications:

- *Versatility in Applications*: Batteries, with a special emphasis on Li-ion batteries, stand as indispensable components across a spectrum of applications. From powering portable electronic devices to propelling the electric revolution in vehicles and serving as essential elements in grid energy storage, their role is central to modern technological landscapes.

Rising demand for High-Performance Batteries:

- *Performance as a Driving Force*: The increasing demand for batteries with enhanced performance characteristics has been a driving force behind technological advancements. Consumers and industries alike seek batteries that deliver higher energy density, prolonged lifespan, and improved efficiency to meet the evolving needs of a dynamic world.

The Nexus of Challenges in Thermal Management:

- *The Unavoidable Thermal Challenge*: However, this pursuit of high performance has ushered in a host of challenges, with thermal management emerging as a critical nexus of concern. The efficient control of temperature within batteries has become paramount, and the failure to address this challenge gives rise to pressing issues that echo across different sectors.

Critical Thermal Challenges:

- *Safety Imperatives*: Thermal runaway, a phenomenon where escalating temperatures trigger self-sustaining reactions within batteries, poses serious safety risks. This is especially crucial in applications like electric vehicles and energy storage, where the failure of a battery can lead to catastrophic consequences.
- *Performance Enhancement*: The performance and efficiency of batteries are intricately linked to temperature. Elevated temperatures accelerate chemical reactions within batteries, impacting their lifespan, energy efficiency, and overall capabilities. Effective thermal management becomes the linchpin for sustained and optimal battery performance.
- *Longevity concerns*: Prolonged exposure to high temperatures contributes to the degradation of battery cells. Heat-induced degradation results in a reduction in capacity and lifespan, necessitating strategies to mitigate excessive heat and maintain temperature variations within permissible limits to ensure the longevity of battery cells.
- *Environmental Considerations*: As the global transition towards cleaner energy gains momentum, the environmental impact of energy storage systems comes under scrutiny.

Sustainable and energy-efficient thermal management strategies are not only imperative for battery performance but also for minimising the environmental footprint associated with their production and disposal.

- *Application-Specific Reliability*: Batteries find applications in diverse settings, each presenting unique operating conditions. From electric vehicles navigating varying terrains to stationary energy storage systems, the challenges in thermal management are multifaceted. Thus, there is a growing need for tailored thermal management strategies that ensure reliability across a spectrum of applications.

The Crux of the Matter:

- *Thermal Management as a Keystone*: Considering these multifaceted challenges, it is evident that the thermal management of batteries stands as a keystone issue that demands immediate attention. The crux of this research lies in navigating these challenges and proposing innovative, sustainable, and efficient thermal management solutions. The overarching goal is to contribute to the development of energy storage systems that not only meet the demands of contemporary applications but also align with the sustainability imperatives of the future.

1.2.1 Aims

This research thesis aims to evaluate research into ANSYS Fluent with applications to TES conjugated with EES to produce post-processing results of an effective passive cooling thermal management strategy targeted at EV batteries such as Li-ion cylindrical batteries. The thesis seeks to propose this approach to engineering for both commercial and industrial applications, providing seamless analyses through effortless interactions improving efficiency and reducing time constraints to designs. This can include extensive applications in the medical, pharmaceutical, renewable/petrochemical, education, automotive, maritime and aviation industries through which varying professionals interact with software and hardware technology.

The TES systems and EES systems are analysed in CFD software. There is always the need to improve how we do things with creativity in analyses and interpretation through varying software and programs that assist designers and developers of all backgrounds. The great advantage is, how the idea or product is efficiently and effectively presented, with numerical analysis a way forward that researchers can use to analyse and visually display their products and findings.

To fully undertake this idea into practicality, research is focused on thermal and electrical energy storage and more specifically on LHS with the use of PCM in conjugation with batteries. The conjugation of the two technologies must also be studied to produce a creative new design to further what is already in literature today. Sufficient knowledge of LHS inclusive of PCM designs and types along with implementing PCMs in electrical devices like batteries must be significantly reviewed. Furthermore, improving the knowledge on the use of passive cooling as an effective battery thermal management system technology up to the present date must be studied intently to execute the post-processing results of the thermal analyses. Moreover, literature on PCMs must be reviewed with replications of the verified results from literature produced alongside data created from new analyses, to ensure that the methodological analysis undertaken is of sufficient standard with the relevant literature up to and including industry standards.

A numerical analysis method was selected to address the design challenges using ANSYS Fluent. This approach involved performing numerical calculations to analyse specific geometries, meshing, boundary conditions, and simulation setups. The goal was to ensure accurate and efficient analysis of the designs. This method offers several advantages, such as repeatability, safety, and environmental suitability, while remaining effective under varying weather conditions and unpredictable environments. Although numerical analysis is emphasised for its practical benefits, the importance of experimental analysis remains recognised and should not be overlooked.

1.2.2 Objectives

The objectives of the Thesis are outlined below, identifying the key tasks that empirically define the set of investigations to which the hypothesis tends to solve the problem specification. The emphasis was intrinsically focused on the aim of the thesis previously highlighted. The thesis is dissected into 3 milestones with the main objectives split into the three as follows:

1st milestone:

Comprehensive Research on TES devices:

- **Objective**: Conduct an extensive investigation into TES devices, with a specific emphasis on LHS utilising PCM, and EES, particularly chemical/electrochemical systems in rechargeable batteries like Li-ion batteries.
- **Rationale**: Understanding the nuances of LHS and its integration with ESS in batteries is crucial for advancing thermal management strategies.
- **Methodology**: Combine literature reviews, experimental data analysis, and computational simulations to explore the principles and applications of LHS and ESS in the context of battery thermal management.
- **Expected Outcome**: In-depth insights into the synergies between LHS and ESS technologies and their potential applications in battery systems.

Numerical Analyses on PCM structures:

- **Objective**: Perform numerical analyses on 2D and 3D, cylindrical, horizontal, and longitudinal structures of selected PCMS, both with and without enhanced heat transfer areas.
- **Rationale**: Investigate the structural and thermal behaviours of PCMs under various geometries to understand the impact of design choices on their performance.
- **Methodology**: Utilise numerical simulations, potentially employing CFD tools, to analyse PCM structures in different configurations.
- **Expected Outcome**: Insights into how different PCM geometries and enhanced heat transfer areas influence their thermal response.

Geometry Preparation and Comparison:

- **Objective**: Prepare geometries 2D and 3D in ANSYS Design Modeler or CAD to replicate chosen benchmarks from the literature. Compare these with new designs featuring enhanced heat transfer areas. Cylindrical, horizontal, and longitudinal structures of the chosen PCMs with and without enhanced heat transfer areas.
- **Rationale**: Assess the impact of design modifications on the thermal performance of PCM structures.
- **Methodology**: Utilise ANSYS Design Modeler or CAD tools to recreate benchmark geometries and develop new designs. Perform comparative analysis.
- **Expected Outcome**: Clear understanding of how design changes affect thermal characteristics.

Meshing and Mesh Independence Analysis:

- **Objective**: Compute the most appropriate mesh for PCM designs, ensuring accuracy and reduced computational time. Use ANSYS Meshing with the elements assigned closer to the domain walls for more accurate computational analysis. Perform a mesh independence analysis. Produce images of the mesh topology and zoomed images of the domain walls
- **Rationale**: Mesh quality influences simulation accuracy; hence, achieving independence is vital.
- **Methodology**: Utilise ANSYS Meshing, assigning elements closer to domain walls. Analyse grid sizes concerning liquid fraction for mesh independence.
- **Expected Outcome**: Optimal mesh configurations for accurate yet computationally efficient simulations.

Application of Boundary Conditions:

- **Objective**: Apply relevant boundary conditions to the selected PCM based on verified literature.
- **Rationale**: Accurate representation of real-world conditions is crucial for simulation validity.
- **Methodology:** Implement boundary conditions consistent with established literature to ensure realistic simulations.
- **Expected Outcome**: Simulations that closely align with real-world scenarios, enhancing the reliability of results.

Convergence and Time Step Analysis:

- **Objective**: Evaluate the most appropriate number of iterations and time step size to ensure the convergence of scaled residuals that satisfies the convergence of velocity, energy, and continuity and estimate computational time for PCM melting/solidification.
- **Rationale**: Achieving convergence and time steps are critical for computational efficiency.
- **Methodology**: Analyse the effects of varying time step sizes on convergence and computational time.
- **Expected Outcome**: Determination of optimal iteration numbers and time step sizes for efficient simulations.

Solidification/Melting Analysis in ANSYS Fluent:

- **Objective**: Employ ANSYS Fluent for solidification/melting analysis to simulate thermal energy behaviour, considering laminar fluid flow within the PCM.
- **Rationale**: Understanding the phase change dynamics of the PCM, is crucial for assessing its thermal energy storage capabilities.
- **Methodology**: Set up simulations with appropriate energy equations involving laminar fluid flow in ANSYS Fluent.
- **Expected Outcome**: Detailed insights into the solidification/melting behaviour of the PCM, aiding in improving energy storage efficiency.

Visualisation of Results:

- **Objective**: Produce contours of temperature and liquid fraction, along with plots of flow times and velocity streamlines of fluid flow. Compare the results from replicated data in verified literature to ensure that the simulation procedure is at the industrial standard.
- **Rationale**: Visual representation enhances the interpretation of complex simulation data.
- **Methodology**: Utilise post-processing tools to generate visualisations in ANSYS.
- **Expected Outcome**: Clear visual representation aiding in the comparison of results with established literature and industry standards.

2nd milestone:

Conjugate Thermal Solution:

- **Objective**: Integrate the newly enhanced heat transfer area into the battery cell and establish a conjugate thermal solution.
- **Rationale**: By combining this enhanced heat transfer area, the goal is to assess its impact on thermal performance concerning a standard analysis.
- **Methodology**: Develop a comprehensive thermal solution model that incorporates the modified heat transfer area, considering relevant parameters such as material properties, geometry, and environmental conditions.
- **Expected Outcome**: Insights into how the enhanced heat transfer area influences the thermal behaviour of the battery cell.

Verification and Validation of CFD Results:

- **Objective**: Employ suitable equipment and software to rigorously verify and validate CFD results.
- **Rationale**: Ensuring the accuracy and reliability of CFD results is crucial for the credibility of the thermal analysis.
- **Methodology**: Utilise available equipment and software, taking into consideration factors such as computational resources, simulation time, and precision requirements.
- **Expected Outcome**: Confirmed accuracy of the CFD results, enhancing the reliability of subsequent analyses and conclusions.

Illustration of Post-Processing Results on ANSYS:

- **Objective**: Demonstrate and interpret post-processing results derived from the thermal analysis using ANSYS.
- **Rationale**: Clear visualisation and interpretation of results are essential for extracting meaningful insights and communicating findings effectively.
- **Methodology**: Employ ANSYS post-processing tools to generate graphical representations of the thermal analysis results. This may involve temperature contours, heat flux distributions, and other relevant visualisations.

- **Expected Outcome**: A comprehensive illustration of the thermal behaviour of the battery cell, showcasing how modifications to the heat transfer area impact various parameters.

3rd milestone:

Conjugate Thermal Solution in Battery Module:

- **Objective**: Integrate the thermal solution with the newly enhanced heat transfer area into a battery module and assess its performance in comparison to standard analysis.
- **Rationale**: Understanding how enhanced heat transfer areas influence the thermal behaviour of an entire battery module is crucial for practical applications.
- **Methodology**: Implement a conjugate thermal solution within a battery module using CFD simulations.
- **Expected Outcome**: Insights into the holistic impact of passive cooling on the thermal performance of battery modules.

Verification and Validation of CFD Results:

- **Objective**: Employ the most effective equipment and software, dependent on availability, for the verification and validation of CFD results.
- **Rationale**: Ensuring the accuracy and reliability of CFD results is paramount for the credibility of the entire study.
- **Methodology**: Utilise appropriate CFD tools and equipment to verify simulated results against theoretical expectations and validate them with experimental data.
- **Expected Outcome**: A validated and verified CFD model that aligns closely with real-world observations, enhancing the reliability of the entire study.

1.3 Research mind map

Figure 1.1 displays a research mind map which follows the main objectives of this research. Highlighted for the literature review section, 4 main study areas were selected for critical review. These included TES, Management of EES devices, PCMs, and conjugation of thermal and electrical energy storage from single cell level to module level. These key areas were then further dissected into the elements that would provide sufficient research to identify areas that would be of interest for research study including journal articles and conference submissions. The literature then follows the research mind map and how the research work successfully fulfils the aim and objectives.

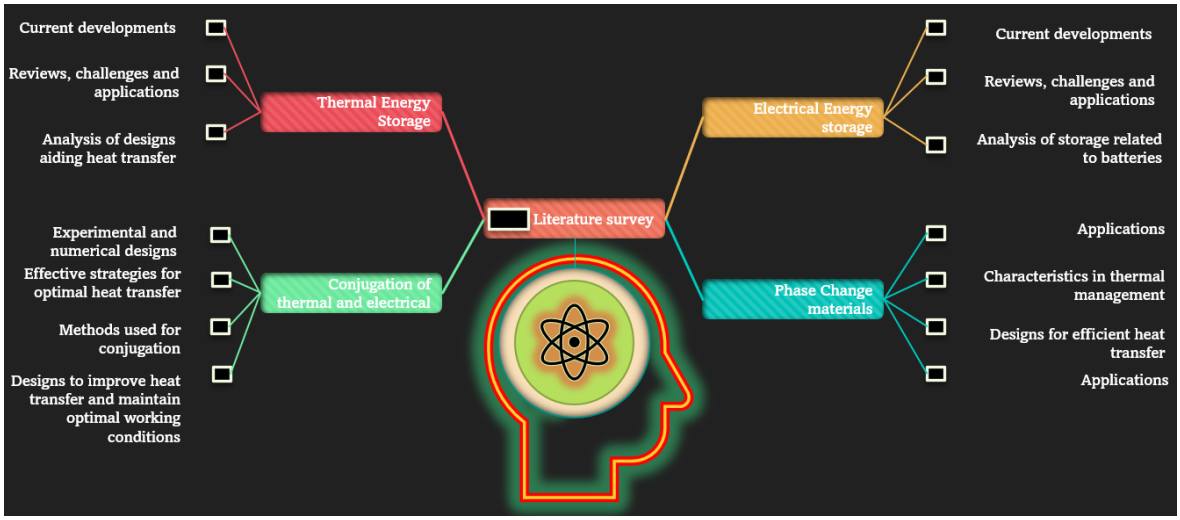

Fig. 1.1 Research Mind Map.

1.4 Research Flowchart

[1] The chosen topic for research/research problem:

a. Determine research interest,
b. Based on aims, objectives and milestones (1 to 3 depending on timeframe in the research timeline),
c. Background reading on the overall topic,
d. Determine the scope and limitations,
e. Any other issues beneficial for interest.

[2] Critical review of literature:

a. Search for relevant literature on the topic: attend webinars/training courses available at the university and offered by Scopus,
b. Gain feedback from supervisors,
c. Determine research strategy based on action plans set in the research timeline using gained techniques from training courses including keywords, phrases, and functions,
d. Conduct strategy using books, search engines, peer-reviewed journal articles, and conference abstracts,
e. Capture key information and store it for drafting of literature.

[3] Methodological approach applicable to the study:

a. Quantitative research analysis,
b. Numerical modelling approach,
c. Chosen applicable software most suitable to strategy including complementary software and research materials such as hardware (journals, meeting records, notes, apps).

[4] Define and prepare the proposal:

a. Search for relevant courses on developing research proposals: attend webinars/training courses available at the university or another university,
b. Align the structure of the proposal according to guidelines,
c. Address research requirements including costings and available equipment/software,
d. Prepare ethical approval form (disclaimer/full ethical approval),
e. Gain feedback from supervisors,
f. This can include abstract submissions.

[5] Prepare investigations and capture appropriate data:

a. Follow numerical/experimental approach,
b. Validate captured data,

c. Verify results,
d. Store data appropriately.

[6] Data interpretation and analysis:
a. Analyse the captured quantitative research data using appropriate data analytics techniques of clear formattable structure,
b. Generate appropriate plots, figures, and tables using the validated data,
c. Formulate findings of results and explanation of the outcome.

[7] Prepare report/write article/review:
a. Ensure the most appropriate resources have been used,
b. Structure report based on pre-requisites,
c. Write an article with a focus on delivering results to a wide variety of audiences,
d. Review the article and rewrite as needed based on comments/suggestions.

Forward View:

This research journey as outlined by the research flow chart in Figure 1.2 commences with the identification of a compelling topic driven by genuine interest and guided by predefined aims, objectives, and milestones. Extensive background reading ensues to shape the research scope, and potential issues are proactively addressed. A critical literature review is then undertaken, leveraging webinars, training courses, and supervisor feedback to craft a robust research strategy. Methodological considerations are meticulously chosen, emphasising the quantitative and numerical modelling approach, aligning with the selected software and necessary research materials. The proposal, shaped through relevant courses and guidelines, encapsulates ethical considerations and research requirements, garnering supervisor input. The subsequent phase involves the direct preparation and capturing of data through numerical or experimental methodologies followed by rigorous validation and verification processes. Data interpretation and analysis, employing advanced techniques, yielding structured findings and meaningful outcomes. Finally, a comprehensive report/article is meticulously crafted, ensuring broad accessibility, and subjected to thorough review and rewriting based on feedback.

Reverse View for Review:

As seen in Figure 1.2 and outlined in this section, if any step in this process is incompletely executed, the research might face setbacks. Failure to articulate a compelling topic with well-defined objectives can lead to aimless efforts. Inadequate background reading may result in a superficial understanding of the subject. A poorly conducted literature review might miss crucial insights and methodologies. Ineffectively chosen methodologies may compromise the research's integrity. A hastily prepared proposal can lead to an oversight in ethical considerations and resource planning. Insufficient

data preparation jeopardises the reliability of findings, while lacklustre interpretation may yield inconclusive outcomes. Neglecting the report's structure and audience relevance undermines the research's impact. Continuous feedback and iteration at each step are pivotal to mitigating such risks and ensuring a robust research outcome.

Fig. 1.2 Research flow chart.

1.5 Thesis Outline

This thesis is structured thoroughly to facilitate a comprehensive exploration of the investigation of thermal management for Li-ion 18650 cylindrical batteries, incorporating PCMs and leveraging multi-level CFD simulations. The sequential organisation of chapters ensures a logical progression of knowledge and insights.

Chapter 2: Critical Literature Review of the Research Topic

In this chapter, an in-depth exploration of existing literature research is presented. The review spans diverse topics, including TES, LHS, PCMs, and the application of PCMs in thermal management systems. Furthermore, it examines thermal and electrochemical battery modelling, highlighting relevant models such as the Equivalent Circuit Model (ECM) and the Newman, Tiedemann, Gu, and Kim (NTGK) model. This chapter concludes with a concise overview and a forward-looking view, setting the stage for subsequent empirical investigations.

Chapter 3: Impact of Fin Type and Orientation on Performance of PCM-Based Double Pipe Thermal Energy Storage Building upon the knowledge gained from the literature review, this chapter focuses on a specific aspect of thermal energy storage – the impact of fin type and orientation on the performance of PCM-based double-pipe thermal energy storage systems. A detailed numerical methodology is employed, involving model development, mathematical approaches, and verification studies. The results and analyses contribute to the understanding of the thermal behaviour of PCMs, laying the groundwork for subsequent investigations.

Chapter 4: Investigative Analysis of EV Battery Cell Performance Under Varying Climate Conditions

This chapter shifts the focus towards the primary subject of Li-ion 18650 cylindrical batteries. It begins with an introduction and proceeds to detail the numerical method including models, assumptions, and computational model setup. Verification studies validate the reliability of the simulations, leading to a comprehensive discussion of results and analyses. Special emphasis is placed on the coupled thermo-chemical and electrical outcomes, providing valuable insights into the performance of EV battery cells under diverse conditions.

Chapter 5: Latent Heat-Based Passive Cooling on the Performance of EV Battery Under Automotive Drive Cycles addressing the practicalities of real-world scenarios. Chapter 5 introduces the concept of Latent heat-based passive cooling applied to EV batteries during automotive drive cycles. This chapter defines drive cycles, outlines the numerical methodology, and presents a meticulous analysis of the results. Through verification and validation studies, the impact of Latent heat jackets on battery performance under different discharging C-rates is explored, offering practical implications for EVs.

Chapter 6: Thermal Performance Analysis of Battery Modules Using Latent Heat Cooling-Based Management System For Real Cycling Modes in Electric Vehicles. Expanding the scope to battery modules, Chapter 6 evaluates the effectiveness of the proposed Latent heat cooling system under real cycling modes in electric vehicles. It begins with an introduction and details the numerical

methodology, including models and assumptions. The chapter encompasses grid and temporal independence studies, validation, technical discussions, and a thorough examination of the proposed passive cooling system's effectiveness. Insights gained contribute to the broader goal of enhancing thermal management strategies.

Chapter 7: Conclusion and Recommendations

This final chapter synthesises the findings from the preceding chapters. It reiterates the main conclusions drawn from the investigations and presents recommendations for future research in the field of Li-on battery thermal management. The chapter serves as a reflective summary, consolidating the contributions made through the research and offering insights into avenues for further exploration.

This structured approach ensures that each chapter contributes progressively to the principal theme of enhancing thermal management for Li-ion 18650 cylindrical batteries. It guides the reader through a logical sequence of knowledge, from theoretical foundations to practical applications and concludes with a reflective synthesis of the research outcomes.

CHAPTER 2: CRITICAL LITERATURE REVIEW OF THE RESEARCH TOPIC

2.1 Chapter Brief

This chapter presents an extensive exploration of the literature underpinning the present study, aiming to elucidate the intricate relationship between TES and EES. Aligned with the outlined aims and objectives in the introduction section, this research endeavour fulfils the specified milestones in section 1.2.2, particularly those related to milestones 1, 2, and 3. The inquiry encompasses a detailed examination of the connection between TES and, more specifically, LHS materials, with a central focus on PCMs—the exploration further delves into the diverse types, designs, and applications of PCMs. Additionally, the literature scrutinises EES and its integration with TES, extending its purview to cellular-level investigations and extending to modular and pack-level research. This comprehensive review lays the foundation for the subsequent analyses and discussions, providing a nuanced understanding of the interplay between thermal and electrochemical considerations in battery modelling, incorporating models like ECM, NTGK, and Newman. Finally, it assesses the potential of passive-based cooling strategies at the single-cell, module, and pack levels with PCM integration.

2.2 Thermal Energy Storage (TES)

With the advent of technological enhancement in the present situation where there is a need to improve on our current standing as human beings in a world encapsulated with potential, many societies thrive on the need to progress civilisation further beyond its current scope. As beings of energy who seek to harness power to further our idealistic cause, men in their insatiable appetite yearn for increased energy becoming parasites, strongly dependent on consistent energy consumption.

According to (Kousksou et al., 2014), energy has become a mainstay in the critical advancement of the civilisation population. Our unquenchable thirst for energy has driven mankind to harness the energy from our natural oil and gas reserves, exhausting carbon energy in the form of fossil fuels. The products which power our very livelihood, however, negatively affect our natural environment in the form of pollution and global warming. Alternative sources of energy in the form of renewable energy and improved efficiency in our use of fossil fuels have become more important shifting the focus from our own needs to the need for a sustainable and energy-efficient planet. In their review, a change to this type of efficient energy storage comes with economic and development barriers including cost factors and transitional implementation with current energy production.

With our current scientific renewable energy extractors such as solar and wind energy dependent on variable seasonal effects, consistent power production is far-reaching. Storage of these energies in excess for timely use is a critical factor for a dominant change in this power production. This is what the world would expect to see in our foreseeable future with the increase in demand for this change according to Sorenson (2015). Storage of these renewable energies provides benefits to our short to long-term requirements even in the presence of fluctuations in energy demand, seasonal, day-to-day and for the transitional requirements between fossil fuels and renewable energy. This is driven by our economic growth and the affluence of our expanding population to harness the power of electrical energy to power our essential products and services.

Efficiently done, renewable energy storage in power applications goes through three separate phases as outlined by (Kousksou et al., 2014), from the charging phase to the storage and finally discharging phase. The amount of storage and power required depends upon the applications specifically suited to its function. As solar energy moves to become the most applicable energy source by today's standards, and soon, conversion of this type of energy occurs through either solar electrical energy or solar thermal energy. Currently, there are three different electrical energy storage technologies except for Thermal Energy Storage (TES) as described by Sorenson (2015) and (Kousksou et al., 2014). These include electrical storage where the energy is stored through battery technology in which chemical energy is transposed to electrical energy. These are most useful in rechargeable batteries such as the Lead-Acid (LA) Battery, Lithium-ion (Li-ion) Battery, Nickel-Based (NB) Sodium-Sulphur (SS) battery and other battery technologies as outlined by Sorensen (2015). Mechanical energy manifests in various utility storage technologies, such as Kinetic Energy (KE) through linear or rotational motion and Potential Energy (PE) represented by methods like Pumped-Hydro Storage (PHS) and Compressed Air Energy Storage (CAES). Additionally, chemical energy finds expression in hydrogen and solar fuels. In contrast, thermal energy takes diverse forms, ranging from thermochemical energy storage involving reversible process and sorption processes to heat storage mechanisms such as Sensible Heat Storage (SHS) and Latent Heat Storage (LHS) and cryogenics. This thesis section predominantly focuses on TES, providing a comprehensive overview of this technology. A specific emphasis is placed on exploring heat storage, with a detailed examination of SHS and LHS.

Figure 2.1 displays the varying types of energy storage (Jouhara, 2020) currently used in power systems. According to their review (Sharma et al., 2009), the campaign to improve quality of life by reducing the emissions from carbon pollution is focused on renewable energy storage in the most ideal form where the energy captured can be transformed to the required application or process. Efficiency in performance and dependability are just two of the important benefits that have major impacts on energy conservation through the reduction of counter-current differences between supply and demand.

Fig. 2.1 Different types of energy storage from the left showing most general to the right showing more specific subsections (Adapted from (Jouhara, 2020)).

The focus of this paper deals with TES and more specifically LHS through solidification from liquid to solid, and melting, from solid to liquid. In their review (Jouhara et al., 2020), the storage of thermal energy is achieved by varying the temperature of the medium by heating or cooling. The energy successfully stored in the medium is then available for future use depending on the application or function where there is a requirement for a temperature change useful in the power generation industry such as heating and cooling in buildings. Integrating TES into the relevant applications provides major benefits important towards the conservation of energy by improving the overall efficiency of the system whilst reducing the harmful impacts of pollution and carbon emissions. They also stated that the integration of solar technology into TES devices can also enhance the technology.

TES can be defined as energy storage technology that stores the energy in the form of thermal meaning through heat or cold. It can be categorised into namely two types, including thermophysical and thermochemical, Sorenson (2015). This storage technology functions effectively through the integration with electricity power output as well as the capability to supply power to electrical systems in off-peak situations and so became highly demanded by various industries outlined in their review

(Kousksou et al., 2014). They also stated that this energy is more often stored as a temporary means through which varying temperatures, even high or low, can be stored, and due to this sinusoidal characteristic, supply and demand can more easily be targeted to specific needs. The lower temperature ranges, often below 200 °C, whereas the higher temperature ranges above this. This means that the technology is useful for heating and cooling applications in which a variation of temperature is needed like in air conditioning (AC) systems, hot and cold-water systems, heating in buildings and even transportation. The energy collected and dispersed can vary depending on the application, but time for discharge must be kept in mind as sustainable long-lasting systems are highly preferable. In this regard, the choice of TES medium is particularly important to successfully fulfil the product or system specification needed. At its core, the TES, regardless of use, should function under the standard of collecting or capturing the energy required in a process known as charging, sustaining the energy over a period, and then releasing the energy when needed, known as discharging. The physical process can then be further classified into Sensible Heat Storage (SHS) and Latent Heat Storage (LHS). While SHS forms a major part of TES, this thesis does not delve into this topic as the focus is more aligned with the LHS technology.

Figure 2.2 displays the processes in which Sensible heat and Latent heat comprise. These are classified under the Physical processes which vary due to the application of storage as stated by (Jouhara et al., 2020). As they outlined in their study, thermal conductivity forms a crucial facet of the charging and discharging process. As part of the selection process for the choice of TES, high storage capacity, in terms of energy density, repeatability in the charging and discharging process, chemically stable with low corrosion and high tensile strength. In their review between the Physical processes and Chemical processes, (Nazir et al., 2019), they explained the methodological approach in both aspects. For the Physical processes, they outlined that the thermophysical properties of the medium are crucially important to the method of heat transfer. They also noted that for Sensible heat, the energy stored is due to the variation in temperature through the heat transfer process of conduction, convection, or radiation of the medium reliant on the value of its specific heat capacity and the value of the temperature variation. Sorenson (2015), and (Cozzolino et al, 2019) also referenced the diverse types of energy storage.

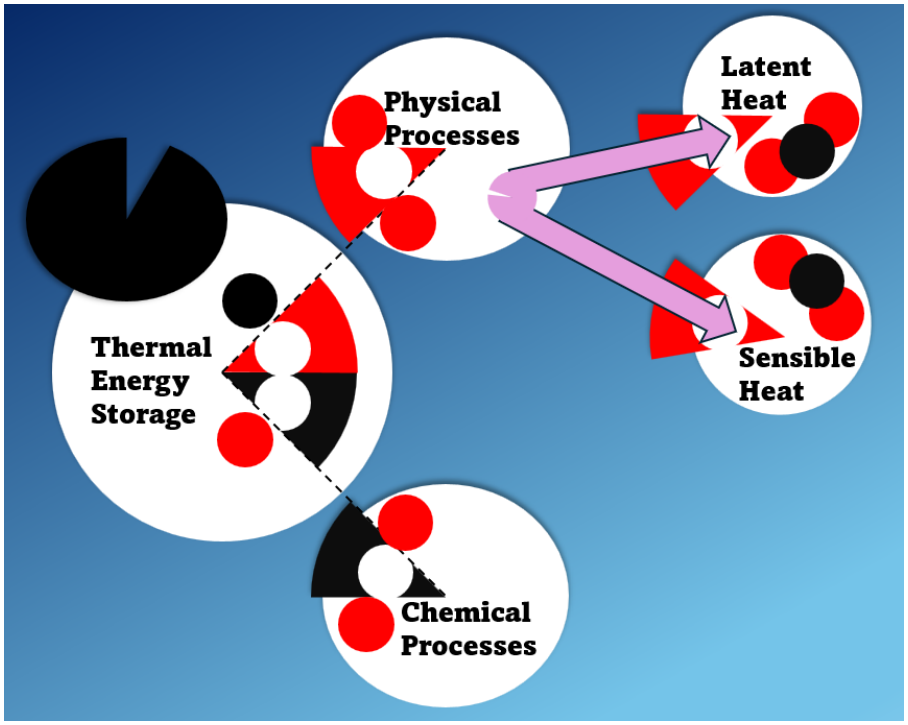

Fig. 2.2 Separation of the physical processes from the chemical processes with Sensible heat and Latent heat (Adapted from (Sorenson (2015), (Cozzolino et al, 2019)).

Reliable materials for this type of heat storage are based on metals and non-metals but, drawbacks such as economic cost and manufacturing as well as low thermal conductivity and low specific heat capacity respectively restrict them to specific applications that are not interchangeable. In this regard, the LHS is more related to constant temperature with its application based upon the phase change of the medium rather than the temperature change. These mediums are most often called Phase Change Materials (PCMs).

In contrast, chemical processes are based on chemical reactions and sorption through reversible reactions. A dissociation reaction occurs resulting from thermochemical heat storage and through reversibility, the energy recovered is through the same principle of charging, storing, and discharging as with all TES applications reviewed by (Nazir et al., 2019).

Illustrated by (Gabriela, 2012), Figure 2.3 displays a plot of temperature with time when a material is heated showing the increase in temperature with time linearly up to point A from origin O, where Sensible heat is dominant. Between points A and B, the temperature does not change but a phase change occurs from solid to a solid-liquid mixture until point B where it is completely liquid. The phase change represents Latent heat where there is no change in temperature with time but a change of phase. From B to C, Sensible heat is dominant again with a further increase in temperature as the material is

fully liquid until it reaches point C where no further increase in temperature occurs with time until D. Latent heat is dominant here again as the material is now in the liquid-vapour stage. At point D, there is another increase in temperature until all the material changes from liquid vapour to complete vapour between points D to E where Sensible heat becomes more dominant.

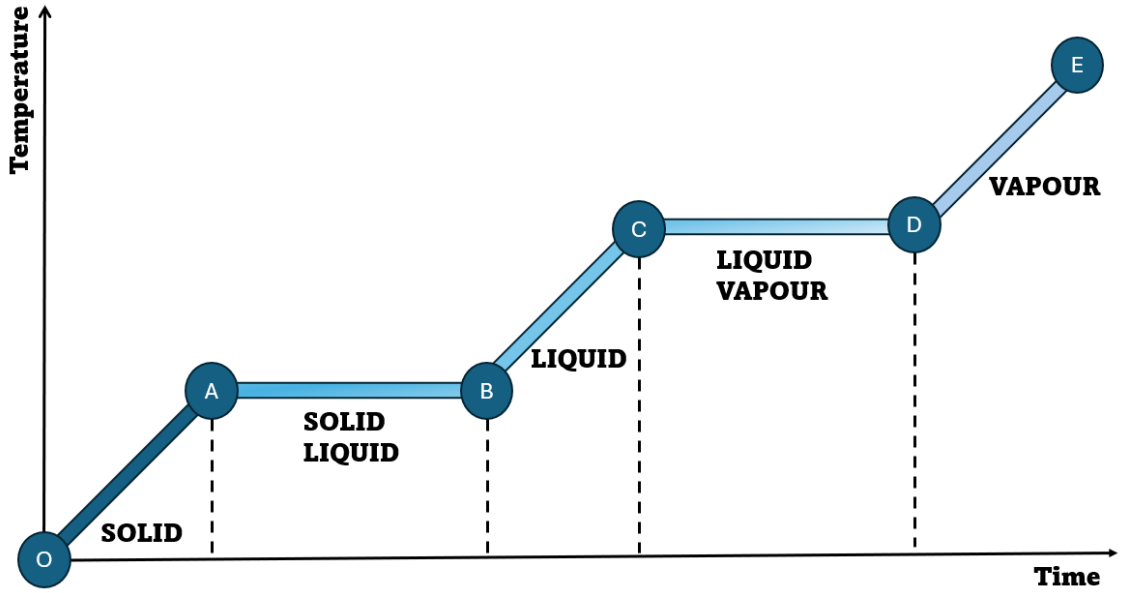

Fig. 2.3 Variation in temperature with time when a substance is heated (Adapted from (Gabriela, 2012)).

Figure 2.4 illustrates not only the components of TES with regards to Sensible heat and Latent heat but also further into these sections with the materials in a specific form comparable to these components. As highlighted in their study, (Sharma et al., 2009), Sensible heat comprises solid and liquid forms while Latent heat has forms including solid-liquid, liquid-gaseous and solid-solid.

Definitions provided in work by Sorenson (2015) and (Zhang et al., 2016) state that Sensible heat storage is based upon the principle of temperature variation with no change in phase by the material through a TES process. The value of the heat storage (q), temperature difference, specific heat capacity ($C_p(T)$), the difference in temperature ($T_{end} - T_{ini}$) and the volume of the material (M) involved as stated in equation (2.1) Sorenson (2015).

$$q = \int_{T_{ini}}^{T_{end}} M.C_p\,(T).dT \qquad (2.1)$$

The material stores the energy based on the three principles of heat transfer including conduction, convection, and radiation and is highly dependent on the immediate environment temperature through which the energy is captured or released by this change.

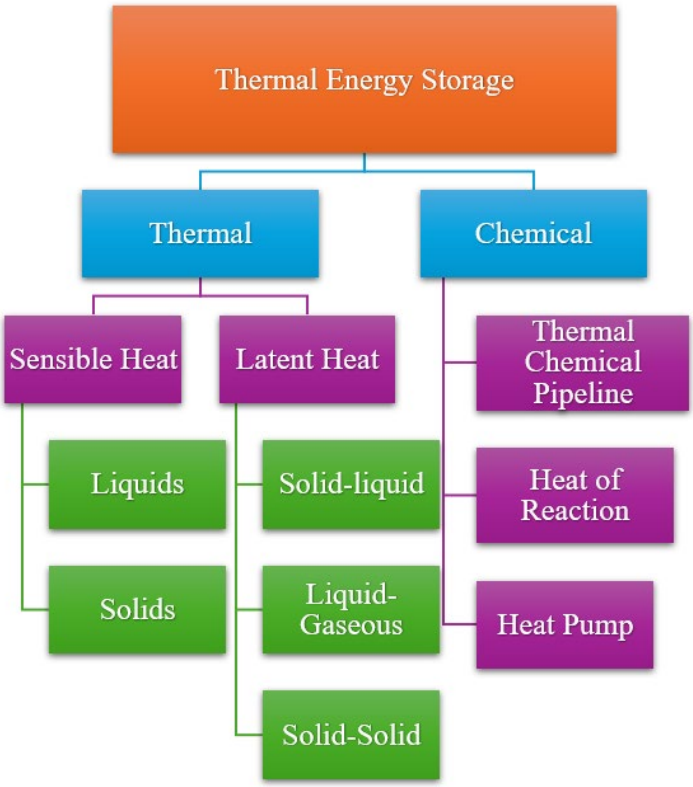

Fig. 2.4 Structure of topics that revolve around Thermal Energy Storage (Adapted from ((Sharma et al., 2009)).

As explained by Sorenson (2015), the literature also supposed that water seems to be the best for this type of energy storage because it is widely available, economical and has good chemical and physical properties and high specific heat capacity. This was also outlined in literature by (Jouhara et al., 2020) as they exclaimed that ceramic as well as oil form good mediums for Sensible heat storage systems. Additionally, (Kousksou et al., 2014), also claimed that water is a good medium for Sensible heat storage, nonetheless, corrosive in the case of mediums as well as only viable in storage within 10 years due to inclement decay of the material life.

As reflected by (Sharma et al., 2009), for temperatures above 100°C, where water usually changes phases to vapour, other materials such as molten salts, varying oils and some liquid metal materials can be used in its place. This was in good agreement with the study by (Jouhara et al., 2020). Water functions both as a storage medium as well as capable of transportation for use in solar energy as colder climates use it for warm tap water and heating. Furthermore, buoyancy effects can be advantageous in water tanks through thermal stratification. This means the removal of mixing to allow the colder-temperature water molecules to sink to the bottom of the tank while the higher-temperature water molecules rise to the top. This is beneficial as it allows the use of similar collected temperatures rather than the slight variation in blending at reduced temperatures, as well as it is assumed that there

would be higher energy available if the accumulated water temperature is less than the blending temperature. When considering large water tank developments, it is necessary to ensure no water loss, reducing heat losses incurred through diffusion through walls. Underground aquifers were considered as well for their large storage capacity and their usefulness for storage during seasonal changes. Open bodies of water can also be used as forms of storage and have been considered but with this form of storage, the research into the specific applications must be considered, however, not dealt with in this review.

As explained in work done by Sorenson (2015) for Sensible solid storage, the mediums used usually operate within low temperatures between 10 °C to above 70 °C, bricks, and its constituents as well as sandwich panels and laminate materials with low specific heat. Work done by (Zhang et al., 2016) also commented on the low economic costs and thermal conductivity. These types of materials are used as compared to liquid, it does not undergo freezing or boiling, (Kousksou et al., 2014). They also conveyed that the same type of material used for the associated piping going to the storage medium should both be the same to reduce the effects of separation from their varying expansion coefficients that reduce the heat transfer process. This type of storage is mostly reserved for buildings, AC, and space heating. They have lower specific heat capacities and so store lower volumes of heat than that of liquid storage. However, they are useful at higher temperature ranges and containment issues are negligible with aspects such as geometrical shape, density in structure, orientation of flow and the category of fluid media chosen must be considered.

Disadvantages of this type of TES include heat loss through self-discharging and minimal energy density. This type of TES has been particularly researched in literature for its usefulness in heating buildings using solid and liquid mediums. Examples of these include water for liquid medium, bricks, concrete, insulated laminate foam material, rocks, earth, sandwich panels and much more, Sorenson (2015). Other disadvantages pointed out in their review, (Kousksou et al., 2014) include bigger storage sizes and large temperature variations directly because of its poor energy storage capacity also outlined by (Zhang et al., 2016). Usually, if this variation is allowed, then the storage size becomes smaller which is not the case for other storage methods. Heat loss is because of the larger storage sizes as well as higher economic costs. Moreover, when considering the use of large storage tanks, which are focused on solar energy, the load, area of zone collection, weather conditions, and operations all manage the economic aspect of the system. They suggested that when considering the geometric designs, low surface area per unit volume can be implemented to negate the effects of heat loss.

2.2.1 Latent heat storage (LHS)

The sectioning of LHS into the three different types of material changes (solid-liquid, liquid-vapour, and solid-solid) when applied to a heat storage process is displayed in Figure 2.5. As described in the literature, (Mohamed et al., 2017), LHS has been regarded as an efficient form of TES. It is reliant on the discharge and charging of the storage medium that goes through phase changes in either of the three forms identified in Figure 2.5 and stated in their review, (Pielichowska et al., 2014). These phase changes occur at a certain temperature depending on the material through the charging of energy commonly known as Latent heat of fusion for changes from solid to liquid and the reverse. Other phase changes consider Latent heat of vaporisation. The temperature causing Latent heat of fusion through the charging process is usually constant until all the storage medium has melted by which it continues to rise if more heat is injected into the process.

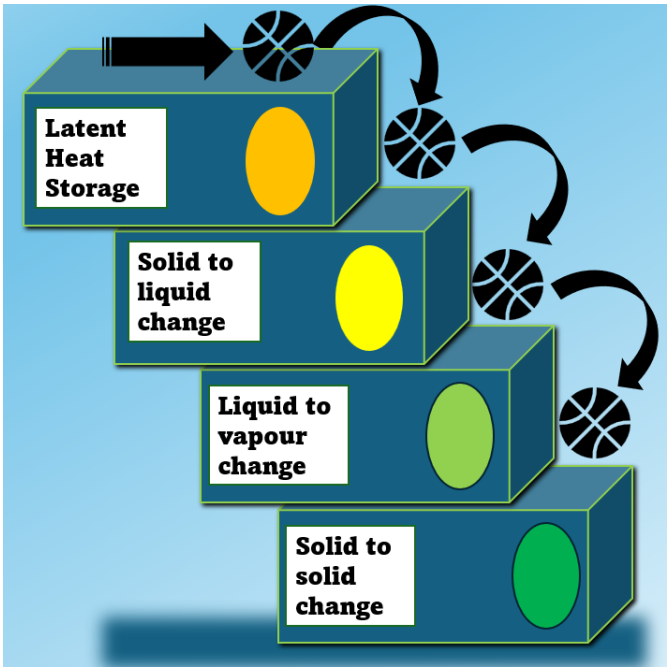

Fig. 2.5 Structure of Latent heat storage into the type of materials used (Adapted from ((Mohamed et al., 2017)).

This can be seen in Figure 2.6 shows the plot increases linearly during Sensible storage where heat is added to the system followed by a constant temperature during Latent heat storage with a small change in pressure and volume and finally to the Sensible storage phase as more energy is supplied and the temperature rises (Mohamed at al., 2017), (Rostami et al., 2020). The variation of temperature with the amount of energy stored as the material is heated showing the area where Sensible heat and Latent heat occurs is displayed in Figure 2.6. The melting and solidification cycles through the Sensible and

Latent heat phases show where the phase change of the PCM occurs at the phase change temperature of the PCM.

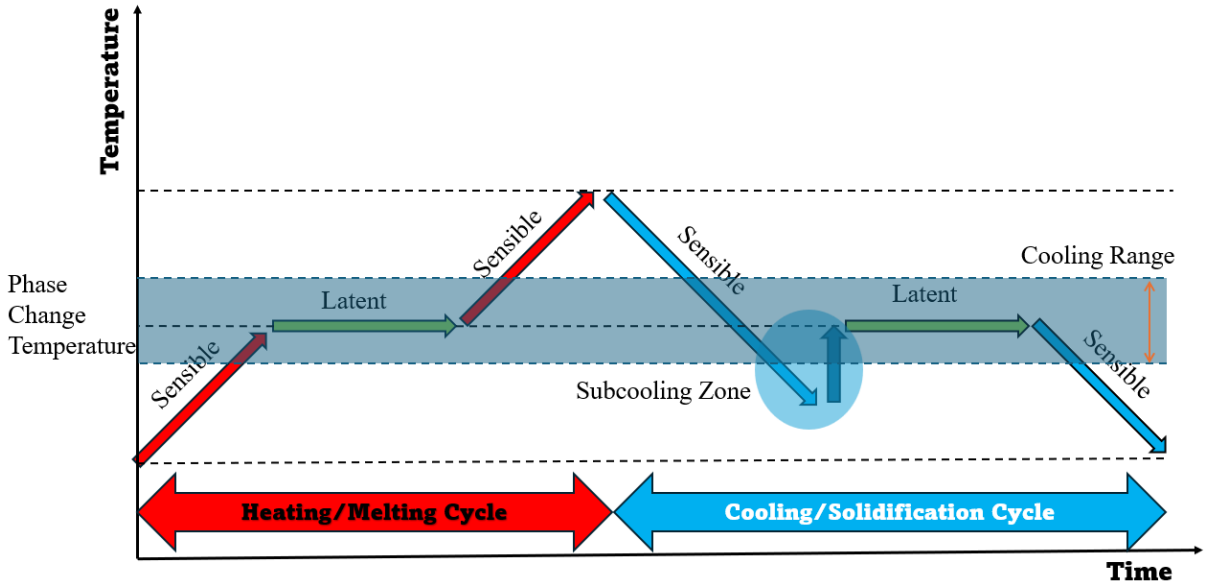

Fig. 2.6 Melting and solidification of the PCM at a phase change temperature (Adapted from ((Rostami et al., 2020)).

The amount of heat stored during the phase change is dependent on the variation in enthalpy of the material through the transition of solid to liquid with the equation as follows (Jouhara et al., 2020):

$$\nabla Q = \nabla H = m\nabla H \qquad (2.2)$$

A study by (Kousksou et al., 2014), characterised Latent Heat as being normally greater than that of Sensible heat for storage materials comprising lower volumes and reduced temperature variation due to fusion or vaporisation at a constant temperature. In most cases, it has been suggested that solid to liquid and vice versa is much more applicable, however, certain complications arise from instability of properties, segregation of phases and supercooling. Studies performed by (Mohamed et al., 2017), (Pielichowska et al., 2014), (Sharma et al., 2009) and (Zhang et al., 2016) were all in agreement with the efficiency of Latent heat being much greater than Sensible heat. It was also stated in their work, (Zhang et al., 2016), that liquid-to-vapour and solid-to-solid change are associated with their complications involving containment capacity and exceptionally low Latent heat, respectively. In this regard, liquid-to-vapour and solid-to-solid are not studied in detail in this research as the focus was on solid-to-liquid change and vice versa.

For the solid-to-solid change, there is little volume change and therefore less heat storage as the material just alters its crystalline structure to another form compared to solid-to-liquid change as stated

in their review, (Sharma et al., 2009), with work by Sorenson (2015) in agreement. There are outlining benefits from using this form, which facilitates less rigour in containment as well as enables greater creativity in design. The studies showed that in terms of this phase change, pentaglycerine has been identified as possibly suitable for solar applications due to its properties. Further research into this material and enhancements can prove beneficial and significant research area, however, it is not dealt with in this paper.

In the case of solid-to-gas and liquid-to-gas changes, greater LHS is available, but due to the nature of these phases to exhibit larger volumes, stricter containment policing must be in place, so they are not applicable in the case of solar energy storage and TES as described by (Sharma et al., 2009), (Pielichowska et al., 2014). They also indicated that for solid-to-liquid changes in mediums, comparatively less heat energy occurs in their transition as opposed to the others identified previously, however, they can charge, store, and discharge larger amounts of heat energy within a small volume and temperature change of the material as seen also in research conducted by (Jouhara et al., 2020). This makes the material economically feasible also discussed by (Pielichowska et al., 2014) and (Mohamed et al., 2017). Moreover, they stated that the heat energy charged can also be retrieved at constant temperatures as well as store greater amounts of energy as opposed to Sensible heat, regardless of small temperature differences between the heat source and the heat sink. This enables LHS to be desirable compared to SHS for TES applications including solar energy storage. For materials, the Latent heat capacity equation is as follows (Jouhara et al., 2020):

$$Q = mC_p dT(s) + mL + mC_p dT \tag{2.3}$$

According to work done by (Jouhara et al., 2020), the interaction of the heat transfer surfaces is an important aspect of TES. As in the case of heat transfer in heat exchangers, the heat transfer process can be either through direct contact or indirect contact. For the indirect contact type, there is a separation wall between the two transfer mediums as there is no mixing between the two mediums but there is still a gradient flow of heat transfer from one medium through the wall to the other medium. For direct contact types, this is not the case, as the two mediums are in contact and can mix. For the latter, due to the absence of a separating wall, temperatures of both mediums can reach smaller temperature differences to saturation, in this case, mass transfer also takes place, Thulukkanam (2013).

One of the major aspects when considering TES and LHS, is that the geometry, function and boundary conditions or parameters, play major roles in the improvement of efficiency of the process. The amount of energy stored and available can include heat transfer improvements such as surface enhancements of the medium, additives to improve thermal conductivity, mass flow rate and inlet temperature of the fluid, dimensional changes, even those through different angular perspectives,

encapsulations and shape the medium takes (Jouhara et al., 2020). This brings into focus, the topic of PCMs and their role in LHS and TES as a whole which will be further discussed in section 2.2.2.

2.2.2 Phase change materials (PCM)

As discussed in the previous section 2.2.1, PCMs characterise the materials used in LHS applications. This medium has been investigated over the past 20 years with the vast nature of the studies themselves incorporating large spectrums of the material which have effortlessly been redefined to determine the best material for the process. PCMs are normally characterised by three (3) states that include, solidifying, melting and gaseous states. It is through these various states of solidifying and melting, that the material can absorb energy in the form of charging/melting, store the energy for a period and discharge/solidify the energy when required. These materials have been actively used to store different forms of TES in real-world applications (Pandey et al., 2018).

During the initial heating, the temperature of the PCM increases as the energy absorbed also increases, until the temperature is at the melting temperature or conversion of phase into liquid, (Mohammed et al., 2017). In this respect, there are PCMs with specific melting temperatures or solidifying temperatures often referred to as the liquidus or solidus temperature. Above or below these temperatures, the PCM can be in a complete state of homogeny in the liquid or the solid state.

This makes them useful in different applications as the phase change temperature of the PCMs varies depending on the type and application it is used. They store the energy during the phase change process within very narrow temperatures and at larger energy densities than in SHS applications (Mohamed et al., 2017), (Sharma et al., 2015), (Sharma et al. 2009), (Pielichowska et al., 2014) and (Kousksou et al., 2014). The equation for LHS capacity with a PCM is shown in the following equation (Mohamed et al., 2017):

$$Q = \int_{T_i}^{T_m} mC_p\, dT + ma_m \Delta h_m + \int_{T_m}^{T_f} m\, C_p dt \qquad (2.4)$$

The equation represents the Sensible heat stored in the PCM during the initial heating phase to increase the temperature, followed by the amount of LHS energy charged or discharged because of the phase change process, and finally an account of the increase in temperature during the liquid phase. The equation most represents the LHS in which the phase conversion is from the solid phase to the liquid phase (Mohamed et al., 2017). This phase conversion for melting is important, as it forms one of the main factors for the choice of PCM material and more specifically, its melting temperature. For obvious reasons in the selection process, the melting temperature of the PCM should be lower than the heat

source and higher than the ambient temperature of the operating environment (Jouhara et al., 2020). As we know, for heat transfer to occur, a differential temperature gradient must be present, as heat is transferred from higher temperatures to lower temperatures due to the differential gradient. In this case, if the temperature of the PCM is higher than the heat source or lower than the ambient temperature of the environment in a melting experiment, the PCM would lose heat and remain in its solid state.

According to work completed by (Mohamed et al., 2017), (Wei et al., 2018), and (Faraj et al., 2021), certain criteria involve choosing the relevant PCM for the various applications for which it is designed. The material is chosen or selected on the basis that it satisfies specific properties whether it be towards the kinetic energy, thermodynamic relation, chemical makeup, and economic factors. In terms of applications related to LHS, the properties must be related to the PCM with the properties shown in Figure 2.7.

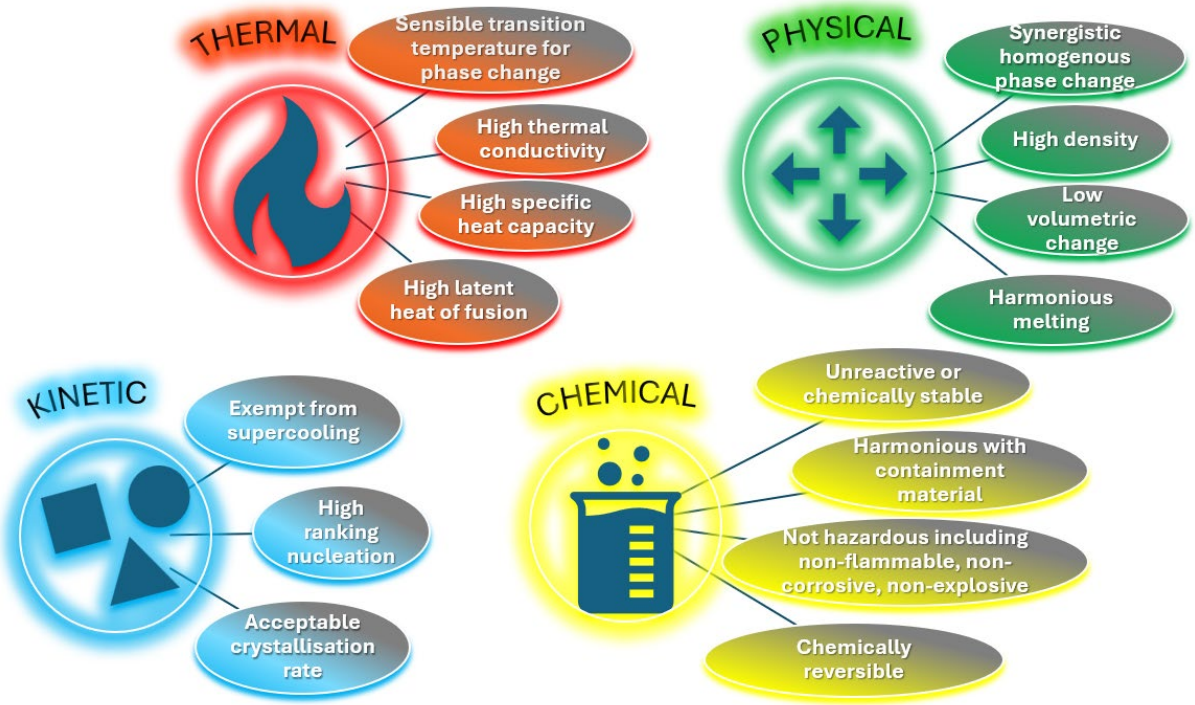

Fig. 2.7 LHS properties of PCM depending on the application (Adapted from ((Mohamed et al., 2017), (Wei et al., 2018), and (Faraj et al., 2021)).

As seen in Figure 2.7, for the thermal properties, it is important specifically for the application that the PCM temperature for phase change is appropriately aligned to the operation temperature. The properties of high Latent heat reduce the volume size ratio of the containment. The high levels of

thermal conductivity and specific heat capacity improve the ability of the PCM to conduct heat per unit area of the PCM (Mohamed et al., 2017). Higher values provide good conductive materials while lower values would only cause the PCM to function as an insulator or poor conductor, which defeats its purpose. Additionally, high conductivity means that the material would have a high thermal diffusivity. In respect of transient heat conduction, this value is representative of how quickly heat conducted would travel through the material, increasing the propagation of heat in the material. This effectively decreases the charging and discharging time through Sensible heat.

To reduce the need for larger containment, a densely packed PCM with little volumetric change during transition is desirable. Low vapour pressures under operational conditions reduce the tangential forces on the container and hence improve its integrity. Harmonious melting prevents segregation in the reversible reaction avoiding loss of efficiency.

Concerning the Kinetic properties of the PCM, supercooling prevents efficient heat extraction so minimal, or no amount of supercooling is preferable. Good nucleation and crystallisation rates also affect the efficiency of the material preventing non-uniform solidification and instances of rapid or slow cooling.

Moreover, for Chemical properties, PCMs degrade due to crystallisation based on chemical instability with containment material chosen or fluid losses. Therefore, the choice of material used in the application for containment of the PCM must be non-reactive, stable, and corrosion-resistant. Also, for any safety protocol based on the intended application, a non-toxic and non-flammable PCM should be investigated. For the material selection process, the PCM material should be economically feasible, widely available for use and in high supply (Pielichowska et al., 2014), (Kousksou et al., 2014), (Sharma et al., 2009), (Wei et al., 2018), and (Liu et al., 2012).

According to (Wei et al., 2018), different methods can be used to select the most appropriate PCM for a particular study or application. These are not limited to experimental approaches, hand calculations or using simulation software. Traditional practices may not be able to capture all the data through research of other published works as they are constrained to either investigation of thermal properties or may lack other issues such as economics and the environment. They also stated that due to the high number of available PCMs, simply choosing one that can fulfil all the requirements of a particular study may be difficult and can take a long duration. They suggested the use of material database software packages like GRANTA EduPack to aid in the selection and creation of PCMs for the application. The software developed by Mike Ashby, contains a database of thousands of materials that can be selected, compared, and modified to even synthesise new materials based on desired properties, cost, and manufacturing process.

PCMs can be classified under certain groups that form a range of subgroups of classifications. According to (Jouhara et al., 2020), PCMs can be classified as organic in composition and can include Paraffins, Fatty acids, Esters, and Alcohols. Inorganic PCMs are mostly composed of Salts, Salt-Hydrates, Metallic compounds, and Metal Alloys. They can also be classified under Eutectic PCMs as Organic-Organic, Inorganic-Inorganic and Organic-Inorganic. These classifications fall under the Solid-Liquid PCMs as highlighted earlier in section 2.2.1. Polymers fall under the category of Solid-Solid PCMs including Cross-linked polyethylene, Polyurethanes, Polybutadiene and Polyalcohols.

These classifications have been illustrated in Figure 2.8 in their study (Nazir et al., 2019). The figure shows the various categories and classifications under TES, more specifically, this section deals with the LHS with the applications of PCMs and their various categories.

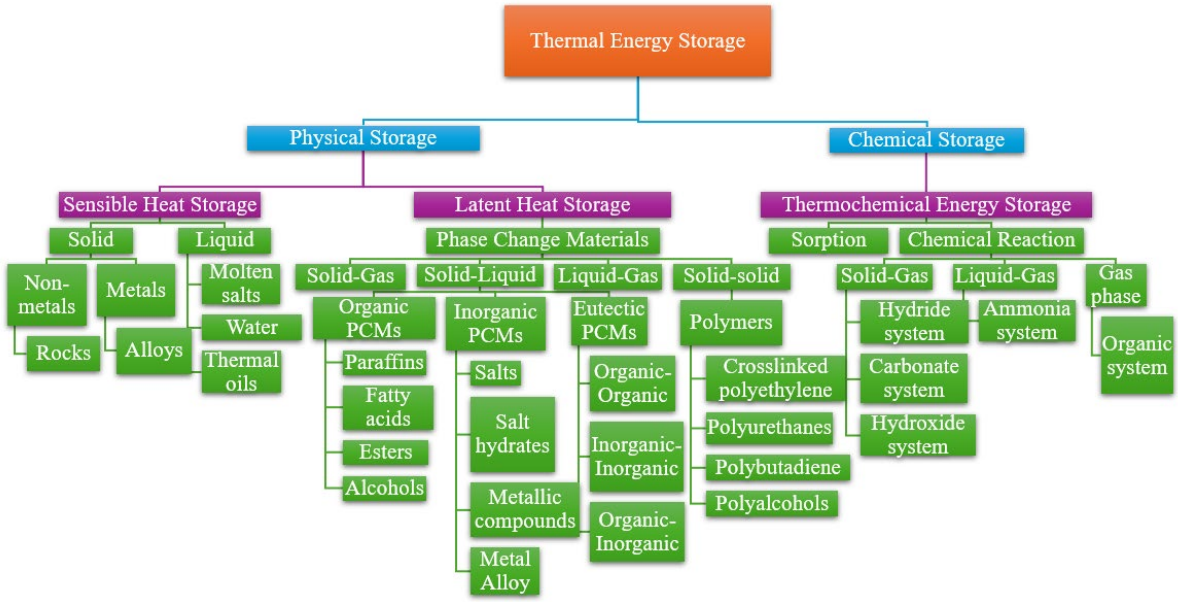

Fig. 2.8 Description of TES with more detail into SHS, LHS and Thermochemical Energy Storage (TCES) (Adapted from ((Nazir et al., 2019)).

In a study completed by (Pandey et al., 2018), they also categorised PCMs into different Organic, Inorganic and Eutectic groups showing similarities and agreement with work done by (Nazir et al., 2019), (Rostami et al., 2020), (Faraj et al., 2021), and (Sharma et al, 2009).

According to (Sharma et al., 2009), (Pandey et al., 2018), (Rostami et al., 2020), and (Sharma et al., 2015), PCMs including the varying types of Organic, Inorganic and Eutectic are attainable through any number of desired temperature limits.

In terms of their Latent heat of fusion and melting parameters, Organic and Inorganic materials can be classified as PCMs. A vast majority of PCMs cannot satisfy the storage requirements considering the melting temperature within the operating parameters. Based on the desired LHS properties (see Figure 2.7), there are no PCMs currently which can facilitate all the requirements, so additional materials must be used in conjunction to bridge the gap between poor properties and the requirements. These can also be implemented as part of the design of the PCM. This can vary from metallic materials that can increase the poor thermal conductivity of PCM, including the supplementary design of added fins, adding nucleating agents to prevent supercooling, and increasing thickness to reduce dissimilar melting (Sharma et al., 2015). As compared to Organic materials, Inorganic materials have twice the amount of LHS capacity ($250 - 400\ kg/dm^3$) to ($128 - 200\ kg/dm^3$). These descriptions will be outlined further in this thesis.

In their research (Pielichowska et al., 2014), potential PCMs have been classified into Paraffin and non-paraffin compounds, Salt hydrates, metallics, and Organic-Organic, Organic-Inorganic Eutectics within the past forty (40) years (see Figure 2.8). They stated that PCMs can be further defined by their phase change temperature.

Low-tier temperature PCMs range below 15 °C, often used for AC and preserving food applications. Mid-tier temperature PCMs, range between 15 – 90 °C and have been the most applicable and used PCM in renewable energy, engineering designs in buildings to improve efficiency, electronics, and other various industries. High-tier temperature PCMs range above 90 °C, mostly used for high-temperature applications including the aerospace industry and where high-temperature operations are required. Whilst research by (Zhang et al., 2016) stated that low-tier temperature PCMs lie below 200 °C and high-tier temperature PCMs lie above 200 °C, they involved a larger temperature range as opposed to work done by (Pielichowska et al., 2014).

Organic materials, described as natural by (Pandey et al., 2018) and (Jouhara et al., 2020), comprise Paraffin compounds and non-paraffin compounds that have certain advantages and disadvantages as compared to Inorganic PCMs. Advantages include thermal and chemical stability, high Latent heat of fusion, non-corrosiveness and generally can be recycled. While, disadvantages include, poor thermal conductivity, flammability, disagreement with polymer and encapsulating containers conferred in their reviews (Zhang et al., 2016), (Jouhara et al., 2020), (Kousksou et al., 2014), (Sharma et al., 2009), and (Sharma et al., 2015).

Paraffin compounds have been extensively used in TES for their characteristic properties which include non-toxic, non-corrosive, constant conductivity during cycles (reduced phase segregation), no supercooling (little crystallisation), low vapour pressure and high fusion heat. They are normally in the straight-chain alkanes group $CH_3 - (CH_2) - CH_3$ (Kousksou et al., 2014) and (Sharma et al., 2009). Considering the various melting points, they have been used to conserve energy in buildings. However, poor thermal conductivity and high-volume expansion make it disadvantageous as well as their high costs in manufacturing and fabrication (Pandey et al., 2018). For LHS systems, technical grade Paraffins are preferred for their low economic costs, reliability, and chemical stability. Below 500 °C, they are chemically stable (Sharma et al., 2009), (Kousksou et al., 2014), and (Sharma et al., 2015).

To reduce the impact of volume expansion, encapsulation methods can be used to improve storage and reduce spill-over. Non-paraffin compounds include fatty acids attained from animals and plants and have better physical and thermal properties as opposed to Organic Paraffin compounds (Jouhara et al., 2020). In a review of the literature (Sharma et al., 2009), (Kousksou et al., 2014) and (Pandey et al., 2018) stated that non-paraffin materials are often diverse in their nature and properties, however, there are commonalities between them that were outlined. Advantages include chemical stability during long periods of operating temperature with no adverse effects of phase segregation or degradation, zero supercooling and the transformation of phases results in high amounts of Latent heat energy storage. Disadvantages include similarities to Paraffins including low thermal conductivity and flammability but may also involve high economic costs for fatty acids, corrosiveness, and toxicity as well as instability at high-tier temperatures and low flash point values. Non-paraffin PCMs vastly outnumber other PCMs relative to their different properties. This group of Organic PCMs consist of fatty acids, esters, and alcohols. These PCMs have innate characteristic hazards such as flammability and should be treated with some caution to avoid open flames or any oxidising agent. The chemical formula that describes fatty acids as desirable PCMs is $CH_3(CH_2)_{2n}.COOH$ (Sharma et al., 2009), (Sharma et al., 2015) and (Pandey et al., 2018). As described in the work by (Sharma et al., 2015), considering their high economic costs, fatty acids display efficient change of phase as compared with paraffin fatty acids and display improved qualities. These include good TES efficiency and chemical stability appropriate to most LHS applications due to the range of melting temperature and harmonious melting. They can also sustain their properties and nature without degrading through cyclic changes of phase change. These materials have been discussed in detail in other research, but this thesis will be void of an in-depth detail of these materials as they have already been evaluated.

Moreover, PCMs also include Inorganic materials that constitute Salt hydrates and Metallics (see Figure 2.8). These materials do not permit supercooling or degradation, (Sharma et al., 2009) and (Pandey et al., 2018). According to their review (Pandey et al., 2018), while Organic materials are

usually carbon-based, Inorganic materials exclude materials involving carbon. Advantages of this type of PCM include good thermal conductivity and two times the amount of LHS capacity as compared with Organic materials (Kousksou et al., 2014). They can also be involved in high-temperature processes and are cheaper as compared to Organic PCMs (Mohamed et al., 2017). In their description, (Jouhara et al., 2020), solid Inorganic materials process the heat energy in different forms of transformation including magnetic, crystallographic structure and order-disorder affecting crystal and amorphous structures. Magnetic and crystallographic structure transformation involves a vast amount of Latent heat. Disadvantages of this type of PCM include phase segregation and separation (reducing the storage capacity), corrosivity (reducing the life span incurring higher costs) and instability as well as subcooling and thus these materials are often used in waste heat recovery in industrial plants. The metallic forms of Inorganic materials have decent properties of thermal conductivity, stability and density that make them well-suited as PCMs as they are irrespective of the disadvantages outlined above.

In the case of Inorganic materials, salt hydrates can be described as crystalline solids of inorganic salts and water, (Sharma et al., 2009) and (Pandey et al., 2018). The phase transformation that involves solid to liquid, consists of dehydration of the salt like the thermodynamic process of melting or solidification. The general formula is stated as $AB\,.\,nH_2O$ with AB set as the inorganic salt in the expression and nH_2O expressed as the number of water molecules present and the chemical formula describing the melting reaction to salt hydrate and water or an anhydrous change is as follows (Sharma et al., 2009), (Pielichowska et al., 2014), and (Kousksou et al., 2014): $AB\,.\,nH_2O \rightarrow AB\,.mH_2O + (n-m)H_2O$ or $AB\,.nH_2O \rightarrow AB + nH_2O$. An increase in Sensible heat energy of salt hydrate separates the crystals into anhydrous state of salt and water or a lower state of salt and water. Since all the solids do not convert efficiently, heterogenous melting occurs causing the denser particles to fall to the bottom of the container while the less dense particles rise to the top of the container. In the case of its poor nucleation properties initiating supercooling, the addition of a nucleation agent to revert or deter this reaction can be a solution to this disadvantage. They are one of the most valued sets of PCMs for their high thermal conductivity and Latent heat of fusion with little volume change in the melting process, also with little corrosivity and toxicity (Zhang et al., 2016).

In terms of melting, three different outcomes include homogenous melting (completely soluble), heterogenous melting (completely insoluble) and semi-homogenous (partially soluble) melting. One major disadvantage of these types of outcomes is that homogenous melting does not take place causing an irreversible process with increasing factors of each cycle. This brings about another disadvantage that involves supercooling the material to ensure proper nucleation, forcing the discharge of stored energy to be released at lower temperatures. Several practical solutions can be used to reduce

the effect of heterogenous melting including mechanical mixing, encapsulation, thickening agents, increased water supply to the process and modifications to the chemical composition of the material in a review of their studies, (Sharma et al., 2009), (Pielichowska et al., 2014), (Kousksou et al., 2014), and (Mohamed et al., 2017). According to work done by (Vikas et al., 2017), the use of paraffin PCM in a rectangular enclosure was used to simulate the melting of the PCM using ANSYS Fluent. One side of the container had constant heat flux while the other sides of the container were insulated. Varying contours of liquid fraction and temperature were generated to review the effect on the PCM from the increase in temperature and the effect of heat transfer on the PCM. Melting was seen to begin from the top of the container with increases in the melting rate as the charging of the PCM progressed. It was seen that initially; conduction was the main form of heat transfer followed by natural convection near the top region.

Another characteristic form of PCMs includes metallics. These include metals with low melting properties as well as metal eutectics. One major disadvantage or deterrent from using this type of PCM is the density and hence weight factor of the material. Although this brings about positives for its high heat of fusion for each volume unit present in the process, unlike other PCMs, this type has high thermal conductivity due to its properties as stated in their study (Sharma et al., 2009) and (Zhang et al., 2016). This was also conveyed in their paper (Pandey et al., 2018) with features such as low specific heat and low vapour pressure also conveyed as properties of metallic PCMS in their review (Kousksou et al., 2014). Also discussed by (Mohamed et al., 2017), these types of PCMs have low heat of fusion for each unit of weight in the process, so due to their weight value, these types may not be considered as stated previously. Another important aspect discussed in their paper was that chemical reactions take place in the solid-liquid type PCMs with the molten metallic alloy and the container. As discussed previously, one of the possible solutions for this is, encapsulation to restrict the interaction between the two materials. In their review, (Pielichowska et al., 2014), these types of metallics or alloys are mostly used in high-temperature processes for their repeatability and thermal reliability. Of these types, they suggested that aluminium, copper, magnesium, and zinc which are bountiful and available, can be used in TES applications for their potential. Aluminium alloys in this case were preferential due to their properties of thermal stability, and heat density and a preferred phase transition temperature was suitable in a wide range of applications. For this reason, aluminium was chosen as the heated material and testing material in the simulation tests conducted throughout this research study.

As opposed to Organic and Inorganic PCMs mentioned previously, another type called the Eutectics has been determined to be a characteristic form of PCMs. This material consists of two or more elements that homogenously melt and freeze creating a crystallisation mixture of minimum melting as stated by (Sharma et al., 2009) and (Pandey et al., 2018). The phase change temperature

remains constant in this type of PCM which can be of the form Organic or Inorganic (Kousksou et al., 2014) and (Jouhara et al., 2020). One advantage of this type of PCM is the absence of phase segregation, since during melting or solidification, both materials either melt or solidify at the same time reducing or eliminating any instance of phase segregation (Zhang et al., 2016). It has been suggested that some PCMs that are also minimum melting types be called Eutectics, but this has been highlighted as incorrect, due to their phase segregation characteristics. These types can be correctly identified as peritectic because of the reaction during the transition phase.

2.2.3 Types, designs, and applications of PCMs

As described above, one of the ways to prevent the interaction of the PCM and the containment media it is in is to encapsulate it as seen in Figure 2.9 for the engineering principle behind the heating and cooling of the encapsulated PCM. As described by (Jouhara et al., 2020), (Wei et al., 2018), and (Nazir et al., 2019), encapsulation minimises any potential leaks that may occur from the molten PCM through the container. This has been one way used to increase the efficiency of the LHS process that involves PCMs. The performance of PCMs using different techniques including improvement to the surface area through encapsulation or the introduction of fins, additives to improve thermal conductivity (Rathore et al., 2019) and enhancements to the PCM themselves have been done through thermodynamic means. Of these methods, with the exclusion of the water-to-ice process, encapsulation is used to restrict the interaction between the PCM and the container or environment, which may cause instability or initiate some physiological change. Encapsulation also improves the mechanical integrity with varying geometries having added benefits or drawbacks.

Three types of encapsulation techniques include macro, micro and nano (Jouhara et al., 2020) and (Nazir et al., 2019). For the macro-encapsulation, the encapsulation shell should be greater than 5 mm as stated by (Rathore et al., 2019) or 1 mm as stated by (Alehosseini et al., 2019) or between 1mm to 1cm as stated by (Nazir et al., 2019). The shape of the encapsulation can be variable and take on many different forms including tubes, triangular, cylindrical, rectangular, cubic or any other shape. Due to the wide variety of designs and shapes, this encapsulation technique is mostly used in building applications. The varying types shown for tube type configurations are shown in Figure 2.10 as well as an illustration of encapsulation of a PCM core material in Figure 2.11.

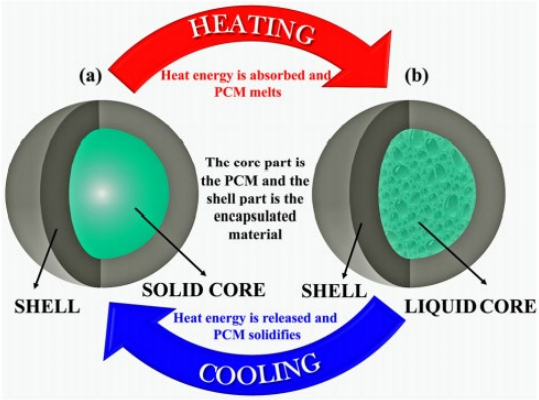

Fig. 2.9 Operating principle for an encapsulated PCM (Nazir et al., 2019).

As described in their study, (Nazir et al., 2019), the core represents the PCM material while the shell represents the encapsulated material. Once the heat is applied to the sufficient melting temperature of the PCM for phase change, an initial solid PCM changes to liquid, storing the energy through LHS. When this heat energy is discharged in the cooling process, the liquid core returns to its solid state. According to research by (Rathore et al., 2019) and (Wei et al., 2018), the encapsulation material should fulfil certain criteria such as good thermal conductivity, high strength, non-toxicity, non-corrosive, non-flammable and chemically (see Figure 2.7) inert with the building materials as well as UV rays and moisture. In their study, (Rathore et al., 2019), they used macro-encapsulation with the building blocks to improve the thermal capacity using steel as the encapsulating material and RT18 as the PCM as shown in Figure 2.12.

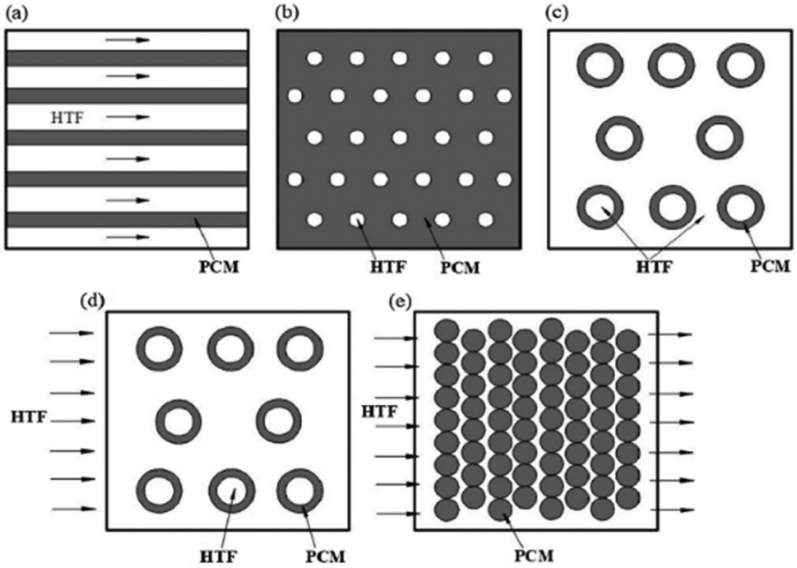

Fig. 2.10 TES storage patterns for tube type configuration; a - flat plate, b - internal flow (shell and tube), c - parallel flow (shell and tube), d - cross flow (shell and tube) and e - packed bed, (Jouhara et al, 2020).

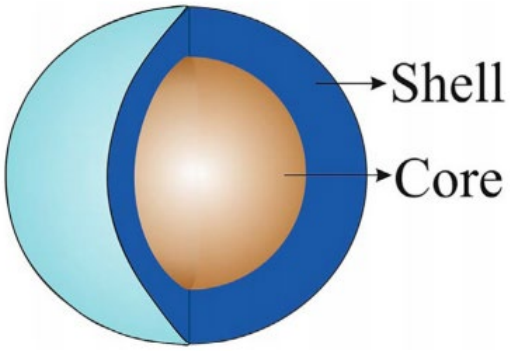

Fig. 2.11 PCM core encapsulated in a shell material (Rathore et al., 2019).

Fig. 2.12 Macro-encapsulated material within the red bricks (Rathore et al., 2019).

In the case of micro-encapsulation, as per their study (Jouhara et al., 2020), improves heat transfer through variation of the surface-to-volume ratio as well as active control for volumetric changes (Pielichowska et al., 2014). As seen in Figure 2.13, these variations include some simple, irregular, multi-core, multi-wall, and matrix designs. Additionally, micro-encapsulation can be implemented in TES building applications as well as other design parameters including chemical and physical, used in medicine, food, and agriculture industries (Jouhara et al., 2020) (Pielichowska et al., 2014). The layer of encapsulating material is usually between $1\ \mu m - 1000\ \mu m$ around the core material either in liquid or solid state. It must be noted that encapsulation improves thermal storage with organic material having less thermal conductivity than inorganic as exclaimed in section 2.2.2.

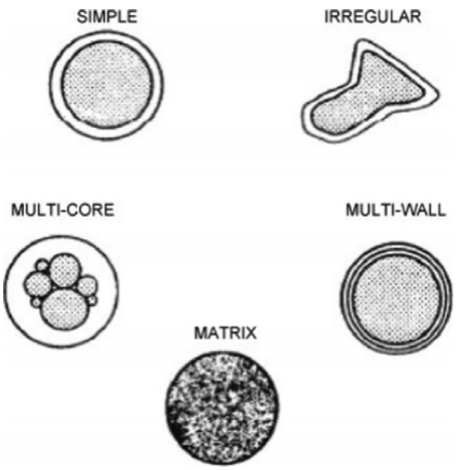

Fig. 2.13 Variation in micro-encapsulation designs (Jouhara et al., 2020).

In their research (Alehosseini et al., 2019), both micro-encapsulation and nano-encapsulation isolate the solid, liquid or gas material within a shell of ideal properties. They stated that this technique is a necessary cause to efficiently apply PCM material to a process. Not only does this technique prevent unnecessary leakage of any liquid material, but it also protects the PCM and enhances its use. It does this by reducing corrosion, and degradation, improving efficiency and reliability and throttling the energy discharged. The only drawback of encapsulation methods is cost implications for desired material properties, shape, design, and strength capabilities as outlined in their review (Pielichowska et al., 2014). The nano-encapsulation is classified with shell sizes between $1 - 1000nm$ or below 1μm (Nazir et al., 2019). The shells must be designed in such a way as to avoid any fracture and have high strength to withstand the volumetric changes during phase transformation. The material can either be a solid material or a combination of materials that can stabilise, accelerate, or retard the TES process. Nano-encapsulated PCMs due to their small size, have high surface area and stability along with their quantum tunnelling and volume effects that are valued in applications involving TES. The main role of encapsulation is the preservation of the PCM core material. They can be achieved through three different techniques as exclaimed in their study (Alehosseini et al., 2019), inclusive of chemical, physio-chemical, and physio-mechanical. This paper does not seek to address any issues or concerns with these methods but merely seeks to identify them in case further research or reading is needed as they are not discussed in detail in this thesis. Figure 2.14 displays the PCM encapsulation techniques for both physical and chemical forms and the methods involved.

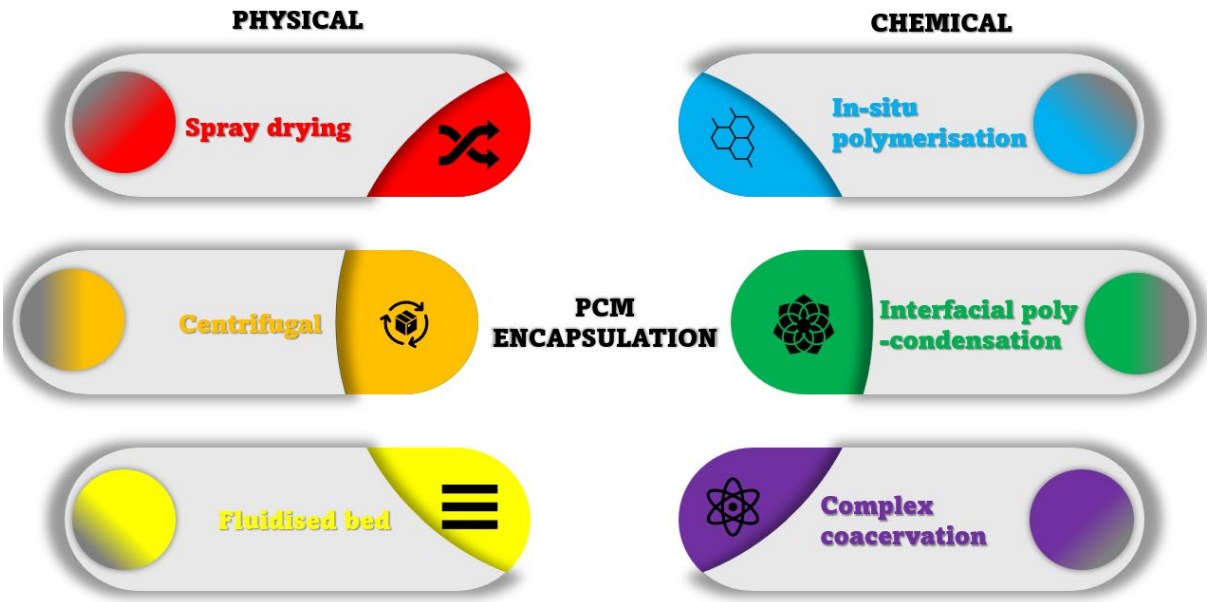

Fig. 2.14 PCMs encapsulation techniques which include both the physical and chemical forms (Adapted from ((Mohamed et al., 2017)).

In their review of PCM encapsulation, (Mohamed et al., 2017) outlined that PCMs in their liquid phase must be encapsulated with the exclusion of water and ice. This agrees with their study (Jouhara et al., 2020). They agreed that leakage is a major issue for containment which encapsulation tries to resolve. Not only does it contain the molten material, but also acts as a barrier to the external environment which may have degrading effects on the PCMs as well as improving the heat transfer by increasing the heat transfer area. They stated that the technology is only viable for insoluble PCMs. As seen in Figure 2.14, the encapsulation techniques, usually for micro-encapsulation, involve a physical and a chemical method through which when compared, the physical method increases the size of the capsules and increases the surface roughness thereby reducing essential storage capacity.

Moreover, PCMs operate efficiently within specific temperature ranges and are suitable depending on the applications. The temperature ranges are grouped into three categories to further isolate the most applicable PCM for its use and function. The ranges follow low temperature between 5 °C and 40 °C, medium temperature between 40 °C to 80 °C, and high temperature between 80 °C to 200 °C and above as outlined by (Jouhara et al., 2020). In terms of applications, generally, the low-temperature range is useful for cooling and heating of buildings, the medium-temperature range is useful for solar and electric devices and processes and the high-temperature range is useful for waste heat recovery and cooling. Depending on the energy storage facility or the temperature range for which the application or process requires, the PCMs that operate efficiently within those requirements are

sensible. It should be noted however, as stated in section 2.2.2, no single PCM has yet been discovered that sufficiently satisfies all the working requirements (see Fig. 2.7) and conditions desirable within any functional areas such as buildings as in the case of their review, (Jouhara et al., 2020).

In their study for phase transition temperature, (Nazir et al., 2019), their classifications for low-temperature, medium-temperature, and high-temperature PCM melting points ranged from 220 °C to 220 °C – 420 °C and above 420 °C, respectively. They stated that for Organic PCMs, whose melting temperature range is below 80°C, the low-temperature range applications are suitable as they usually efficiently operate between 100 – 200 °C. They stated that salt hydrates usually have melting points below 220 °C, whereas Inorganic salts have melting points up to but not above 1000 °C. These types of PCMs are normally used in cyclic operations that involve temperatures covering 500 °C and above, including TES applications for high temperatures. Their study indicated that metal alloys and inorganic eutectics are suitable for solar applications due to their extremely high melting temperatures, which are usually about 770 °C. Organic PCMs are usually employed in low melting temperature applications and, the Inorganic PCMs for their high melting temperatures would be ideal for high melting temperature applications.

In their review of high-temperature PCMs, (Liu et al., 2012) salts and metals, and their eutectic forms are viable for solar power plant applications since their melting temperature properties are generally higher than 300 °C but less than 550 °C. Above these temperatures need to be investigated further. They outlined salts and eutectics for their applications as PCMs are viable above 300 °C based on their thermophysical properties. They included the inorganic compound, melting temperature, heat of fusion, density, specific heat, thermal conductivity, and thermal expansion coefficient as well as the same properties for inorganic eutectics. They were chosen based on their availability and economic costs. As such, studies have been conducted creating numerical models of cylindrical enclosures investigating the melting and solidification of high melting point PCMs. Metals and their alloys were also listed and analysed for their properties, since salts and their composites are limited by their corrosivity, thermal conductivity and their volumetric changes, (Wei et al., 2018). Work done by (Zhang et al., 2016) also looked at the inorganic material properties viable for use as PCMs between 300 °C and 800 °C, listing the same properties as seen in work done by (Liu et al., 2012). They looked at these types of PCMs due to their widespread availability and their economic costs, however, as stated previously, these materials are limited by their low conductivity, therefore, appropriate methods must be investigated to improve the efficiency of the charging and discharging of energy. Even in the examples highlighted, it was shown that Sensible heat technologies outperform the LHS PCMs technology due to this disadvantage. Therefore, techniques to improve the thermal conductivity of the PCMs are currently being investigated by researchers.

In this section of the research, the applications of PCMs were closely looked at to give examples of where these PCMs have been used and any possibilities of further use, discovered in research of the literature. According to (Pielichowska et al., 2014), various PCMs with the properties identified in the literature have been used in industrial applications such as buildings, textiles, automotive, medical, industrial, electrical, and solar energy. The electrical and medical industries have been the latest applications in which the technology of LHS PCMs was implemented or studied. The construction sector, however, requires more advanced TES technology that has been studied and more research required in that field.

In terms of building applications, as discussed earlier, TES used in the cooling and heating of buildings (Jouhara et al., 2020), (Pandey et al., 2018), (Sharma et al., 2009), (Sharma et al., 2015), (Faraj et al., 2021), (Gonzalez et al., 2021), (Pandey et al., 2021), and (Nazir et al., 2019) are becoming essential due to the variety of temporal weather and environmental conditions (Pandey et al., 2018). Domestic heating or cooling has often been bombarded by the varied changes in weather related to hot or cold climates and the fluctuating electrical energy required during daylight hours and nighttime, varies depending on the climate region. Applying LHS passive PCM technology reduces the strain caused by these cyclic and fluctuating differences, (Pielichowska et al., 2014). These passive devices are defined such that they do not require an external mechanical device to assist the system with energy to heat or cool. The earliest instalments of this technology including paraffins, dated back to the 1980s for greenhouse buildings in countries such as Japan, the United States, and Germany. If the most suitable PCM material was chosen, the greenhouses were managed efficiently for energy storage and humidity. In comparison, the active storage systems were used for low peak loads, applied mainly at night to reduce the need for energy consumption. PCMs are studied in this case for photovoltaic (PV) devices (Jouhara et al., 2020), (Pandey et al., 2018), (Browne et al., 2016), (Sharma et al., 2009) and floor heating, (Gonzalez et al., 2021), where they have characteristically similar temperatures for the Solid-Liquid PCM with added fins to improve the thermal conductivity and performance (Pielichowska et al., 2014).

PCMs have also been used in the heating and cooling of water, with materials used like encapsulated salt hydrates, PCM-graphite composites and PCM modules studied for their effects. Other applications for PCMs have seemed to be directed towards Latent functional thermal fluids (LFTF), otherwise known as double-phase fluids, which offer larger values of specific heat than their single-phase alternatives. These are often in the form of emulsions of PCM materials suspended in a heat transfer fluid with suggestions that this may increase the thermal performance of the process with potential applications in technologies that they can be adapted for (Pielichowska et al., 2014).

Solar Energy Storage (SES) is one of the major applications for which PCM material would absorb the energy during daylight hours for discharge at nighttime (Rostami et al., 2020). In their review, (Pielichowska et al., 2014), PCMs were shown to improve the performance with their use, providing alternatives to traditional devices. Over half of current Solar power plants use LHS technology in the form of molten salts, however, their use accompanies drawbacks such as high economic cost, high volume, and large facilities, (Jouhara et al., 2020). The use of PCMs also displayed good performance for thermal management in air-based solar heating systems for low-temperature applications in a parametric study presented by (Pandey et al., 2018), (Sharma et al., 2009), and (Sharma et al., 2015) as well as for solar thermal technology in power plants. They described the various uses and applications in solar air heating applications relating to conventional air heaters, finned heaters, corrugated heaters, double exposure, double flow, and two-pass solar air heaters. They also reviewed solar cookers, free cooling and building applications. Their work can be reviewed in detail in their paper, but this study does not present a comprehensive review of various applications but descriptions of where LHS PCMs can be incorporated.

Another application is seen in their work (Pielichowska et al., 2014) and (Nazir et al., 2019) regarding smart textiles technology, in which over 40 years ago, the National Aeronautics and Space Administration (NASA) designed fibrous PCM microcapsules for example nonadecane in space suits, to reduce the effect of temperature fluctuations experienced in space. They described the use of thermal fibres dipped in PCM solutions, coated, or encapsulated; however, these were not suitable for thermal storage as they were very unreliable and could not withstand the cyclic processes. Therefore, the use of micro-capsules has been further developed and deemed much more suitable for use in smart textiles for TES. Their study also described using the smart textile technology biomaterials and biomedical applications for use as bandages or burn wounds. Other types of applications with smart textiles include blankets, layered clothing and sportswear which involves microcapsules PCMs between 1 and 30 μm spherical in diameter, (Sharma et al., 2015).

In their study, (Zhang et al., 2016), they reviewed LHS technology applied to cryogenics. These liquid energy carriers usually have temperatures below -150 °C. High energy density liquid natural gas has sufficient properties that can provide an alternative to fuels. Their internal energy is decreased, and their exergy is increased in storage with daily energy loss to the environment less than 1 %. They are, however, 40 % efficient, although this can be improved using the Rankine cycle as outlined in their review. They also reviewed LHS with steam accumulators. These accumulators use the liquid-gas phase change in a pressurised container with steam and water. The energy is stored in the liquid phase as it is economically viable as opposed to the storage of saturated or superheated steam. More on this can be reviewed in their study of accumulators, (Zhang et al., 2016).

PCMs' use in electronics in the form of heat sinks has also been studied and implemented with improved functional characteristics and power in hand-held devices, such as cellular phones, laptops, tablets, and cameras (Fan et al., 2013) and (Pielichowska et al., 2014). Handheld electrical devices are usually designed for short periods of operation before charging and so implemented PCMs give greater positive potential with chip technology often maximised between 85 °C to 120 °C. Temperatures exceeding these limits run the risk of overheating. Their study (Fan et al. 2013) investigated the effects of adding internal fins to PCM heat sinks, for the effects of melting on the performance using organic PCMs. Their results highlighted that the finned heat sink with higher melting temperatures sustained the device below overheating temperatures for a longer period. The addition of fins to the heat sink reduced the thermal resistance and hence improved the heat transfer regardless of the PCMs used in the experiment. It was suggested that melting temperature and the addition of fins must be considered for PCM selection. Investigations conducted by (Mahmoud et al., 2013) also examined the effects of fins in parallel, cross and honeycomb configurations, with results comparable to that of (Fan et al. 2013) with the results of the honeycomb arrangement at better economic cost compared with machined fins having about the same effect on the thermal performance. The use of fins of varying thickness and height was also studied by (Hosseinizadeh et al., 2011), indicating improved results with larger fin thickness because of reduced thermal resistance and better heat transfer. However, the volume of PCM was reduced for larger fin thickness and impacted upon the LHS capacity of the system, as any increase in the fin thickness had no further effect on the performance. With regards to the fin height, the taller the fins, the better melting performance was seen as a greater region of the PCM interacted with the fins thus, enhancing the effect of natural convection and improving the heat transfer. Their results also showed that the initialisation of melting was slower with a reduced melting time when both the increase in fin thickness and length were assessed. In a study performed by (Ali et al., 2018), different designs of pin-fins from circular to rectangular to triangular with and without a PCM were examined. In their analysis, the triangular design was determined to be the best followed by the rectangular then the circular. It was stated that the surface area ratio for the triangular fins was much less than the others as well as a higher number of fins was present. Improving the number of fins seems to have benefits for heat transfer but must be noted that studies showed that after a threshold fin thickness was reached, there was no improvement further in performance. This was considered for the fin designs in conjunction with PCM use for an analysis performed on the number of fins as well as the similar or equal surface area to volume ratio for the fin and the volume of the PCM used.

PCMs have also been used in the automotive industry, for cooling the internal combustion engine (ICE) and thermal heating in the car. They reviewed in their study, (Pielichowska et al., 2014), applications in which TES PCM was used for pre-heating engines to reduce emissions and time for the

engine to reach operating temperatures during start-up in colder climates. Research conducted by (Zhu et al., 2018) examined the performance of partially filled PCM heat sinks with metal foam (copper) as in TES applications, fin design, metal foams and use of extended surfaces to increase the surface area applied to heat sinks. They stated that the application of metal foam improves the heat transfer as opposed to the other design enhancements. They analysed the filling height ratio, pore size and the effect on performance. The results showed performance improvement when the filling ratio was increased, with little to no impact due to pore size at lower power as compared with higher power, and full filling was not cost-effective as compared with partial filling, seemingly beneficial to efficiency. According to a study performed by (Baby et al., 2014), a finned PCM heat sink was analysed with an unfinned PCM heat sink and a heat sink without any PCM as a standard assessment under different power levels at constant operation, varying heat inputs and loads. The finned heat sink showed improvement over the other cases with the varying power levels or heat not as efficient and less economical. Another study performed in their work (Debich et al., 2020), examined a rectangular PCM heat sink with different numbers of fins and varying the PCM material as well as the input power levels (Baby et al., 2014). The PCMs examined in this research were salt hydrate, paraffin and N-eicosane for their thermal performance on the system. Their results showed that a smaller number of fins used in the PCM sink had improved the thermal storage energy charging phase while an increased number of fins improved the thermal energy discharging phase. It was also noted that in comparison with the other PCM materials for this experiment, the PCM N-eicosane had better thermal performance than the other selected PCMs, especially in the charging phase. In this paper, further studies were highlighted using this PCM for its properties and operating temperature ranges. It should be noted that other experiments using PCM heat sink in combination with other LHS technologies have also been looked at in unique cases such as in their study (Kozak et al., 2013), in which they tried to enhance conduction and convection rates due to a hybrid design using an eicosane PCM based heat sink with a forced draft fan heat sink placed above it. They noted that more research was needed to study the effects of using a variety of sink designs. Another study performed (Kansara et al., 2021) investigated the effects of varying Grashof's number to affect gravitational performance on a selection of PCMs in a control module with pin-fins to identify whether this had any effect on the melting performance of the PCM. Their results showed that during the initial melting phase, conduction was more prevalent than natural convection as well as more dominant during the solidification process. This was verified during a replication analysis for melting in a concentric cylinder as seen in chapter 3 of this paper.

One of the major drawbacks of the utilisation of PCMs is their properties of low thermal conductivity as mentioned previously. Thermal conductivity can be described as the capacity of a body of material or substance be it solid, liquid or gas to conduct heat, (Kumar et al., 2020). As explained in

their review (Liu et al., 2012), the thermal conductivity for most PCMs is around 0.5 W/mK which is low for heat transfer. This corresponds to the discharging of stored energy through solidification of the liquid to solid phase change where the energy is transferred to the exchanger surface. However, the energy transferred is minimal due to the low thermal conductivity and hence low heat transfer, (Mohamed et al., 2017).

All PCMs including the Organic and Inorganic types have low thermal conductivity properties usually between 0.1 to 0.6 W/mK which inherently causes the slow charging and discharging of heat energy, (Pielichowska et al., 2014). A review by (Mohamed et al., 2017) stated even though Inorganic PCMs have higher thermal conductivities than Organic PCMs, they are not able to improve heat transfer by any significant amount. In this case, the heat exchange is limited. However, they stated that there are varying methods to improve the thermal conductivity of the PCM as well in agreement, according to their study, (Pielichowska et al., 2014), a multitude of techniques have been studied and implemented that can improve the thermal conductivity. These techniques highlighted in their study, (Mohamed et al., 2017), exclaimed that the enhancements can be in the form of heat pipes, metal foams, increased porosity materials, and increases to the surface area through extended fins or metallic matrices. They suggested that the fins made of varying metals including aluminium, steel, and copper chosen based on their physical properties can be used to improve the thermal conductivity of the PCM. The fins can be arranged longitudinally or circular governed by the heat transfer fluid passing through the pipe of the shape of the containment whether it be cylindrical or rectangular. The shape of the fins has also been studied in detail with comparisons to thickness, helical shape, length, and number of fins showed improvement in the thermal performance of the PCM. In their study, (Mohamed et al., 2017), improved heat transfer was seen in the thickness of the fin compared to no fin material as well as helically shaped fin compared to dimpled, and cone and the number of fins had insignificant effects on the thermal performance.

In their review, (Zhang et al., 2016) and (Wei et al., 2018), also identified that fins can be used to increase the heat transfer rate which can be designed either axially or radially to tubes which agrees with the work by (Liu et al., 2012), where they stated that adding the finned design is a cheaper alternative than encapsulating the PCM which can be expensive above 200 °C melting temperature. The materials used for the fin material can be highly conductive materials such as metals like aluminium, steel, copper, and graphite to raise the thermal conductivity. Different arrangements and designs of the finned structures have been reviewed in detail by researchers.

They indicated, (Liu et al., 2012), (Liu et al., 2016), (Pielichowska et al., 2014), (Zhang et al, 2016), (Nazir et al., 2019), (Sharma et al., 2015), (Wei et al., 2018), (Rostami et al., 2020), and (Jouhara

et al., 2020) that in addition to this method, the thermal conductivity of the PCM can be improved using finned tubes/finned surfaces with high conductivity material, the implementation of a metal matrix, micro-encapsulation of the PCM and applying porosity. These methods enhance the thermal conductivity of the PCM by increasing the surface area by changing the structure through fins or porosity. According to Newton's law of cooling and Fourier's law of heat conduction as shown in equations 2.5 and 2.6, respectively, the rate of heat transfer can be improved by either increasing the convection heat transfer coefficient by adding forced convection via a pump or fan or through extended surfaces by increasing the surface area directly proportional to heat transfer.

Newton's law of cooling: $Q_{convective} = hA_s(T_s - T_\infty)$ (2.5)

Fourier's law of heat conduction: $Q_{conduction} = -kA\frac{dT}{dx}$ (2.6)

This can also include adding to the PCM, materials that have high thermal conductivities. These materials improve the Sensible heat transfer phase to increase the temperature of the material. Nano-enhanced PCMs with an injection of highly conductive nanomaterials into the PCM discussed in their paper, (Kumar et al., 2020), enhance the thermal conductivity of the PCM without the added weight if metal foams or fins are used. As seen in Figure 2.15, the ideal characteristics of PCMs are highlighted as described in this review showing the preferred qualities required for efficient TES applications.

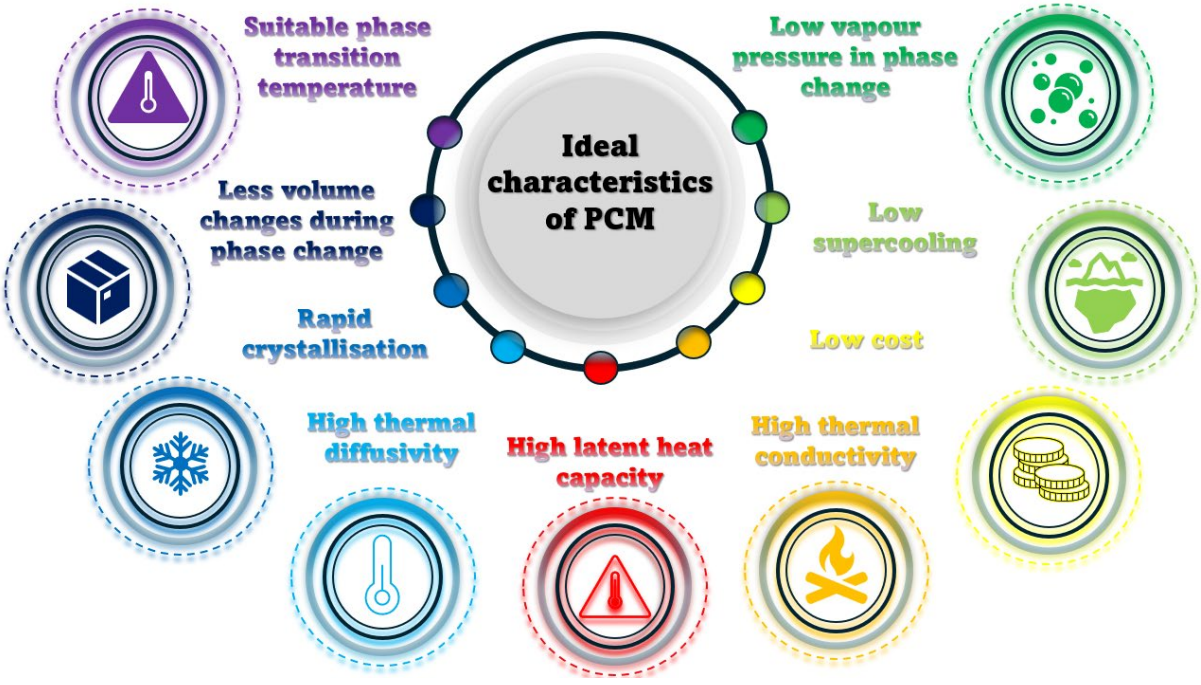

Fig. 2.15 Preferred characteristics of PCM materials useful for LHS TES applications (Adapted from ((Kumar et al., 2020)).

Composite materials with porosity as well as graphite can have substantial improvements in the thermal conductivity of the PCM even up to 70 W/mK as stated in their study (Liu et al., 2012). This can be done by either entrenching with porous graphite, with metal foam showing greater improvement in performance as opposed to expanded graphite, (Mohamed et al., 2017). Distribution of the graphite into the PCM through mechanical means or compression of both materials was assessed in their study (Liu et al., 2012). Results through experimentation showed improvement in the thermal conductivity and hence heat transfer of the PCM. The investigation of open-cell metal foams has also been studied by (Cozzolino et al., 2019) with an experimental prototype design with stacks of metal foams including straight and U-tube designs. Results showed improved thermal performance with modifications in layout designs for future experiments which can have applications viable to the commercial sector as well as residential. The use of fluidised beds concerning particulate solid material was also suggested in their study (Liu et al., 2012). The physical properties of the materials generate the fluidisation effect for which porosity, diameter, and density form key properties that are affected using this method. They were also in agreement that macro, nano, and micro-encapsulation to improve the thermal conductivity of the material as described above. Other methods mentioned include graphite composites, cascades of PCM, and the use of metal matrices can also have positive effects on the thermal conductivity of the material.

Moreover, in terms of nanomaterials addition to the PCM to enhance the thermal conductivity, a review conducted by (Nazir et al., 2019) stated that the nanomaterials come in various shapes and sizes. These can include particles, sheets, fibres, wires, rods and or nano-sized droplets. Two methods have been suggested that can be used to produce the nano-fluids referred to as the one-step or two-step method. The 1st method involves the coinciding production and distribution of the nanoparticles throughout the fluid while in the 2nd method, the nanoparticles are produced separately with an agitative method performed when distributing the nanoparticles throughout the fluid. Results showed that there was a valuable rise in the conductivity of the PCM through the addition of nanomaterials. A study performed by (Choi et al., 2014) and (Liu et al., 2012) also investigated the effects of improving the thermal conductivity of PCM through the addition of nanomaterials and carbon additives which showed a more than 20 % increase in performance with graphite material outperforming graphene in their study. Their article also summarised that there are other ways to improve the thermal conductivity of the PCM other than the use of nanomaterials and encapsulation, such as an increase in the porosity of the PCM. Implanting metal foams with highly conductive metals such as aluminium, nickel, copper, expanded graphite and polyethylene showed considerable improvement in the thermal conductivity of the PCM compared with the general Organic PCM, paraffin, as well as Inorganic PCMs. Their work also agreed that the use of extended surfaces such as fins or the use of PCMs with varying properties depending on

the arrangement, can also have a positive impact on the thermal performance of the PCM and as such the TES system.

As seen in Figure 2.16, the use of multiple PCM arrangements can be integrated into a series layout to improve the efficiency of the TES system if the relevant properties and volume of PCMs coincide with one another, (Liu et al., 2012) (Wei et al., 2018). This approach maintains the heat flux between the transfer mediums. In this case, one PCM would usually have a reduction in heat transfer due to a reduction in temperature difference in the direction of flow. The figure shows that the reduction in the temperature difference is supplemented by the corresponding PCM in the line-up that has a higher melting temperature and so continues in the pattern whilst the fluid flows through the heat exchanger. This effect is also valid for the reverse direction in the discharging phase.

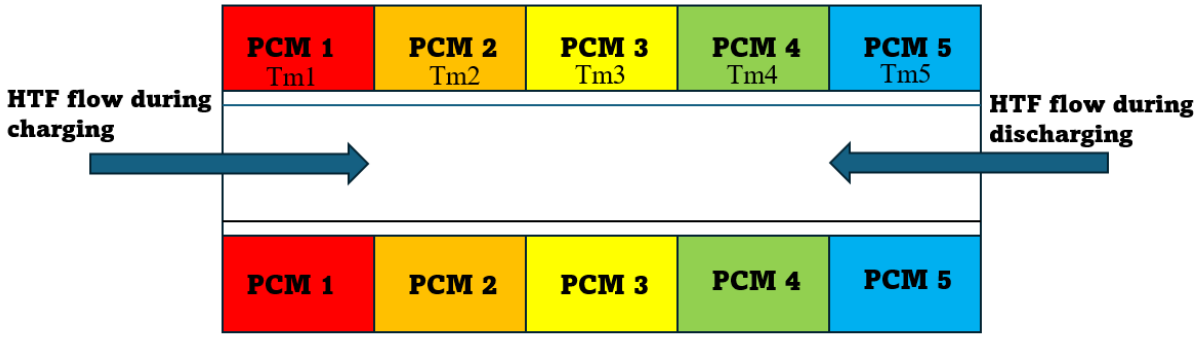

Fig. 2.16 Multiple PCM arrangement in a shell and tube heat exchanger (Adapted from ((Liu et al., 2012)).

Research conducted in their paper (Liang et al., 2020) investigated the effects of changing the geometric parameters of the shell and tube heat exchanger, as well as the effects of the type of fluid flow for the heat transfer fluid on the volume ratio of the PCM. The research was used to identify the most ideal PCM volume ratio. Paraffin wax was used as the PCM in this work with the shell and tube heat exchanger oriented in the vertical position. The inner and outer tube diameters were varied with the effects of changing the PCM volume and thermal conductivity analysis of the output temperature, efficiency, and effectiveness in the presence of laminar and turbulent fluid flow. Their results indicated that energy storage was improved when the size of the shell and tube heat exchanger increased due to the increase in heat transfer area. The increase in effective thermal conductivity had little effect on the energy storage unless the PCM volume ratio was above a critical value. It was also seen that laminar flow outperformed turbulent flow for the heat transfer fluid.

Compared with other materials, it was stated that Aluminium, for its good properties for thermal conductivity and low density and cost was preferred over other metals, as well as the most ideal material to use to improve heat transfer with corrosion resistance. Intermediate heat transfer fluid has also been used with the interaction of the PCM useful for liquid-vapour phase change. Heat pipes with high thermal conductivity have also been implemented as intermediaries between the PCM and the heat transfer fluid. They function as interfaces between the heat transfer fluid and the PCM through vaporisation or condensation designed in various ways, (Mohamed et al., 2017). This technique effectively increases the heat transfer in the TES system. Other methods involve studies of the combination of techniques performed by researchers and scientists to identify whether it is congruent, (Nazir et al., 2019).

A numerical investigation involving a combination of rectangular fins and heat pipes was evaluated by (Diao et al., 2019). Their study assessed rectangular fin thickness and height in a longitudinal arrangement around sections of a heated pipe array with water passing through a TES tank unit. Their analysed results showed a U-type phase change dependent on the configuration of the fins. For their design, the fin height increased, and improved thermal performance whilst fin thickness remained inconsequential due to the PCM used. Another study using a combination of heat transfer techniques was completed by (Ren et al., 2019). Their study involved using a lattice Boltzmann method to understand the charging process of copper nanoparticle-enhanced PCM (N-eicosane) along with a comparison between rectangular fins and triangular fins made of copper in a square container. Results showed for this analysis that substituting a rectangular fin with two triangular fins of constant length improved the charging time. The nanoparticles had a positive effect on heat transfer if the temperature of the heated surface remained below 324K, with any further increase reacting negatively. It was also noted that for their analysis, bottom surface heating rather than side heating proved better TES results with corresponding fin location.

In their study (Parsazadeh et al., 2018), a vertical heat exchanger tube with partially filled horizontal circular fins was numerically investigated with two forms of heat transfer enhancement, namely, using fins and nanomaterials. The PCM was paraffin wax and aluminium oxide was used as the nanomaterials. Varying angles of the fins and location along the inner tube were investigated for effects on the charging process. It was noted from their results that during early conduction at the initial state, the added materials to improve heat transfer had little to no effect only until after ¼ of the PCM melted. The amount of heat transfer taking place at the bottom was improved using the fins whilst the natural convection had improved heat transfer at the top of the heat exchanger. It was also seen that the addition of the nanoparticles had reduced the heat transfer performance, with the fins as natural convection to the top half was inhibited. The vortices produced around the fins were also impacted by

the angle of the fins to the inner tube improving heat transfer. A study involving the improvement of heat transfer in LES systems with a combination of heat pipes, fins and copper foam in a vertical arrangement was done by (Zhang et al., 2020). Their study encompassed four varying cases including heat pipe with PCM alone, heat pipe with fins, hat pipe with copper foam and a combination of heat pipe with horizontal partial fins and copper foam filling the whole container. Their results showed for a constant PCM volume, the increased number of fins had better performance over the reduced fin, copper foam combination. The lowest total time for both processes was seen in the copper foam, fin, and heat pipe combination as well as this setup had the best conduction results. The copper foam and heat pipe combination had the lowest improvement in heat transfer as the copper foam would have reduced the effects of natural convection in the upper half of the container.

Another method involving the use of PCMs to improve the thermal efficiency and overall heat transfer includes the variation in where the PCM is packed into the containment device such as a tube. In their study (Chen et al, 2020), the variation between placing the PCM on the inside of the inner tube or with the annular space in a shell was investigated. The variations have been referred to as the cylinder model and pipe model, respectively. They investigated this with a tube heat exchanger for both melting and solidification of the PCM as well as variation between the triplex tube and elliptical-shaped tubes. They were investigated for horizontal and vertical positions to compare which orientation was best suited. Their results indicated that the horizontal elliptical design and triplex tube design had better performance than the vertical and circular designs.

Varying plate-fin heat exchangers with varying configurations were studied by (Riahi et al., 2018). The vertical shell and tube heat exchanger was designed with a vertical plate fin configuration with heat transfer fluid entering and leaving the system through various flow models. The enthalpy-porosity method with constant heat flux imposed on the bottom surface of the system with insulated sides was used for the evaluation of temperature distribution in both the charging and discharging processes. Their analysis outlined an economical system showing that a low-temperature gradient in the charging phase and a high-temperature gradient in the discharging phase, subsequently has a consistent rate of heat transfer. They suggested from their work that zone separation plays an important aspect in similar designs and should be considered. Another variation in this research was done by (Jia et al., 2019) considered PCM encapsulation through a spherical capsule with varying pin fin designs to investigate the effects on thermal efficiency. 3D models of the capsule filled with a PCM composite capric acid-lauric acid-oleic acid (CA-LA-OA) were filled with varying numbers of partially filled and fully extended pin fins with different lengths and thicknesses. Charging and discharging of the PCM was simulated with the corresponding temperature and liquid fraction produced similar results.

2.3 TES application and management of electrical energy storage devices

Globally, there has been an outreach for the transition towards electric vehicles (EVs) and the reduction of emission levels has propelled nations, including the EU, China, France, Britain, and Norway, to recommend EV adoption via stringent deadlines backed by policies and funding. The governments are incentivising EV sales centred on emissions and prices with strong support for charging infrastructure. The International Energy Agency (IEA) therefore has suggested a substantial EV growth, which has been estimated to be 1.3 million units (Lin et al., 2021) by the year 2030. Emissions that emanate from internal combustion engines (ICE) contribute significantly to certain regions, particularly in the European Union, which account for around one-fifth of the carbon dioxide (CO_2) emissions. These harmful gases have detrimental effects on flora and fauna including the natural environment. Policies introduced by government bodies have adopted energy portfolios with a focus on zero-emission vehicles and potential bans on using ICE in major cities (Mohammad et al., 2022). The global population is threatened by the growing energy crises, and the impact on the environment has been detrimental, yet the demand which energy resources including fossil fuels, for example, oil, continues to rise forced by economic progress. Demands for these reviews have been indicated by the BP Statistical Review of World Energy 2016 and BP Energy Outlook 2016, which has contributed to the underlying need for cleaner alternatives in the use of EVS, hybrid electric vehicles (HEVs) and including plugins (PHEVs), have in their potential to reduce pollutants and greenhouse gas emissions.

Despite the challenges associated with safety, cost, lifespan, and susceptibility to temperature-based degradation, Li-ion batteries are a critical component in driving these vehicles due to their high energy, power, long life, and low discharge rates (Wen et al., 2020). Addressing these concerns, particularly, thermal issues, has brought about the need for effective battery thermal management systems (BTMS) for prolonged life and performance. Narrow temperature ranges between 15 °C to 35 °C (Liu et al., 2017 and Liu et al., 2019) and in different cases 20 °C to 40 °C are deemed pivotal, with severe impact on the capacity and safety. Mitigating risk to prevent damage and hazards and to ensure safe operation of Li-ion necessitates managing temperature both during the discharge and charging phases (Xia et al., 2017). Efficient management of temperature and a balanced temperature within battery packs can improve safety and lifespan. The temperature has a profound impact on the performance of Li-ion batteries, and the development of an efficient BTMS, demands a deep understanding of various aspects of thermal generation, transport, and heat dissipation (Liu et al., 2019) from a single-cell level to module and pack. A compromise on operating temperature and uniformity leading to the extreme, can negatively affect cycle life leading to localised degradation (Gulfam et al., 2019) and thermal non-uniformity.

Depicted in Figure 2.17, presents a comprehensive view of a multi-objective optimisation approach as seen by (Lin et al., 2021 and Liu et al., 2019) for economic-conscious charging. This coupled integration defines an interesting model in which economy, energy and time management have been closely related to charging cost, temperature and charging time, respectively. These Li-ion batteries spearheaded towards zero emission solutions have seen in their development, oxide cathodes and graphite anodes which improves energy density and long life cycle in comparison to other battery technologies. A promising trajectory by research seen by (Jiang et al., 2020) indicates improvement in cost, safety and energy efficiency albeit, barriers which affect performance in energy, power and low-temperature operations. Beyond human comfort level, extreme temperature is exacerbated in multiple battery connections creating inconsistencies and overall degradation.

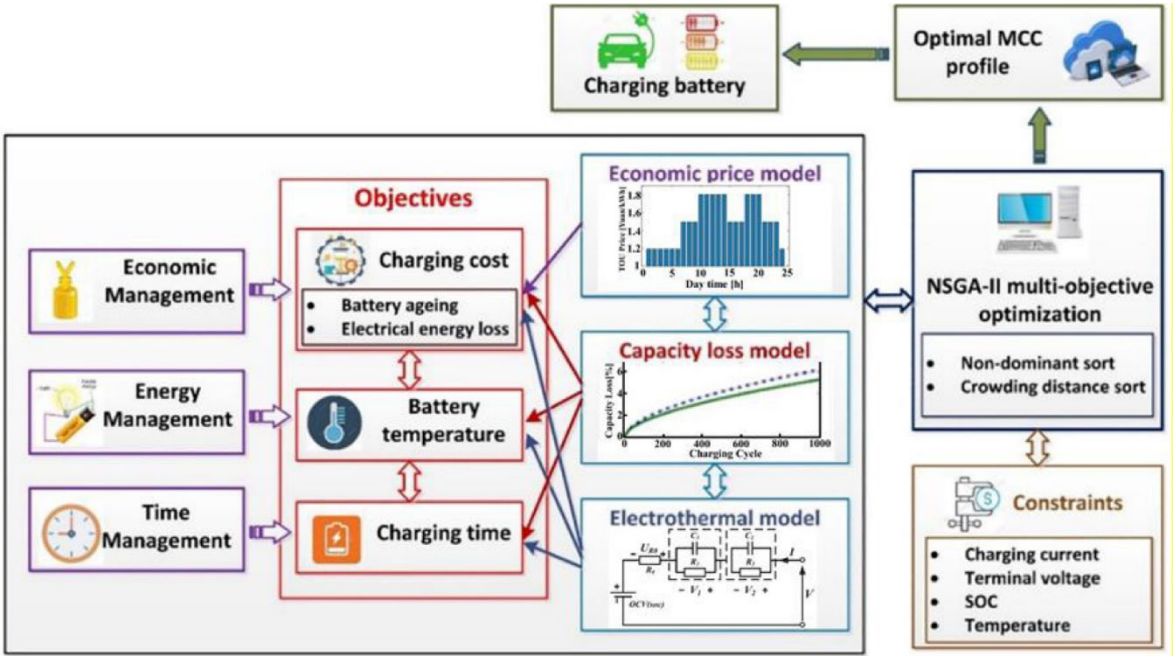

Fig. 2.17 Overall multi-objective optimisation framework for economic-conscious charging (Lin et al., 2021 and Liu et al., 2019).

Within the last four decades, thermal systems utilising phase change materials (PCMs) have undergone a remarkable transition. Reversible processes which involve matter phase change between states such as solid, liquid and gas sensitive to thermal changes, encompass the storage and release of Latent Heat (LH). These PCM materials can be in either organic or inorganic form including paraffin waxes and salt hydrates respectively, and switch between states of matter exhibiting very distinct melting and solidification temperatures (Gulfam et al., 2019). Technological advancements that purposely create PCM material with attributes clinical to thermal management and control have been scientifically explored to produce different types and ranges of PCMs with manipulated properties.

Gaining acknowledgement for low-temperature TES, PCMs can be useful in many areas such as battery and photovoltaic thermal management. Paraffin PCMs (Verma et al., 2019), (Greco et al., 2015), and (Bais et al., 2022) have been showing promise can enhance thermal management, although there are many challenges which focus on the low thermal conductivity. This can limit their use as cooling alternatives, however, passive cooling with linear temperature increase until phase change occurs during which temperature stabilisation and consistency may be beneficial in certain applications. The available LH, conductivity and phase change temperature can be useful in Li-ion battery applications and thermal balance, maintaining the battery's optimum temperature range. Other characteristics also include almost negligible volume change in transition, stability, non-toxic, non-flammable, cost-effective and widely available as mentioned in their work (El Idi et al., 2021), (Du et al., 2018), and (Sharma et al., 2015).

Figure 2.18 (Xia et al., 2017) displays different levels of research to develop a highly efficient and robust BTMS system to understand heat transport and dissipation. Both the single cell and module display the direction of the heat source and sink including boundary conditions from the input and corresponding output. The single cell deals with heat generation in steady or variable conditions while the module level deals with the dissipated heat including cell-to-cell temperature differences and control. These differences are often within a maximum of 5 °C.

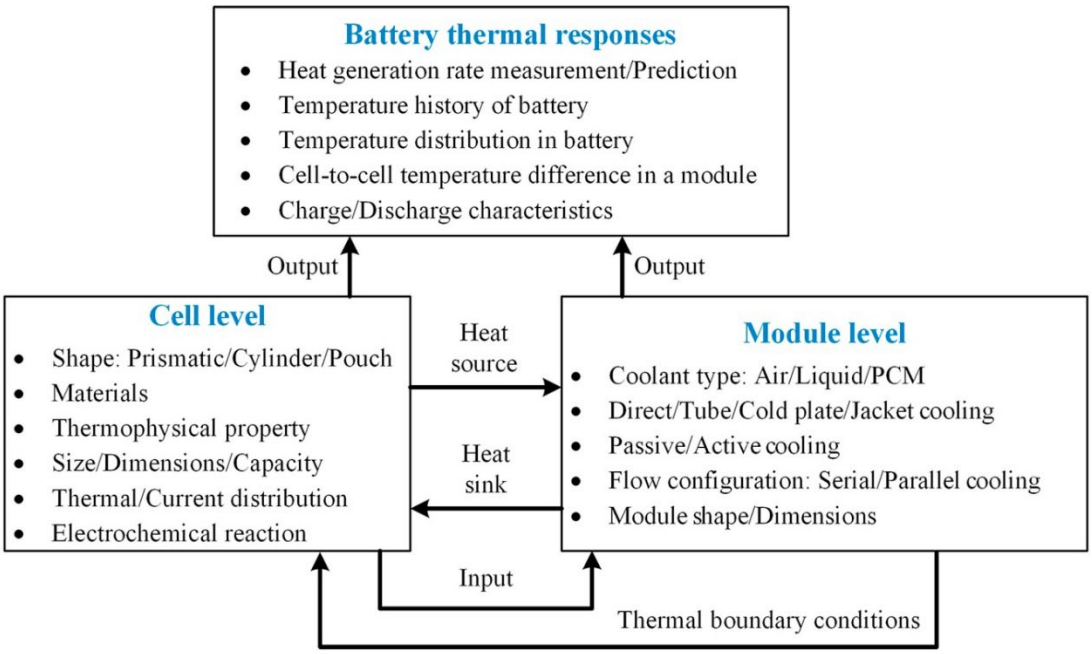

Fig. 2.18 Thermal issues at cell and module levels. (Xia et al., 2017).

Exceeding the 5 °C temperature difference between cells in a module can lead to issues including prolonged exposure that can trigger problems such as diminished capacity in cold climates and thermal

runaway at higher temperatures (Sharma et al., 2015), (Kim et al., 2019), (Zhou et al., 2023). There are numerous BTMS that have emerged to maintain thermally optimum temperatures in Li-ion batteries. Techniques have included air cooling/heating (Ahmad et al., 2023), (Kausthubharam et al., 2021), (Luo et al., 2023), (Mahek et al., 2023), (Verma et al., 2023), (Yang et al., 2023), (Zhang et al., 202024) liquid cooling/heating (Chavan et al., 2023), (Dai et al., 2024), (Fan et al., 2023), (Guo et al., 2023), (Wang et al., 2022), (Xie et al., 2023), (Xu et al., 2023), (Ye et al., 2023) heat pipe (Bernagozzi et al., 2023), (Hu et al., 2022), (Maghrabie et al., 2022), (Septiadi et al., 2022), (Weragoda et al., 2023), (Zhang et al., 2020) and PCMs. The most simple and cost-effective is air cooling but limited to low heat transfer efficiency and high sensitivity to temperature. Liquid cooling has higher heat transfer coefficients, however, additional parts and components are required and more costly whilst heat pipes increase weight and complexity. In contrast, PCMs offer energy-efficient and component-free thermal management (Olabi et al., 2022), (Alami et al., 2022), (Zhang et al., 2021), (Luo et al., 2022). Often composed of multiple cells in different arrangements, Li-ion batteries in series and parallel face many challenges including low-temperature efficiency and thermal runaway. Li-ion batteries have been designed in many ways with larger battery cells more susceptible to localised (Bai et al., 2019) heat accumulation.

The use of PCMs can be used to absorb the heat regardless of the cell size and should be designed such that the LH capsules prevent temperature spikes and an optimal balance for thermal conductivity and LH. Non-uniform temperatures lead to short-circuits and local degradation, thus maintaining the temperature below 40 °C is crucial. PCM volume/thickness including additives and varying composite materials has been examined with cell-to-cell spacing (Jilte et al., 2019) also an effective method for efficient heat dissipation. Flow passages and spacings in multicellular arrangements can improve overall battery performance if cells are thermally affected by other cells. Studies on encapsulation techniques for PCM melting and solidification based on different geometries have been summarised in their studies (Mohaghegh et al., 2021). These materials absorb, store and release LH (Malik et al., 2016) whilst maintaining almost constant system temperature. It also aids in reducing the effects of thermal imbalance between cells with encapsulation with coupled systems gaining momentum. PCM-based thermal storage leverages high thermal storage capacity where near-constant temperature represents the best efficiency with aligned melting temperatures (Fallahi et al., 2017). It is seen that passive cooling using PCMs can provide a compact alternative to active cooling methods with the effect of absorption of heat during phase change, delaying effects and prolonging battery life, low thermal conductivity may cause internal temperature gradients with studies to enhance thermal conductivity using material with high thermal conductivity (Murali et al., 2021), (Maqbool et al., 2023), (Tan et al., 2023), (Wang et al., 2023), (Lee et al., 2023), (Zhang et al., 2023) can enhance

the PCM performance. A study by (Reuben et al., 2020) also highlighted that form-stable PCMs can be negatively impacted by contact resistance and lack of flexibility. Flexible foam PCMs were stated to enhance thermal contact and resistance. Some studies also focus on thermal abuse and potential thermal runaway scenarios to evaluate whether a PCM-based thermal management technique can address the implications which can arise. One such study for a proposed module with a cooling plate system (Kshetrimayum et al., 2019), analysed a battery module even damaged by nail penetration to gain insight into preventing thermal runaway in various conditions.

There are many applications which involve diverse engineering domains in which computational fluid dynamics (CFD) software can be used to efficiently enhance thermal solutions. This numerical method enables benefits such as cost and time saved but also contains optimisation tools and functions for increased efficiency. Modelling techniques to ensure longevity including diverse battery modelling behaviour for the thermal aspects of Li-ion batteries use electrochemical-thermal models in computational tools. These tools can be used in conjunction with experimental data or studies (Al-Abidi et al., 2013) to analyse the heat generation, dissipation and distribution within cells to fully understand temperature control and safety for these storage devices. There are existing models which have limited capabilities but the use of detailed models is computationally intensive. Methods in the estimation of the state of charge (SOC) and state of health (SOH) employ models that solely rely on data processing with different battery models offering co-estimation which can improve the accuracy with a proposed electrochemical model (Panchal et al., 2018) based on the electrical circuit.

This review focuses on BTMS which uses different numerical computational modelling of PCM-based thermal management. Despite progress in thermal characteristics, there is a lack of comprehensive discussion on battery electrical models using computational software based on different battery types and models as well as the effect on PCM-based thermal management with an emphasis on ambient and maximum temperature during different cycling modes. This study aims to address this gap and highlight modelling performance-related challenges in accurate BTMS using LH-based materials and composites. This chapter is further structured into two main sections with the exclusion of the conclusion. Section 2.3 introduces the phase change theory of PCMs including battery modelling using computational software like ANSYS and COMSOL including proposed battery modelling techniques with an overlapping field of PCMs summarised. Section 2.4 elaborates on thermo-physical characteristics of PCM-based thermal management solutions covering the type of battery modelling, arrangement of battery cells, cooling method, discharging or charging rate, continuous cycling or drive cycle modelling and ambient and maximum temperature based on SOC. It also includes an extensive list of research papers covered during the review with an attempt to review ideal modelling development and characterisation techniques for improved thermal management systems. The chapter concludes with

a critical discussion addressing thermal system design including composites with possible recommendations. This section reviews the existing work for thermal cycle options for next-generation batteries and multi-physical cooling BTMS performance and temperature management for EV battery-powered systems. It goes into detail on thermo-chemical and electrical modelling of batteries including simulation techniques during phase transition and the feasibility of the PCM based thermal management. Heat transfer concepts and their applications are explained including an in-depth analysis of the advantages and disadvantages of the different modelling host systems and optimisation measures for any technical challenges that may arise, providing real solutions for the future of BTMS research.

2.3.1 Thermal and electrochemical battery modelling

Li-ion batteries use electrochemical redox processes as their primary mode of operation and work as rechargeable EES. Exothermic processes and ohmic losses (Shahjalal et al., 2021) which happen in the charge transport release heat. In this event, the cell temperature increases consequentially affecting neighbouring cells impacted in a battery module or pack. The change in temperature results in an entropy change that then affects the thermal performance of the battery and can be intensified with different C-rates. Distinct profiles are shown visually in Figure 2.19 (A) (Jeon et al., 2014), (B) (Goutam et al., 2017), and (C) (Li et al., 2021), with an illustration of the temperature distribution across cylindrical cells, pouch cells and prismatic cells. For intricate battery configurations which are characterised by interconnected modules that form packs, cells within are predisposed to significant heat generation, thus thermal management and uniform temperature distribution become pivotal for cell life. Left unaddressed, non-uniform temperature increases can potentially escalate to more serious problems such as thermal runaway. This phenomenon's quantitative description is encapsulated in the heat generation equation, elaborated in various studies (Qian et al., 2019), (E et al., 2021), (Yoo et al., 2019), (Huang et al., 2022), (Ping et al., 2021), (Williford et al., 2009) which acts as a foundational equation that characterises this behaviour. Heat transfers due to conduction and convection (Qian et al., 2019) during BTMS design and simulation are shown in eqn. (2.12) and (2.13).

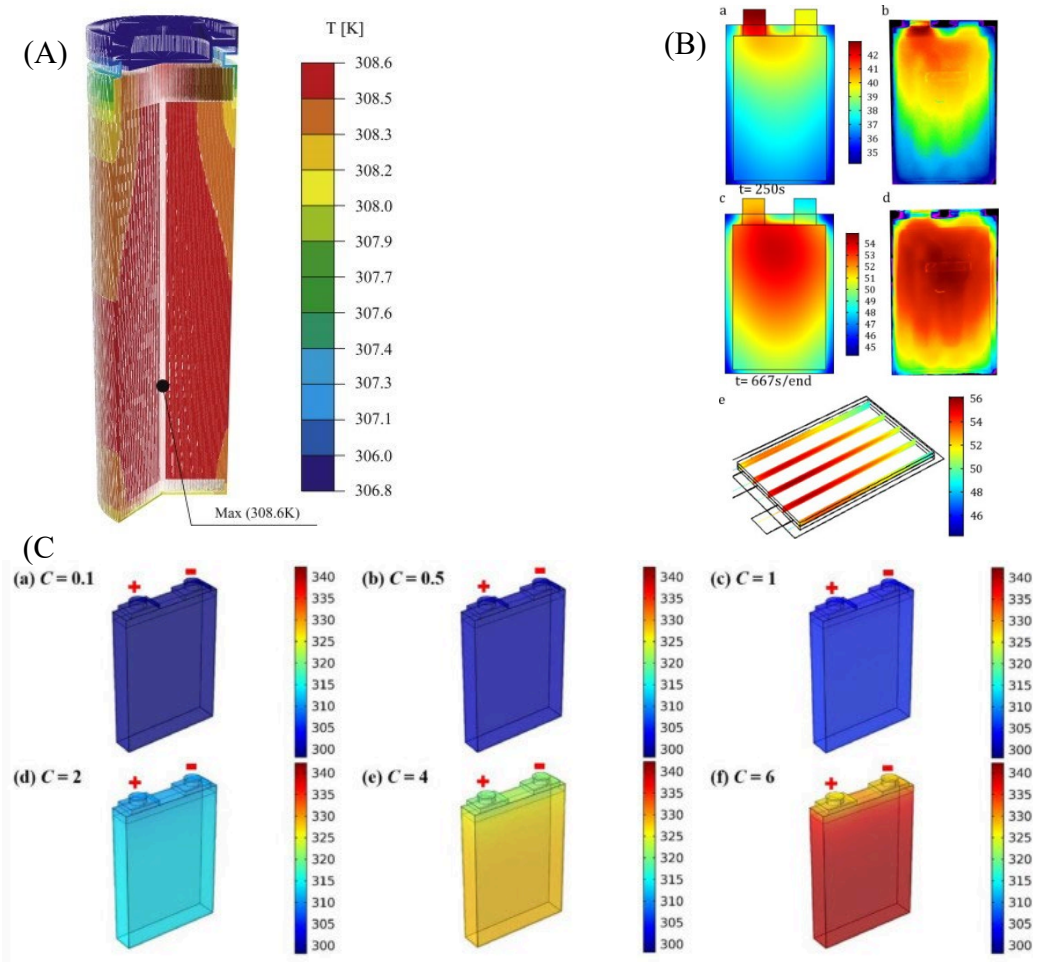

Fig. 2.19 Battery cell surface and profile temperature, A) cylindrical cell (Shahjalal et al., 2021), B) pouch cell (Jeon et al., 2014) and C) prismatic cell (Goutam et al., 2017).

The following expression by Bernardi represents the heat generation model:

$$q = \frac{I}{V}[E_{ocv} - E_v + T\frac{dE_e}{dT}] \tag{2.7}$$

Where the battery current is, I; open circuit voltage, E_{ocv}; cell voltage, E_v; battery temperature, T; a low-value temperature coefficient, $\frac{dE_e}{dT}$. Low coefficient term is overlooked with the difference $[E_{ocv} - E_v]$ acting as the total battery resistance, giving the joule heat energy:

$$E_{ocv} - E_v = IR_i \tag{2.8}$$

Enthalpy change equation:

$$q = mc_p \frac{dT}{dt} \tag{2.9}$$

Where the mass of the battery is, m; specific heat capacity, c_p.

The new equation, substituting (2.7, 2.8 and 2.9) therefore:

$$\frac{1}{I}\frac{dT}{dt} = \frac{R_i}{mc_p} + \frac{T}{mc_p}\frac{dE_e}{dT} \tag{2.10}$$

$$q = I^2 R_i + IT\frac{dE_e}{dT} \tag{2.11}$$

Heat transfer in the battery cell due to conduction according to Fourier's law:

$$q = -k\frac{dT}{dx} \tag{2.12}$$

While convection heat transfer between cell surface and ambient conditions:

$$q = hA(T_{cell} - T_{air}) \tag{2.13}$$

Gaining insights into the dynamics of heat generation and dissipation within the Li-ion cell is paramount due to its profound influence on the overall performance of the Li-ion battery since its temperature plays a crucial role. The phenomenon of heat generation within the battery is intricate, inherently tied to electrochemical reaction rates, and undergoes variations over time with changing temperature conditions. This intricate interplay is illustrated in Figure 2.20 (A) (Panchal et al., 2017), where the active materials embedded within both the positive and negative electrodes are fundamental components influencing the Li-ion content of the cell.

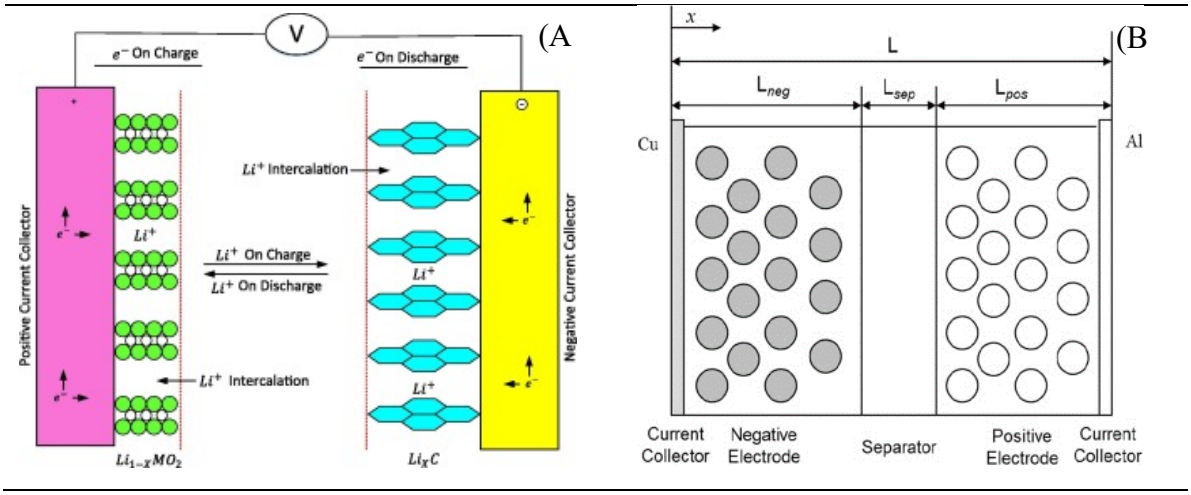

Fig. 2.20 Li-ion cell schematic, A) charge/discharge cycling process (Panchal et al., 2017) and B) physical model (Peng et al., 2016).

A standard Li-ion cell has fundamental components including a positive electrode, a negative electrode, an electrolyte, and a selectively permeable membrane through which Li-ions traverse and a protective shell. Distinct layers come together; a copper current collector, a negative electrode, a separator, a positive electrode, and an aluminium current collector seen in Figure 2.20 (B) (Panchal et al., 2017), and (Zhang et al., 2022). The negative electrode employs the carbon material, while the positive electrode incorporates lithium-containing compounds such as LiFePO4, LiMn2O4 and Li (NiCoMn)O2. The core operation of the Li-ion batteries involves the movement of Li-ions between the two polar terminals.

The behaviour of the active materials in these electrodes is noteworthy; they facilitate the extraction or insertion of lithium ions from or into the particles without inducing significant structural alterations. During the charging phase, Li-ions are extracted from the active material in the positive electrode, subsequently being inserted into the negative electrode (Panchal et al., 2017), and (Zhang et al., 2022). Conversely, during the discharge cycle, lithium ions traverse the electrolyte to reach the positive electrode. These electrochemical reactions transpiring within both the positive and negative electrodes contribute to the overall reactions which govern the battery's performance. The specific electrochemical reactions pertinent to each electrode, as well as the overarching comprehensive reaction, are succinctly captured from the following equations as seen in (Panchal et al., 2017).

For the positive electrode:

$$LiMO_2 \overset{charge/discharge}{\Longleftrightarrow} Li_{1-x}MO_2 + xLi^+ + xe^- \quad (2.14)$$

For the negative electrode:

$$C + xLi^+ + xe^- + LiMO_2 \overset{charge/discharge}{\Longleftrightarrow} Li_xC \quad (2.15)$$

Total reaction:

$$LiMO_2 + C \overset{charge/discharge}{\Longleftrightarrow} Li_xC + Li_{1-x}MO_2 \quad (2.16)$$

In the context of studying battery thermal behaviour, mathematical models based on different dimensions (Gulfam et al., 2019), and (Sharma et al., 2015) including zero-dimensional (lumped parameter modelling), one-dimensional (1D) (Martínez-Rosas et al., 2011), two-dimensional (2D) (Samba et al., 2014), and three-dimensional (3D) (Guo et al., 2013) models, are commonly used. These lower-dimensional models offer simplifications of the comprehensive 3D model tailored to specific battery scenarios. For instance, a 2D model can be viewed as a 3D model with homogeneity along one dimension, allowing that one dimension to be omitted. This simplification strategy is exemplified by the 2D current distribution developed in their research (Mastali et al., 2015). Additionally, various cell-level thermal models, classified by their physical mechanisms and dimensions, have been explored. The models identified (1D, 2D and 3D) include electro-thermal, electrochemical thermal, and thermal runaway propagation models (Sharma et al., 2015) which analyse the heat generated from Li-ion batteries and thermal dissipation which profoundly affect performance. The heat generated is because of the irreversible activation, joule heating and reversible reactions from entropy change. The connection between battery performance and temperature is significant. Reduction in performance can negatively affect its capacity and power which are impacted when active materials are converted into inactive and where there is an increase in impedance, respectively. The intricacies of these processes underline the role of operation temperature in Li-ion battery performance. This understanding has led to the development of comprehensive thermal models, which aid in predicting internal temperature distribution and improving battery performance while minimising experimental costs.

Analysing the thermal behaviour of Li-ion batteries, which profoundly impacts their performance and safety, is pivotal at all levels of arrangements including single cell up to pack level. While alternative methods are available, experiments and numerical thermal simulations have emerged as the predominant methods. However, the experimental route presents limitations which may include tailoring conditions to individual experiments, making it arduous and time-consuming to explore battery behaviours across diverse ambient environments of discharge rates. There are also disparities between the core temperature and surface temperature measurements which might inadequately represent the maximum battery temperature. Internal temperature measurements using thermocouple temperature sensors may prove to be too impossible to achieve given the compact battery casing. Contrastingly, numerical simulations (Wen et al., 2020) offer versatility by adapting to different conditions through parameter adjustments. Furthermore, these simulations enable the depiction of thermal behaviours across various sections of the battery despite the minor deviations from experimental conditions, the numerical approach is favoured. This method also employs thermal enhancement for configurations and BTMS systems. In subsequent sections, numerical simulations are examined, highlighting their versatility in controlling different boundary conditions and parameters. Additionally, in-depth exploration is conducted on the use of equivalent circuit models (ECM) and electrochemical models, specifically the Newman, Tiedemann, Gu, and Kin (NTGK) models, as well as the Newman P2D model.

2.3.2 Equivalent circuit model (ECM)

Researchers have been exploring the design of optimal charging protocols using models based on the equivalent circuit model (ECM). These models are integrated into optimisation problems with single or multiple objectives and constraints. The optimisation problems involve employing first-order (Parvani et al., 2015), (Zheng et al., 2015), and (Nemes et al., 2019) or higher-order (Khamar et al., 2014) ECMs (Jiang et al., 2014), (Xiaopeng et al., 2014), (Tomaszewska et al., 2019) to characterise the cell behaviour. Diverse cost functions are formulated to achieve maximum charging efficiency and minimise charging loss during fast charging. Loss in charging is determined by factors such as internal resistance, current rate, and charging time. Optimisation on ECM models was reviewed by (Xiaopeng et al., 2014) to reduce temperature and battery degradation. Their study also highlighted that while ECMs capture external battery characteristics, one drawback is that they lack insights into internal state information, particularly side reactions from charging and lithium deposition. Therefore, electrochemical models have increasingly become preferential in their capability to address this drawback. Nonetheless, ECM models have proven sufficient to evaluate battery cycling performance. ECM simplify complex electrochemical battery behaviour using basic electrical components. Unlike

detailed electrochemical models, ECMs require fewer parameters (Yang et al., 2023), making them efficient and widely used. Commonly, Thévenin-based and impedance-based models categorise these approaches. Impedance models employ a constant phase element, while the Thévenin models use voltage sources, resistors, and RC pairs (Feng et al., 2015). These models have been studied to be twice the computational speed compared to impedance models. The simple internal resistance model, a Thévenin variant, uses a voltage source and resistor to represent battery internal resistance (Guo et al., 2022). While it is easily integrated into BTMS systems, it may lack simulation accuracy.

A 1D basic equivalent circuit model (Zheng et al., 2015) is depicted in Figure 2.21 (A) represents the internal resistance of a battery. It consists of an ideal voltage source connected to a resistor symbolising the battery's internal equivalent resistance. This uncomplicated model is easily incorporated into various BTMS due to its simplicity. However, its simulation accuracy often falls short. A more comprehensive model shown in Figure 2.21 (B) is the second-order ECM (Khamar et al., 2014) which encompasses components such as resistances and capacitance, open circuit voltage (OCV) with battery terminal voltage. This model presents increased accuracy, clarity, and comprehensiveness. The model employs a capacity and a current-controlled current source on the left, derived from runtime-based models, to represent battery capacity, state of charge (SOC), and runtime. Furthermore, the model incorporates an RC network, akin to Thévenin models to simulate transient responses. To establish a link between SOC and OCV, a voltage-controlled source is integrated. This proposed model amalgamates components and dependencies from previous models, resulting in a simplified extraction process and facilitating compatibility with Cadence. Notably, it seamlessly predicts runtime, steady state, and transient response, capturing the dynamic electrical characteristics of batteries including useable capacity, OCV and transient response. In their review (Guo et al., 2014), the estimation of state-of-power (SOP) can still be accurately modelled using the simple 1st-order RC ECM model as seen in Figure 2.21 (A) due to its ease of implementation and simplicity. Nevertheless, this model has significant limitations when compared to real-world scenarios. They stated that the structure cannot precisely replicate specific reactions and non-linear behaviours of Li-ion batteries which can include hysteresis effects and diffusion. Moreover, the SOC greatly affects the parameters, current and temperature. Failure to account for these discrepancies undermines the model's accuracy for different battery states and operating conditions. Therefore, various models (Guo et al., 2022), (Shen et al., 2019) of SOC estimation refine the structure and incorporate parameter variability.

As reviewed in their study (Shen et al., 2019), the ECM employs circuit elements such as constant voltage sources (representing OCV), resistances (indicating electron and ion movement difficulty), and RC networks (depicting battery polarisation) to emulate battery I-V traits and transient actions. This model finds a balanced compromise between understanding external dynamic behaviour

and gaining insights into internal or microscopic behaviour. Equivalent circuits (ECs) can be broadly classified into two types: those in the time domain and those in the frequency domain. They emphasised that the time-domain ECMs construct components to replicate external attributes like voltage and current. These models are extensively employed in EV management systems due to their simplicity and parameter identification. The Thévenin model allows for enhanced polarisation between the electrodes and electrolyte and encompasses a more precise transient response. Various sophisticated ECMs have been developed to comprehensively capture intricate battery electrochemical processes, enabling accurate battery state estimation. Other models (Wu et al., 2014), (Mousavi et al., 2014) which were discussed in their review included alongside the ones discussed, the Impedance-based model, the Runtime-based model, the combined electrical circuit-based model, and the generic-based model. Modelling and simulation are prominent tools for exploring and refining battery cell and BTMS designs. These methods offer insights into various battery behaviours, encompassing electrical, electrochemical, and thermal aspects, to predict performance under controlled conditions. Two primary modelling categories are employed: electrochemical models, which provide comprehensive data on cell electrochemical actions using sets of partial differential equations, and electrical equivalent circuit models that simplify complex electrochemistry by representing it as electronic components like capacitors and resistors. The electrical equivalent circuit model, such as the internal resistance model with a resistance and ideal voltage source, simplifies the electrochemistry. More complex variations enhance the accuracy. While electrochemical models are precise, they demand substantial computing resources, making them less suitable for power and dynamic system studies. Simplified models, like order-reducing models, aim for faster simulations.

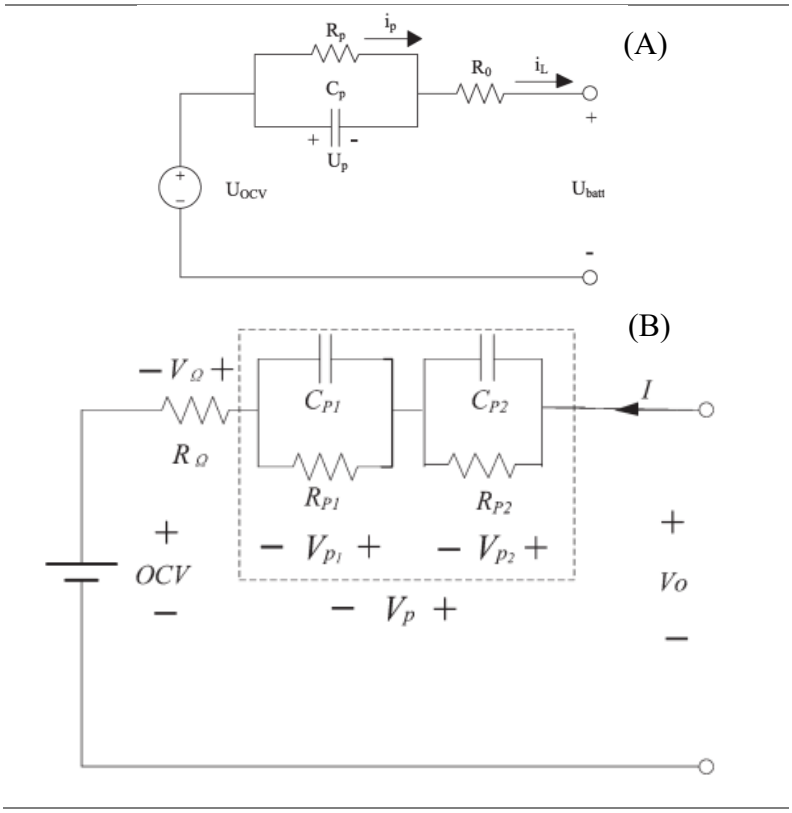

Fig. 2.21 Li-ion cell schematic of, A) first-order RC equivalent circuit model (Parvani et al., 2015) and B) second-order equivalent circuit model (Khamar et al., 2014).

For the first-order RC equivalent circuit model (Guo et al., 2013):

$$U_v = U_{OCV} - R_p I - U_p \tag{2.17}$$

$$equal U_{p,j+1} = \exp(-\frac{\Delta t}{R_p C_p} U_p + R_p[1 - \exp(-\frac{\Delta t}{R_p C_p})]\, I_j \tag{2.18}$$

For the second-order RC equivalent circuit model, the multi-scale multi-domain (MSMD) approach for the thermal and electrical analysis (Tomaszewska et al., 2019), (Chen et al., 2006):

$$\frac{\partial \rho C_p T}{\partial t} - \nabla.(k\nabla T) = \sigma_+ |\nabla \emptyset_+|^2 + \sigma_- |\nabla \emptyset_-|^2 + \dot{q}_{ECh} + \dot{q}_{short} + \dot{q}_{abuse} \tag{2.19}$$

For the second-order RC equivalent circuit model, the electric circuit represents:

$$V = V_{OC}(SOC) - V_1 - V_2 - R_s(SOC) I(t)$$

$$\frac{dV_1}{dt} = -\frac{1}{R_1(SOC)C_1(SOC)}V_1 - \frac{1}{C_1(SOC)}\ I(t)$$
$$\frac{dV_2}{dt} = -\frac{1}{R_2(SOC)C_2(SOC)}V_2 - \frac{1}{C_2(SOC)}\ I(t)$$
$$\frac{d(SOC)}{dt} = I(t)/3600Q_{ref} \quad (2.20)$$

Heat is a pivotal factor that directly impacts the thermodynamic attributes of batteries. Influencing variables like the rate of temperature alterations. Conversely, battery temperature also yields an effect on parameters such as resistances, influencing voltage. This relationship is noteworthy, as higher temperature may lead to reduced internal resistance as well as reduced battery voltage when the current is high. To effectively represent this and accurately numerically simulate battery characteristics and the dynamic changes, a coupled electrochemical and thermal model (Özdemir et al., 2021), (Tran et al., 2020) has been reviewed. In this coupling mode, both the electrochemical model which represents electrical properties as well as the thermal model based on the heat equations are concurrently integrated. A set of partial differential equations (PDEs) offers precise insights into battery voltage and temperature responses. This thermo-electric coupling can be generated using 1D, 2D and 3D electrochemical and thermal models for different batteries of different chemistry. It is noted that this model employs the ECM model in which the electrical characteristics are supplemented with a thermal model to represent simple real-world battery applications under various dynamics. Comparison of the performance of different ECM models (Tran et al., 2020) for various common Li-ion battery chemistries including lithium iron phosphate (LFP), lithium nickel manganese cobalt oxide (NMC), lithium manganese oxide (LMO) and lithium nickel cobalt aluminium oxide (NCA). The first, second and first-order hysteresis models were analysed under dynamic and non-dynamic current profiles. Results indicated that all three ECM models can accurately predict battery voltage, with better performance observed in dynamic current profiles. They also stated that the choice of ECM should be modified to the specific Li-ion battery chemistry, highlighting that the significance is fundamental in selecting the appropriate models with real-world battery chemistry and BTMS applications.

In electronics applications, high-energy density rechargeable Li-ion batteries are advantageous, but the inherent heat generation becomes problematic, escalating with discharge rates. Managing this thermal issue is crucial within Li-ion BTMS. In their study (Kirad et al., 2021) cooling of a battery module comprising 30 Li-ion batteries using forced air. The numerical models centred around both single cell and module arrangement with the influence of longitudinal and transverse spacing variations between cells for the impact of velocity and discharge rate studied. Results indicate that transverse spacing significantly affects cooling efficiency and temperature uniformity. High temperatures and cell-

cell temperature differences significantly impact the ageing and thermal runaway of Li-ion batteries. Research conducted by (Liang et al., 2021) investigated the BTMS method using ECM on a 168-cell pack under a 5C discharging rate. Electrical and thermal behaviours were simulated through an electrical model (Simulink) and heat transfer model, (ANSYS fluent). Results show that high tolerance levels and ageing contribute to elevated local cell temperature and substantial temperature discrepancies in battery packs. The flat-heat-pipe-based BTM maintained the temperature below 50 °C and within a 5 °C temperature difference. The increasing demand for battery storage systems in applications such as EVs and the importance of internal heat production for maintenance of battery temperature between 15 °C – 45 °C is essential. Active and passive cooling techniques like liquid and air cooling as well as passive in PCMs and heat pipes are actively being explored. A study by (Padalkar et al., 2023) used the ECM battery modelling technique, which is versatile regardless of active or passive cooling for ANSYS using previous data. Grouping of cells to introduce turbulence in forced-air cooling, resulting in a 21.2 % reduction in temperature rise and a 12.7 % decrease in power as noted. A study by (Yang et al., 2023) analysed the thermal performance of air-cooled BTMS for a honey-comb cylindrical battery pack with 24 Li-ion cells. CFD using ECM modelling evaluated the cooling efficiency and velocity distribution with findings showing a reduction in maximum temperature and temperature difference compared to a standard module. The thermal impact on the performance, lifespan, and safety of Li-ion batteries necessitates effecting cooling solutions. A tree-shaped channel heat sink was designed by (Ran et al., 2023) for Li-ion battery cooling compared with existing fractal and serpentine channels. Employing an electrical thermal and fluidic physics simulation based on the ECM model, the temperature distribution's effect on battery pack consistency was explored. Different arrangements of series and parallel configurations were assessed for initial temperature during discharging and charging. The results indicated that the new design had superior heat dissipation and more parallel cells in the module had a negative impact on the battery consistency and increased the average temperature rise and the temperature difference between cells.

A combination with PCM is a promising innovation including those with PCM nanocapsules. According to their study (Qaderi et al., 2022), an 18650 Li-ion battery pack with water nano-encapsulated PCM BTMS was analysed using the ECM battery model. Results revealed benefits up to 34 % and 51 % for average and maximum cell temperature compared to just water-based systems. Over 78 % improvement in temperature uniformity was also observed. In a study for combining a hybrid BTMS with PCM and liquid cooling (Wang et al., 2022), numerical modelling using a 3D thermal ECM model for battery behaviour, power consumption, weight and efficiency were analysed with a system with PCM only. Results indicated that at high C-rates, the PCM cooling may not be sufficient for large-

format Li-ion batteries. Temperature uniformity and maximum temperature difference were kept at a minimum with the integration of the ECM model for thermal analysis with economic considerations.

2.3.3 Newman, Tiedemann, Gu, and Kim (NTGK) model

Li-ion batteries are the favoured choice among secondary batteries, surpassing lead-acid, and nickel-metal hydride (NiMH) batteries due to their superior energy density, extended life cycles, and reduced self-discharge rates. They have been embraced in hybrid, plug-in hybrid, and electric vehicles, playing a significant role in reducing emissions and resolving energy storage limitations (Wu et al., 2019), (Zhang et al., 2017). Yet, while Li-ion batteries offer higher energy and power density, they also exhibit increased heat generation, making them highly susceptible to temperature variations during operation. The heat generation within these batteries, driven by chemical reactions, reveals reversible heat predominance at low discharge rates and irreversible heat dominance at higher rates (Du et al., 2017). As demands for increased power rise, ensuring the thermal safety of Li-ion batteries is paramount. Research focusing on the thermal behaviour of Li-ion batteries is crucial to maintaining safe operating temperatures as defined by (Liu et al., 2019), (Adeniran et al., 2023), (and KÖK et al., 2020), ensuring temperature variation among cells stays within a 5 °C range (KÖK et al., 2020). This approach guarantees optimal battery performance while avoiding overheating risks. The integration of simulation software and experimental validation methods has become an essential practice within the battery industry.

A diverse range of software tools is available each offering distinct models. This study emphasises three primary models: ECM, NTGK, and P2D. While the Single Potential Empirical Battery model demonstrates advantages in fully resolved model geometry, its limitations become evident when simulation battery systems and their associated electrochemical events. Conducting a single-cell simulation using this model could become computationally burdensome (Adeniran et al., 2023). The multi-scale, multi-dimensional (MSMD) approach, however, addresses this limitation by viewing the entire battery as an orthotropic continuum. The second key model, NTGK, is widely used by others (Liu et al., 2019), (Adeniran et al., 2023), (KÖK et al., 2020), (Hussain et al., 2023). Is a simple semi-empirical electrochemical model proposed in (KÖK et al., 2020). This model relies on experimentally derived parameters to establish a relationship between volumetric current density and voltage (Hussain et al., 2023). Primarily suited for battery pack simulation with constant discharge rates (C-rates), the NTGK model requires fewer parameters and is easier to compute, offering an advantage in cases of limited cell technical data availability. Nevertheless, certain discharge performance data is essential for determining specific parameters (Adeniran et al., 2023).

In the pouch cell modelling phase, for example, the internal structure comprises distinct layers such as positive and negative electrodes, porous separators, current collectors, and electrolytes, each individually modelled with similar shapes and structures. The exterior of the cell is enveloped in an aluminium/plastic composite, with the porous separator situated between the positive and negative electrodes. Despite the structure being 3D, the electric current flow between the electrode pairs is observed as a 2D structure. Simulating the repetitive electric field flow demands significant modelling time and computational resources. Thus, to streamline the process, the cell is simplified by modelling a single pair of positive and negative electrodes (Adeniran et al., 2023). For further details regarding the battery's internal structures, (Kwon et al., 2006) can be referred to. In adopting the NTGK model for simplicity, several assumptions are made: the short distance between the electrodes results in a perpendicular current flow; the electrode is considered an equivalent network of electrode material and current collector resistors linked in parallel; the temperature differences across the cells stacks are overlooked due to their thinner dimensions in comparison to the electrodes; and the cell is treated as a single domain, with the physical parameters being an average of the subdomains (Hussain et al., 2023).

The NTGK model serves as an efficient approach (Zhang et al., 2020) to predict rapid heat generation within Li-ion batteries, aiding in evaluating electrochemical heat and temperature variation between battery cells. Researchers have leveraged the NTGK model to explore cooling techniques and temperature uniformity in simple hacks (Ho et al., 2020). The model uses equations to solve battery temperatures based on cell voltage and current (Molaeimanesh et al., 2020). Nevertheless, it presents certain limitations, such as lacking the Arrhenius equations (Zhang et al., 2020), which hinders temperature distribution feedback, resulting in a single I-V curve under specific discharge conditions. Despite these limitations, the model's simplification, ease of parameter adjustment, and efficient computational time outweigh its drawbacks.

To reduce computational time, Reduced order models (ROMs) are used with additional assumptions. However, caution is needed when employing ROM methods due to potential information loss (Cheng et al., 2014). Yet, this loss does not significantly impact results in particular applications like soc estimation and voltage prediction. Passive and active cooling systems have been used to cool Li-ion batteries historically utilising air or liquid systems. Both systems contribute significantly to BTMS, reducing thermal runaway possibilities (Kim et al., 2019), (Narasimha et al., 2022). Nevertheless, traditional cooling methods as noted by (Kim et al., 2019) and (Narasimha et al., 2022), are complex in design installation and have limited effective temperature ranges. PCMs, however, address these challenges. As Li-ion battery temperature surpasses the PCM's melting point, the phase transition process manages the temperatures. However precise NTGK settings are necessary to model the moment of melting accurately. The activation of the Solidification/Melting models as described by

(Cheng et al., 2014) and understanding the enthalpy formulation are essential concepts in solving phase change problems.

2.3.4 Newman P2D model

This section explores a comparison between a rigorous pseudo-two-dimensional model and two simplified models for simulating the cycling performance of Li-ion cells. It assesses the advantages and limitations of each approach. According to research (Santhanagopalan et al., 2006), findings reveal that a simple ordinary differential equation (ODE) model is highly accurate in predicting potential over time for discharge rates up to 1C. However, for rates beyond 1C, it is advisable to incorporate certain simplifications into the rigorous model to improve computational efficiency. Each modelling approach has its strengths and weaknesses. The porous electrode model offers detailed insights into battery processes but is computationally intensive. The single particle model, while significantly faster, simplifies some physical processes, potentially compromising accuracy. Incorporating polynomial approximations into the porous electrode models strikes a balance between complexity and computational efficiency.

In the context of simulating Li-ion cell performance across multiple cycles, it is crucial to choose models that provide a trade-off between accuracy and computation time. By using a parabolic approximation for solid-phase concentration, these approximate models significantly reduce computational time while maintaining accuracy, making them suitable for cyclic simulations. As seen in their research (Santhanagopalan et al., 2006), (Xu et al., 2015), Figure 2.22 (A) illustrates the pseudo-two-dimensional (P2D), (B) shows the single particle (SP) model and (C) the 3D computational domain and a 1D pouch cell during discharge. The P2D model envisions the solid phase as spherical particles with radial diffusion as the primary transport mode with concentration and potentials varying solely along the x coordinate. A constant open circuit potential is assumed for a side reaction, leading to capacity fade. The SP model involves the representation of each electrode with a single spherical particle which disregards the limitations posed by the solution phase and maintains assumptions regarding the side reaction. A third approach with combines the parabolic approximation with the P2D model retains the complexity of the porous electrode theory but is mathematically simpler. The approaches offer various trade-offs between complexity and computational efficiency in modelling Li-ion battery performance. Equations (2.21) and (2.22) outline the summarisation of the P2D model.

Positive electrode

$$Li_{1-y}MO + yLi^{+} + ye^{-} \overset{\frac{charge}{discharge}}{\Longleftrightarrow} LiMO \tag{2.21}$$

Negative electrode

$$LiC_6 \overset{\frac{charge}{discharge}}{\Longleftrightarrow} xLi^{+} + x\,e^{-} + Li_{1-x}\,C_6 \tag{2.22}$$

The P2D model develops the ohmic porous-electrode model by introducing diffusion in the electrolyte and solid phases as seen in Figure 2.22. A concentrated solution theory depicts the internal behaviour of Li-ion batteries which encompass positive and negative porous electrodes, separators, and current collectors (Ramadesigan et al., 2012). They serve as a versatile foundation that accommodates the evolution into battery systems which lead to the development of other models. Although the model has an intriguing and useful physics-based approach for the accurate prediction of variables, it still represents overly complex coupled nonlinear partial differential equations (PDEs) across multiple dimensions. The computational depth results in simulation times ranging from seconds to minutes, but the model offers enhanced predictive capabilities due to its incorporation of internal factors.

Electrochemical models have emerged in the exploration of Li-ion batteries, building upon the groundbreaking work by Newman. These models have been thoroughly examined and evaluated for their applicability in advancing battery design, as discussed but the authors and in their work (Abada et al., 2016). Among these models, the P2D model has become the cornerstone, incorporating the idea of solid material represented by uniform spherical particles within each electrode. It excels in capturing the battery's intricate physical processes and predictive capabilities. However, as mentioned in this review, the computational demands have prompted researchers to seek simpler models which offer faster simulations with the absence of the full range of cell processes. The models vary depending on the dimensionality including 1D, 2D, 3D and even lumped models (Zichen et al., 2021). The electrochemical model discussed here is a representation of a cell unit, with a primary emphasis on heat generation within porous electrodes and the separator. This model is depicted in Figure 2.22 (A) where the anode, separator, and cathode correspond to the thickness, respectively. The model simulates the movement of Li-ions, beginning with their release from the porous negative electrode into the electrolyte. As seen in their study, (Ren et al., 2022), they travel through the electrolyte, reaching the porous positive electrode, where they undergo reactions with the active particles, completing the discharge process.

A study on energy capacity and resistance amongst cells for a 1D electrochemical-thermal model for a 53 Ah pouch cell to evaluate parallel-connected cells used an integrated COMSOL Multiphysics and coupled electrical circuit model in MATLAB (Hosseinzadeh et al., 2018). Results indicated that variations in cell depth of discharge and temperature gradients across parallel connections increase with higher load currents and interconnect resistances.

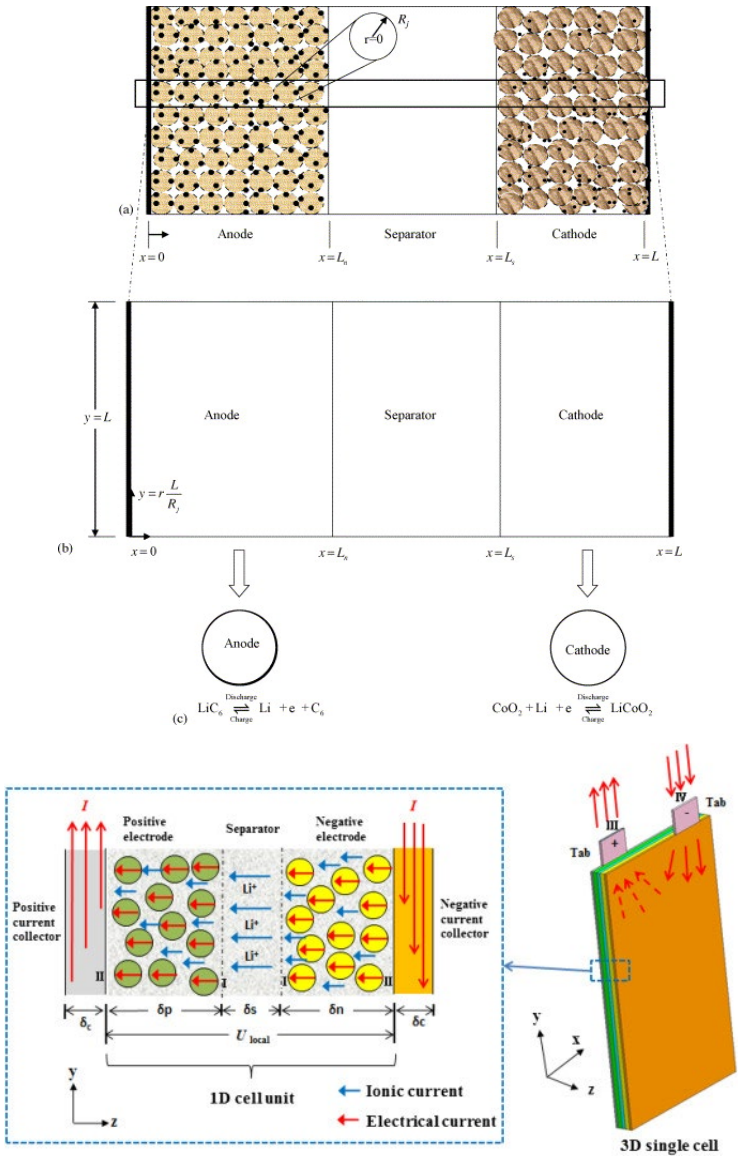

Fig. 2.22 Pseudo two-dimensional (P2D) model, single particle model (SP) and schematic of 3D computational domain and 1D cell during discharge (Santhanagopalan et al., 2006), (Xu et al., 2015).

The variations accelerate cell ageing and may pose safety concerns if left unmanaged. It was stated that a reduction in the number of parallel cells can improve the performance by up to 12 % where otherwise, high electrical loads can exacerbate temperature issues, particularly near the terminals.

Research seen in their study (Weilong et al., 2020) analysed the mechanical effects within Li-ion batteries employing a P2D model that couples mechanical stress with diffusion physics to predict voltage, temperature, thickness change, and stress distribution in a Li-ion cobalt oxide-graphite pouch cell. Results indicate that the standard 2D P2D model without the enhanced stress diffusion tends to overestimate stress levels up to 50 % and an increase in discharge cell capacity by 5.4 %. The stress levels correlate with Li-ion concentration gradients, with high C-rates, such as in fast charging and significant at the electrode-separator interface.

Both electrochemical and thermal behaviours were studied (Xu et al., 2015) during discharge, with the assessment of SOC distribution amount 1D cell units on a prismatic LiFePO4 battery using a pseudo-three-dimensional model. In this case, the battery with current collecting tabs was treated as 3D and the local cell units as 1D. This model considered mass, charge, and energy conservations along with electrochemical kinetics. It was noted that the placement of the positive and negative current collecting tabs significantly impacts potential, local reaction rates, heat generation, and temperature distribution within the battery. Tabs on the opposite sides yielded more uniform electrical and thermal distributions than those on the same side. The model was solely developed for the discharging states with future research on the expansion to charging processes which would require parameter modifications.

A 1D electrochemical-thermal model used to analyse a 53 Ah large format battery utilising NMC chemistry across diverse operational scenarios was studied (Hosseinzadeh et al., 2018). The continuous charging and discharging from 0.5 C to 5C were analysed for the EV operation using urban drive-cycle conditions (WLTP Class 3) and high-performance EV operation resembling track racing. The model combined a 1D representation of one electrode pair with a 3D thermal model, capturing cell-scale temperature distribution. The model was based on the coupling to reduce computational costs and sufficiently predict the temperature distribution at the cell scale. The key findings from the study revealed the significant influence of ambient temperature on battery performance including an increase in heat generation from increased internal resistance.

A study on battery capacity fade in Li-ion cells for natural convection, forced and PCM cooling in hybrid analysis investigated a 6 series 2 parallel battery pack (Zadeh et al., 2022). A 3-D electrochemical and thermal model, incorporating Newman's P2D model using ANSYS, was used to predict the heat generation and temperature distribution within the battery especially the impact of temperature on capacity fading. It was noted in the results that air cooling falls short of temperature limits and PCM cooling improves temperature uniformity with accumulation of heat.

A pseudo-two-dimensional electrochemical using COMSOL, coupled with a lumped thermal model to analyse the electrochemical and thermal behaviour of a commercial 18650 LFP cell was used to understand the impact of various factors including electrical contact resistance and current on the battery performance and temperature distribution (Saw et al., 2013). The model effectively integrated the detailed geometry and layered structure of the battery components for natural convection and heat dissipation correlated from experimental validation. The results showed that reaction heat was identified as the primary heating source about 80-85 % during charging and discharging. The significance of electrical contact resistance was identified, which led to temperature gradients across the cell and highlights the importance of proper cooling for EVs, especially for fast-charging applications.

A CFD model using ANSYS for predicting the transient temperature distribution in a prismatic LiPo battery cooled by natural convection during various discharge cycles was analysed (Magri et al., 2023). The model combined Newman's P2D electrochemical approach with CFD analysis using experimental validation of the accuracy of the CFD simulations. The parameters are crucial for battery modelling, often challenging, assumed, and validated, and useful for similar battery simulations. The study highlighted how computational modelling can replace expensive and time-consuming physical testing, benefiting battery manufacturers and researchers.

Research conducted (Hashemzadeh et al., 2022) on improving Li-ion battery modelling with the consideration of concentration-dependent electrolyte properties often neglected in simplified models proposed a nonlinear modified SP model to function as a simplified electrochemical-based model. It was studied to address the shortcomings of constant-property models using a simplified full-order electrochemical model with a reduction in the number of equations. An approximation was used for improved accuracy which was validated against experimental data. Results indicate that the new model had a reduction in computation time compared to the full-order P2D model and the importance of electrolyte properties in high C-rate applications. A 3D battery model on the study of the internal physiochemical characteristics of a 10 Ah LiPo battery was analysed in their work (Li et al., 2015) using COMSOL. Results revealed that the most significant gradients in the properties occurred at the transition region between the electrode plates with the cell. Consequently, the design of tabs within a battery should be carefully considered as well as the role of the anode in terms of the overpotential of the battery during the discharging phases. The critical challenge of managing heat in 10 AhLiFePO4 battery modules was analysed for high-temperature regions in their work (Ping et al., 2018). Combining PCM with a fin structure to mitigate extreme temperature and enhance temperature uniformity using paraffin waxes with a 1D-electrochemical and 3D thermal coupling using a P2D model in COMSOL. Results indicated that the choice of PCM for lower melting temperature improved the thermal performance but had limitations due to low conductivity, which was enhanced with a fin structure,

reducing the maximum temperature to 51 °C for high C-rates. It was also noted that there was a reduction in the risk of failure using the combination.

2.4 Passive-based cooling effects on battery thermal management systems (BTMS) for real cycling modes in electric vehicles

2.4.1 Integration of PCMs in Battery systems

Traditionally, phase changes have been categorised based on the state of matter involved. However, it has been observed that an additional type of phase change occurs within the solid state as indicated in their review (Xia et al., 2017) and as depicted in Figure 2.23. There are alterations in the crystal structures for the solid-state phase change which contributes to fractional LH to the overall phase change phenomenon. This is particularly noticeable in the differential scanning calorimeter curves in paraffin waxes. A classification was formed by associating the fundamental types of structural and state changes with PCMs. Paraffin waxes are versatile PCMs with attributes suitable for various thermal applications. However, their unique features, including thermal, mechanical, responsive, and chemical properties, demand tailored approaches for each application.

For the thermal management systems, paraffin waxes require compositional adjustments to overcome their low thermal conductivity while preserving Latent heat (LH). Mechanical enclosures are usually preferred due to their minimal leakage, which is advantageous to polymers. A balance between thermal and operational performance is pivotal toward high storage density while reducing heat times including LH which can often lead to bulkier designs. As seen in their review (Xia et al., 2017) thermo-mechanical, thermo-responsive and thermo-chemical systems were analysed which use varying properties, shapes, and inertness to meet certain constraints including smart surfaces and biomaterial design approaches which hold immense potential across various thermal applications. Although, the implementation hinges on design, material, and methodologies.

A BTMS (Qian et al., 2019) is essential for regulating the temperature of battery packs, especially Li-ion batteries commonly used in commercial applications. Temperature significantly impacts the battery performance, as chemical reactions within the battery are temperature dependent as seen in this review. Research has shown that temperature variations can lead to uneven temperature distribution within battery cells causing reduced lifespan and performance. Battery temperature changes occur due to heat generated during the charging and discharging processes. This heat is a result of various factors, including ohmic heat, heat mixing, enthalpy heating and entropy changes during the electrochemical reactions. Managing this heat generation is critical, particularly for Li-ion batteries in

EVs and HEVs. BTMS plays a crucial role in maintaining battery pack performance and longevity by regulating temperature. Researchers have made significant contributions to the field of battery thermal management, aiming to address the challenges posed by temperature variations in EVs and HEVs. There have been studies on heat generation (Madani et al., 2023), (Kandukuru et al., 2023), (Broatch et al., 2022), (He et al., 2023), (Velumani et al., 2022), (Siddique et al., 2018), (Tete et al., 2021) and the most likely areas of heat accumulation which may lead to non-uniform temperature distribution leading up to low performance and reduced useful life. A chart showing the classifications of the battery cooling system is illustrated in Figure 2.24 (Tete et al., 2021), which outlines the various categories of power consumption including active and passive cooling as well as other key parameters including the heat transfer medium, whether there is direct or indirect cooling, orientation of battery system example series and parallel and other techniques.

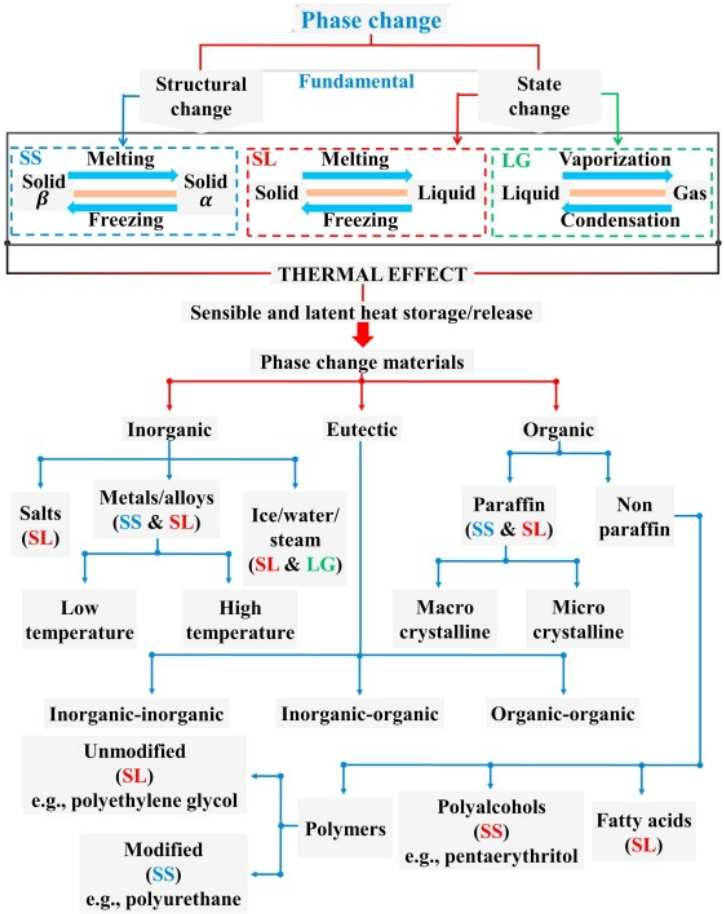

Fig. 2.23 Phase change dependent classification from the fundamental changes to thermal effects and PCM types (Xia et al., 2017).

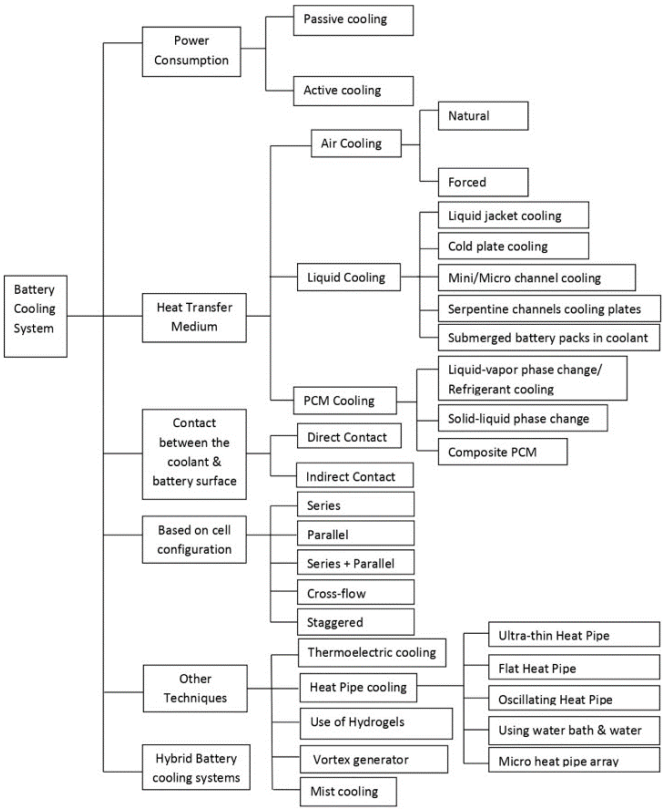

Fig. 2.24 BTMS classification (Tete et al., 2021).

The field of BTMS has witnessed an array of rigorous investigations, combining both experimental and numerical approaches. These studies span across multiple tiers, encompassing research conducted at the cell, module, and pack levels. The primary objective has been to unravel the intricate thermal behaviours of batteries operating under various conditions. A notable facet of this research has been the extensive use of mathematical modelling, often leveraging Computational Fluid Dynamics (CFD) techniques, which have been instrumental in understanding and enhancing BTMS. Experimental research as seen in their review (Tete et al., 2021) occupies a pivotal role in this domain, serving as the cornerstone upon which our understanding of BTMS is built. It offers the means to discern the nuanced relationship between variables, shedding light on the influence of one parameter upon another. Researchers have diligently contributed to the development of both numerical and experimental platforms which are tailored to the unique challenges posed by the thermal management of Li-ion batteries. Both the impact of the structural, and operational variables on the performance and longevity of Li-ion batteries include objectives to discuss in this review. Present battery and BTMS technologies in EVs face challenges: their performance relies on temperature, state, and health factors. High discharge rates often lead to uneven temperature distributions within the battery, potentially decreasing its lifespan. Cold weather necessitates additional power for heating, causing energy losses. Thermal runaway, especially during high-speed charging and repeated cycles, poses a risk, potentially

damaging cells, or battery packs. Recycling and disposal of batteries have environmental implications. Moreover, the main obstacle to economical EVs is the cost of Li-ion batteries, with potential cost reductions offering significant savings. Future battery development focuses on extending lifespan, boosting power capacities, and enabling rapid charging to enhance EV feasibility as studied (Choudhari et al., 2020).

BTMS are crucial for maintaining Li-ion batteries within the ideal temperature range. Li-ion batteries are sensitive to temperature, so BTMS ensure the battery pack's temperature stays optimal. In this regard, the BTMS must be practical, energy-efficient, and cost-effective as stated in their review (Kim et al., 2019), ideally not exceeding 20 % of the system weight or interfering with other components. Effective cooling is vital, keeping the maximum temperature below 40 °C and the minimum temperature below 15 °C. This is also respective of the C-rate, single charging/discharging and whether consecutive cycling or drive cycle modelling is applied. These parameters along with the ambient temperature assessed were recorded in the summary tables. Harnessing LH during phase transitions in the use of PCMs can play a pivotal role in BTMS. These PCMs must possess specific attributes like high LH, appropriate phase transition temperatures, minimal volume changes, good thermal conductivity, non-toxicity, and chemical stability. Solid-liquid PCMs, especially eutectic materials are favoured in power BTM for their stability and minimal volume changes during phase shifts. Organic PCMS, like paraffin, are widely used due to their chemical stability, affordability, and corrosion resistance, though they have limitations like low thermal conductivity and flammability. Enhancements like low thermally conductive materials such as metal copper foams, improve thermal performance. These cooling method enhancements have been identified in this review in the summary tables. Although different cooling methods such as air cooling, liquid cooling, heat pipes and thermoelectric coolers (TECs) are researched to have effective thermal management, there are many challenges associated with using these active methods. In the case of PCM cooling, challenges like volumetric expansion and low thermal conductivity during phase shifts are experienced so strengthening using PCM sleeves with materials such as graphite, metal fins, encapsulations or foam improves the thermal conductivity (Ranjbaran et al., 2023), (Sun et al., 2019), (Zhang et al., 2023), (Zhang et al., 2022). They can also be enhanced using nanotubes and nanomaterials which will be discussed in this review.

As a culmination of these research efforts, this section includes a comprehensive summary of significant findings drawn from a synthesis of numerical simulations, where different CFD approaches have been used to model single-cell, module and pack systems that employ PCM (Wazeer et al., 2022) as a cooling method along with enhancements to this method. Tables 2.1, 2.2 and 2.3 within the article have been thoughtfully organised based on these criteria. This amalgamation of insights represents a

valuable resource for advancing our understanding of BTMS using PCMs and the numerical approaches used and informs on the development of more robust and efficient thermal management solutions.

The realm of BTMS has witnessed extensive research, employing both experimental and numerical methodologies, spanning various levels, including cell, module, and pack. The primary objective has been to understand the complex thermal behaviours of batteries under diverse conditions. Mathematical modelling, particularly leveraging CFD techniques, has played a crucial role in comprehending and enhancing BTMS. Experimental research holds a pivotal role, providing a foundation for understanding BTMS intricacies and the relationships between various variables.

Current battery and BTMS technologies in EVs face challenges, including temperature sensitivity, uneven temperature distribution, energy losses in cold weather, thermal runaway risks, and environmental concerns. Future battery development aids in extending lifespan, increasing power capacities, and enabling rapid charging to enhance EV feasibility. Effective BTMS is essential for maintaining Li-ion batteries within an ideal temperature range, considering factors like weight, energy efficiency, and cost-effectiveness. Cooling is vital, with parameters such as maximum temperature, minimum temperature, C-rate, and environmental conditions playing a crucial role. PCMs are key components in BTMS, harnessing Latent heat during phase transitions. PCMs should possess specific attributes like high Latent heat, approximate phase transition temperatures, minimal volume changes, thermal conductivity, non-toxicity, and stability. Enhancements, such as using materials like metal copper foams and nanomaterials, improve PCM cooling performance.

2.4.2 Single-cell PCM integration

A study (Yang et al., 2023) explored passive cooling techniques using PCM to regulate a Panasonic 18650 PF Li-ion battery cell for use in EVs and HEVs with validation results less than 1 % deviated between numerical and experimental data, with stringent safety measures imposed to mitigate risks. The PCM introduced a substantial impact on thermal performance, notably under normal ambient conditions (25 °C), extending it by 20 % post single discharge. This accumulated into an impressive 340 % overall performance enhancement, ensuring consistent temperature maintenance across different cycles. The study also investigated the impact of circumferential PCM thicknesses with 3 mm sufficient for effective performance extension. Notably, in high-temperature environments (40 °C and 55 °C) there were still stable battery temperatures and even in low temperatures (-20 °C and 0 °C) where the PCM does not melt due to melting temperature, consistent thermal performance over consecutive cycling was displayed.

A water-nano encapsulated PCM with nano-capsules dispersed in water, for the thermal management of an 18650 Li-ion battery pack was seen in research (Qaderi et al., 2022) which employed momentum, electrochemical, and energy equations to analyse the system. The results indicated that PCM utilisation can significantly reduce the average and maximum temperatures of battery cells up to 34 % and 51 %, respectively, compared to traditional water systems. Additionally, there was an enhancement in the temperature uniformity up to 78 % with a slight increase in Li-ion concentration difference for both the solid and liquid phases and a reduction in the battery voltage.

A thermal management system using pin fins, PCM and expanded graphite (EG) for high discharge scenarios exceeding a Panasonic NCR18650BD battery's 2C limit was studied (Wazeer et al., 2022) for the battery's electrical and thermal behaviours simulated for different discharge rates (0.5C, 1C and 2C) validated with experimental data. The study investigated the heat generation profile for high discharge rates (2C, 3C, and 4C) and explored the effectiveness of various heat sinks, with fins and without using Eicosane PCM. Results showed a reduction in temperature by up to 22.7 °C compared to a plain heat sink. The introduction of the EG and the addition of fins added weight to the system but maintained low battery temperatures and temperature uniformity.

The critical issue of battery overheating in EVs by introducing an effective thermal management system for battery modules focused on preventing heat propagation and thermal runaway for up to three 18650 cells damaged due to nail penetration was examined in their work (Kshetrimayum et al., 2019). The Newman P2D model, short circuit model and thermal abuse model were used to accurately estimate intense heat generations under various conditions. The results demonstrated that the proposed system with combined PCM and micro-channel cooling plate maintained the maximum temperature of neighbouring cells below 89.85 °C to prevent the thermal runaway across the entire module.

The growth of EVs and HEVs faces a significant obstacle due to the need for larger Li-ion batteries that can manage heat safely. In their study (Al-Hallaj et al., 2002), a 1D thermal mathematical model to simulate the thermal behaviour of commercial Li-ion cells incorporated experimental and heat generation data for simulations revealed that cells maintain uniform temperature under low cooling rates but are significantly affected by variations at higher cooling rates. The Li-ion batteries exhibit unique cooling characteristics that make them highly suitable for a passive thermal management system reliant on phase change heat effects. They stated that there is high potential for the use of PCM-based thermal management systems, especially in extremely cold ambient conditions and space applications. Moreover, it emphasises the cost advantages it can offer compared to active cooling systems. A thermal management system for Li-ion pouch battery modules investigated the use of phase change slurry (PCS)

comprised of water and n-octadecane microcapsules within a mini-channel cooling plate to manage the battery temperature was studied in their work (Bai et al., 2019). The study analysed a 3D thermal model and employed an orthogonal matrix to balance the cooling performance and energy consumption. The findings indicate that the PCM slurry outperformed the pure cooling method but diminishes once beyond a critical mass flow rate. It was deemed that at an appropriate concentration rate and above 35.85 °C, the energy efficiency of the slurry is improved. Two BTMS systems for Li-ion batteries in HEVs and EVs as seen in their work (Chen et al., 2020) explored active air cooling and passive PCM cooling. A comprehensive model integrating electrochemical and thermal aspects was used and validated. The key findings revealed that active air cooling effectively maintains battery temperature up to 50 °C, while passive PCM cooling struggles at high temperatures but provides a more uniform temperature distribution. Air cooling extends Li-ion cycle life, especially at lower velocities, and is cost-effective according to their work. Research work (Verma et al., 2019) examines the efficacy of PCM/compressed expanded graphite (CENG) cooling for battery cells, providing a competitive alternative to forced convection methods. The study employed a simplified 1D model, demonstrating practicality and accuracy and the influence of built density on system performance. Results indicate that as density increased the gains in efficiency diminished. To enhance the performance further, reducing the convection resistance emerged as a crucial factor. However, a notable concern of the temperature gradient which exceeds 10 °C within the battery needed further investigation.

As ongoing areas of research, a more streamlined approach to the design and optimisation of PCM/CENG cooling systems for battery packs was promising as the choice of various inputs to create the test case allowed for versatility. Composite PCM (cPCM) consisting of paraffin and expanded graphite (EG) for BTMS was explored (Gu et al., 2022). Optimal dimensions for a cPCM were identified and led to the proposal of an innovative BTMS design with air and cooling fins with validated data for an ambient 20 °C with a 2C discharging rate using a lumped model in COMSOL. The function of the cPCM was to cool the core of the Li-ion batteries, while the air with the addition of fins, cooled the upper and lower sections. The simulations using COMSOL Multiphysics demonstrated that the model consistently reduced temperatures by 2 – 4 °C compared to the base design under a high discharge rate condition at 30 °C. This approach was also seen to significantly reduce the weight of the Li-ion battery packs. Different configurations of the fins also improved the heat transfer. A study which introduces ECM battery modelling for BTMS utilising PCM and liquid cooling used an enhanced extended Kalman Filter (EKF) for real-time battery temperature estimation without extra sensors. Compared to free cooling, the approach lowered the battery temperature by 7.35 °C at a 3C discharge rate with a 1.7 °C difference (Hou et al., 2022), assessed at various discharge rates, inlet flow rates, and

PCM thicknesses. The model exhibited an accuracy within 5 % of experimental results. The model proposes a real-time electrical and thermal signal prediction in large battery packs and BTMS analysis.

A numerical heat transfer analysis using ANSYS fluent in their work (Javani et al., 2014) explored the passive thermal management in EVs and HEVs using PCMs integrated with Li-ion cells. PCMs absorb and release heat during phase changes, mitigating temperature spikes in cells. The study employed a numerical approach with varying PCM thicknesses and assessed the impact on cell temperature distribution. A 12 mm PCM reduced the maximum temperature, while a 3 mm thickness provides a 10 % more uniform temperature distribution. Transient conditions revealed that PCMs rapid cooling effect within 7 minutes at heat generation rates and emphasises thicker PCMs for improved thermal management. Mesh generation using COMSOL was seen in their work (Karimi et al., 2022) in a study which explored high-power dual-cell Li-ion capacitor modules using PCMs combined with aluminium mesh grid foil.

The main goal of the research was to maintain system temperature within a safe range while improving uniformity and costs. Three different cooling methods were analysed which included pure PCM, dual PCM and the PCM combined with aluminium through experimentation and validated with a 1D-electrothermal and 3D-thermal model. Results showed that the PCM combination reduced the maximum temperature of the module by 20 % compared to forced convection with optimal thickness examined to balance the cost and temperature. The dual-PCM combination system also further enhanced temperature reduction and demonstrated promise for efficient and cost-effective thermal management. In their study (Karimi et al., 2021), research investigated the thermal management for Li-ion capacitors in high-power applications. Various cooling systems, including air-cooled and liquid-cooled active systems as well as passive systems with PCMs, aluminium mesh, heat sinks and heat pipes were all examined. The experimental results were validated using COMSOL Multiphysics software. The PCM and liquid-cooled hybrid with PCM reduced the maximum temperature of the system.

Figure 2.25 displays battery single-cell geometry for cylindrical (A-D), prismatic (E), and pouch (F) respectively, showing the orientation and location of the PCM for different cell types seen in research.

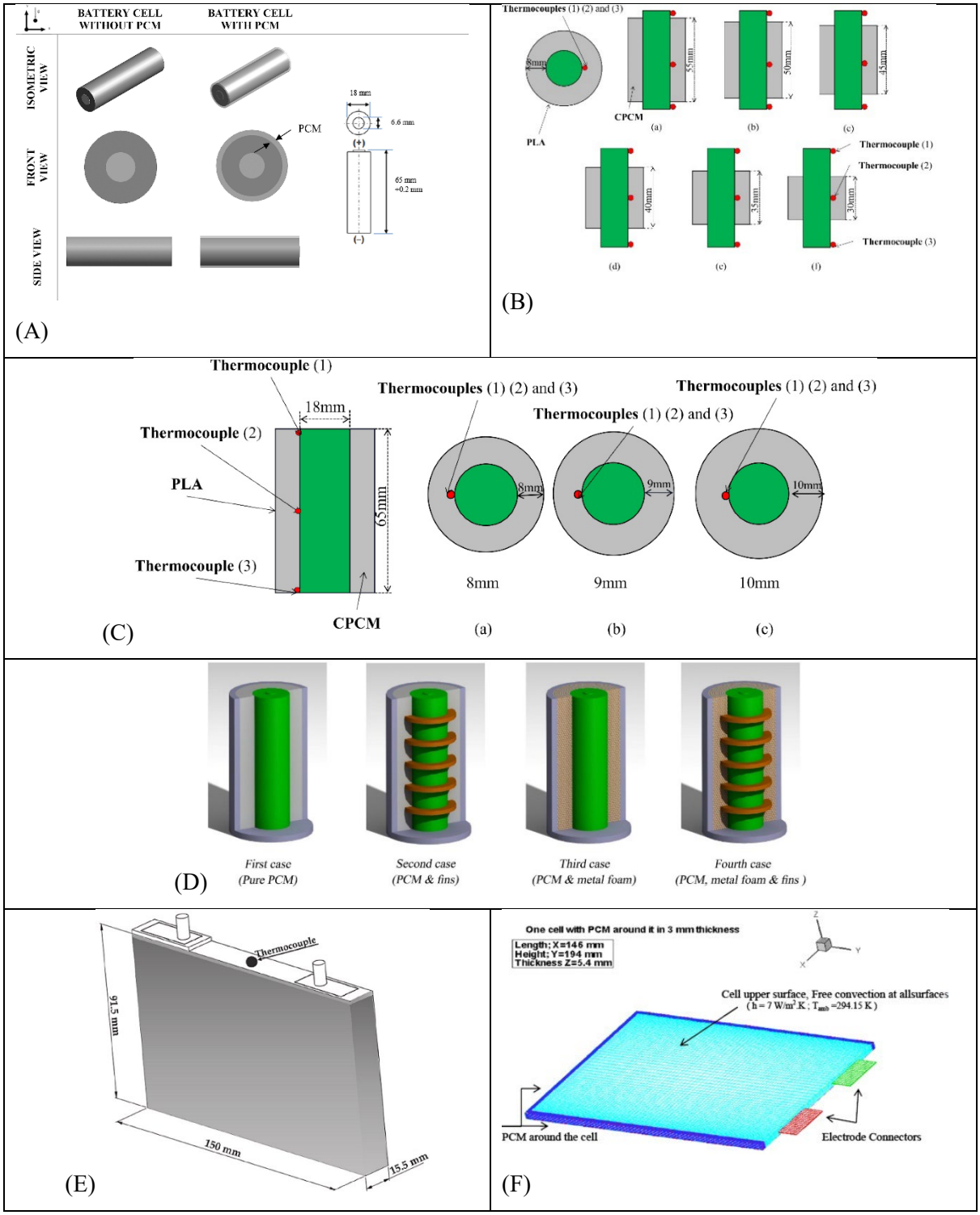

Fig. 2.25 Schematics of PCM-based cooling for single-cell batteries proposed by A) (Yang et al., 2023), B) (Gu et al., 2022), C) (Gu et al., 2022), D) (Khaboshan et al., 2023), E) (Karimi et al., 2022), F) (Javani et al., 2014).

In another study (Karimi et al., 2021), the combination of features which include double-layer capacitors and Li-ion batteries was investigated. During high-power operations, the storage devices generate heat which impacts their performance and longevity. An integrated system which included PCM, and heat pipes aimed to maintain the temperatures below 40 °C under continuous 150 A for 1400 s. The experimental and numerical analysis compared the hybrid system with PCM and natural convection with the heat pipe. Results showed that the hybrid passive system significantly reduced the temperatures by 35 % compared to a standalone system and improved the temperature uniformity. In their study (Ma et al., 2022), the improvement of BTMS for electric tools requiring high currents (10 - 15 C) and high temperatures (40 °C) was investigated. The batteries used in the system were Samsung 18650 20R NCM batteries and explored the temperature distribution from the battery core to the surface under these extreme conditions. PCMs were applied for thermal control. Results showed that while the PCMs effectively reduced the surface temperatures, core temperature reduction was limited, which caused a significant temperature difference and noted the impact of PCMs on battery lifetime, with increased capacity but accelerated ageing (90 – 250 %) under extreme conditions. A study which focused on the development of effective BTMS for Li-ion batteries used in EVs (Najafi et al., 2023) used four configurations with a combination of PCM, metal foam, and various fin shapes designed to maintain optimal surface temperatures during high-current discharging (3C-rate) in diverse environmental conditions. The results showed that the most effective BTMS, incorporating PCM, metal foam and fins, reduced the battery surface temperatures and delayed PCM melting compared to just PCM alone. It was noted that different fin shapes had minimal impact on performance and practical applications should consider environmental factors in cylindrical Li-ion batteries.

Efforts to develop effective BTMS for Li-ion batteries in EVs used different configurations with a combination of PCM, metal foam, and various fin shapes. The most effective BTMS, incorporating PCM, metal foam and fins, reduced battery surface temperature and delayed PCM melting compared to PCM alone (Najafi et al., 2023). A summary of the single-cell PCM-based thermal management systems for pure and enhanced PCM designs including numerical modelling, cell types, battery chemistry and cooling method is illustrated in Table 2.1 (A). An additional supplementary Table 2.1 (B) outlines the discharging/charging rates and ambient and maximum temperature seen in the research. The studies also analysed whether continuous discharging/recharging processes were completed including drive cycle modelling.

Table 2.1A. Summary of work conducted for the single cell model BTMS (materials).

Serial	Authors	Modelling	Cell type	Battery Chemistry	Capacity Ah	# of cells /module	Cooling method	IF PCM - Type/Melting Temp/Pure
1	Yang et al., 2023	ECM	Cylindrical	Lithium-ion	2.9	1	PCM	N-octadecane/298.15 K-302.15 K/pure
2	Qaderi et al., 2022	P2D	Cylindrical	LiFePO4 / Graphite	1.5	24	water nano-encapsulated PCM (NEPCM)	N-octadecane/298.15 K-302.15 K/pure
3	Akula et al., 2022	P2D	Cylindrical	NCR18650BD	2.98	1	Pure PCM/fins (expanded graphite)	Eicosane/
4	Kshetrimayum et al. 2019	P2D	Cylindrical	Lithium-ion	1.5	10	microchannel cooling plate and PCM	
5	Al-Hallaj et al., 2002		Cylindrical	Lithium-ion	10, 30, 50, 100	1	liquid cooling/PCM	
6	Bai et al., 2019b	ANSYS	Pouch	LiFePO4 / Graphite	20		PCM slurry	20 % n-octadecane, 80 % water
7	Chen et al., 2020	COMSOL	Cylindrical	LiFePO4 / Graphite	2.3	16	PCM	
8	Greco et al., 2015	SYRTHES	Cylindrical	Lithium-ion		1	PCM composite	
9	Gu et al., 2022	COMSOL	Cylindrical	Lithium-ion	3.3	1	PCM composite (paraffin and expanded graphite)	paraffin wax
10	Hou et al., 2022	COMSOL	Pouch	LiFePO4 / Graphite	22	1	liquid cooling/PCM	
11	Javani et al., 2014	ECM	Pouch	Lithium-ion		1	PCM	
12			Prismatic	Lithium-ion	2.3	1	PCM/Al	
13	Karimi et al., 2022		Prismatic	Lithium-ion	2.3	1	air/liquid/PCM cooling/PCM/Al	pure paraffin
14	Karimi et al., 2021		Prismatic	Lithium-ion	1	1	PCM and flat pipe	pure paraffin (25 - 32 °C)
15	Ma et al., 2022		Cylindrical	NCM	30	1	PCM and graphite	paraffin wax (45-58°C)
16	Najafi et al., 2023	ANSYS	Cylindrical	Lithium-ion		1	PCM, metal foams and fins	n-eicosane

Table 2.1B. Summary of work conducted for the single cell model BTMS (conditions).

Serial	Authors	C rate	Consecutive cycling (100% - 0%)	Drive Cycle	Single charge/discharge	Ambient Temp C	Max Temp C
1	Yang et al., 2023	1C	Yes	No	Yes	25	60
2	Qaderi et al., 2022	0.2C-2C	No	No	Discharging	26	40
3	Akula et al., 2022	2C, 3C, 4C	No	No	Discharging	24	60
4	Kshetrimayum et al. 2019	1C	No	No	Discharging	26.85	89.85
5	Al-Hallaj et al., 2002	1C-3C, 5C, 7C, 9C	No	No	Discharging	26.85	63.85
6	Bai et al., 2019b	1C, 1.5C, 2C, 3C	No	No	Discharging	26.85	53.47
7	Chen et al., 2020		No	No	Discharging	25	46.96
8	Greco et al., 2015	0.1, 0.5C, 1C	Yes	No	Yes		
9	Gu et al., 2022	0.5C, 1C, 1.5C, 2C	Yes	No	Discharging	25	39.85
10	Hou et al., 2022	1C	Yes	Yes	Yes	0, 10, 20, 30, 40, 50	56
11	Javani et al., 2014		No	No	Discharging	20	75
12	Karimi et al., 2020	2C, 3C, 4C	Yes	No	Yes	20	60
13	Karimi et al., 2022	1C, 2C, 3C	Yes	No	Yes	30	45
14	Karimi et al., 2021	1C, 2C	Yes	No	Discharging	21	43.85
15	Ma et al., 2022	1C	No	No	Discharging	25	45
16	Najafi et al., 2023	1C	No	No	Discharging	23	60
1	Yang et al., 2023	1C	No	No	Discharging	23	55
2	Qaderi et al., 2022	15C	No	No	Discharging	40	75
3	Akula et al., 2022	3C		No		31.85	

2.4.3 PCM-based cooling in modules

The critical issue of Li-ion battery thermal management in EVs to prevent catastrophic thermal runaway has been studied (Hussain et al., 2023). They introduced an efficient and cost-effective BTMS using PCM. The research employed a 3D simulation, analysing single batteries and battery packs under extreme conditions. The NTGK model in ANSYS is used for battery performance and thermal analysis, further enhanced by PCM solidification, and melting models. The study evaluated ambient temperature, discharge rate, and heat transfer effects on BTMS performance and identified effective ambient PCM combinations. Under high discharge rates, the PCM-based BTMS significantly reduced the maximum battery temperature, enhancing safety and providing insights into large-scale applications based on tailored PCM selection and environmental conditions.

Performance enhancement of Li-ion batteries in EV which looked to address the issue of reduced mileage due to high temperature was studied in their work (Talele et al., 2021). Their study introduced a passive thermal management system using PCMs for 60-cell 18650 Li-ion batteries commonly used in automobiles. The PCM was applied around the battery cells to delay the temperature rise using numerical simulations in ANSYS fluent and a neural network approach for optimisation. Paraffin wax and RT-18 PCM configurations were compared with the paraffin wax showing better performance due to its lower melting point. The study correlated the time delay with the liquid fraction rate and indicated that higher liquid fraction rates increased the time delay and allowed for more efficient energy utilisation.

A hybrid cooling plate for thermal management of Li-ion batteries in EV, with a combination of both active liquid cooling and passive PCMs cooling as seen in their research (Akbarzadeh et al., 2021). The hybrid design was shown to be 36 % lighter than traditional aluminium plates, offering weight savings. ANSYS CFD and experimental testing were used to validate the performance. Results showed that the hybrid cooling plate reduced the energy consumption for circulating coolant by up to 30 % compared to the aluminium plates and provided better temperature uniformity. In colder conditions, there was a delayed temperature drop which reduced the need for active heating and little downtime. Moreover, the hybrid liquid cooling plate embedded with PCM was seen in their study (Akbarzadeh et al., 2022). The hybrid system combined both the active and passive cooling methods to investigate the performance using ANSYS for a 48 V battery module under low currents with passive cooling, medium currents with triggered liquid cooling and high currents with constant liquid cooling. The study also investigated the PCM's ability to prevent rapid temperature drops in cold environments when the battery is switched off. Results showed that the passive cooling kept the module within the desired temperature range at low current with the hybrid model showing reduced energy consumption. The maintenance of battery temperature also impacts the requirement for warming the battery after short stops.

Research on the impact of battery configuration, for spacing between batteries in a liquid-to-vapour battery cooling system (Al-Zareer et al., 2019a) where the batteries were partially or completely submerged in a coolant pool near the battery optimal temperature. The heat generated from the battery exceeds the saturation temperature leading to evaporation and cooling. Four configurations were assessed under varying discharging rates (4C, 5C, and 6C) using COMSOL with results showing that decreasing the battery spacing increases the maximum battery temperature but improves the thermal uniformity. In another study (Al-Zareer et al., 2018a), a refrigerant R134a was used as the cooling method which integrates a comprehensive model combining a 1D electrochemical model with a 3D heat and mass transfer model to effectively simulate and assess the battery performance for partially

submerged batteries. As R134a absorbed the heat, it transformed into vapour and cooled the battery surfaces not in contact with the liquid which is then expelled and subsequently condensed back to liquid in the conditioning system. The system was assessed under various conditions, including 600s charging and discharging at 5C and a 10-minute motorway drive cycle. The results demonstrated that the PCM-based BTMS surpasses conventional air and liquid cooling systems, ensuring lower maximum battery temperature and achieving more uniform temperature distribution across the module. Moreover, (Al-Zareer et al., 2018b) assessed a boiling-based heat transfer method to effectively control battery temperature during high-power charging and discharging with propane as a cooling and energy source. The resulting vapour from heating was used to produce electrical energy for charging or driving the vehicle. The tests were performed under charging and discharging cycles with results indicating that the battery temperature was maintained below 35 °C as well as reducing the temperature difference between cells. Further research on the PCM R134a to enhance battery lifespan and reduce charging duration was seen in their work (Al-Zareer et al., 2020) for spacing configurations. The results indicated that the compact refrigerant-based thermal management system maintained the battery maximum temperature under 35 °C with temperature variations within 4 °C when 80 % of the battery is submerged. The study demonstrated that the liquid-to-vapour battery cooling system offered competitive performance compared to liquid and air-cooling systems. A comparative analysis of BTMS with a focus on the liquid-to-vapour PCM systems was studied (Al-Zareer et al., 2019b) and compared convectional thermal management methods. Results included that tube-based systems excel for prismatic batteries, pool-based reduce maximum temperatures for cylindrical batteries by 30 %, and 80 % coverage is needed to achieve similar temperature reductions for prismatic batteries with both methods found superior to other proposed systems with enhanced heat transfer characteristics, but further exploration needed.

Thermal management challenges in fast-charging Li-ion batteries with a focus on cooling methods like liquid cooling and hybrid cooling with PCMs were seen in their study (Amalesh et al., 2022). Three design configurations of a prismatic module charged at 8C rates were assessed through numerical simulations in ANSYS. The findings highlighted the superiority of liquid cooling over hybrid methods for fast charging. Factors like coolant flow direction and PCM thermal conductivity significantly impact the cooling efficiency, while PCM melting temperature and Latent heat play a minor role. It was noted that a minimum cooling flow rate is required to maintain battery temperatures below 40 °C during fast charging, and PCM-based hybrid cooling required enhancements in thermal conductivity. A hybrid BTMS combining active air cooling and passive PCM within a Li-ion battery module analysed eighteen cases with various cell arrangements, module compactness levels, and PCM thicknesses were simulated in ANSYS in their work (Bamdezh et al., 2020). Results indicated that only

one case, which featured aligned cell arrangement, maximum compactness, and minimal thickness experienced unsafe cell temperature increases. Across all the cases, the maximum temperature difference within the battery module remained under 1.5 °C, which demonstrated the hybrid's ability to maintain uniform temperature distribution among cells.

The increase in the PCM thickness reduced the average cell temperatures, particularly when the active cooling was less powerful. A passive thermal management system for Li-ion batteries to prevent thermal runaway using inorganic composite PCM (cPCM) consisting of sodium acetate trihydrate (SAT) and EG was analysed in their study (Cao et al., 2022). The results revealed that SAT/EG effectively inhibits thermal runaway propagation with a battery compared to unprotected conditions or insulation materials without a rise in the temperature. The material combination displayed substantial heat storage capacity and can be deemed a promising candidate for thermal runaway protection. A hybrid BTMS combining liquid cooling and PCM with varying EG contents to enhance battery module temperature uniformity and cooling performance (Chen et al., 2022) analysed a matrix which adapts the heat transfer efficiency along the liquid flow direction due to the difference in EG contents. Investigation into layout options, segment lengths, and structural parameters through CFD at 4 C-rate and 308.15K ambient temperature was shown to significantly reduce maximum temperature and temperature difference. Additionally, an increase in the cell spacing was also found to reduce the maximum temperature and temperature difference.

A study which focused on the enhancement of the thermal performance of a 5x5 Li-ion battery arrangement using PCMs was analysed (Choudhari et al., 2021) and highlighted the heat during discharge and charge. PCM cooling, known for its high Latent heat capacity and lightweight nature, was evaluated. Results indicated that while PCM was effective at lower discharge rates (1C, 2C, and 3C), there was an accumulation of heat in the interior of the module. Different fin structures were introduced and studied including convection and structure of fins on charging and discharging cycles. There was an indication that the potential to reduce maximum temperature and improve PCM melting fraction was observed. Effective thermal management is vital as seen in the studies highlighted in this review with energy storage systems reliant on Li-ion batteries. In their study (Coleman et al., 2016), minimum cell-to-cell spacing in direct, liquid-cooled battery modules using a metal/wax composite during single-cell failures was analysed. This included different heat sink materials and interface qualities. The simulations covered transient load scenarios which revealed that composite materials perform well under normal conditions but struggle in compact designs.

A study on the performance, lifespan, safety, and reliability of Li-ion battery modules, particularly with high discharge rates (Hekmat et al., 2022) was analysed for temperature distribution

among cells and their surfaces using a combined model with PCM and liquid cooling channels for prismatic cells. The results revealed that the maximum temperature difference among cells was reduced and ensured better temperature uniformity. It was noted that flow rate can improve the temperature control for cells with non-uniform heat generation. A numerical investigation of cooling for a cubic module of nine cylindrical Li-ion batteries which employed nanofluids in separate ducts surrounding the battery assembly was immersed in PCM (Jiang et al., 2022). The simulations explored the impact of nanoparticle volume fraction and duct height over time. Results indicated that over 60 % of the PCM melted during that time and higher nanoparticle volume fractions enhanced the heat transfer coefficients for both the nanofluids and PCM while reducing the pressure drop inside the ducts. PCMs were used in a study (Kadam et al., 2023) which were enhanced using graphene nanoparticles for thermal management of 12 cylindrical Li-ion cells using SOLIDWORKS for the 3D model and validated using ANSYS thermal simulations at different C-rates and PCM thicknesses. The results revealed that an increase in the PCM thickness reduced the battery pack temperature but increased the weight, necessitating a trade-off between temperature control and pack weight. Paraffin PCM was noted as a cost-effective solution when combined with graphene for a hybrid cooling system for high-temperature scenarios. A thermal management system using PCM for Li-ion batteries in an electric scooter was investigated in their work (Khateeb et al., 2004). This passive system controls battery temperature without active cooling components, offering a compact, lightweight, and energy-efficient solution. Simulations assessed a battery sub-module with nine Li-ion cells surrounded by a PCM with a melting point between 41 °C and 44 °C. Aluminium foams and fins were considered as an enhancement to the PCM performance with results demonstrating the PCM's effectiveness, especially with the addition of aluminium fins and maintaining battery temperatures within safe operating conditions. The active air-cooling alone proved inadequate and the PCM's potential as a cost-effective thermal management solution.

The combination of Convolutional Neural Networks (CNNs) and Finite Element Method (FEM) was developed (Kolodziejczyk et al., 2021) to assess the thermal properties of cPCM composed of copper and foam. The predicted thermal properties were then used in a multiscale model to simulate the thermal management of a Li-ion module during charging/discharging cycles. Results indicated that the CNN-based model accurately evaluated thermal management with high precision and may provide an alternative to time-consuming FEM solutions. In their work (Lazrak et al., 2018), the challenges with EV market penetration by improving battery energy performance and thermal management were studied. The focus was on the integration of PCM to enhance the heat transfer. It investigated the influence of the PCM's melting temperature on the system using two numerical models including 1D and 3D which were developed for system design and PCM selection. The study also introduced a

method to enhance the thermal heat transfer within the PCM using copper grids. The results demonstrated a reduction of at least 5 °C compared to the reference system with optimisation in future research directions.

A study (Wang et al., 2021a) which focused on enhancing the thermal safety of Li-ion batteries using PCMs has been studied with the introduction of silicone coupled with PCM to analyse different thicknesses and thermal conductivities of PCM. Results demonstrated that based on the battery system, the PCM and silicone configuration exhibited optimal performance when compared without the silicone and reduced the battery temperature up to 24 °C during the 4C discharge rate. The challenge of excessive heat generation in Li-ion batteries during operation (Wang et al., 2021b) with the mitigation to performance and safety while maintaining energy efficiency and cost-effectiveness. A passive PCM system around the pouch cell was numerically investigated based on heat production and PCM heat transfer principles. The findings revealed that the PCM units effectively reduced the maximum cell temperatures and temperature differences, exhibiting good heat storage and temperature equalisation capabilities. Insulation of the PCM units was seen to prolong the cooling times and temperature retention. The study explored the impact of PCM design parameters, including thermal conductivity, viscosity, Latent heat, PCM unit thickness and unit shell thermal conductivity using PCMs.

In a study which underscores the growing need for efficient battery cooling systems, driven by the expanding applications of Li-ion batteries in electric vehicles (Mousavi et al., 2021), PCM and mini-channel cold plates were designed for prismatic cells in ANSYS. The orientation of battery modules was explored for its impact on BTMS performance, which revealed a substantial temperature difference between orientations. The coupled system proved superior in maintaining a lower maximum battery temperature under constant heat generation compared to active cooling. A hybrid system for PCM and liquid cooling for prismatic battery modules were studied (Mousavi et al., 2023). Each module was comprised of four battery cells enclosed between vertical mini-channel plates, complemented by horizontal PCM plates. The hybrid approach resulted in several advantages including lower maximum battery temperatures, improved temperature uniformity, enhanced power efficiency and superior driving cycle performance compared to active cooling.

Figure 2.26 illustrates PCM-based cooling in modules showing the orientation and location of the PCM for different cell types as seen in research. A summary of the module PCM-based thermal management systems for pure and enhanced PCM designs including numerical modelling, cell types, battery chemistry and cooling method is illustrated in Table 2.2 (A). An additional supplementary Table 2.2 (B) outlines the discharging/charging rates and ambient and maximum temperature seen in the research.

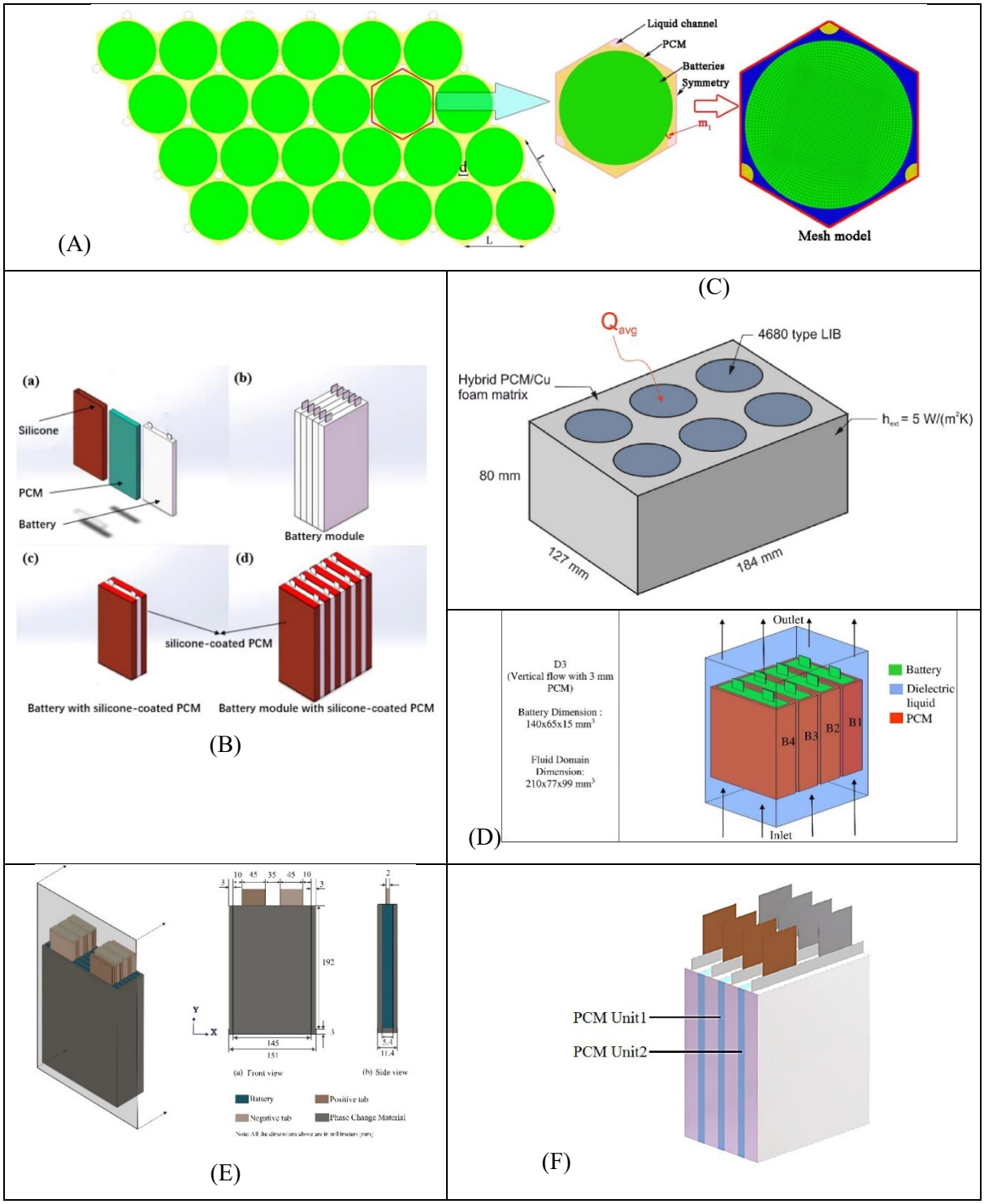

Fig. 2.26 Schematics of PCM-based cooling for modules proposed by A) (Chen et al., 2022), B) (Wang et al., 2021a), C) (Kolodziejczyk et al., 2021), D) (Amalesh et al., 2022), E) (Hussain et al., 2023), F) (Wang et al., 202021b).

The studies also analysed whether continuous discharging/recharging processes were completed including drive cycle modelling.

Table 2.2A. Summary of work conducted for the module model BTMS (materials).

Serial	Authors	Modelling	Cell type	Battery Chemistry	Capacity Ah	# of cells/module	Cooling method	IF PCM - Type/Melting Temp/Pure
1	Hussain et al., 2023	NTGK	Pouch	LMO	14.6	1 and 6	Pure PCM	N-octadecane/composite paraffin/RT-58
2	Talele et al. 2021	ECM	Cylindrical	Lithium-ion (LiCoO2/Graphite)	20.8	60	active and passive cooling (paraffin wax and RT-18 PCM)	paraffin wax and RT-18 PCM
3	Akbarzadeh et al., 2021	ANSYS	Prismatic	NMC	43	12	liquid cooling plate/PCM	paraffin graphite composite
4	Akbarzadeh et al., 2022	ANSYS	Prismatic	NMC	43	12	liquid cooling plate/PCM	paraffin graphite composite
5	Al-Zareer et al., 2019	COMSOL	Prismatic	Lithium-ion		12	cold plate/propane, ammonia, R134a refrigerants (liquid to vapour)	
6	Al-Zareer et al., 2018a	COMSOL	Prismatic	Lithium-ion		12	cold plate/propane, ammonia, R134a refrigerants (liquid to vapour)	
7	Al-Zareer et al., 2018b	COMSOL	Cylindrical	Lithium-ion	1	12	PCM (liquid to vapour)	R134a
8	Al-Zareer et al., 2020	COMSOL	Cylindrical	Lithium-ion	1	12	PCM (liquid to vapour)	R134a
9	Al-Zareer et al., 2019	COMSOL	Cylindrical	Lithium-ion	1	12	PCM (liquid to vapour)	R134a
10	Amalesh et al., 2022	ANSYS	Prismatic	Lithium-ion	10	4	PCM	RT35
11	Bamdezh, et al., 2020	ANSYS	Cylindrical	Lithium-ion (LiCoO2/Graphite)		6	PCM	RT27
12	Cao et al., 2022	ANSYS	Cylindrical	Lithium-ion		10	PCM	cPCM
13	Chen et al., 2022	ANSYS	Cylindrical	Lithium-ion	3	24	hybrid cPCM and cooling channel	cPCM (paraffin RT44HC and graphite)
14	Choudhari et al., 2021	ANSYS	Cylindrical	Lithium ion	2.2	25	PCM and fins	paraffin RT44HC
15	Coleman et al., 2016	ANSYS	Cylindrical	generic	30	4	PCM and liquid cooling/cell-cell spacing	liquid wax
16	Hekmat et al., 2022	ANSYS	Prismatic	Lithium-ion	5.5	5	cooling channels and PCM	
17	Jiang et al., 2022	COMSOL	Cylindrical	Lithium-ion		9	alumina/water nanofluids and PCM	N-octadecane
18	Kadam et al., 2023	ANSYS	Cylindrical	Lithium-ion		12	graphene nanoparticles and PCM	RT58 (331K)
19	Khateeb et al., 2004		Cylindrical	Lithium-ion	2	9	Al foam/fins and PCM	paraffin wax (40-44°C)

20	Kolodziejczyk et al., 2021	COMSOL	Cylindrical	Lithium-ion		6	PCM composite	paraffin wax (41-49°C)
21	Lazrak et al., 2018	ANSYS	Cylindrical	Lithium-ion		15	PCM and metal foam	
22	Wang et al., 2021a	COMSOL	Pouch	Lithium-ion	16	5	PCM	
23	Wang et al., 2021b	ANSYS	Pouch	Lithium-ion	10	4	PCM	
24	Mousavi et al., 2021	ANSYS	Prismatic	Lithium-ion		5	PCM and mini channel cool plates	n-eicosane
25	Mousavi et al., 2023	ANSYS	Prismatic	Lithium-ion		4	PCM and mini channel cool plates	

Table 2.2B. Summary of work conducted for the module model BTMS (conditions).

Serial	**Authors**	**C rate**	**Consecutive cycling (100% - 0%)**	**Drive Cycle**	**Single charge/discharge**	**Ambient Temp C**	**Max Temp C**
1	Hussain et al., 2023	1C-5C	No	No	Discharging	26.85	60
2	Talele et al. 2021	1C, 1.5C, 2C	No	Yes	Discharging	x	56-59
3	Akbarzadeh et al., 2021		No	Yes	Discharging	25	60
4	Akbarzadeh et al., 2022		No	Yes	Discharging	25	60
5	Al-Zareer et al., 2019	6C	No	Yes	Yes	25	45
6	Al-Zareer et al., 2018a	1C-6C, 7.5C	Yes	No	Yes	25	49
7	Al-Zareer et al., 2018b	5C	Yes	Yes	Yes	25	35.5
8	Al-Zareer et al., 2020	6C, 7C, 8C	Yes	Yes	Yes	25	35.5
9	Al-Zareer et al., 2019	4C,5C,6C	Yes	No	Yes	25	40
10	Amalesh et al., 2022	8C	No	No	Charging	30	60
11	Bamdezh, et al., 2020	3C	No	No	Discharging	20	40.85
12	Cao et al., 2022	1C	No	No	Discharging	25	58
13	Chen et al., 2022	1C, 4C	Yes	No	Yes	35	60
14	Choudhari et al., 2021	1C, 2C, 3C	Yes	No	Yes	13	71.85
15	Coleman et al., 2016		No	No	Discharging	40	118
16	Hekmat et al., 2022	1C, 2C	Yes	No	Discharging	21.85	38.85
17	Jiang et al., 2022	1C	No	No	Discharging	23.85	48.85
18	Kadam et al., 2023	1C, 2C, 3C	Yes	No	Discharging	34.85	60
19	Khateeb et al., 2004	2.4C	No	No	Discharging	20	70
20	Kolodziejczyk et al., 2021	0.1C, 1C, 3C, 4C	No	No	Yes	25	36.85
21	Lazrak et al., 2018	1C	No	No	Discharging	22	48
22	Wang et al., 2021a	1C, 2C, 3C	Yes	No	Discharging	20	64.3
23	Wang et al., 2021b	5C	Yes	No	Discharging	26.85	51.85
24	Mousavi et al., 2021		Yes	No	Discharging	26.85	96.85
25	Mousavi et al., 2023	1C, 2C, 3C	Yes	Yes	Discharging	26.85	76.85

2.4.4. Battery pack-level PCM integration

Research on BTMS which explored heatsinks with fluid channels and multiple PCMs (Mohammad et al., 2023) revealed that increasing the PCM thickness significantly reduced the battery temperatures while liquid cooling outperformed air cooling, especially at high temperatures. Moreover, a denser stack enhances the cooling efficiency. The enhancement of thermal management of Li-ion batteries used in solar vehicles was studied (Moraga et al., 2016) to enhance the efficiency using seven different configurations of PCMs for their effectiveness in reducing the battery temperatures during discharge rates. The results indicated that heat conduction primarily influences battery cooling when PCMs are employed, with PCM melting occurring within minutes. Two configurations, one with multiple PCMs and another with a single layer of PCM, significantly reduced the maximum battery temperatures by approximately 20.9 °C and 23.2 °C compared to the non-PCM battery. Other factors mentioned of importance of the PCM selection and positioning for efficient thermal management in solar racing cars, where space, weight, and aerodynamics are critical factors.

Research as seen in their work (Patel et al., 2022) focused on selecting the most suitable PCM for BTMS with a consideration of various charging rates and ambient temperatures. The study evaluated critical parameters like maximum battery temperature and maximum temperature difference using PCM for ambient temperature over charging rate with RT42 and RT50 and found the most effective for keeping the battery below 60 °C in various conditions. It was also noted that high melting temperatures, significantly above or below ambient temperature were less effective for battery performance. A comprehensive electrochemical-thermal model, using FEA analysis to evaluate the performance of BTMS using nano-encapsulated PCM slurry cooling for Li-ion battery packs was studied as seen in their work (Qaderi et al., 2023). Experimental validation and the NN model were used for analysis with key factors including Reynold's number for low ambient convective heat transfer and ambient temperature close to solidus temperature. Results showed close agreement with the optimisation outcomes. The application of 1-Tetradecanol as a PCM in a BTMS for EV using LiFePO4 batteries using ANSYS CFD (Rajan et al., 2022) to investigate the PCM's behaviour during its melting process within a cylindrical enclosure and determine the effectiveness in maintaining battery temperatures within acceptable ranges was studied. Copper foam was used to enhance the thermal conductivity of the PCM with the results showing an indication that there was a significant reduction in battery temperature rise, especially with the addition of the copper foam. The study suggests that this PCM-based system was well suited for EVs, particularly during high heat generation scenarios and the importance of spatial arrangement and PCM placement.

Research into three hybrid BTMS configurations using PCM, and air coolant was studied (Safdari et al., 2020) for circular, rectangular, and hexagonal PCM vessels containing 12 Sony battery cells to assess the thermal performance across various charging and discharging rates. The results highlight the circular PCM configuration's overall effectiveness due to efficient Latent heat use. However, the rectangular design with uniform air channels proved superior in high-rate charging or discharging conditions. The research emphasises the impact of PCM vessel shape on BTMS efficiency with factors such as battery temperature and PCM liquid fraction. An approach to extending the lifespan of outdoor base station standby batteries using semiconductor thermoelectric devices and PCMs coupled BTMS was researched (Song et al., 2018) using a 3D model battery pack. The results indicate that arranging the semiconductor thermoelectric devices on two flanks in the smallest size direction enhances temperature uniformity and heat preservation. The method kept the battery within the optimal temperature range even during discharging and charging processes.

As seen in their work (Verma et al., 2022), a passive cooling solution which combines PCM with longitudinal rectangular fins was investigated with different PCM thicknesses and fin lengths to enhance performance. Key findings revealed that the cooling system equipped with fins significantly reduced the battery pack temperature depending on the PCM thickness. The use of fins improved the temperature uniformity and extended the active time window of the PCM melting-solidification cycle. The combination of PCM and fins to control temperature, especially in hot climates was investigated (Verma et al., 2022). Various configurations were analysed and revealed that the operation of PCM and fins, with specific mass and length ratios achieved a cooling effect.

A hybrid liquid cooling plate system combined with Z-type parallel cooling channels with PCM, and aluminium foam composites was studied (Yang et al., 2023) for nine plate designs including one without PCM. The results demonstrated that the optimum hybrid design significantly reduced the power consumption while maintaining proper cooling performance, particularly at lower discharging rates. In a study on the issue of thermal runaway propagation in power battery packs for EVs, traditional methods to inhibit heat propagation often involve heat insulation materials or increased battery spacing. In response to this, a study (Zhang et al., 2022) introduced using non-uniform thermal conductivity PCMs alongside liquid cooling. By strategically combining high and low thermal conductivity PCM, the system showed balance in heat transfer and insulation. The numerical analysis demonstrated that this approach effectively managed the heat dissipation during normal operation and restricted thermal runaway within a safe range and along a defined path. Increased thermal conductivity aids heat dissipation but accelerates thermal runaway spread, while decreased conductivity mitigates propagation but may reduce overall heat dissipation.

Figure 2.27 illustrates battery pack-level PCM integration for the orientation and location of the PCM for different cell types seen in research.

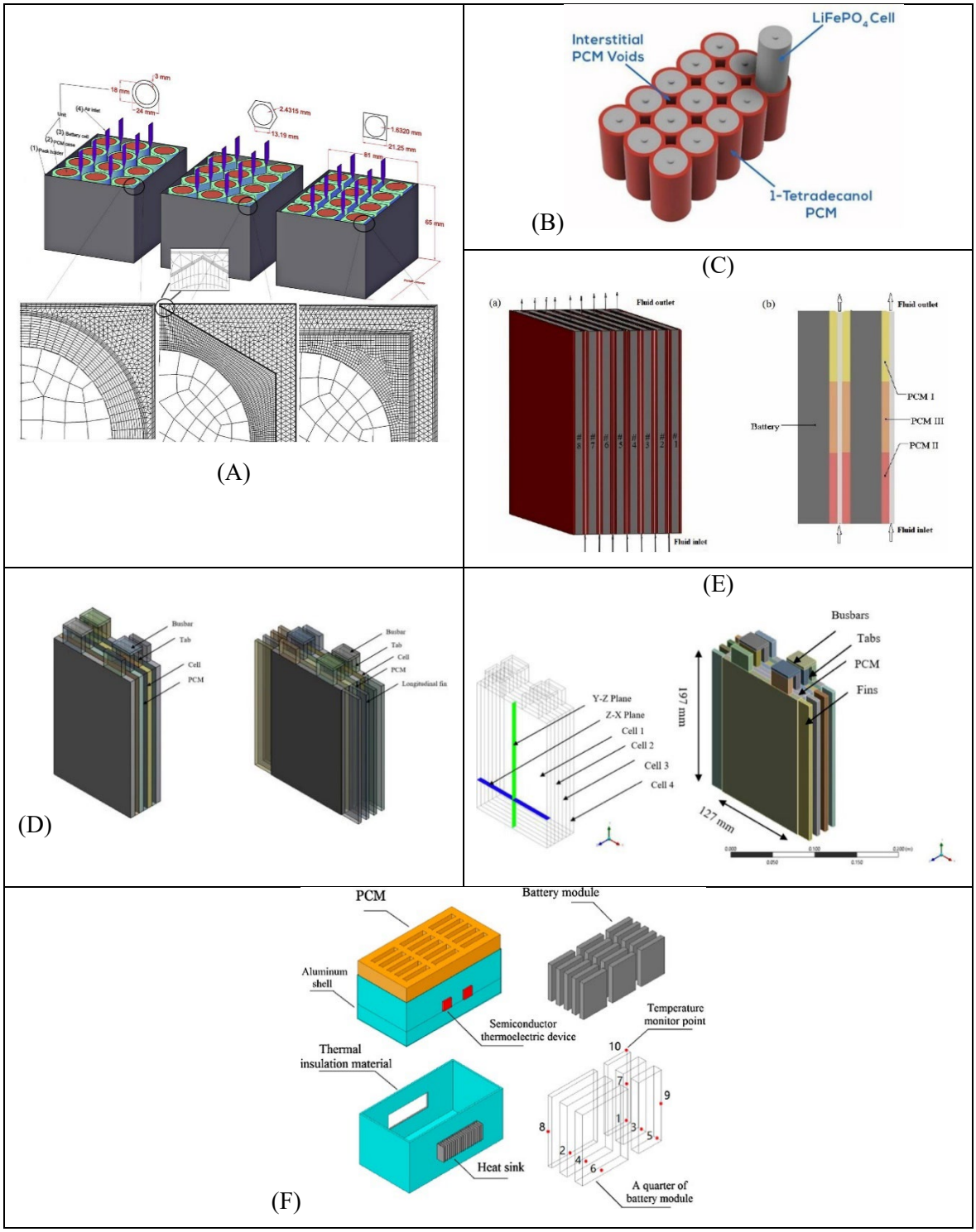

Fig. 2.27 Schematics of PCM-based cooling for packs proposed by A) (Safdari et al., 2020), B) (Rajan et al., 2022), C) (Mohammed et al., 2023), D) (Verma et al., 2022a), E) (Verma et al., 2022b), F) (Song et al., 2018).

A summary of the pack PCM-based thermal management systems for pure and enhanced PCM designs, including numerical modelling, cell types, battery chemistry and cooling method, is presented in Table 2.3 (A). An additional supplementary Table 2.3 (B) outlines the discharging/charging rates and ambient and maximum temperature seen in the research. The studies also analysed whether continuous discharging/charging processes were completed, including drive cycle modelling. Additionally, the study highlighted the importance of choosing PCMs with melting temperatures that align closely with ambient conditions for optimal battery performance. These insights collectively contribute to the ongoing advancement of BTMS strategies for diverse applications, especially in the realm of solar racing cars, where space, weight and aerodynamics are paramount considerations.

Table 2.3A. Summary of work conducted for the single pack model BTMS (materials).

Serial	Authors	Modelling	Cell type	Battery Chemistry	Capacity Ah	# of cells/modules	Cooling method	IF PCM - Type/Melting Temp/Pure
1	Mohammed et al., 2023	ANSYS	Prismatic	Lithium-ion	15	8	air, silicon oil, ethylene-glycol, water, PCM	
2	Moraga et al., 2016	ANSYS		Lithium-ion		6	PCM	capric acid, eicosane, decahydrate sodium carbonate
3	Patel et al., 2022	ANSYS	Cylindrical	Lithium-ion	2.4	25	PCM	RT21, RT24, RT31, RT42, RT50
4	Qaderi et al., 2023	COMSOL	Cylindrical	Lithium-ion	1.5		Water Nano-encapsulated PCM slurry	
5	Rajan et al., 2022	ANSYS	Cylindrical	LiFePO4	18	45	PCM	1-Tetradecanol
6	Safdari et al., 2020	ANSYS	Cylindrical	Lithium ion	1.8	12	PCM and air	
7	Song et al., 2018	ANSYS	Prismatic	Lithium-ion	80	60	PCM	
8	Verma et al., 2022a	ANSYS	Pouch	LiFePO4	20	4	Fins and PCM	
9	Verma et al., 2022b	ANSYS	Pouch	LiFePO4	20	4	Fins and PCM	
10	Yang et al., 2023	ANSYS	Prismatic	Lithium-ion	45	21	PCM aluminium foam composite and liquid routing	Paraffin wax, RT35
11	Zhang et al., 2022	COMSOL	Cylindrical	Lithium-ion	3.3	15	PCM and liquid cooling	

Table 2.3B. Summary of work conducted for the single pack model BTMS (conditions).

Serial	Authors	C rate	Consecutive cycling (100% - 0%)	Drive Cycle	Single charge/discharge	Ambient Temp C	Max Temp C
1	Mohammed et al., 2023	5C	No	No	Discharging	26.85	41.85
2	Moraga et al., 2016		Yes	No	Discharging	21	84.65
3	Patel et al., 2022	1C, 2C, 3C 0.2C	Yes	No	Discharging	30 26.2	60
4	Qaderi et al., 2023	1C, 2C	Yes	No	Discharging	30.85	46.85
5	Rajan et al., 2022	2C	Yes	No	Discharging	25	70
6	Safdari et al., 2020						
7	Song et al., 2018		Yes	No	Discharging	19.85	49.85
8	Verma et al., 2022a		Yes	No	Discharging	40	79.85
9	Verma et al., 2022b	3C	Yes	No	Discharging	40	79.85
10	Yang et al., 2023	1C, 2C, 3C	Yes	No	Discharging	25	70
11	Zhang et al., 2022	3C	Yes	No	Discharging	25	300

2.5 Concise overview and forward-looking view

2.5.1 Concise overview

The comprehensive review assessed, passive-based cooling systems have emerged as a promising solution for efficient battery thermal management in various applications, including EVs and renewable energy storage. This approach leverages materials like PCMs and innovative design strategies to maintain optimal battery temperatures without active cooling mechanisms like fans or pumps. Through extensive numerical simulations, researchers have explored and refined these passive cooling systems, offering insights into their benefits and drawbacks.

Benefits of Passive-based cooling:

- Enhanced safety: Passive cooling systems significantly reduce the risk of thermal runaway in Li-ion batteries. By using PCMS with phase change properties, they can absorb and dissipate excess heat, preventing temperature spikes that can lead to catastrophic failures.
- Energy Efficiency: Unlike active cooling systems that consume additional energy, passive cooling is energy-efficient. It relies on the natural thermal properties of materials, minimising the overall power consumption of the system.
- Reduced weight and complexity: Passive cooling designs are typically lightweight and straightforward in construction. They do not require bulky cooling equipment like radiators or pumps, making them ideal for applications where weight and space are at a premium, such as EVs.

- Maintenance-Free: Passive cooling systems have fewer moving parts, which translates to lower maintenance requirements and longer service life. This can result in cost savings over the lifetime of the battery system.
- Environmental friendliness: The absence of active cooling components reduces the environmental footprint of battery systems. This aligns with the growing emphasis on suitable energy solutions.

Drawbacks of Passive-based cooling:

- Limited cooling capacity: Passive systems may struggle to manage high heat loads or rapid temperature changes, limiting their applicability in demanding scenarios.
- Design complexity: Developing effective passive cooling solutions often requires intricate design considerations and material selection, which can be complex and time-consuming.
- Lack of control: Passive systems have limited control over thermal conditions, especially in dynamic environments where temperature fluctuations are frequent.
- Size constraints: The space required for efficient passive cooling can be substantial, potentially limiting its use in compact devices.
- Heat dissipation challenges: In different applications, passive cooling alone may not provide sufficient heat dissipation, necessitating the integration of active cooling elements.

Benefits of Numerical simulations:

- Cost-efficiency: Numerical simulations are often more cost-effective than conducting physical experiments, especially when testing diverse design iterations.
- Rapid prototyping: Simulations enable rapid prototyping and evaluation of different cooling configurations, accelerating the design process.
- Parametric studies: Researchers can perform parametric studies to explore a wide range of scenarios, helping to identify optimal designs and configurations.
- Data insights: Simulations provide valuable insights into heat transfer, temperature distribution, and system performance under various conditions.
- Risk mitigation: Simulations allow for the assessment of system behaviour and performance without the need for physical prototypes, reducing development risks.

Drawbacks of numerical simulations:

- Limited accuracy: Simulations may not always perfectly represent real-world conditions due to assumptions, approximations, and variations in material properties.
- Complexity and computational demands: Modelling complex heat transfer processes can be computationally intensive and time-consuming, requiring substantial computational resources.
- Data requirements: Accurate simulations depend on precise material property data, which may not always be readily available.
- Validation challenges: Ensuring simulation results align with physical reality often requires extensive experimental validations, adding complexity to the research process.
- Overlooking real-world complexity: Simulations may oversimplify real-world complexities, such as transient effects or environmental variability, potentially leading to discrepancies between simulations and actual performance.

2.5.2 Forward-looking view

The integration of passive-based cooling systems into various battery applications holds great promise. As the demand for efficient and safe energy storage solutions continues to grow, these systems can play a pivotal role. However, there are key areas that require attention and further research:

- Experimental validation: While numerical simulations provide valuable insights, it is essential to validate these findings through extensive experimentation. Real-world testing can confirm the accuracy of simulation models and their ability to predict performance accurately.
- Material development: The development of advanced PCMs with tailored properties is a critical area of research. PCMs with improved thermal conductivities, Latent heat capacities, and phase change temperatures can enhance the effectiveness of passive cooling systems.
- Optimised designs: Researchers should continue to explore innovative design configurations that maximise the benefits of passive cooling. This includes optimising the arrangement of PCMs, the use of heat exchangers, and novel materials.
- Scalability: Passive cooling systems must be scalable to suit various applications, from small electronic devices to large-scale energy storage systems, Researchers should focus on designing solutions that are adaptable across different sizes and power requirements.

- Integration with active systems: In scenarios, combining passive and active cooling mechanisms may offer the best results. Research should explore hybrid systems that leverage both approaches to provide optimal thermal management.

In conclusion, passive-based cooling systems, supported by numerical simulations, offer a compelling solution to the thermal management challenges of modern energy storage systems. While simulations are valuable tools for initial design and assessment, they must be validated through experimentation. Continued research and innovation in materials, design, and scalability will further enhance the efficacy of passive cooling systems, contributing to the growth of sustainable energy technologies and safer, more efficient battery systems for a wide range of applications.

2.6 Chapter summary

This literature review Chapter has assessed a substantial body of research about TES, emphasising the various types of energy storage mechanisms, with a particular focus on LHS. A comprehensive analysis of PCMs was conducted, encompassing diverse types, designs, and applications. Furthermore, the integration of EES devices with TES was scrutinised, evaluating the feasibility of different integration methods. The chapter strategically directed its attention to the objectives delineated in this thesis, aligning with the reviewed literature in pursuit of milestones 1, 2, and 3. The discourse within this Chapter not only reviews literature relevant to these milestones but also lays the groundwork for the subsequent stages of research, with study Chapters published or submitted for review. Moving forward, Chapter 3 delves into a more detailed examination of TES, focusing specifically on the impact of fin type and orientation of PCM within a double-pipe heat exchanger. It should be noted that the Chapter has been published as seen in the list of publications based on heat transfer improvement to a specific PCM during melting and solidification.

CHAPTER 3: IMPACT OF FIN TYPE AND ORIENTATION ON PERFORMANCE OF PHASE CHANGE MATERIAL-BASED DOUBLE PIPE THERMAL ENERGY STORAGE[1][2]

3.1 Chapter Brief

This Chapter builds upon the critical review of TES and EES integration presented in the preceding Chapter 2. While the previous Chapter 2 extensively explored the broad landscapes of TES, including LHS, PCMs, and their varied applications, this Chapter 3 focuses on addressing a specific challenge within PCM materials, their inherently low thermal conductivity. The aim revolves around enhancing the thermal performance of PCMs through the strategic incorporation of highly thermally conductive materials and the introduction of structurally formed fins. These fins, classified as either flat or corrugated and arranged longitudinally or transversally, aim to improve natural convection heat transfer during PCM melting. The Chapter employs a comprehensive numerical study, encompassing verification and validation processes based on existing literature. The findings, which highlight the considerable impact of fin type and orientation on PCM thermal performance, have been disseminated through a journal article and conference presentations, as documented in the Publications section of this Thesis.

3.1.1 Introduction

A combination of high energy density in a constant temperature process (Sardari and Bahai et al., 2020 and Sharma et al., 2009) describes the Latent heat storage (LHS) technology as opposed to Sensible heat storage (SHS) where the temperature of the material changes with time. One major disadvantage of (LHS), is the property of low thermal conductivity in phase change materials (PCMs) as outlined in Sharma et al., 2009). This property affects the thermal equilibrium of the system creating an imbalance in thermal energy storage (TES) (Mohamed et al., 2017). To alleviate this process, various

---

[1] **Nicholls**, R.A, Moghimi, M.A., and Griffiths, A.L., Impact of fin type and orientation on performance of phase change material-based double pipe thermal energy storage, *Journal of Energy Storage*, 50, 2022, pp 104671. https://doi.org/10.1016/j.est.2022.104671

[2] **Nicholls**, R.A, Moghimi, M.A., and Griffiths, A.L., A comparative study of corrugated fins during melting of phase change material in a double pipe heat exchanger, *Proceedings of the 17th UK International Heat Transfer Conference*, Manchester, United Kingdom, Paper number 116, April 2022. http://cfd.mace.manchester.ac.uk/ukhtc21-proc/papers/O-12-5.pdf

techniques could be implemented such as extended surfaces, metal matrices and materials added with high thermal conductivity, encapsulation of the PCM as demonstrated in (Liu et al., 2012, Jouhara et al., 2020, Nazir et al., 2019, Rathore et al., 2019 and Deng et al., 2019) as well as different configurations of PCMs and multiple PCM arrangements as described in Liu et al., 2012) and heat pipes. There has been a significant amount of research involving all these methods, this study concentrates on the utilisation of extended surfaces (fins) due to affordability in economic cost and manufacture as well as the added benefits of increased heat transfer surface area, (Deng et al. 2019).

Latent heat storage technology is used to improve the system energy storage capabilities by storing the thermal energy in the form of a charging or melting process and releasing that stored energy in the form of a discharging or solidification process, (Jouhara et al., 2020), also dependant on geometric container designs (Zayed et al., 2020). A fast or shorter melting time that would absorb the thermal energy followed by a delayed or longer solidification time would be ideal for any TES applications considering PCM melting temperature and applied heating, (Mekrisuh et al. 2020). Previous studies have analysed the effects of natural convection (Nemati et al., 2020) in the upper region of LHS devices, showing that conduction is the main heat transfer mechanism in the lower region. An effective use of coupling the two modes of heat transfer can improve the performance of the LHS device.

A study performed by (Cao et al., 2018) investigated the impacts of natural convection on the PCM melting efficiency of an eccentric horizontal DPHX. Their study revealed that natural convection for the experiments of melting and solidification significantly impacted the melting method. A further analysis investigating the effect of natural convection by (Joybari et al., 2017-2019), evaluated a front-tracking method for the pure conduction and combined conduction-convection cases. As for the pure conduction case, natural convection is inherently ignored which produces melting fronts in a circular pattern radiating outwards from the inner tube. This method, however, contradicts the buoyancy effects because of density variations. Further studies on the effects of natural convection on melting and solidification were conducted (Yadav et al., 2020), (Soliman et al., 2021), and (Mahdi et al., 2019). Their results showed a reduction in the melting time when natural convection was considered for the initial majority conduction heat transfer followed by convection. Vortices generated because of natural convection once interacted with the majority of PCM can improve the melting performance. When designs were inserted that impeded natural convection, the melting performance decreased. Studies involving eccentricity and thermal improvement for PCM charging and discharging were conducted by (Darzi et al., 2012), (Dhaidan et al., 2013) and (Kadivar et al., 2019) which investigated natural convection in the upper region of containers.

Finned PCM materials have been used in a variety of different containments, positions and orientations as seen in (Kalapala et al., 2021), (Rathod et al., 2015), (Mahdi et al., 2019), (Gurturk et al., 2020), (Yagci et al., 2019), (Siyabi et al., 2019), (Kousha et al., 2017), (Seddegh et al., 2016) and (Seddegh et al., 2015). Results showed that the orientation influenced the liquidus temperature, specifically when the LHS system was oriented in the horizontal position and approximately 40 % improvement in charging and solidification of the PCM with fins. It was seen that the horizontal orientation for the non-finned tube showed better performance than the vertical orientation. However, when the fins were added in both scenarios, the orientation of the tubes did not severely impact the outcome of the results. A numerical study by (Tian et al., 2020) investigated the effects of fin materials including copper, aluminium, carbon steel and steel-302 for a container compared with no fins. It was shown that there was a reduction in melting time of up to 41 % for the copper and aluminium materials and the highest energy storage in the steel302 material.

In research conducted by (Sharifi et al., 2011), the impact of horizontal fins on three different physical properties including the fin number, thickness and length was investigated. The effect of natural convection was considered in the melting process compared with no fins added to the PCM. Results indicated that fast melting preceded slow melting affected by the addition of fins. An experimental analysis performed by (Kamkari et al., 2014) also investigated the effects of PCM melting for rectangular fins horizontally and partially constructed. Their results showed improved melting performance for the systems with fins, however, the rate of heat transfer was reduced as the number of fins increased, and this brought about a reduction in the convection currents. (Arici et al., 2020) investigated the effects of rectangular fin lengths and positions investigated for PCM melting performance, they showed that there was a reduction in melting time with the addition of fins of up to 50 %. For the location of the fin, the Liquid Fraction varied up to a 40 % increase for the side heating and up to 68 % increase for the bottom heating compared to the unfinned Case. Further studies on fin length, number and thickness have been studied for PCM melting and solidification as seen in (Joshi et al., 2019), (Qin et al., 2017), (Biwole et al., 2018), (Shahsavar et al., 2020), (Darzi et al., 2016) and (Pu et al., 2020) with natural convection heat transfer considered for finned and unfinned Cases. Results showed negligible effects on the melting performance for reduced fin lengths at the top of the container as there was a reduction in temperature uniformity and a rise in heat transfer with increasing fin number. There was also a reduction in melting for larger diameter fins until a threshold where any increase in the diameter, negatively affected the results. The fins placed closer together near the bottom of the HE had the best charging results. The studies which compared uniform and non-uniform arrangements, (Yu et al., 2020), identified in agreement with previous studies, that fin location can improve the efficiency of the LHS device by improving the net heat transfer. Increases in fin size such as the diameter should

be investigated accordingly as this may reduce the performance by inhibiting natural convection currents.

Considerations towards axial and co-axial fin arrangements have also been reviewed for their effects on natural convection as seen in their studies (Jmal et al., 2015), (Al-Abidi et al., 2013), (Mahdi et al., 2018), (Yuan et al., 2016), (Tang et al., 2021), (Nie et al., 2020) and (Marri et al., 2020). These are particularly useful in PCM solidification, regardless of orientation as they improve the heat transfer mechanism, especially in the case of uneven distributions. The number of fins was varied and analysed for the solidification rate of the PCM which showed as the fin number increased, the solidification time was negatively impacted due to restrictions of convective flow. The results of solidification showed that the full-length longitudinal fin design had the best solidification time. A reduction in the fin thickness and increase in length showed better results as compared with other cases. (Sarani et al., 2020) investigated the solidification process and energy storage for a triplex tube heat exchanger (TTHE) where partial fins were compared with full fin arrangement and with varying fin numbers. Their conclusions showed that the partial fins improved the solidification time as compared to the full fin arrangement. In their research, (Abdulateef et al., 2017) examined a horizontal TTHE with PCM including longitudinal fins and triangular fins attached to the inner tube. The triangular fin arrangements outperformed the longitudinal fin arrangements, with the external triangular fins performing the best for the charging process. Further to this, (Nemati et al., 2020) investigated the effect of elliptical horizontal annular fins and the effect of natural convection for vertical and horizontal arrangement showing that the fin spacing is an important consideration for performance. (Hosseini et al., 2015) investigated the PCM melting performance in a horizontal DPHX with longitudinal fins at varied lengths and Stefan numbers. Their results showed that the higher the Stefan number, the better the melting performance by increased vortex production, until it does not affect the melting rate. It was also concluded that the length of the fins proved more effective than increasing the Stefan number, with the drawback of higher economic costs. Research concerned with the variation of fin numbers in a horizontal DPHX with varying wall fluxes and Nusselt numbers was performed in their study (Cao et al., 2018). The higher number of fins reduced the melting time, however, as the fin number increases, the efficiency reduces, and the melting time starts to increase. A study on wall boundary conditions and fin number for constant wall temperature and constant heat flux by (Ye et al., 2018) showed that constant wall temperature was more considerable for melting but limited in the solidification stage.

(Kazemi et al., 2018) analysed the effects of longitudinal fin angle in a horizontal triplex tube heat (HTTE) exchanger. Their analysis showed that a 60 °C angle between the triple fin arrangement, proved the best results for melting efficiency, with the lowest melting time than the other arrangements, while for the double fin, a 45 °C angle had the best results. (Deng et al., 2019) also investigated the

effects of varying double fin angles in a concentric shell and tube heat exchanger (STHE) showing improvement in fin angle and length for an improvement in melting performance. Research conducted by (Khan et al., 2020) investigated the impact on buoyancy, energy storage, and the charging process of partial longitudinal fins at varying angles for a horizontal DPHX. Their results showed that the Y-fin orientation with a single fin in the lower region proved the best results for melting time as compared with a single fin in the upper region. Even though fin angle is an important aspect in the improvement of the heat transfer process, this was not inherently studied in this paper, as symmetrical vertical double fins in a horizontal container were sufficient to perform the analysis for the effect on performance. Further research can be conducted on varying the angles and number of the corrugated fins in future studies.

In research highlighted, the shape of the fins as well as positioning can play a vital role in the heat transfer process to either aid or reduce the efficiency. Many studies have analysed the variation of fin shape and location with a consistency of comparing novel shapes with basic shape structures, such as flat fin designs, to identify whether there is any significant improvement to the melting/solidification rate or energy storage. Additionally, there have been studies performed investigating the shape of the fin from a unique perspective. These studies analysed the effects of specially designed fins and include a combination fin (triangular and rectangular) (Gurturk et al., 2020), snowflake fin (Sheikholeslami et al., 2016), longitudinal-triangular fin (Liu et al., 2019), Y-shaped fin (Keshteli et al., 2020), and spider web fins (Qaiser et al., 2021). Their results showed that the partial rectangular fin performed the best concerning the others with reduced solidification time in the order of the snowflake fins, longitudinal fins, and no fin systems. It is noteworthy that the addition of fins improved the thermal conductivity of the LHS devices by around 40 % as identified by other studies previously for the charging process and more than 40 % improvement in the solidification compared to flat fins. (Duan et al., 2020) investigated the effects of varying fin numbers and spiral fins with varying degrees of pitch compared with the flat fins design. Results showed that smaller spiral fin numbers improved the heat transfer process. (Aly et al., 2019) studied the impact on the solidification rate for differently shaped fins (varying corrugation) compared with flat fins for a concentric DPHX. Results showed plots of solidification rates and contours of Liquid Fraction with a reduction of about 30 % in solidification rate. The time for solidification reduced as the fin height increased. It was also seen that an increase in the number of wavelengths negatively impacted the efficiency.

Charging and discharging processes of TES equipped with corrugated fins either longitudinally or transversally as well as transversal flat fins have not previously been studied to the author's best knowledge. This study builds upon previous knowledge to further investigate the improvement of the LHS systems by using differently shaped fins and orientations added to a horizontal DPHX. The PCM

in the annular space is subjected to both the charging and discharging processes, inclusive of five different Cases (A - E) as displayed in Figure 3.1, which are analysed. This study evaluates a comprehensive understanding of fin orientations and types of charging and discharging processes for a DPHX. These fin models and orientations were simulated to understand the best improvement in the thermal conductivity of the PCM and to improve the heat transfer of TES. The structure of this investigation is as follows: initially the model description is presented, including mathematical modelling, assumptions, and boundary and initial conditions. This section is followed by validation and verifications including grid, temporal, and mushy zone independency analysis. The charging and discharging processes of TES results and a discussion comparing all five tests' Cases (unfinned, longitudinal flat fins, longitudinal corrugated fins, transversal flat fins, and transversal corrugated fins) are presented. Finally, the study concludes by summarising the most important findings of the research.

3.2 Numerical method

3.2.1 Model

Case A builds upon the validation process as per (Darzi et al., 2012) and (Kadivar et al., 2019) in which the PCM was placed in the annular space, subjected to a constant temperature from the inner cylinder, and the outer cylinder was adiabatic, with the physical and computational domain seen in Figure 3.1. A symmetrical design was considered to reduce the computational effort as well as disregard the thickness of the inner and outer cylinder walls. Unlike Case A, also referred to as the base Case in this study, all the other Cases shown in Figure 3.1 have the addition of fins to improve the thermal conductivity of the PCM and to enhance the heat transfer process, as this method can be found in the literature with Cases similarly defined.

To investigate the performance of the corrugated fin design, flat fins were compared in this analysis. For the horizontal DPHX, the fins were placed longitudinally and transversally in separate Cases which involved 2D and 3D computational domains. For Case B, 2 longitudinal flat fins were each placed on the top and bottom of the heat exchanger which was also symmetrically constrained as seen in Figure 3.1. For Case C, 2 longitudinal corrugated fins were placed in the same positions as in Case B to make a valid comparison between them. In Case D, transversal flat fins were added to the design to analyse the variation in fin position to determine their performance seen in Figure 3.1. A 3D computational domain was considered to observe both the charging and discharging process for the transversal finned Cases more easily. Symmetry was also applied to reduce the computational time for the more complex Cases. For the final Case, Case E, transversal corrugated fins were added to the

domain as in Case D with the exact cross-section design parameters as in the longitudinal Case. All 5 Cases were then numerically evaluated using commercial CFD software concerning their performance of Liquid Fraction melting time, temperature and streamlines to investigate their performances.

The cross-sectional view of the concentric horizontal DPHX (Case A) shown in Figure 3.1 had an outer diameter of 40 mm, and the inner diameter was set to 21.5 mm. The thickness of the inner and outer walls of the domain was overlooked due to the high thermal conductivity of the metallic shell. In addition to this study, only one-half was used due to the geometry symmetry condition to reduce the computational effort. A constant temperature was imposed on the inner tube wall while the outer wall was insulated. The annular space was filled with PCM N-eicosane. It's noteworthy that the PCM was subcooled by 1K before initialisation. An enthalpy-porosity model was used to evaluate the charging and discharging process of the PCM.

To evaluate the impact of corrugated and flat fin designs, these fins in longitudinal and transversal orientations were added to the base design (see Figure 3.1) in each of the separate Cases. For the transversal cases, the flat fins and corrugated fins are placed on similar sides of the design. Moreover, to reduce the computational burden, longitudinal Cases and the unfinned Cases were numerically modelled in 2D while transversal Cases were modelled in 3D. To ensure consistency for the charging and discharging processes, the volume of the PCM was kept constant for all Cases, the outer diameter was re-sized, while the inner diameter was unchanged as seen in Table 3.1 showing the dimensions used specifically for the longitudinal Cases.

Table 3.1. Dimensions of the Cases in this study for outer diameter, inner diameter, and fin area.

Dimensions	**Unfinned (Case A)**	**Longitudinal Flat fins (Case B)**	**Longitudinal Corrugated fins (Case C)**	**Transversal Flat fins (Case D)**	**Transversal Corrugated fins (Case E)**
Outer Diameter, (mm) D_o	40	40.76	40.756	40	40
Inner Diameter, (mm) D_i	21.5	21.5	21.5	21.5	21.5
Fin area, (mm^2)	NA	12.052	11.984	1037.5	1433.2

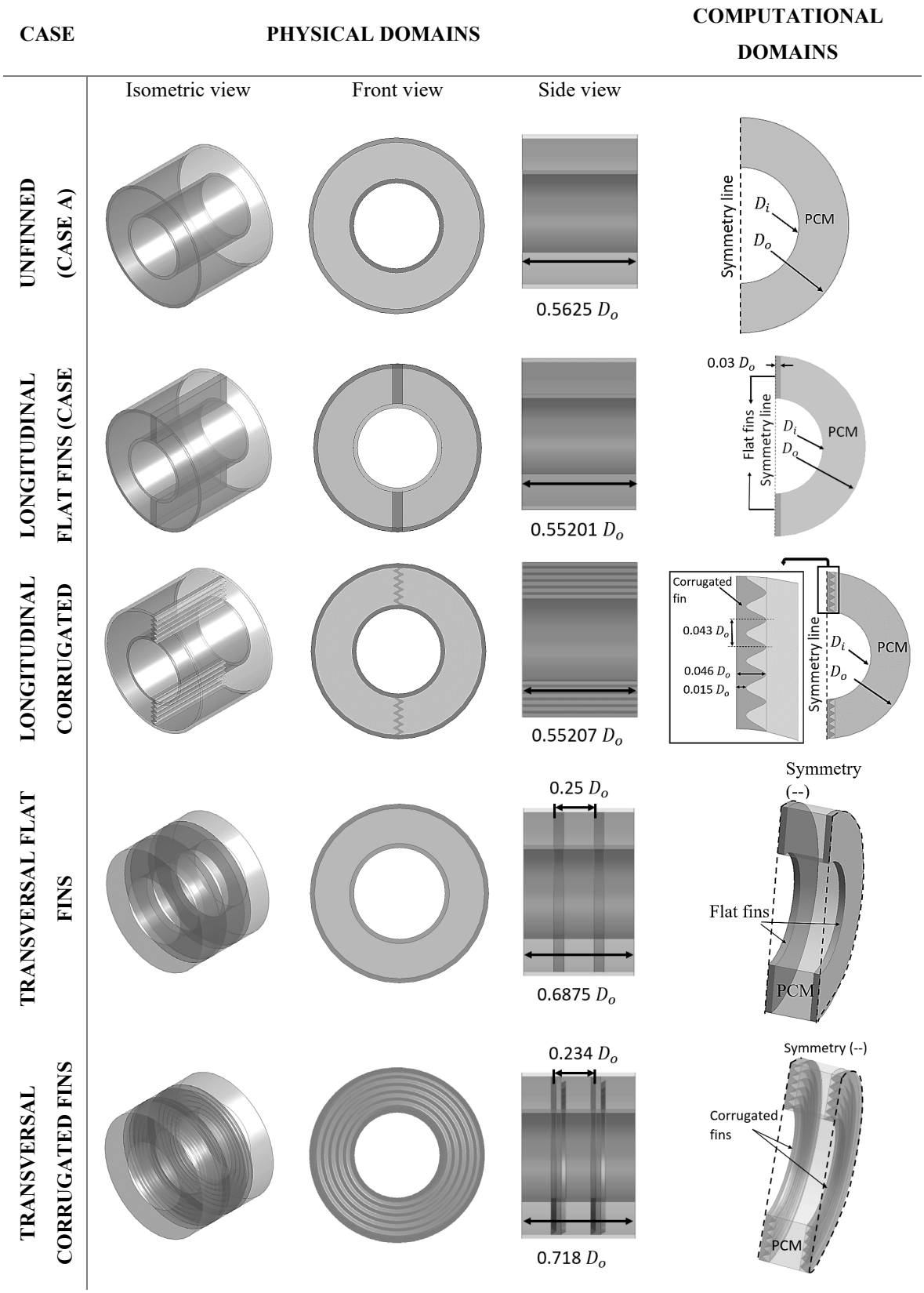

Fig. 3.1 Schematic of symmetrical Cases displaying physical (isometric, front, and side views) and computational domains. Cases A-C were modelled in 2D while Cases D-E were modelled in 3D with figure showing lines of symmetry.

3.2.2 Mathematical and numerical approach

The simulation of the charging and the discharging processes for the design models were performed using ANSYS Fluent 2020 R2, where an enthalpy-porosity technique is used (Voller et al., 1987 and Swaminathan et al., 1992)

For this setup, the cells in the computational domain are explicitly correlated to a quantity known as the Liquid Fraction (Voller et al., 1987). This area represents the liquidus form of the control volume, established from the balance of enthalpy, and evaluated for each iteration. The liquid-solid interface known as the mushy zone is assessed with an equivalency of porosity to Liquid Fraction and considered as the porous zone. ANSYS Fluent applies sink terms to both the momentum and turbulence models to effectively evaluate these changes to the solid areas. The mushy zone is determined as a "pseudo" medium bounded between the values of 0 and 1 with the prior being the solidification and the latter considered when the material has liquified. In this case, the porosity and the velocity are considered null (Brent et al., 1988).

The thermophysical properties of the PCM, walls and fin materials considered for the analysis are listed in Table 3.2.

The energy equation that corresponds is as follows with symbol definition in Nomenclature:

$$\frac{\partial}{\partial t}(\rho H) + \nabla.(\rho \vec{v} H) = \nabla.(k \nabla T) + S \tag{3.1}$$

Where H is derived as follows:

$$H = h + \Delta H \tag{3.2}$$

$$h = h_{ref} + \int_{T_{ref}}^{T} C_p \, dT \tag{3.3}$$

and ΔH is derived as follows:

$$\Delta H = fL \tag{3.4}$$

$$f = \begin{cases} 0 \\ 1 \\ \frac{T - T_{solidus}}{T_{liquidous} - T_{solidus}} \end{cases} ; \begin{cases} T < T_{solidus} \\ T > T_{liquidous} \\ T_{solidus} < T < T_{liquidous} \end{cases} \tag{3.5}$$

S is the source term derived from the momentum sink as follows:

$$S = \frac{(1-f)^2}{(f^3+\varepsilon)} A_{mush} \quad (3.6)$$

ε is a number equal to 0.001, to prevent an invalid result when divided by zero

A_{mush} is the mushy zone constant generally between $10^4 - 10^7$, (Talebizadehsardari et al., 2021); 10^5 was studied for the solidification process while 10^8 was studied for melting process in this analysis (see 3.3.3).

Substituting the Eqs. {3.2}- {3.5} into Eq. {3.1} yields the energy equation as

$$\frac{\partial \rho h}{\partial t} + \nabla.(\rho \vec{v} h) = \nabla.(k \nabla T) - \frac{\partial \rho f L}{\partial t} - \nabla.(\rho \vec{v} f L) + S \quad (3.7)$$

Substituting Eq. (3.6) into (3.7) gives the momentum equation in the following:

$$\frac{\partial \rho \vec{v}}{\partial t} + \nabla.(\rho \vec{v} \vec{v}) = -\nabla P + \nabla.(\mu \nabla \vec{v}) + \rho g + \frac{(1-f)^2}{f^3+\varepsilon} \vec{v} A_{mush} \quad (3.8)$$

With the inclusion of the forces due to gravity, buoyancy-driven flows known as natural convection flows are caused by the deviation in density due to temperature. The natural convection, in this case, occurs within an enclosed domain and so the Boussinesq Approximation is valid to initialise faster convergence for a reference density (constant) and temperature shown in the following equations:

$$(\rho - \rho_0) g \approx -\rho_0 \beta (T - T_0) g \quad (3.9)$$

Which is a valid approximation when

$$\beta (T - T_0) \ll 1 \quad (3.10)$$

Eq. (3.8) can be written over as

$$\frac{\partial \rho_0 \vec{v}}{\partial t} + \nabla.(\rho_0 \vec{v} \vec{v}) = -\nabla P + \nabla.(\mu \nabla \vec{v}) + (\rho - \rho_0) g + \frac{(1-f)^2}{f^3+\varepsilon} \vec{v} A_{mush} \quad (3.11)$$

The governing equation for continuity is as follows:

$$\frac{\partial \rho}{\partial t} + \nabla.(\rho \vec{v}) = 0 \tag{3.12}$$

The non-dimensionless numbers ∇ = DV, $\vec{v} = \frac{\vec{v}D}{\alpha}$, $H = \frac{H}{L}$ and $T = \frac{T - T_s}{L/c_p}$ (3.13)

D = 2 ($R_{out} - R_{in}$), the energy equation for the non-dimensionless terms is as follows:

$$\frac{\partial (H)}{\partial F_o} + \nabla.(\vec{v}H) = \nabla.(\nabla \mathrm{T}) \tag{3.14}$$

where Fourier Number, $F_o = \frac{\alpha t}{D^2}$

Table 3.2 Thermophysical properties of PCM, walls and fin materials. (Darzi et al., 2012, Kadivar et al., 2019 and Al-Abidi et al., 2013).

	PCM (N-eicosane)	**Aluminium (fin)**	**Aluminium (Inner cylinder)**	**Plexiglass (insulation)**
Density (kg/m^3)	770	2719	2719	1190
Cp (Specific Heat) ($J/kg-K$)	2460	871	871	1470
Thermal Conductivity ($W/m-K$)	0.1505	202.4	400	0.19
Viscosity ($kg/m-s$)	0.00385			
Thermal Expansion Coefficient ($1/K$)	0.0009			
Pure Solving Melting Heat (J/kg)	247600			
Solidus Temperature (K)	308.15			
Liquidus Temperature (K)	310.15			

3.2.3 Assumptions

The following assumptions were considered for the numerical models analysed in this study:

- A transient analysis was considered for the charging and discharging processes for the domains under laminar, incompressible, and viscous model flows,
- The thermophysical properties of the materials except density are constant,
- Density variation is estimated under the Boussinesq approximation,
- A pressure-based solver for incompressible flows using the VOF multiphase model was used with the gravity of 9.81 m/s^2 acting in the negative y-direction/axis,
- Viscous dissipation because of larger velocity gradients is ignored,
- The thickness of the inner and outer cylinders is ignored to reduce computational effort.

3.2.4 Initial and boundary conditions

The following represented the conditions to repeat the simulation validation as well as used in the set-up for all Cases. The outer cylinder of the DPHX was adiabatic so no heat losses to the environment were considered. The PCM was initially subcooled by 1K, and a constant temperature of 329.15K was applied to the inner cylinder while the outer cylinder was insulated. The thermal conductivity for the inner cylinder was set to 400 (W/mK). The initial temperature of the PCM was set to 308.15K for the charging process and 329.15K for the discharging process. The PCM used in the analysis was N-eicosane listed in Table 3.2.

3.3 Verification study

3.3.1 Special grid independence study (mesh)

A structured mesh consisting of quadrilateral cells was generated using the ANSYS Fluent 2020R2. A grid independence analysis for all Cases for various grid sizes was evaluated to ensure the solutions were independent of the mesh size. A full analysis listed in Table 3.3 shows percentage deviations of Liquid Fraction of different grids (coarse, selected, fine) from the selected grids at specific Fourier numbers ($F_O = 0.01$). The largest deviation was approximately 5 % or less for the coarse grids and less than 3 % for any increase in refinement for the fine grids.

Table 3.3 Impact of grids (coarse, selected, fine) on Liquid Fraction values (with percentage deviation from the selected grid number) at a time step size of 0.005s for $F_O = 0.01$.

Cases		**Grid Type**		
		Coarse	**Selected**	**Fine**
Case A	**Cell No**	2600	4000	6000
	liquid fraction (% deviation)	0.1067 (1.04%)	0.1066	0.1066 (2.92%)
Case B	**Cell No**	2700	4200	6200
	liquid fraction (% deviation)	0.1526 (2.72%)	0.1522	0.1517 (0.00%)
Case C	**Cell No**	21248	27248	35248
	liquid fraction (% deviation)	0.1649 (5.04%)	0.1672	0.1644 (0.48%)
Case D	**Cell No**	140000	160000	180000
	liquid fraction (% deviation)	0.4410 (0.00%)	0.4410	0.4409 (0.00%)
Case E	**Cell No**	283920	354880	378800
	liquid fraction (% deviation)	0.5568 (1.03%)	0.5626	0.5506 (2.12%)

Table 3.4 lists the quality of elements for the selected mesh type listed. The selected number of elements was not only sufficient to conduct the simulations (based on the mesh independence study discussed earlier) but also had high-quality grids. In that regard, the recorded Orthogonal Quality and Skewness for all the selected mesh Cases are greater than 0.96 and less than 0.15, respectively. Figure 3.2 shows images of the selected meshed Cases.

Table 3.4 Mesh quality study of selected grid.

Cases	**Number of elements**	**Number of nodes**	**Orthogonal Quality (average)**	**Skewness (average)**
Case A	4000	4131	0.99982	0.0125
Case B	4200	4335	0.99703	0.0485
Case C	27248	27529	0.98401	0.1059
Case D	160000	169371	0.99982	0.0125
Case E	354880	368874	0.96684	0.1332

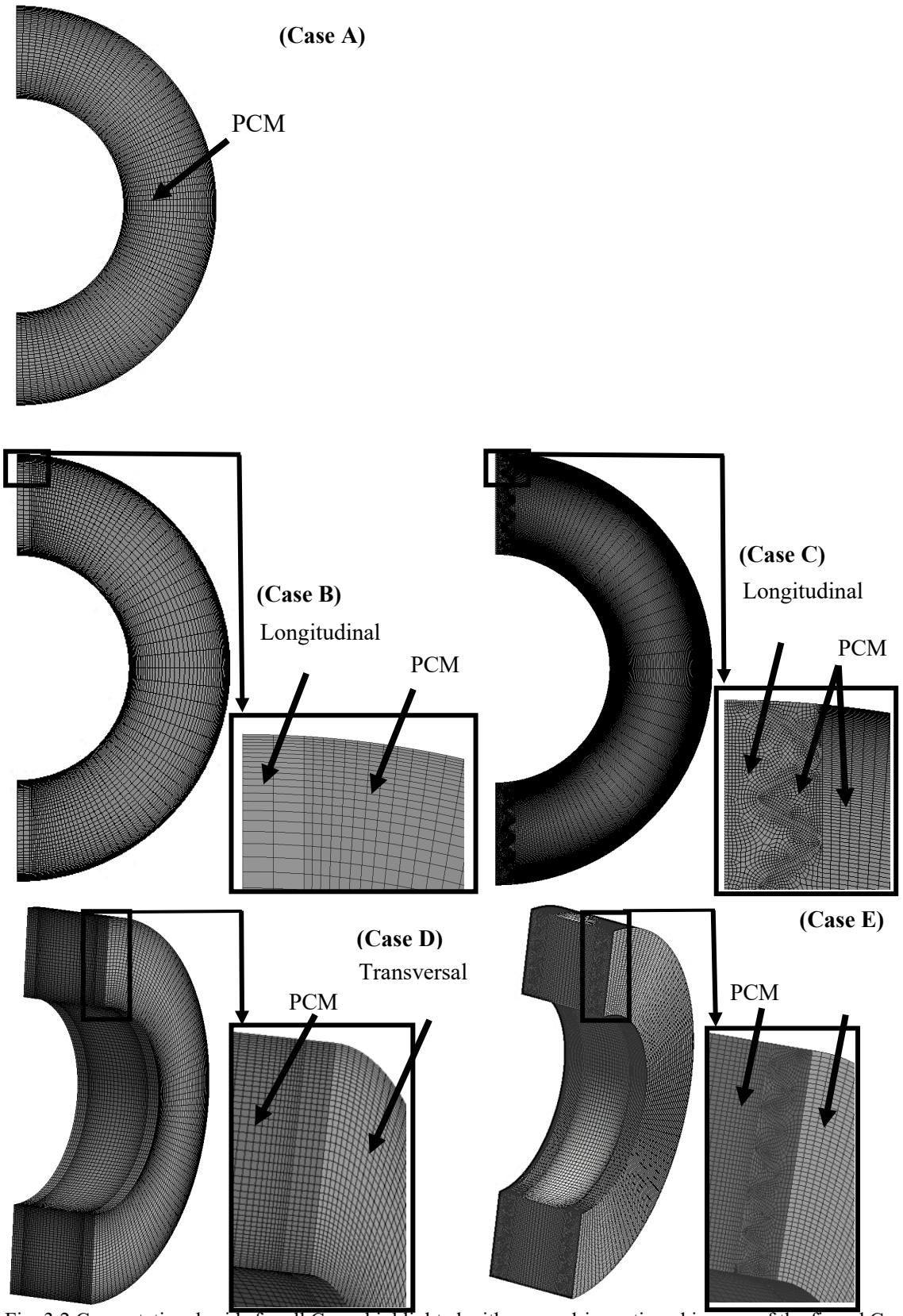

Fig. 3.2 Computational grids for all Cases highlighted with zoomed-in sectioned images of the finned Cases to show mesh topology.

3.3.2 Temporal independence study (time-step)

Table 3.5 shows the time-step independence study and aims to investigate the impact of time-step on Liquid Fraction and their percentage deviation from the selected time-step size (0.005 s). A temporal independence study for the Liquid Fraction is performed for Cases A - D for time-step size at 0.001 s, 0.003 s, 0.005 s (selected), and 0.007 s with maximum iterations per time-step set at 70 for a fixed-type time advancement. For Cases A - D, a fixed time-step size of 0.005 s was sufficient as also seen in the validation for work done. For Case E, the time-step size was significantly reduced to 1^{-6} to maintain uniform and steady convergence, which led to smooth charging, and increased steadily from 1^{-6} to 0.1 in increments of 0.01, until it was sufficient for proper convergence in an adaptive-type time advancement method (this study has not been reported for the sake of brevity). The smaller time-step size showed a reduction in Liquid Fraction percentage deviation as opposed to the higher time-step size for Liquid Fraction percentage deviation of less than 7 %.

Table 3.5 Impact of various time-step size(s) on Liquid Fraction and percentage deviation from selected time-step size shown in bracket for F_o=0.01. It should be noted that an adaptive method was used for Case E with a time-step size modified from $1e^{-6}$ to.

Cases	**Time-step size(s)**			
	0.001	**0.003**	**0.005 (selected)**	**0.007**
Case A	0.1067 (0.38%)	0.1066 (0.02%)	0.1066	0.1028 (3.58%)
Case B	0.1522 (0.00%)	0.1522 (0.00%)	0.1522	0.1468 (3.52%)
Case C	0.1672 (0.00%)	0.1672 (0.00%)	0.1672	0.1616 (3.32%)
Case D	0.2362 (5.28%)	0.2362 (5.28%)	0.2494	0.2329 (6.62%)

3.3.3 Mushy zone constant independence study

An evaluation of the impact of mushy zone constant values, A_{mush}, on the trend of melting for Case B is displayed in Figure 3.3. As shown at $A_{mush} = 10^4$, the melting rate is seen to be faster than $A_{mush} = 10^9$ due to the increase in volume of the mushy zone negatively affecting the natural convection. It can also be seen that during conduction heat transfer in the initial stages of the charging process ($<F_O = 0.03$), the melting rate was almost independent of the mushy zone constant. As a result of natural convection, buoyancy effects force the molten PCM to rise with increased Bernard cells and vortex generation which leads to increasing the melting rate.

During the convection heat transfer, the value of the mushy zone constant affects the melting rate. This is conversely true for the solidification process, as conduction is the main mode of heat transfer, and as such, the value of A_{mush} is insignificant to the solidification rate. This bolstered the neglection of the mushy zone independence study for the solidification process and as such $A_{mush} = 10^5$ was realised to be sufficient.

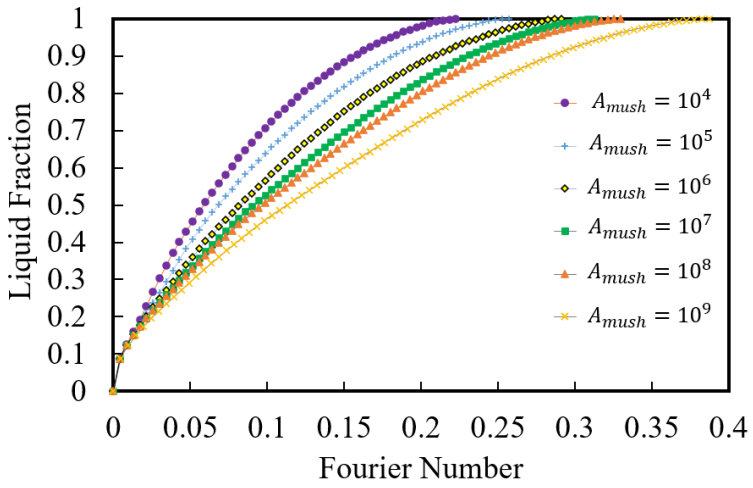

Fig. 3.3 Charging phase Liquid Fraction versus Fourier Number (F_O) for longitudinal flat fin (Case B) for A_{mush} values from 10^4 to 10^9.

The addition of highly conductive fin materials created larger temperature and Liquid Fraction percentage deviations as seen in Table 3.6. This table shows the impact of Mushy Zone constant values, A_{mush} on Liquid Fraction and their percentage deviation for all Cases in the early ($F_O = 0.01$ when conduction is dominant), mid ($F_O = 0.05$ when having mixed conduction and convection), and late stages ($F_O = 0.1$ when convection is dominant) of the charging process. A comparison between A_{mush} values of 10^5 and 10^8 shows a small Liquid Fraction percentage deviation for the unfinned Case at the early stage compared to the late stages. The addition of fins in Case B-C shows a larger Liquid Fraction percentage deviation at the final stage due to the increase in conduction heat transfer and less so for the transversal fin Cases. The variation in A_{mush} values can significantly affect the charging process with values below 10^5 and higher than 10^8 contributing to inaccurate predictions of the melting front. The accuracy of the melting front seems to tend to value closer to 10^8 (see Figure 3.3) and is in line with experimental work in literature and as such was chosen for the charging process in this study. It must be noted that the Liquid Fraction percentage deviation was higher in the late stages ($F_O = 0.1$) for Case A-C while smaller for Case D and E.

Table 3.6 Impact of Mushy Zone constants, A_{mush},, 10^5 and $10^8$for all Cases (A-E) showing Liquid Fraction - percentage deviation at time-step size of 0.005s at early ($F_O = 0.01$), mid ($F_O = 0.05$)) and late stage ($F_O = 0.1$) charging process.

Cases	**Mushy Zone constant, A_{mush}**	**Liquid Fraction (percentage deviation from $A_{mush} = 10^8$)**		
		Early-stage $F_O = 0.01$	**Mid-stage $F_O = 0.05$**	**Late-stage $F_O = 0.1$**
Case A	$\mathbf{10^5}$	0.1066 (1.41%)	0.2724 (7.78%)	0.6113 (21.27%)
	$\mathbf{10^8}$	0.1051	0.2512	0.4813
Case B	$\mathbf{10^5}$	0.1521 (1.12%)	0.3606 (8.93%)	0.5833 (10.99%)
	$\mathbf{10^8}$	0.1504	0.3284	0.5192
Case C	$\mathbf{10^5}$	0.1672 (2.27%)	0.3808 (12.24%)	0.6039 (14.04%)
	$\mathbf{10^8}$	0.1634	0.3342	0.5191
Case D	$\mathbf{10^5}$	0.4410 (3.15%)	0.9132 (6.14%)	0.9997 (0.78%)
	$\mathbf{10^8}$	0.4271	0.8571	0.9920
Case E	$\mathbf{10^5}$	0.5626 (7.27%)	0.9198 (3.82%)	1.000 (0.18%)
	$\mathbf{10^8}$	0.5217	0.8847	0.9982

3.3.4 Computational model setup

To perform the simulations, ANSYS Fluent 2020R2 is used to evaluate the solutions for charging and discharging alongside the energy equations for a laminar flow viscous model. The PISO scheme is used for the pressure-velocity coupling with second-order upwind applied to the Momentum and Energy equations and PRESTO for pressure including spatial discretization along with a first-order implicit transient formulation.

The under-relaxation factors for the solution control for pressure, density, momentum, Liquid Fraction, and energy is 0.3, 1, 0.7, 0.9 and 1, respectively. Convergence conditions for continuity, momentum and energy are set to absolute criteria of 10^{-5} for every timestep.

3.4 Results/analysis and discussion

3.4.1 Validation

The computational setup for the enthalpy-porosity technique using the Boussinesq approximation for the charging process was validated against the Liquid Fraction presented in (Darzi et al., 2012). Their study analysed the melting of PCM (n-eicosane) in the proposed base Case displayed in Figure 3.1.

Figure 3.4 displays the comparison of the Liquid Fraction contours against the literature which shows close similarities with the phase change developments. Additionally, the Liquid Fraction versus Fourier Number (F_O) was captured numerically during the charging process and validated against literature which shows good agreement with the results. The coloured contours of the Liquid Fraction as per the legend show the solid-liquid and mushy zones which were affected by a gravitational force acting in the negative (y) direction. The result from this study accurately predicts the PCM melting front movement per Fourier Number (F_O) for this design. Please note that only for the sake of validation study, for this section the A_{mush} was selected as 10^5 because the chosen literature results were numerical studies based on $A_{mush} = 10^5$.

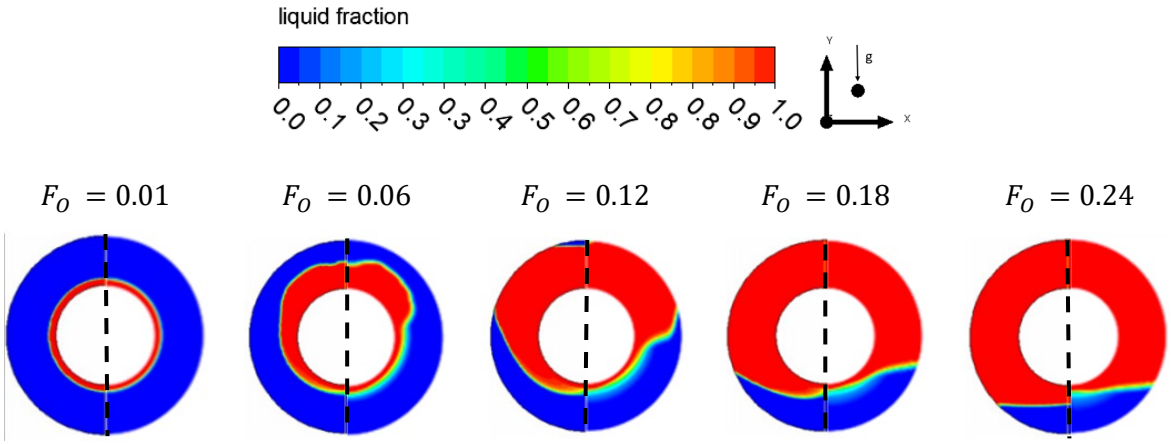

Fig. 3.4 Charging phase Liquid Fraction contours (see legend) with the numerically validated data from the literature (Darzi et al., 2012) shown on the left semi-circle and the present study shown on the right semi-circle, at specific Fourier Number (F_O) intervals with time-step size at 0.005s.

As an additional verification step, the trend of the charging process for unfinned Case (Case A) was compared with the literature in Figure 3.5. As shown, the captured results of $A_{mush} = 10^5$ closely in line with the numerical data from the literature (Darzi et al., 2012). This is attributed to the fact that those literature were numerical studies which got their results at $A_{mush} = 10^5$ while as discussed earlier in this study, for the charging process $A_{mush} = 10^8$ is the most appropriate value. The A_{mush} value does not seem to greatly affect the solidification process and the $A_{mush} = 10^5$ was deemed sufficient to complete this part of the study.

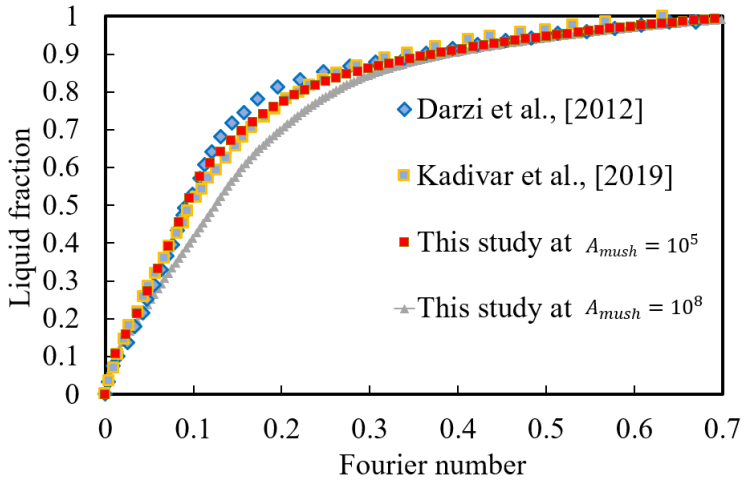

Fig. 3.5 Numerical results validation of the charging process for Liquid Fraction versus Fourier Number (F_O) with the present study at 10^5 and 10^8 mushy zone constants compared with literature (Darzi et al., 2012 Kadivar et al., 2019).

3.4.2 Charging process

The Liquid Fraction contours showing Cases A - E for progression in the melting process per Fourier Number (F_O) is shown in Figure 3.6 with a colour legend showing the variation between the solid and liquid phases of the PCM, as well as the area of the solid-liquid interface, known as the melting front. When the Liquid Fraction is zero (0), the PCM is completely solid and represented by the blue coloured region while when the Liquid Fraction is one (1), the PCM is completely liquid and shown by the red region.

As seen in Figure 3.6 Case A, during the initial stages of the charging process at $F_O = 0.01$, a liquid circular layer wraps evenly around the inner cylinder during the initial mode of heat transfer such as conduction, this transfers heat from the heated inner surface to the contact region of the PCM. Similarly, as seen for Cases B and C, the phenomena occur where the liquid region encircles the circumference of the inner cylinder. Additionally, due to the insertion of the flat fins in Case B and the corrugated fins in Case C, a thin layer of liquid forms on the surface of the fins. For the finned Cases, due to conduction, the heat was transferred from the heated surface to the aluminium fins as they were in contact with the heated surface. The thermal conductivity of the inner surface was set at a high value of 400 W/mK, so when the temperature of the surface was increased to 329.15K, the temperature rise would be transferred instantly since the surface had no thickness.

Cases A-E for isotherms are shown in Figure 3.7 with the Cases showing streamlines on the left in black lines, and the isotherms on the right, the legend shows the temperature values of the contours. This figure shows the temperature rise from 308.15K near the inner cylinder region verifying that the rise in temperature of the PCM beyond its liquid temperature state, changed the phase of the PCM from solid to liquid. The thermal conductivity of the aluminium fins is much higher than the PCM and would conduct heat at a much faster rate, raising the temperature of the heated surface very quickly as compared to the low conductivity PCM. At $F_O = 0.01$, the temperature of the fins is comparable to the heated surface, so a similar layer of liquid occurred over its surface.

As the temperature of the PCM increases further, a temperature gradient is formed, generating differences in the density of the PCM in the form of buoyancy forces, thus increasing the liquid region of the PCM after $F_O = 0.01$, and the higher temperature fluid rises. This is shown for Case A, B and C in Figure 3.6 where a larger region of the PCM is melted in the top half of the exchanger, caused by natural convection while the bottom half of the PCM is affected by conduction only.

This was verified in Figure 3.7 for Case B and C where the temperature contours and streamlines show the regions of the highest temperature and excitation velocity of the molecules around the inner cylinder and at the surface of the fins. In its initial stages, this showed that the insertion of metallic fins to improve the thermal conductivity of the system had a positive effect on its melting performance. The isotherms and streamlines shown for Case A, B and C, illustrate that the higher temperature plume of liquid rises to the top half of the exchanger with vortex cells, known as Bernard cells showing the recirculation in the streamlines. A greater region of recirculation cells can be seen in Cases B and C as the fin addition improved heat transfer. Based on Figure 3.8 illustrates results obtained for Liquid Fraction versus Fourier Number (F_O), for the finned Cases (B and C), at least 15 % of the PCM was liquified compared to just 10 % for Case A.

At $F_O = 0.06$, Case A melted approximately 28 %, Case B melted approximately 38 % and Case C melted approximately 39 %. This was illustrated in the Liquid Fraction contours as a larger region of the PCM was fully melted in Case B and C with only the finned design liquid phase touching the outer cylinder (see Figure 3.6). Beyond $F_O = 0.12$, the liquid reaches near the outer surface of the cylinder for Case A showing increased vortex cells (see Figure 3.7), however, Case B and C had a smaller region of solid PCM with even larger vortex cells, and a larger recirculation zone. At this stage, the solid PCM was melted approximately 48 % for Case A and 60 % for, B and C, respectively. The process of melting continues further at $F_O = 0.18$ with more of the PCM melted, and a region of solid PCM at the bottom of the cylinder with the PCM Liquid Fraction at 66 % for Case A and 78 % for, B

and C, respectively. At $F_O = 0.24$, Case B and Case C have 8 % of solid PCM at the bottom of the cylinder and Case A with 23 % of solid PCM in the lower region (see Figure 3.6).

A further analysis was performed comparing the charging processes for the transversal flat (Case D) and corrugated (Case E) fins (see Figure 3.1). The same design for the corrugation was also applied to the transversal Case to effectively analyse which arrangement showed better performance. Analogous to the longitudinal Cases in Figure 3.6 for Liquid Fraction contours and Figure 3.7 for the isotherms and streamlines, the transversal Cases are presented under the same boundary conditions. However, as seen by Fourier Number (F_O) for the complete Liquid Fraction for the transversal Cases compared to the longitudinal Cases in Figure 3.8, the transversal finned Cases had a greater reduction in melting time compared to the base Case and longitudinal Cases.

As seen in Figure 3.6, the PCM is fully solid for both transversal Cases, until at $F_O = 0.01$. The temperature of the fins was equal to the heated surface temperature (as seen in the side view), and a greater region of the top half of the PCM was melted, as compared to the bottom region at $F_O = 0.06$. This can be attributed to natural convection due to buoyancy effects at the top region, which fully liquified while the bottom region was still largely affected by conduction heat transfer with solid PCM remaining. The side view displays the PCM melting from the high-temperature zones near the fins and the melting front moving towards the centre with the sectioned plane view (see Figure 3.6) showing a greater region of solid PCM in the midplane. The Liquid Fraction contours for Case D and E fully melted at $F_O = 0.12$ and $F_O = 0.1$ respectively, with complete red contours at $F_O = 0.12$. The isotherms for Case D and E shown in Figure 3.7 illustrate the temperature distribution with Fourier Number (F_O), which is significant as the overall temperature of Case E is slightly less than Case D with stronger convection currents on the left and a greater amount of the PCM at the highest temperature.

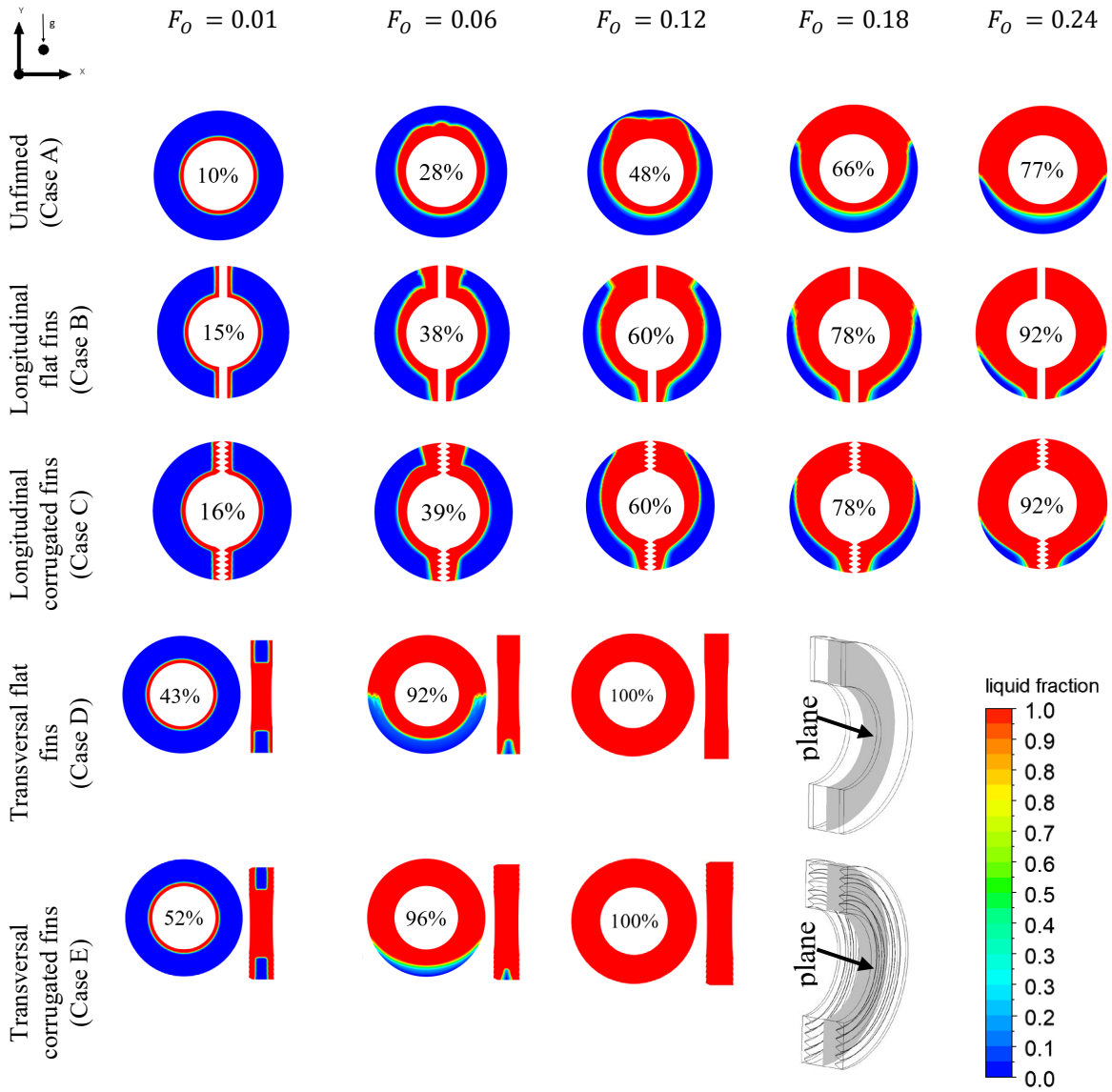

Fig. 3.6 Numerical Liquid Fraction charging for all Cases (A - E) showing percentage of Liquid as per legend. Case D and E are shown at sectioned mid-planes and accompanied with their side views.

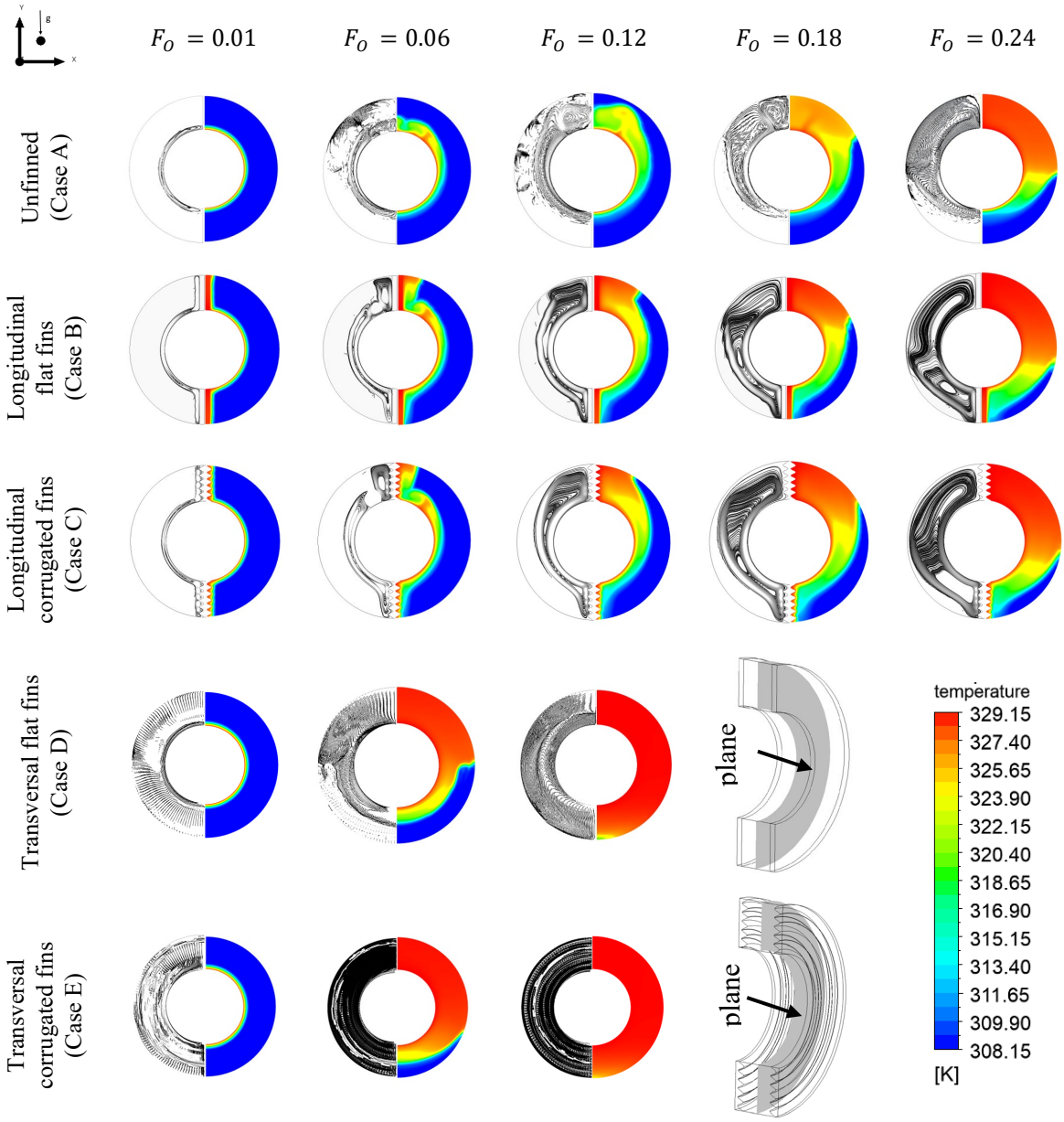

Fig. 3.7 Numerical charging streamlines on the left and isotherms of PCM temperature on the right for all Cases (A - E). Case D and E are shown at sectioned mid-planes and accompanied with their side views.

Figure 3.8 shows the plot of Liquid Fraction versus Fourier Number (F_O) for the finned Cases as well as the unfinned Case. The plots show the numerical data of the contours described in Figure 3.6 showing the transversal finned Cases with reduced melting time, as opposed to the longitudinal finned Cases (B-D) as well as the unfinned Case (Case A). It was seen that there was a 60 % and 58 % reduction in melting time for Case B and Case C respectively compared to Case A. There was approximately 86.5 % and 88 % reduction in melting time for Case D and E respectively, as compared to the base Case

(Case A), with Case E, outperforming all other Cases in terms of melting efficiency. The plot of Liquid Fraction versus Fourier Number (F_O), was largely linear until about $F_O = 0.05$ for the transversal Cases, then it began to curve, and approximately after $F_O = 0.25$ for the longitudinal Cases, compared to after $F_O = 0.2$ for Case A. The deviation in the curve represents the time at which the melted PCM reached the surface of the outer cylinder showing that the convection currents had a major impact on the reduction of the melting time in the upper region.

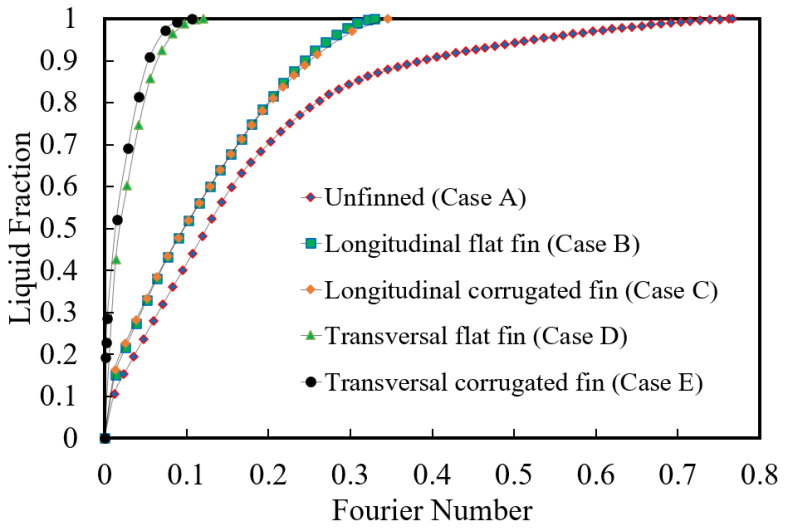

Fig. 3.8 Liquid Fraction versus Fourier Number (F_O) comparison of the charging process for all Cases.

3.4.3 Discharging process

Conversely from the charging process, the solidification or discharging process releases the energy stored by the PCM in the designated system. This is the last phase of the entire process and also contributes to the efficiency of the system and determines the feasibility of the application for the requirements of the TES application.

Contours of Liquid Fraction versus Fourier Number (F_O), for all Cases during the solidification process are shown in Figure 3.9, with the colour legend similar to the melting process. The red indicates a Liquid Fraction of one (1) and PCM temperature of 329.15K while the blue indicates a Liquid Fraction of zero (0) and PCM temperature of 308.15K. At the end of the charging process, the temperature of the PCM was heated up to approximately 329.15K, which was the same as the temperature of the heated surface. To accurately monitor the system in this study, the initial temperature of the PCM was set to

329.15K, and the temperature of the heated surface of the inner cylinder was set to 308.15K with the outer cylinder adiabatic, to prevent heat losses.

As seen in Figure 3.9, at $F_O = 0.72$ for Case A and the longitudinal Cases (B and C), a layer of solid PCM envelops the inner cylinder while the liquid PCM at Liquid Fraction one (1) rises to the top half of the system, and the lower temperature or more dense PCM sinks to the bottom of the system. In this case, conduction was the main mode of heat transfer during discharging. For Cases A, B and C, the solid PCM also forms around the surface of the flat fins and corrugated fins with denser PCM collecting at the bottom. For Case A, 28 % of the PCM was solid while 35 % and 36 % were solid for Case B and C respectively. At $F_O = 2.86$, the solidification of the PCM continues and the solid PCM volume around the inner cylinder and fins increases, as well as in the lower region near the bottom of the annulus. Based on the Liquid Fraction contour colours, Case A still had some molten PCM near the top of the annulus with 57 % solidification while Case B and C were at 67 % and 68 % respectively. This process continues for $F_O = 5.72$, $F_O = 8.58$ and $F_O = 11.44$ showing solidification at 74 %, 83 % and 89 % for Case A, 81 %, 88 % and 93 % for Case B and 82 %, 89 % and 93 % for Case C, respectively (see Figure 3.9). It was noted that full solidification was completed at $F_O = 26.02$, $F_O = 23.4$ and $F_O = 23.6$ for Case A, Case B and Case C, respectively.

Consequently, due to the solidification of the PCM from the inner cylinder and the fins for the finned Cases, the heat transfer process is significantly reduced, as the layer of solid PCM forms a thermal barrier due to its low thermal conductivity, compared to the aluminium inner cylinder. This can be seen in Figure 3.10 showing a plot of Liquid Fraction versus Fourier Number (F_O) for all the Cases (A - E) with the unfinned Case showing the slowest discharging rate.

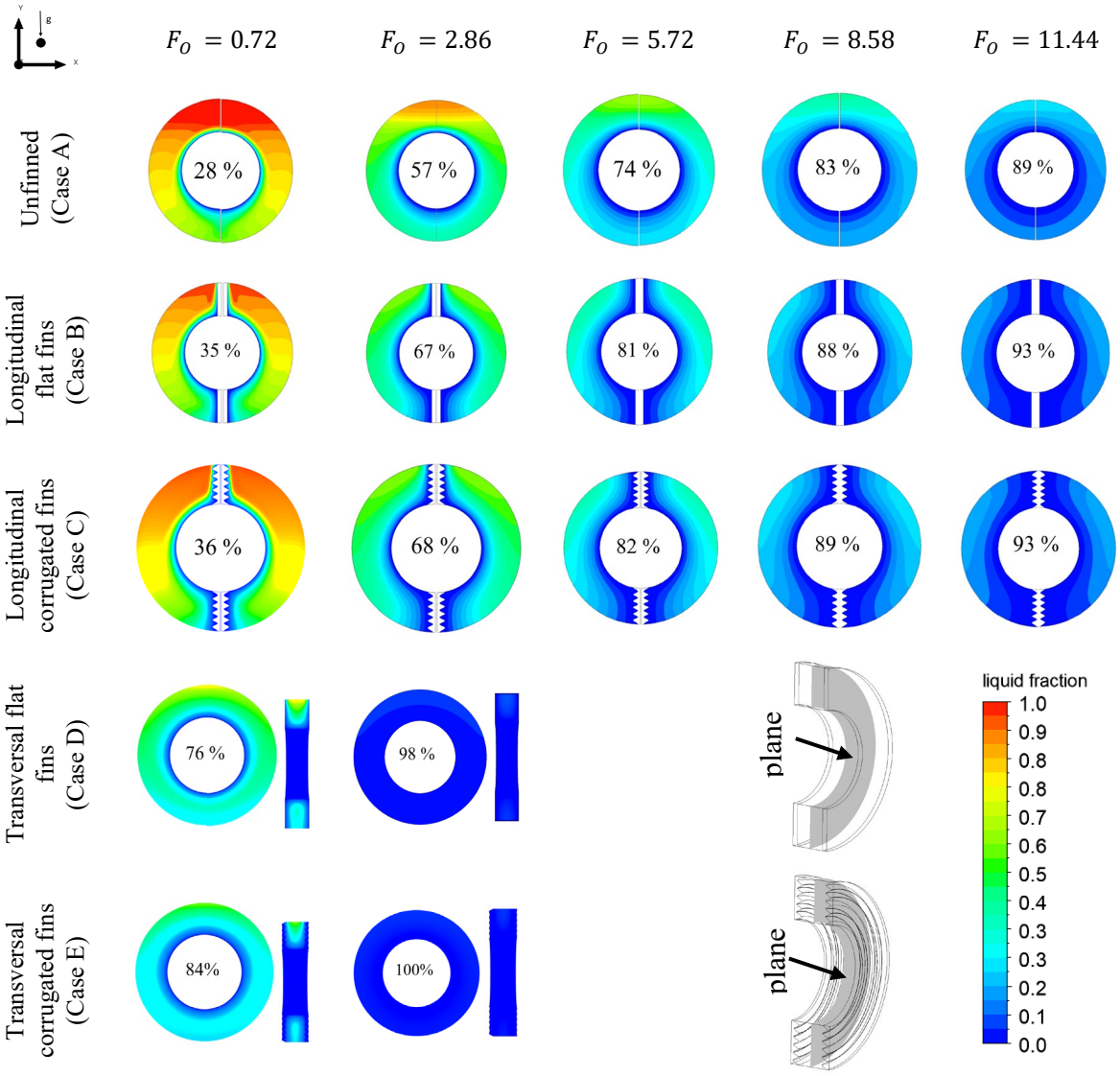

Fig. 3.9 Numerical Liquid Fraction for all Cases showing percentage of solid as per legend during the discharging process with contour colours as seen in the legend. Case D and E are shown at sectioned mid-planes and accompanied with their side views.

Similarly, for the longitudinal Cases, the same boundary conditions applied to the PCM was set to 329.15K, and the heated surface was set to 308.15K. It is worth noting that at the initial state, the fins start at the same temperature as the PCM. Also, the solidification rate and the total time taken for the PCM to fully solidify in the transversal Case (D and E), are much less than the other Cases (A-C) as shown in Figure 3.10.

At F_O = 0.72, like the longitudinal Cases, the solid PCM layer envelops the inner cylinder with much more of the PCM solidified at this stage compared to the longitudinal Cases as the solid PCM

moves from the fins to the centre of the domain. The domain centre solidifies much slower as its furthest away from the fins. Case D solidified approximately 76 % at this stage while Case E solidified at approximately 84 %. As the solidification continues, for the transversal Cases, the PCM at the bottom half of the annulus continues to solidify at a faster rate than the PCM in the top half, which was significantly progressed showing that the PCM was 98 % solid at $F_O = 2.86$ for Case D and 100 % solid for Case E. As seen in Figure 3.10, the solidification rate for the transversal corrugated fin (Case E), is faster than the transversal flat fin (Case D) as well as the other Cases (A-C). The total process time was observed to be faster for the finned Cases than the unfinned Case with (1.13x times) $F_O = 23.730$ Case B, (1.12x times) $F_O = 23.945$ Case C, (8.7x times) $F_O = 3.53$ Case D and (11.5x times) $F_O = 0.67$ Case E.

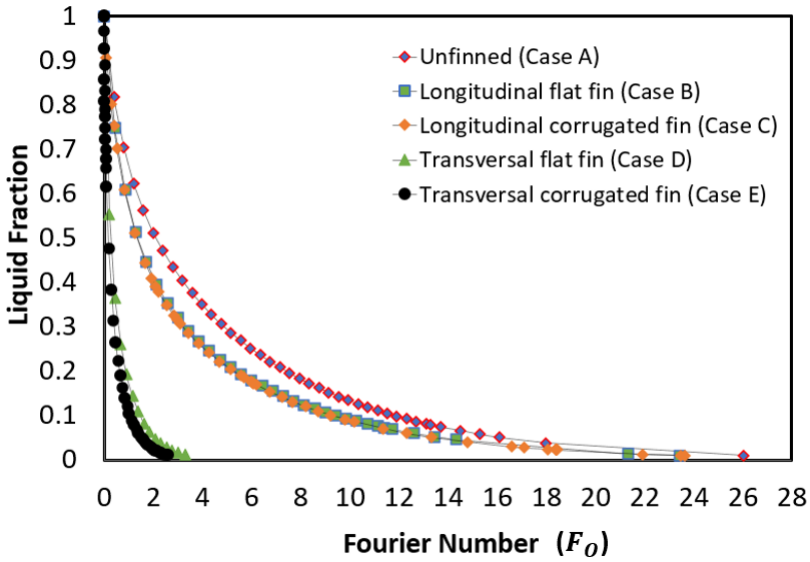

Fig. 3.10 Liquid Fraction versus Fourier Number (F_O) comparison of the discharging process for all Cases.

This is significant, as depending on the application, for shorter charging and discharging times, the transversal finned Cases may be applicable for faster charging and discharging processes. Moreover, even though the transversal corrugated fin Case (Case E) had a shorter overall processing time than the transversal flat finned Case (Case D), the cost of design and manufacturing considerations as well as complexity and precision of corrugated fins in a small container may be less feasible. It should be noted although, that there was a 1 % deviation smaller corrugated fin area for the longitudinal Cases (B and C) and a 28 % increase in fin area for the transversal corrugation (Case E) over flat fin (Case D). The same cross-sectional area of material had a 27 % increase in surface area for the transversal corrugated Case (Case E) compared with the flat fin Case (Case D) to improve heat transfer.

Further to this, an optimisation technique may be considered to determine the best shape of corrugation for frequency in wavelength to improve upon the processing time dependent on the application requirements. The longitudinal finned Cases (B and C) significantly reduced the charging time as compared to the unfinned Case (Case A) as described in this investigation. However, there was only an 11 % reduction in the solidification time. This can be viewed as advantageous to TES systems for a faster rate of charging as well as lengthy discharge times.

3.5 Conclusions

In this study, corrugated fins were analysed for their effects on the performance of a horizontal DPHX arranged longitudinally and transversally. A numerical investigation involving five varying Cases (unfinned, longitudinal flat fins, longitudinal corrugated fins, transversal flat fins, transversal corrugated fins) in charging and discharging processes was conducted. N-eicosane PCM filled the annular space subjected to constant temperature on the inner pipe walls and outer pipe walls adiabatic in the concentric LHS system with the fins attached to the inner cylinder. The subsequent conclusions are outlined below:

- The results obtained for comparable analysis were similar to predicted numerical data from the literature, showing 0.1 % deviation and 0.009 % deviation for total melting time. In all Cases for melting, primarily the main mode of heat transfer was conduction, and in the presence of molten PCM after a specific time, convection was the main mode of heat transfer. For all Cases during charging, heat transfer occurred more readily in the top half of the PCM as it melted faster while at the bottom, it melted much slower. The contours of PCM temperature and velocity streamlines were also similar, with the Liquid Fraction contours showing the greatest regions of recirculation at the highest PCM temperatures. It was noted that at 10 % of complete melting, the longitudinal corrugated fin (Case C) had a higher percentage Liquid Fraction (26 %) as opposed to the longitudinal flat fin (Case B) (25 %) during the initial conduction heat transfer.
- When the Cases were compared for melting rate, the transversal corrugated fin (Case E) had the fastest rate of melting and overall melting time with a reduction of 88 % compared to the unfinned Case showing a significant improvement in heat transfer. The longitudinal corrugated fin Case had a 58 % reduction in melting time which was 2 % slower than the longitudinal flat fin Case, overall, the transversal corrugated fin (Case E), was 11.5 times faster than unfinned Case. The cross-sectional area was approximately 1 % varied for the corrugated fin compared to the flat fin. Although

there was no significant improvement in heat transfer when the longitudinal fin Cases were compared, the same cross-sectional area for the corrugated fin had a significant improvement in heat transfer in the transversal orientation (27 % improvement). Further work on increasing the number of transversal corrugated fins, fin angles, corrugation optimisation, PCM material and fin material can be considered for additional investigations.

- During the discharging process, conduction was the main mode of heat transfer for all Cases as the lower region of the PCM solidified faster than the upper region.
- Both the longitudinal flat fin and corrugated fin Cases performed similarly for discharging energy for a longer period than the transversal finned Cases. The transversal corrugated fin (Case E) had 91 % reduction in solidification time while the transversal flat fin (Case D) had 88 % reduction. Both the longitudinal flat (Case B) and corrugated (Case C) had 16 % reduction in solidification time. This showed above 70 % reduction in solidification time when the transversal Cases were compared to the longitudinal Cases.
- The overall results highlighted gave a new understanding into transversal fins as compared to longitudinal fins and their effect on natural convection in a horizontal DPHX for melting and solidification. This is particularly useful in future optimisations to conduction and convective heat transfer in PCMs especially in renewable energy storage devices that require fast charging and lengthy discharging, such as electrical devices.

3.6 Chapter Summary

This research Chapter evaluated the enhancement conducted for Thermal Energy Storage (TES) and analysed an improvement in the passive energy storage materials such as Phase Change Materials (PCMs). An improvement in the thermal conductivity of N-eicosane using fins made of aluminium was specifically studied to identify the best improvement in thermal performance for fin orientation (longitudinal and transversal) and fin-type (flat and corrugated). The Chapter analysed specifically how the PCM can be thermal enhanced with a research study on the subject that aligned with the research conducted in the literature review Chapter 2 as well as for the milestones and objectives of this research work. The results of the study were subsequently published in a Journal article and presented at a Conference as outlined in the Publications section and form part of the completed work for the thesis. Moving forward, the subsequent Chapter 4 continues the narrative, exploring the integration of TES

and EES. The Chapter discusses the integration method and goes into detailed literature for this conjugation specifically passive cooling as discussed in the previous Chapter 3 as well as the Literature review in Chapter 2. The numerical approach including verification and validation techniques as well as results was subsequently discussed.

CHAPTER 4: INVESTIGATIVE ANALYSIS INTO EV BATTERY CELL PERFORMANCE UNDER VARYING CLIMATE CONDITIONS COUPLED LATENT HEAT STORAGE BASED PASSIVE COOLING [3][4]

4.1 Chapter Brief

In the previous Chapter, an investigation into the thermal performance enhancement of passive cooling LHS PCMs analysed the effects of fin-type (flat and corrugated) and orientation (longitudinal and transversal). The literature review Chapter 2 gave a general overview of TES, and the materials used (PCMs) with the previous Chapter 3 specifically examined the thermal improvement for melting and solidification of PCMs. This Chapter is devoted to the conjugation of TES materials that facilitate LHS such as PCMs with EES devices such as Li-ion batteries. A battery thermal performance analysis was conducted on a specific 18650 cylindrical battery cell outlining three key performance parameters such as the Temperature, State of Charge (SOC) and Power and used as the basis for comparison when the battery was jacketed with PCM around the circumferential area. The heat generated from the battery during charging and discharging was captured and directly transferred to the PCM to melt the PCM until all the material was fully liquified. The data was numerically captured using ANSYS Fluent with results validated and verified using numerical and experimental data from literature. The coupled thermo-chemical and electrical results are presented based on various climate conditions as well as the type and volume of PCM surrounding the battery. This study Chapter is in line with the objectives set about in Chapter 1 and seeks to partially fulfil the targets set in milestones 1 and 2. This study is classed as a cellular study, as a single cell was analysed with future work on battery modules to be reviewed to further fulfil milestone 2 targets. The results of this study Chapter were presented at a Conference and published in a journal article as seen in the list of publications.

---

[3] Yang, M., **Nicholls**, R.A, Moghimi, M.A., and Griffiths, A.L., Performance management of EV battery coupled with latent heat jacket at cell level, *Journal of Power Sources*, 558, 2023, pp 232618. https://doi.org/10.1016/j.jpowsour.2022.232618

[4] **Nicholls**, R.A, Moghimi, M.A., and Griffiths, A.L., Can passive cooling be a practical solution for the thermal management of battery in electric vehicles, *Proceedings of the 16th International Conference on Heat Transfer, Fluid Mechanics and Thermodynamics and Editorial Board of Applied Thermal Engineering*, Amsterdam, Netherlands.

4.1.1 Introduction

Renewable energy storage is becoming widely acceptable as an alternative source of energy storage and is a viable candidate in the application of zero-emission vehicles such as HEVs and EVs. Increased energy demands and consumable resources have dictated the main source of energy in the form of fossil fuels. Unfortunately, industrial processes that employ these sources, have negatively impacted our natural environment in the form of rising worldwide temperatures thus causing a surge in energy demand and rising heat generation. As a result of these global changes there is an ever-increasing requirement for renewable energy sources to meet this demand and thus reduce/slow down the impact on our climate (Nicholls et al., 2022).

This study seeks to highlight these renewable energy resources in the form of EES (Chen et al., 2009), (Cho et al., 2015), (Ferreira et al., 2013) and (Hameer et al., 2015) and Thermal Energy Storage (TES) (Alva et al., 2018), (Fang et al., 2007) and (Kuravi et al., 2013), they have gained attention in their role of reducing the carbon emissions. Increased attention towards these types of "green" transport as outlined by (Kim et al., 2019) has driven the capitalization of EV and HEV production in recent years.

According to (Meunzel et al., 2015), the rechargeable Li-ion battery with its small volume has received great interest due to its high energy density, long life cycles, low self-discharge rate, high voltage and chemical stability when compared with other rechargeable batteries. Studies have shown that when operated at standard ratings, the optimal battery performance is achieved (Tomaszewska et al., 2019). Li-ion batteries are extremely sensitive to temperature, and it can have an impact on the battery life cycle, stability, and performance as well as operational safety (Behi et al., 2020, Panchal et al., 2018, Kshetrimayum et al., 2019 and Balakrishnan et al., 2006). According to (Ki et al., 2019, Muenzel et al., 2015, Behi et al., 2020, Panchel et al., 2018 and Kshetrimayum et al., 2019), deviation from the optimum working temperatures can cause a reduction in the electrical as well as high temperatures causing thermal runaway and potential of fire and explosion.

Even the distribution of battery temperature has been found to aid in the thermal and electrical response of the battery (Verma et al., 2019 and Wang et al., 2015). Li-ion battery cells operate safely between the temperatures of 20 °C to 40 °C (Landini et al., 2019 and Jilte et al., 2019), this can vary slightly according to the manufacturer and battery type (Muenzel et al., 2015). Fluctuations outside this optimum operating temperature range can cause two types of harmful effects namely: overheating and undercooling. Large temperature gradients from the effects of divergent surface temperature negatively affect the battery performance, therefore maintaining uniform temperature distribution across the battery would aid in its stability (Landini et al., 2019), (Jilte et al., 2019) and (Hosseini et al 2012),

commonly known as Battery Thermal Management Systems (BTMS) (Verma et al., 2019), (Wang et al., 2015), (Selokar et al., 2019) and (Javani et al., 2014). BTMS is usually focused on active cooling by using a variety of techniques and materials including air (Jilte et al., 2019) and liquid cooling (Sardari et al., 2020) and (Talebizadehsardari et al., 2021). These techniques are required to maintain the optimum battery temperature however they increase the complexity of the EVs and HEVs. There is a significant increase in loading for driving (e.g., fan, pump) and delivering (e.g., channels, pipelines), a cooling medium to and from the batteries. Therefore, if passive cooling alone can provide the cooling capability in the batteries, the BTMS system will be much simpler and lighter, as unnecessary devices and equipment for driving and delivering active cooling medium will be eliminated from the system.

A comprehensive review of PCMs (Sharma et al., 2015) and (Du et al., 2018) of low (-20 °C to 5 °C), medium-low (5 °C to 40 °C), medium (40 °C to 80 °C) and high (80 °C to 200 °C) temperatures were analysed on the impact of applications. Medium-low and medium-temperature PCMs are more directly related to electronic cooling as a heat sink and in some cases a heat source where the low thermal conductivity of the PCM becomes useful for maintaining stable operating temperatures for purely passive cooling (Veerakumar et al., 2016). Natural convection melting, volume, and cell spacing between cell-scale models are all considerations alongside the thermal conductivity that affects the performance of PCMs as a cooling medium for the thermal management of batteries. These also include battery voltages and uniform temperature for experimental and numerical approaches involving multi-scale multi-dimensional physics models, (El Idi et al., 2021), (Huang et al., 2020), (Lu et al., 2013), (Murali et al., 2021) and (Xia et al., 2017).

Research has shown that coupled electrochemical battery and thermal PCM systems have stabilised the temperature (Wang et al., 201), (Landini et al., 2019), (Rao et al., 2011), (Shahjalal et al., 2021), (Sun et al., 2021), (Oh et al., 2019), (Budiman et al., 2021), (Cao et al., 2020a), (Cao et al., 2020b), (Chen et al., 20190, (Nicholls et al., 2022), (Moradi et al., 2017), (Du et al., 2018) and (Malik et al., 2016). In this instance, heat energy produced from the battery is readily absorbed by the PCM to store the energy as LH (Talebizadehsardari et al., 2017) and (Nicholls et al., 2022). PCMs store LH during phase changing as the temperature increases and reaches its liquidus temperature point. During this phase change, the temperature of the PCM remains constant, which is useful in thermal applications including free cooling, air conditioning (AC), passive cooling, heat recovery systems and solar energy storage systems (Sardari et al., 2020), (Moradi et al., 2017) and (Du et al., 2018).

One of the main parameters that influence the performance of the battery is the State of Charge (SOC) (Yang et al., 2021). The SOC usually denoted as a percentage of the remaining capacity is constrained between its fully charged position at 100 % and the fully/deep discharged position at 0 %

and as an approximation since the State of Health (SoH) and the Remaining Useful Life (RUL) (Xu et al., 2022) and (Ungurean et al., 2017) should be considered.

The focal point of this study is to evaluate the impact of passive cooling on Panasonic 18650PF Li-ion battery cell (PCM cooling conjugated with an EES) under various conditions with measured thermal and electrical indicators of performance (SOC, Temperature, and Power) applied in EVs and HEVs, which to the best of author's knowledge has not previously been investigated. This study focuses on two cases including a single battery cell (with and without PCM) which undergoes cycles of consecutive discharging and recharging under climatic conditions including extreme winter -20 °C, winter 0 °C, ambient 25 °C, hot summer 40 °C, and extreme hot/desert 55 °C temperatures. Notably, this study takes into consideration the safety concerns of these thermally reactive materials and reduces the possibility of potential hazards such as fire and explosion. As such, temperature safety limits (charging 0 °C to 45 °C, discharging -20 °C to 60 °C) and voltage (2.5 V to 4.2 V) were imposed on all test cases as well as other constraints. Furthermore, an evaluation study on the effect of the PCM jacket thickness around the cell (1 mm, 3 mm, 5 mm, and 7 mm) is investigated to identify the significance of the volume of the storage system and to effectively reduce the added weight. The study also investigates a variation in PCM applicable to the change in ambient weather conditions.

The structure of the study follows a numerical method detailing the models, mathematical and numerical approaches, assumptions and boundary conditions and verification including numerical (special grid, temporal, and mushy zone) and experimental results validation, results and discussion followed by conclusions.

4.2 Numerical Method

4.2.1 Models

The schematic domains of the battery cell are displayed in Figure 4.1 for a cylindrical 18650PF Panasonic Li-ion battery cell as well as the geometrical dimensions. Isometric, front, and side views show battery cells with and without a jacketed PCM. The outer walls of both cases, with and without PCM, are set to be adiabatic and hence thermally unaffected by the environment. The dimensions show that the outer diameter and length of the active zone for this battery cell are 18 mm and 65 mm respectively, while the outer diameter and height of the tabs are 6.6 mm and 0.2 mm, respectively.

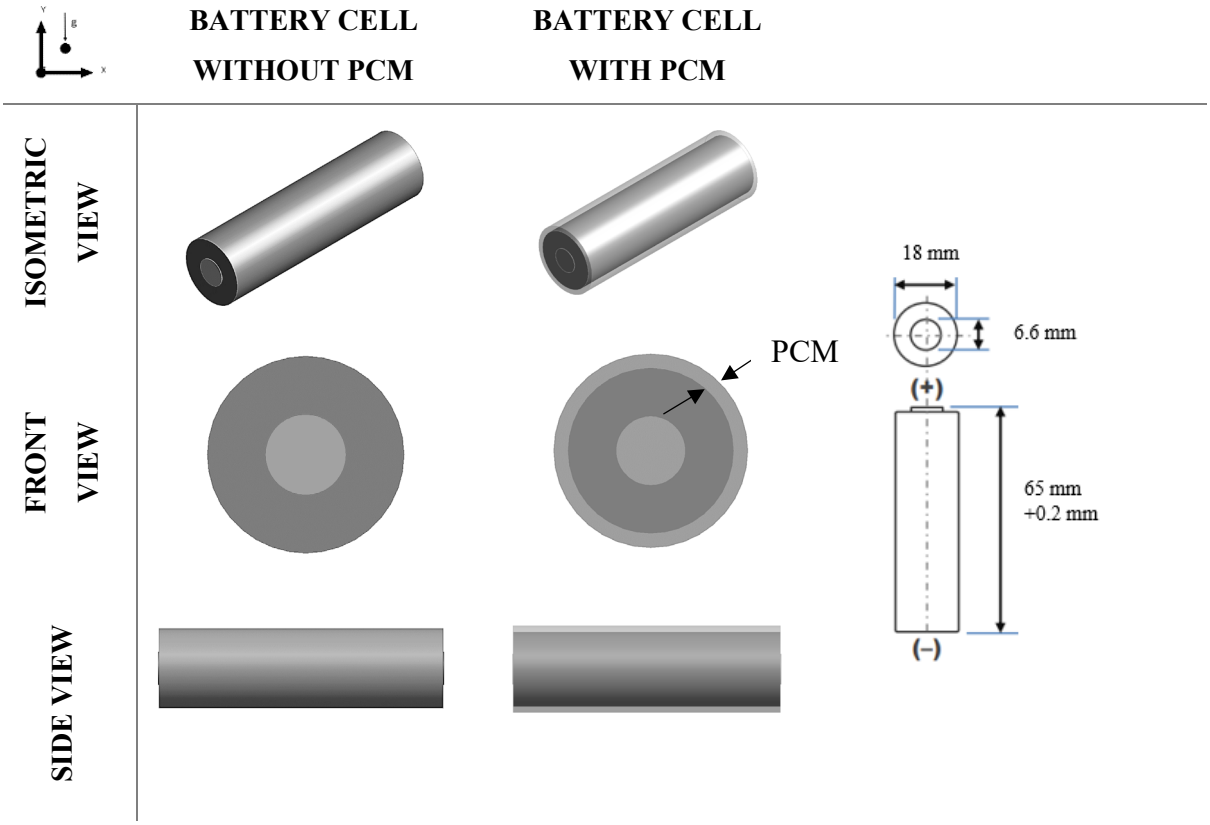

Fig. 4.1 Schematic of cylindrical 18650 battery cell displaying isometric, front, and side views for battery cell without PCM as well as the jacketed battery cell with PCM.

4.2.2 Mathematical and numerical model approach

For PCM modelling, an enthalpy-porosity formulation was used to solve the fluid flow equations for melting and solidification instead of tracking the melting/liquid-solid front (Voller et al., 1987) and (Swaminathan et al., 1992). In the cases where the volume of the cell is liquid, a quantity known as liquid fraction was used to correlate these cells based on the enthalpy balance evaluated at every iteration. A "pseudo" porous zone known as the mushy zone, was quantified by the liquid fraction with minimum and maximum values of zero at solidification and 1 at melting, respectively. The values of the mushy zone region were associated with the porosity from solidification to fully melted, 0 to 1 and in the case where the full solidification of the material takes place, the porosity, as well as velocity, are null. Sink terms applied to momentum and turbulence were used to assess the phase change variation of the solid zones (Brent et al., 1988). The thermophysical properties of the PCM and walls are listed in Table 4.1.

The numerical approach for modelling the PCM zone for melting and solidification (Nicholls et al., 2022) relates to the following:

The energy equation relates to the following and is stated as:

$$\frac{\partial}{\partial t}(\rho H) + \nabla.(\rho \vec{v} H) = \nabla.(k \nabla T) + S \tag{4.1}$$

Where H is derived as the sum of sensible enthalpy, h, and the latent heat, ΔH:

$$H = h + \Delta H \tag{4.2}$$

$$h = h_{ref} + \int_{T_{ref}}^{T} C_p \, dT \tag{4.3}$$

and latent heat, ΔH, is defined as:

$$\Delta H = fL \tag{4.4}$$

The liquid fraction, f, is derived as

$$f = \begin{cases} 0 \\ 1 \\ \frac{T - T_{solidus}}{T_{liquidous} - T_{solidus}} \end{cases} ; \begin{cases} T < T_{solidus} \\ T > T_{liquidous} \\ T_{solidus} < T < T_{liquidous} \end{cases} \tag{4.5}$$

S is the source term derived from the momentum sink as follows:

$$S = \frac{(1-f)^2}{(f^3 + \varepsilon)} A_{mush} \tag{4.6}$$

ε is a number equal to 0.001, to prevent an invalid result when divided by zero

A_{mush} is the mushy zone constant between $10^4 - 10^7$, (Talebizadehsardari et al., 2021) and (Nicholls et al., 2022); 10^5 was studied for the melting process in this analysis (see 4.3.3)

Substituting the Eqns. (4.2) - (4.5) into Eq. (4.1) yields the energy equation as

$$\frac{\partial \rho h}{\partial t} + \nabla.(\rho \vec{v} h) = \nabla.(k \nabla T) - \frac{\partial \rho f L}{\partial t} - \nabla.(\rho \vec{v} f L) + S \quad (4.7)$$

Substituting Eq. (4.6) into (4.7) gives the momentum equation in the following:

$$\frac{\partial \rho \vec{v}}{\partial t} + \nabla.(\rho \vec{v} \vec{v}) = -\nabla P + \nabla.(\mu \nabla \vec{v}) + \rho g + \frac{(1-f)^2}{f^3 + \varepsilon} \vec{v} A_{mush} \quad (4.8)$$

With the inclusion of the forces due to gravity, buoyancy-driven flows known as natural convection flows are caused by the deviation in density due to temperature. The natural convection in this case occurs within an enclosed domain and so the Boussinesq Approximation is valid to initialise faster convergence for a reference density (constant) and temperature as shown:

$$(\rho - \rho_0) g \approx -\rho_0 \beta (T - T_0) g \quad (4.9)$$

Which is a valid approximation when:

$$\beta (T - T_0) \ll 1 \quad (4.10)$$

Eq. (4.8) can be re-written as:

$$\frac{\partial \rho_0 \vec{v}}{\partial t} + \nabla.(\rho_0 \vec{v} \vec{v}) = -\nabla P + \nabla.(\mu \nabla \vec{v}) + (\rho - \rho_0) g + \frac{(1-f)^2}{f^3 + \varepsilon} \vec{v} A_{mush} \quad (4.11)$$

The governing equation for continuity:

$$\frac{\partial \rho}{\partial t} + \nabla.(\rho \vec{v}) = 0 \quad (4.12)$$

The non-dimensionless numbers ∇ = DV, $\vec{v} = \frac{\vec{v} D}{\alpha}$, $H = \frac{H}{L}$ and $T = \frac{T - T_s}{L / c_p}$ (4.13)

D = 2 ($R_{out} - R_{in}$), the energy equation for the non-dimensionless terms are:

$$\frac{\partial(H)}{\partial F_o} + \nabla.(\vec{v}H) = \nabla.(\nabla \mathrm{T}) \tag{4.14}$$

where Fourier Number, $F_o = \frac{\alpha t}{D^2}$

The numerical approach for modelling the battery cell zone:

A coupled thermal-electrical simulation is used to evaluate the heat generation rate for normal operation, the Multi-Scale Multi-Domain method (MSMD) is used. This method uses a multi-domain, multi-physics approach based on the problem definition where the distributed temperature is analysed along the battery length scale.

The thermal and electrical fields are solved using the following differential equations:

$$\frac{\partial \rho C_p T}{\partial t} - \nabla.(k\nabla T) = \sigma_+ |\nabla \emptyset_+|^2 + \sigma_- |\nabla \emptyset_-|^2 + \dot{q}_{ECh} + \dot{q}_{short} + \dot{q}_{abuse} \tag{4.15}$$

Where σ_+ and σ_- are the effective conductivities for the positive and negative electrodes, $\emptyset_+$ and $\emptyset_-$ are phase potentials for the positive and negative electrodes, $\dot{q}_{ECh}$ is the electrochemical reaction heat due to electrochemical reactions, $\dot{q}_{short}$ is the heat generation rate due to battery internal short-circuit and $\dot{q}_{abuse}$ is the heat generation due to the thermal runaway reactions under the thermal abuse condition. For normal operation and no internal short circuit, $\dot{q}_{abuse}$ and $\dot{q}_{short}$ are set to zero. The Equivalent Circuit Model (ECM) in Figure 4.2 replicates the battery electrical behaviour in an equivalent circuit and engages six parameters based on the work from (Chen et al., 2006) that monitors the electrical performance of the battery during cycles.

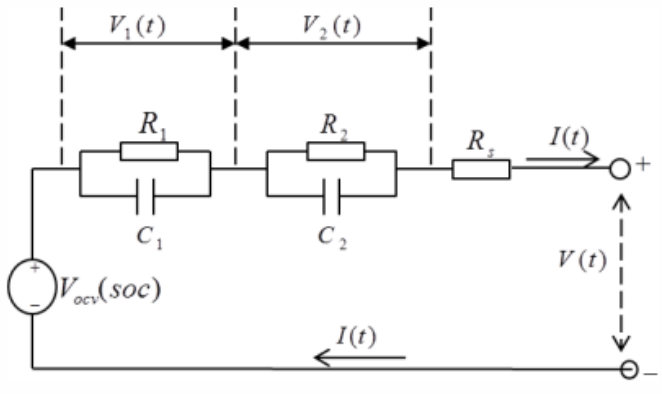

Fig. 4.2 Schematic of electric circuit corresponding to the ECM.

The electric circuit equations corresponding to the voltage-current correlation are computed by the following:

$$V = V_{OCV}(SOC) - V_1 - V_2 - R_s(SOC)I(t) \tag{4.16}$$

$$\frac{dV_1}{dt} = -\frac{1}{R_1(SOC)C_1(SOC)}V_1 - \frac{1}{C_1(SOC)}\ I(t) \tag{4.17}$$

$$\frac{dV_2}{dt} = -\frac{1}{R_2(SOC)C_2(SOC)}V_2 - \frac{1}{C_2(SOC)}\ I(t) \tag{4.18}$$

$$\frac{d(SOC)}{dt} = I(t)/3600Q_{ref} \tag{4.19}$$

Where V is the battery cell voltage that can obtained either from the circuit solution in Figure 4.2 the Circuit Network solution method or calculated as $\emptyset_+ - \emptyset_-$ from the MSMD solution method. For a given battery, the open circuit voltage, resistors' resistances, and capacitors' capacitances are functions of the battery's state of charge (SOC) and temperature. The functions are defined as fifth-order polynomial forms (Equations 4.20 – 4.25) used for the derivation of the coefficients of the discharging and recharging.

$$R_s = a_0 + a_1(soc) + a_2(soc)^2 + a_3(soc)^3 + a_4(soc)^4 + a_5(soc)^5 \tag{4.20}$$

$$R_1 = b_0 + b_1(soc) + b_2(soc)^2 + b_3(soc)^3 + b_4(soc)^4 + b_5(soc)^5 \tag{4.21}$$

$$C_1 = c_0 + c_1(soc) + c_2(soc)^2 + c_3(soc)^3 + c_4(soc)^4 + +c_5(soc)^5 \tag{4.22}$$

$$R_2 = d_0 + d_1(soc) + d_2(soc)^2 + d_3(soc)^3 + d_4(soc)^4 + d_5(soc)^5 \tag{4.23}$$

$$C_2 = e_0 + e_1(soc) + e_2(soc)^2 + e_3(soc)^3 + e_4(soc)^4 + e_5(soc)^5 \tag{4.24}$$

$$V_{OCV} = f_0 + f_1(soc) + f_2(soc)^2 + f_3(soc)^3 + f_4(soc)^4 + f_5(soc)^5 \tag{4.25}$$

The source terms corresponding to Equation 4.15 are derived as:

$$j_{ECh} = I\ \frac{Q_{Nominal}}{Q_{ref}\,Vol} \tag{4.26}$$

$$\dot{q}_{ECh} = j_{ECh}\ \left[V_{OCV} - V - T\ \frac{dU}{dT}\right] \tag{4.27}$$

Where I is the current, and V_{OCV} is the open circuit voltage.

Table 4.1 Thermophysical properties of battery cell (active zone), PCMs and insulation walls (Kousha et al., 2017 and Mohaghegh et al., 2021).

	18650 Battery cell	**Pos Tab**	**Neg Tab**	**PCM (N-octadecane)**	**PCM (RT44HC)**	**PCM (Stearic acid)**	**Plexiglass (insulation)**
Density (kg/m^3)	2092	2719	8978	770	700	1150	1190
Cp (Specific Heat) ($J/kg-K$)	678	871	381	2196	2000	2830	1470
Thermal Conductivity ($W/m-K$)	18.2	202.4	387.6	0.148	0.2	0.29	0.19
Viscosity ($kg/m-s$)				0.003	0.0033	0.0078	
Thermal Expansion Coefficient ($1/K$)				0.00091	0.00076	0.0008	
Pure Solving Melting Heat (J/kg)				243500	250000	186500	
Solidus Temperature (K)				298.15	314.15	327.5	
Liquidus Temperature (K)				302.15	317.15	337.1	

4.2.3 Assumptions

To analyse the numerical models presented in Figure 4.1, the following assumptions are made:

- The battery cell is initially fully charged,
- All physical properties of the battery cell are constant,
- A transient laminar fluid flow analysis applied for the discharging and recharging of the battery including viscous and incompressible flows,
- Heat transfer in the battery cell is due to conduction,
- ECM model parameters affecting the electrochemical and thermal properties of the battery are due to the discharging and charging coefficients for the fifth-order polynomial form data type,
- Gravitational acceleration of 9.81 m/s^2 acts downward in the negative y-direction including Boussinesq approximation due to natural convection heat transfer and modelling of the PCM melting and solidification,
- Excluding density, all PCM properties are constant,
- Molten PCM fluid flow is laminar, incompressible, and viscous.

4.2.4 Safety Constraints

Safety limits were imposed in this study that influenced the battery voltage and temperature during charging and discharging to prevent degradation of the battery, overcharging, thermal runaway, fire, and explosion. In that regard, the following restrictions are imposed for battery charging and discharging in the simulations experimental work:

- Simulation cut-off voltage (Maximum/Minimum voltage limits) is set to 4.2 V and 2.5 V, respectively.
- Simulation cut-off temperature (maximum temperature limits) is set at 45 °C and 60 °C, respectively. I.E., in the simulation cut-off is imposed where any further increase in temperature will compromise the integrity of the battery leading to hazardous situations.

4.2.5 Initial and boundary conditions

To analyse the numerical models presented in Figure 4.1, the following initial and boundary conditions are considered:

- Adiabatic (zero heat flux) outer circumferential walls applied for all models (outer battery walls and PCM walls for the cases with and without PCM) to prevent heat loss to the environment. In other words, the proposed systems are isolated,
- Adiabatic (zero heat flux) walls applied to battery tabs,
- Battery cell and PCM thermophysical properties and insulation material are listed in Table 4.1,
- Initial PCM temperature is set to solidus temperature for the models with PCM, and battery cell temperature set to ambient temperature specified (extreme winter weather -20 °C, winter weather 0 °C, ambient weather 25 °C, hot summer weather 40 °C, and extreme hot/desert weather 55 °C).

4.3 Verification study

4.3.1 Special grid independence study (mesh)

The special grid independence analysis ensures that the cases studied were independent of the grid sizes. An analysis of grid independence was performed using the meshing feature that created a structured meshing including quadrilateral cell results. The analysis compared the different grid sizes ranging between coarse, selected and fine defining larger to smaller cells, respectively. The comparison with and without PCM showed little deviation (less than 1 %) between the different grids. An adequate number of elements was chosen for the battery cell with (86877 elements) and (84801 elements) without PCM had high average Orthogonal Quality (greater than 0.95) and low Skewness (less than 0.25).

4.3.2 Temporal independence study (time-step)

A temporal independence study (time-step) with the influence of the time-step size on the Temperature for the first discharge of the battery cell at an ambient temperature of 25 °C was performed at fixed time-step size at 10 s, 50 s, 100 s (selected), and 150 s for the battery cell without PCM. For this case, the percentage deviation was less than 0.1 % for the selected time-step size of 100 s and was seen as sufficient to conduct the study. For the other case where the battery cell is jacketed with a PCM, a manual adaptive type of time-step size was used to achieve converged results. This ensured that the movement of the melting front and the mushy zone region was accurately captured to effectively evaluate the heat transfer effects due to conduction, convection, and natural convection.

4.3.3 Mushy zone constant independence study

The mesh independency study was performed to understand the impact of the mushy zone constant values, A_{mush}, from $1e^4$ to $1e^8$ on the melting of the PCM N-octadecane due to the thermal influence generated from the battery cell. In this case, the ambient battery temperature was 25 °C and was deep discharged at 1C rate. Results had little to no impact on the temperature as well as the PCM liquid fraction (approximately 1 %). This can be attributed to the small volume (5973 mm^3) of PCM (3 mm circumferential diameter) used in this analysis, as larger volumes of PCM can significantly impact the natural convection (Nicholls et al., 2022). It is during this phase of convection heat transfer which is associated with the rate at which the PCM melts. This study has only incorporated the melting phenomenon of the PCM and does not consider the solidification. In solidification, the mushy zone constant would be overlooked since conduction heat transfer would be the dominant heat transfer

mechanism. It is noted that ~ 65 % of the PCM was melted at the end of the first discharge, which indicates that the majority of the PCM was liquid with a percentage deviation of ~1 % for all cases compared to the selected case ($1e^5$).

4.3.4 Computational model setup

ANSYS Fluent 2021 R1 is used to numerically simulate all cases including discharging and recharging of the battery cell, as well as melting of the PCM using a pressure-based solver adequate for laminar viscous model flows. A transient time analysis was used with the implemented Pressure Implicit Splitting Operator (PISO) scheme for the pressure-velocity coupling. Momentum and Energy equations were analysed using second-order upwind, while for pressure, PRESTO! was used in the spatial discretization. The under-relaxation factors for pressure, density, momentum, energy, and liquid fraction were set to 0.3, 1, 0.7, 1 and 1, respectively. The convergence criteria were set to 1 micro for each timestep.

4.4 Results/analysis and discussion

4.4.1 Validation

Figures 4.3 (A) and (B) display the results of the validation of PCM melting and battery cell discharge respectively, captured from literature (Nicholls et al., 2022), (Kirad et al., 2021), (Kollmeyer et al., 2017), (Darzi et al., 2012), and (Kadivar et al., 2019) with less than 0.1 % deviation compared with the present study. Using the captured data for the Panasonic battery cell seen in (Kirad et al., 2021), the coefficients of the fifth-order polynomial form were calculated as seen in equations (4.20 - 4.25) and used as the inputs for the MSMD ECM model. Following the insertion of the assumptions and boundary conditions, the cell was discharged from an ambient temperature at 25 °C at a rate of 1C and heat transfer coefficient at 7 (W/m^2K) with adiabatic outer walls. The PCM assessed in the validation case was N-eicosane (Nicholls et al., 2022) which showed close agreement with the melting of the PCM and the phase change over time. This PCM validation study is shown to predict the melting front movement with close accuracy and a similar analysis is conveyed in this present study with the most suitable PCM.

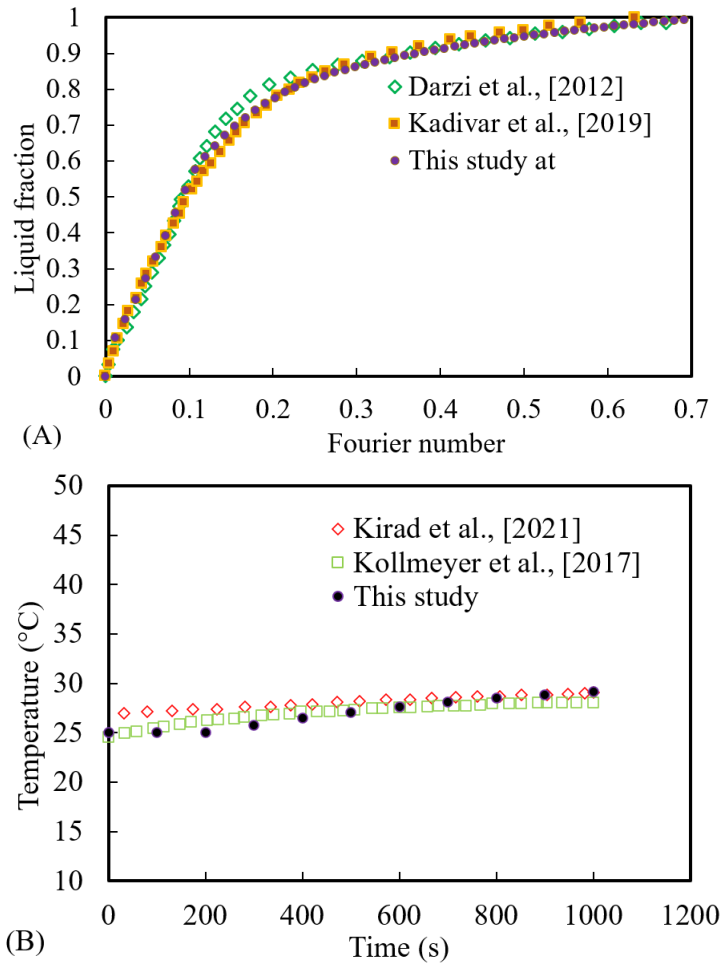

Fig. 4.3 Validation study results: A) Validation of the PCM melting for liquid fraction versus Fourier Number (F_O) for the present study compared with numerical data from the literature (Darzi et al., 2012), and (Kadivar et al., 2019); B) Validation of the battery cell thermal analysis for Temperature (°C) versus Time (s) for the present study compared with numerical and experimental data from the literature (Kirad et al., 2021 and Kollmeyer et al., 2017) at reference ambient temperature of

25 °C.

4.4.2 Coupled Thermo-chemical and electrical results

The results of the combined thermo-chemical and electrical study of the battery cell in the presence and absence of PCM for the following investigations are presented in this section and sub-sections:

- Investigation on the impact of PCM on the battery cell performance under charging and discharging cycles to ascertain its suitability to be considered as a thermal management system for battery cells.
- Investigation on the impact of PCM circumferential thickness (1 mm, 3 mm, 5 mm, and 7 mm) on battery performance to determine the most appropriate size for thermal management of batteries.
- Investigation on the impact of ambient weather conditions on PCM effectiveness for the thermal performance of batteries to design batteries with a lengthened stability in the process of discharging and recharging cycles even in extreme weather conditions.

4.4.2.1 Impact of PCM on battery performance under charging and discharging cycles

The objective of this study was to ascertain whether adding PCM as passive cooling is a suitable solution to enhance the battery performance under charging and discharging cycles. Results of the coupled thermo-electrochemical impact on the battery cell with jacketed PCM are displayed in Figure 4.4.

The results show the three indicators of battery performance used in this study namely, State of Charge (SOC), Temperature and Power at the initial temperature of 25 °C at the fully charged state. Figure 4.4 (A) displays a zoomed image with the complete discharge at a rate of 1C of the battery from initial SOC at 1 for both cases of the battery cell with (shaded symbols) and without (unshaded symbols) PCM. From the initial fully charged position, the battery temperature increased linearly during the first discharge until it reached a temperature of approximately 48 °C (in the absence of PCM). It must be noted that the safe operating temperature range for this type of battery cell is between -20 °C to 60 °C during discharge. This meant that in the absence of the PCM, the battery cell temperature was safely within this range. As shown in this Figure, during this first discharge, the SOC for both cases (with and without PCM) linearly decreased from the initial fully charged position at 1 and was fully/deep discharged at 0. Power drops from maximum power (~12W to ~8W) since there was a drop in the voltage of the battery as it discharged. The addition of the PCM jacket around the battery cell (3 mm circumferential diameter), kept the temperature constant and well within the optimum working temperature range (20 °C to 40 °C), showing that the thermal performance of the battery had improved due to the LH available from the PCM. This in turn extended the battery life cycle by a further 20 %

(~600 s) in comparison to the standalone battery cell as shown by the electrical performance captured (SOC and Power).

During the process of discharging, the PCM absorbed the heat generated from the battery cell by conduction heat transfer and the PCM began to melt as the liquidus temperature had been reached. At this stage, the liquid fraction of the PCM (molten PCM) was ~64 %, which indicated that there was still solid PCM with available LH capacity. To better understand the impact of PCM on the temperature distribution of a battery, in Figure 4.4 (A) a localised temperature contour layover is plotted at the initial and final conditions for the battery cell without PCM. Please note, as in the presence of PCM the battery temperature did not change significantly, the contour has been excluded in this figure. Also note, to display maximum temperature, the lower and upper limit of the colour bar varies between 321.05K to 321.18K, respectively, therefore a reader can better indicate the location of the maximum temperature of the battery in the overlayed contour. As shown in the overlayed contour, the highest temperature is accumulated at the core of the battery and decreases as it moves towards the battery tabs. This showed that the heat generated is at the centre of the battery where the focus of the LH material should be applied. The indication of the highest temperature zone was particularly useful for the designation of surrounding PCM. This initial discharging gave insight into the practicality of combining PCM with a constant volume for a single discharge with the applied assumptions and boundary conditions.

Moreover, a supplementary study (extended version of Figure 4.4 (A)) seen in Figure 4.4 (B), analysed the effects of PCM on the electrical and thermal performance of the battery involving continuous cycles of discharge and recharge, to ascertain a timespan, that the proposed model operated safely within its limits as discussed in section 4.2.4. In this case, the PCM enveloped the core of the battery only excluding the tabs (see Figure 4.1). Like Figure 4.4 (A), the boundary conditions and assumptions remained the same with the initial SOC at 1, temperature at 25 °C and a discharge rate of 1C. It is noteworthy that, as discussed in section 4.2.4, the discharging (60 °C) and charging (45 °C) cut-off temperature limits and voltage limits between 2.5 V and 4.2 V, a continuous cycle of discharge and recharge was performed (see Figure 4.4 (B)). In the absence of the PCM, as previously pointed out, the temperature of the battery cell reached ~48 °C after the first deep discharge, and well within the discharge temperature safety cut-off limit (60 °C). However, a further continuous recharge could not be completed since the battery temperature was above the charging safety limit (45 °C) for the upcoming process of charging, therefore in practice, the battery had to be cooled before the charging started. However, as seen in Figure 4.4 (B), further continuous charge and discharge cycles were applicable for the case with PCM. After the first discharge, the battery temperature was not significantly increased from its initial temperature of 25 °C since LH was still available from the PCM (36 %) to perform further cycles. Immediately after the first discharge (at 3600 s), the first charge was initialised. During

this cycle, the battery cell temperature was still relatively constant with a minimal increase in temperature until the PCM had fully melted at 30 °C indicated by a liquid fraction of 1 (at 5300 s). Since the volume of the PCM was completely molten, all the LH capacity available was used up and there was a transition to Sensible Heat (SH) where no further change in phase can occur, but the temperature of the material continued to rise. In this case, the battery cell temperature started to rise sharply (see Figure 4.4 (B)) almost mid-way through the charging until the end of the first charging (at 7300 s). At this stage, the temperature had reached ~40 °C and was still reasonably within the safe operating temperature range as the PCM contributed significantly to this. The SOC at the end of this cycle did not fully reach the initial starting charge at 100 % since there was a restriction in the maximum voltage (4.2 V), as discussed in section 4.2.4. Nonetheless, since at this stage in the cycling, the battery cell temperature was ~40 °C and well below the discharging cut-off limit (60 °C), it means that the process could continue safely into another discharge. At the end of this second discharge (at 10305 s), the temperature was at 54 °C and notably beyond the charging cut-off limit (45 °C) and therefore was unable to proceed to the second charge. By considering a complete cycle to include complete discharging followed by recharging, the introduction of the PCM extended the battery life cycle up to one ½ cycles or 3.4 times in comparison to that without a PCM, based on the conditions previously specified.

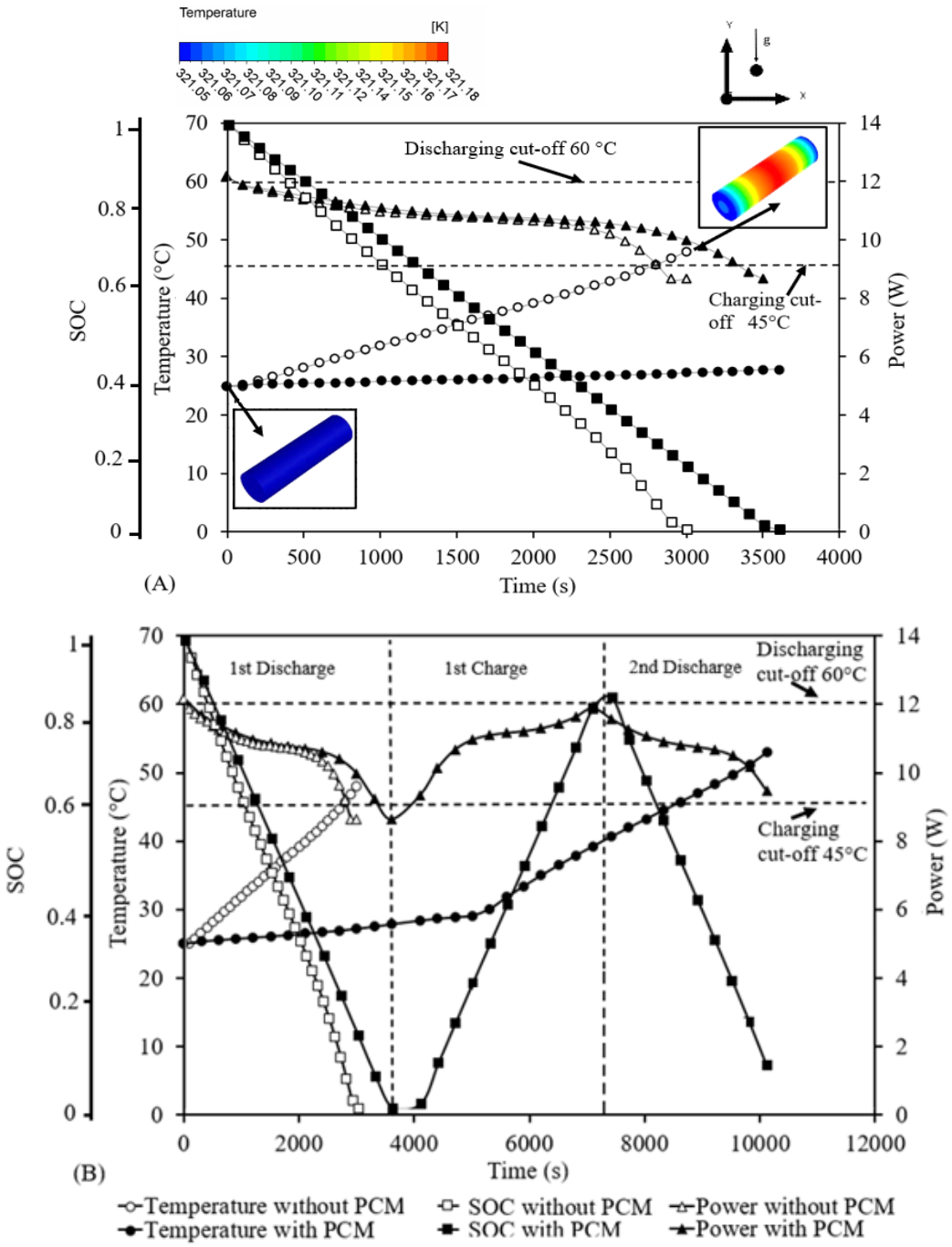

Fig. 4.4 Comparison of battery cell performance including SOC, Temperature (°C), and Power (W) versus Time (s), in absence and presence of 3mm jacketed PCM at 25 °C ambient temperature; A) during a single battery discharge with overlayed localized temperature contours; B) Consecutive cycles of battery discharge and recharge.

4.4.2.2 Impact of PCM circumferential thickness on battery performance

As the introduction of PCM proved itself as a promising passive cooling technique, a complementary study was implemented to ascertain the most suitable PCM size for battery performance. The study analysed the PCM jackets with 1 mm, 3 mm, 5 mm, and 7 mm thicknesses whilst considering N-octadecane as PCM material. Figure 4.5 presents the results of the proposed complementary study. In Figure 4.5 (A), a single battery cell underwent deep discharge at the initial temperature of 25 °C at a rate of 1C is displayed with a comparison of the battery cell without (unshaded symbols) and with (shaded symbols) PCM of varying thicknesses. PCM thicknesses of 3 mm, 5 mm and 7 mm performed similarly showing constant temperature. However, the 1 mm thickness was completely molten at ~2400 s after which a sharp increase in the temperature was observed until the battery was completely discharged (3900 s). This represented a change in the jacket from LH to SH where no further change in phase occurred, but rather, the temperature continued to rise. This can be thought of intuitively, as the greater the volume of PCM, the greater the amount of LH available.

This study was further extended into Figure 4.5 (B), where continuous cycles of discharge followed by recharge were performed for all the cases for varying thicknesses of PCM. As seen for the 1 mm PCM thickness, the SH was dominant up to ~2400 s after initialisation. As with the battery cell without PCM, the temperature was beyond the charging cut-off (45 °C) and was unable to proceed to the next cycle (at 3000 s). As seen for the 3 mm, 5 mm, and 7 mm PCM thickness, further cycles were performed. For all cases, the temperature remained constant for a longer time if there was LH present in the PCM (not fully liquid). As previously stated, when the PCM was fully molten, the LH was used up and so SH was dominant, and the temperature started to rise sharply. It shows that as the PCM thickness surrounding the battery cell increased, the battery was able to endure more discharge/recharge cycles. In this case, the 3 mm PCM lasted for 1 ½ cycles, 5 mm for 2 ½ cycles and the 7 mm lasted for 3 cycles whilst taking into consideration the discharging and charging cut-off temperature limits and voltage limits that affect the electrical performance of the battery. The figure also displays the overlayed battery temperature contours in the absence and presence of PCM with varying thicknesses. These contours illustrate the variation of temperature in the cell in different instances.

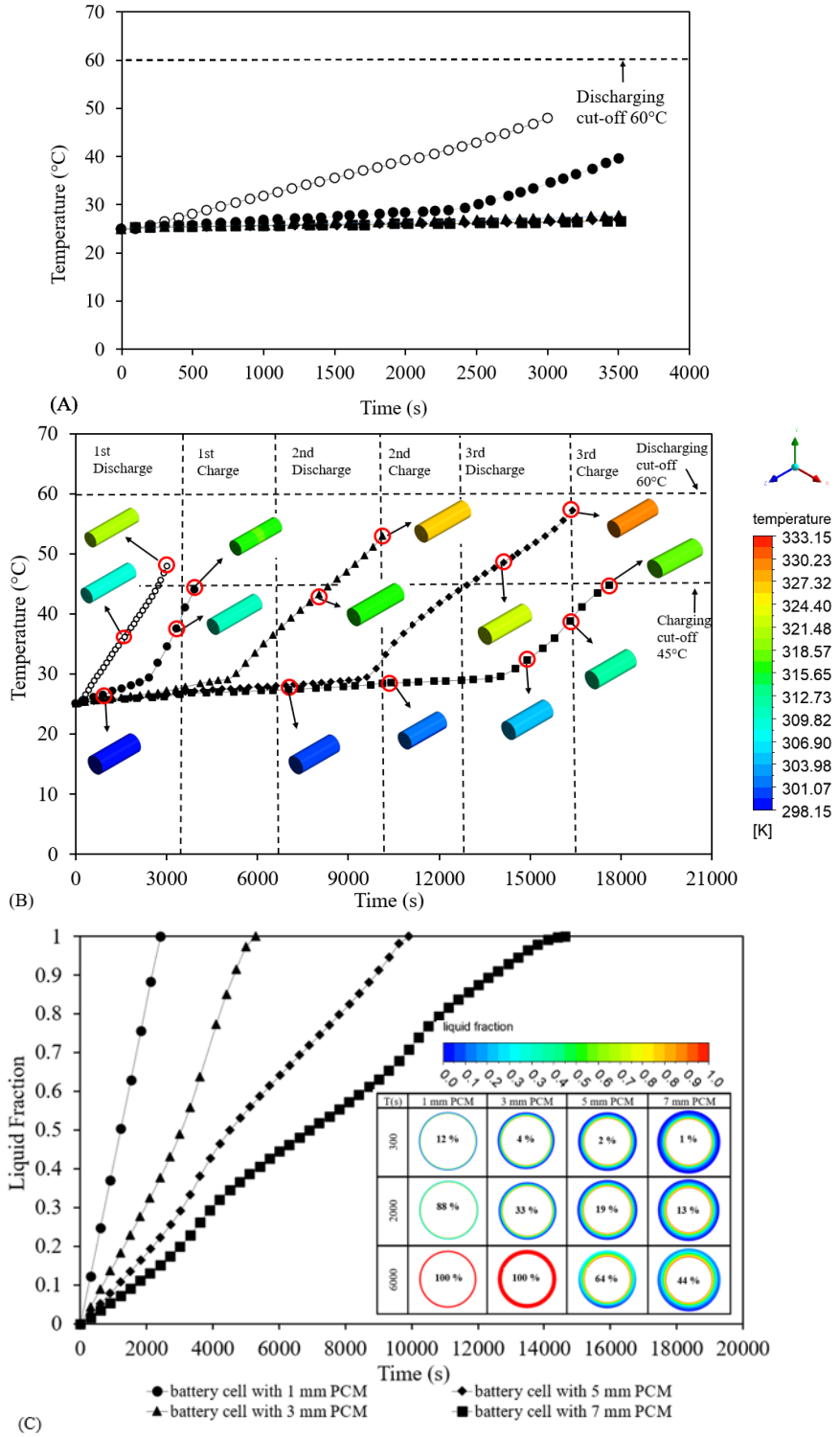

Fig. 4.5 Impact of jacket PCM thickness: A) Comparison of battery cell Temperature in presence and absence of various circumferential PCM Jacket thicknesses at ambient temperature of 25 °C during single battery discharge; B) Temperature (°C) versus Time (s) in consecutive cycles of battery discharge and recharge with temperature contours at specific instances; C) Liquid fraction versus Time for the melting of the PCM N-octadecane for the battery cell consecutive cycles with liquid fraction contours at specified instances.

In terms of selecting the optimum volume of PCM to provide the best improvement in thermal performance, the 3 mm jacket PCM thickness around the 18650 cylindrical battery cell was sufficient to illustrate that thermal performance can be prolonged if the electrical performance is also stable within the limits. When considering jacketing the battery cell with PCM, the available space and volume surrounding the cell must be taken into consideration, as ideally the weight of the BTMS should be kept to a minimum.

Figure 4.5 (C) shows the liquid fraction versus time for the various sizes of PCM N-octadecane, melting during the consecutive discharging and recharging cycles. The circumferential thickness of PCM was significantly affected by the heat generated, showing that the larger volume liquifies much slower. Liquid fraction contours at front views display the percentage of PCM fully melted at specific times. The battery cell with 1 mm and 3 mm PCM was fully melted after 6000 s and the natural convection is not clearly shown due to small volume sizes. However, for the battery cell with 5 mm and 7 mm PCM, the natural convection during melting is illustrated with a greater volume of solid PCM near the bottom as opposed to the top as shown by the coloured legend. In this case, the volume of PCM could be further increased to prolong the thermal efficiency of the battery. However, considerations towards the weight of the BTMS must be acknowledged as this can have a negative impact on the performance of the vehicle. Based on this study, 3 mm PCM was considered sufficient to extend the thermal performance without having a significant impact on the volume and weight of the system.

4.4.2.3 Impact of ambient weather conditions on the effectiveness of PCM jacket for thermal management of battery cells even under extreme weather conditions

Furthermore, a study performed on the impact of ambient weather conditions from normal to extreme conditions investigated the effectiveness of PCM for thermal management. For this study, varying the ambient temperature conditions for a test case for a single cell battery include -20 °C (extreme winter weather), 0 °C (winter weather), 25 °C (regular ambient weather), 40 °C (hot summer weather) and 55 °C (extreme hot/desert weather). It should be noted that at extremely low temperatures, such as -20 °C, there is an increase in internal resistance and consequently cold start of the battery which was not taken into consideration in this study but could be useful for further investigations. With decreased temperatures, the internal resistance of the battery cell increases, and capacity drops due to slower chemical reactions. Figure 4.6 displays the comparison of all the cases with and without PCM N-octadecane under the various ambient weather conditions after a deep discharge as used previously in this study along with RT44HC and Stearic acid.

At 25 °C, an insignificant rise in temperature is seen as time passes, since the PCM is already molten and acts as a LH system during a single discharge. Below 25 °C, the ambient temperature weather conditions did not reach the liquidus temperature of the PCM N-octadecane and so the PCM temperature would increase linearly (as the SH is active) until it reaches that melting point (the system acts as LH). For these low temperatures, the N-octadecane (PCM) takes longer to liquefy and can undergo further cycles of discharging and recharging until it is fully molten, and the LH returns to SH. For the hot temperatures outlined (40 °C and 55 °C), the PCM N-octadecane was fully molten (at 100 s) and so the LH already turned to SH, since there was no further change in phase. The battery temperature reached the discharging cut-off limit of 60 °C at 2,800 s and 700 s for 40 °C and 55 °C, respectively. In this case, only ½ cycle could be performed whilst safety limits were taken into consideration. It can be concluded from Figure 4.6, that the PCM N-octadecane (see properties in Table 4.1) were sufficient up to 25 °C (from extreme cold to ambient weather conditions), due to its solidus and liquidus temperatures. However, the thermophysical properties of PCM N-octadecane are not sufficient for t temperatures higher than 25 °C. This study shows that based on the geographical weather market manufacturers can design enhanced batteries with PCM based. As the thermal properties of the PCM N-octadecane were inadequate to keep battery temperature stable for extremely hot weather conditions, another complimentary study was conducted to investigate the impact of different PCM types on the thermal management of the battery. To alleviate the drawback of PCM N-octadecane in the hot weather conditions, two different PCMs were considered for the hot summer weather at 40 °C (RT44HC) and the extreme hot/desert weather at 55 °C (Stearic acid) (see Table 4.1).

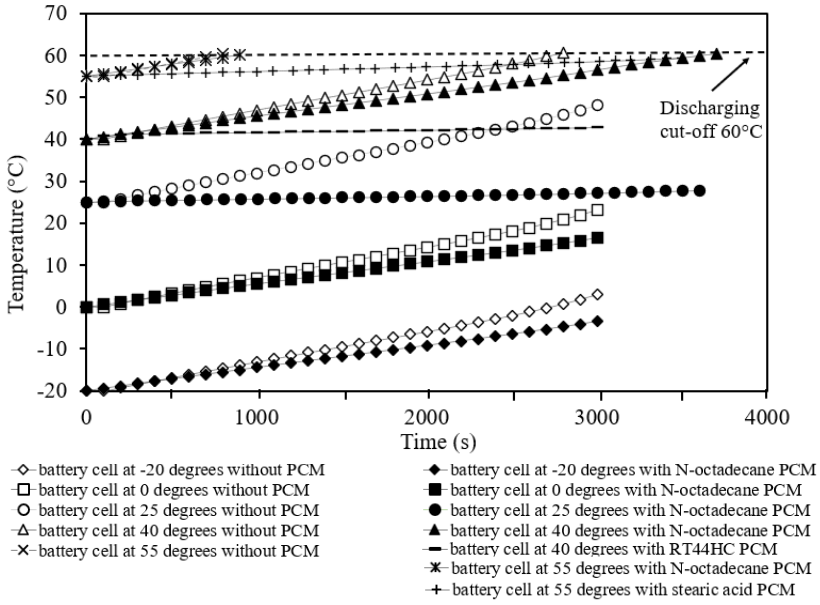

Fig. 4.6 Comparison of all cases for battery cell discharge with and without PCM N-octadecane at varying initial ambient temperatures of -20 °C, 0 °C, 25 °C, 40 °C and 55 °C.

Figure 4.7 shows the impact of the variation of PCM for consecutive discharge and recharge cycles. For the cases below 25 °C, SH was still dominant during the first discharge as the liquidus temperature of the PCM N-octadecane had not been reached as previously seen in Figure 4.6. Unfortunately, due to the extremely high temperature of 55 °C, only a single discharge was performed (see Figure 4.6) since the temperature was beyond the discharging cut-off limit (60 °C). However, there was still a 440 % improvement in the thermal performance of the battery to maintain a constant temperature at the end of deep discharge (~4.4x longer). It must be noted that these high temperatures are uncommon, but it is complementary to the results of the possibility of practically using PCM as a passive cooling approach for BTMS designs.

Consecutive discharge and recharge cycles were performed, and the results are shown in Figure 4.7. For the hot summer weather at 40 °C, the battery cell without PCM could only undergo the 1st discharge before reaching the cut-off temperature (at 2800 s), however, when the PCM was introduced, the battery underwent consecutive charging and was still below the charging cut-off temperature (at 6000 s) and so finally a 2nd discharge was completed (at 7700 s). LH was active for the first complete cycle of discharge and recharge, however, after this stage, the PCM was fully molten, and SH was active resulting in the sharp increase in temperature during the 2nd discharge. Both cases for 0 °C and -20 °C without PCMs completed consecutive discharge and recharging cycles (1 ½ and 3 cycles respectively) with a steady increase in the temperature until the safety cut-off limit was reached. Similarly, the cases of 0 °C and -20 °C with PCM completed multiple cycles with steady increases in temperature until the PCM started to melt and LH was active. At this region, the battery cell temperature remained constant even up to and after three consecutive cycles for the 0 °C case and up to the fifth discharge for -20 °C. This was significant as the battery operated at the optimum temperature up to 2 ½ full cycles and 4 ½ full cycles for the 0 °C case and -20 °C, respectively. After these cycles (at 13800 s for 0 °C and 24300 s for -20 °C), SH was active and no further cycling was performed. The results show that once the most appropriate PCM was chosen based on thermal properties and ambient conditions, the combined PCM and battery model can maintain its optimum operating conditions for longer.

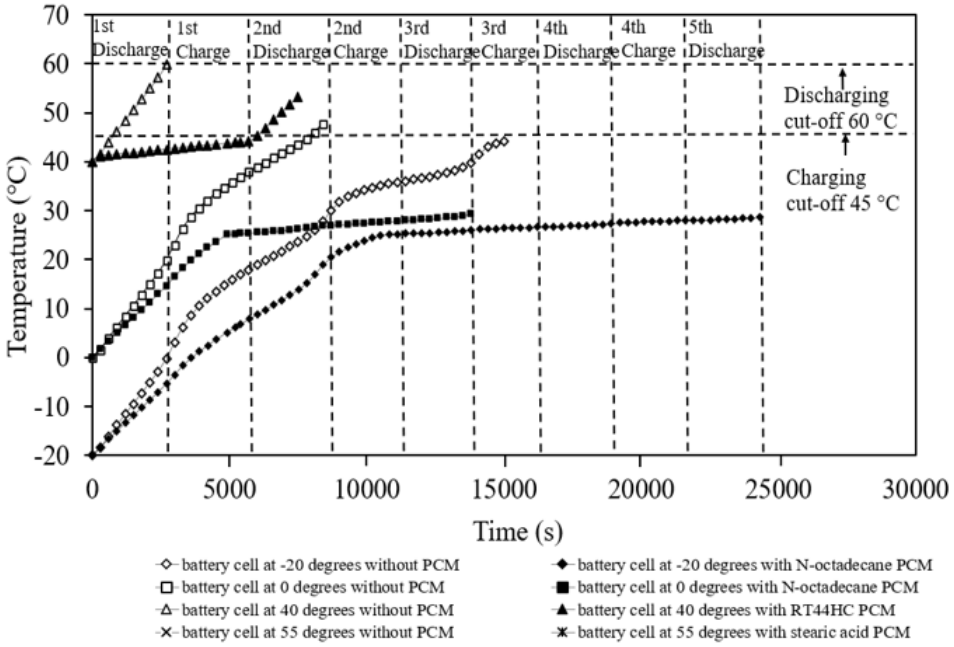

Fig. 4.7 Comparison of battery cell with (shaded symbols) and without (unshaded symbols) PCM showing the coupled electrochemical and thermal results of Temperature (°C) versus Time (s) at varying initial ambient temperatures of -20 °C, 0 °C, 40 °C and 55 °C for consecutive cycles of battery discharge and recharge.

4.5 Conclusions

In this study, an 18650 Li-ion cylindrical battery cell was conjugated with PCM to analyse the effects of passive cooling on the thermal performance under consecutive cycles of charging and discharging in varying ambient weather conditions including extreme winter weather -20 °C, winter weather 0 °C, ambient weather 25 °C, hot summer weather 40 °C, and extreme hot/desert weather 55 °C. Variations of circumferential PCM thicknesses including 1 mm, 3 mm, 5 mm, and 7 mm were analysed for the most appropriate PCM thickness and included variations of PCM for the changing weather conditions. Two cases were analysed one with PCM and one without so that all the heat generated by the battery was directly transferred to the PCM. The conclusions from the study are:

- The results of the validation study showed less than 0.1 % deviation from the literature with the study results and verification study for the special grid (mesh), temporal (time-step) and mushy zone variations showing that the selected values were sufficiently independent.

- The impact of PCM for regular ambient weather conditions at 25 °C, prolonged the thermal performance of the battery cell by 20 % after a single discharge and was effective at maintaining

a constant temperature for multiple cycles with a total extension of 3.4x (340 % performance improvement). In this first case study, results were positive in the direction of PCM-based thermal-balanced cooling (passive cooling) that provided steady battery temperature control and can function as a standalone BTMS based on the conditions set in this work.

- The impact of circumferential thickness compared PCM jacket sizes of 1 mm, 3 mm, 5 mm, and 7 mm thickness whilst considering N-octadecane as PCM, showed that 3 mm was sufficient for extending the thermal performance.

- Appropriate PCMs chosen for higher temperatures at 40 °C and 55 °C with initial results of discharging, showed constant battery temperature. However, at 55 °C temperature only achieved a single discharge since it reached the cut-off limit, but there was still a 440 % improvement (4.4x) in the thermal performance. This temperature is not common but complimentary to the study. Similarly, the 40 °C weather condition without the PCM only underwent a single discharge before reaching the safety cut-off limit, but the addition of the PCM further extended the thermal performance up to 1 ½ cycles.

- For lower temperatures (-20 °C and 0 °C) only SH was observed since the PCM was not at the melting temperature. Consecutive cycles for the 0 °C and -20 °C with PCM remained constant even up to and after 2 ½ and 4 ½ consecutive cycles, respectively displaying 160 % and 162 % thermal performance improvement.

The results show the choice of PCM-based passive cooling on thermal properties and the ambient conditions, can maintain the optimum battery operating conditions for longer.

4.6 Chapter Summary

This research Chapter evaluated the research conducted for the conjugation of TES with EES. The study focused on the cellular level of a Li-ion 18650 cylindrical battery cell jacketed with PCM around the circumferential area. The study analysed the effects of the introduced PCM on the battery and focused on three main elements of battery performance, namely, Temperature, State of Charge (SOC) and Power. Using these three indicators of battery thermal performance, the added PCM was shown to be an improvement in the thermal stability of the battery, even performing multiple consecutive cycles of charging and discharging as the thermal performance had been enhanced with the introduction of the passive cooling material. The study highlighted various weather conditions as well

as the volume of PCM surrounding the battery cell. This Chapter evaluated the integration of the TES with EES as identified as part of the main objectives of this research and acts as a starting point for further research at the modular level. It is noted that this Chapter was a continuation of studies for a Conference presentation as highlighted in the Publications section and has been published in a Journal. Moreover, in the following Chapter 5, a shift from ideal theoretical continuous loading to haphazard variations as a result of real-world driving cycles is investigated. Notably, the impact on the performance of the single cell with and without passive cooling is investigated for different driving cycles from harsh to casual to evaluate the thermal reaction of the chosen PCM within a specific ambient condition. Additionally, the Chapter goes into detail about the variation of discharging C-rates on the performance of the single cell when passive cooling was introduced as compared to without.

CHAPTER 5: LATENT HEAT BASED PASSIVE COOLING ON THE PERFORMANCE OF EV BATTERY UNDER AUTOMOTIVE DRIVE CYCLES [5]

5.1 Chapter Brief

In the previous Chapter, an investigation into the conjugation of TES and EES analysed the impact of an 18650 Li-ion cylindrical battery cell jacketed with PCM. The cell was assessed under continuous cycles of charging and discharging with various PCMs, the impact of PCM circumferential thickness on battery performance and the impact of ambient weather conditions on the effectiveness of PCM jackets for thermal management even under extreme weather conditions. An overall introduction to PCMs and battery thermal management based on passive cooling and the effectiveness of different battery models were reviewed in the literature review in Chapter 2. The previous chapter expanded on this research area for performance under various climate conditions. Chapter 5 is focused on the utilisation of passive cooling for BTMS for cylindrical cells employing the Latent heat (LH) jacket under various real-world automotive drive cycles as opposed to continuous charging/discharging cycles. In this case, the challenge addressed involved the understanding of the haphazard behaviour which impacts the battery's performance and its thermal stability. The drive cycles were collected from literature and online sources which comprised both aggressive and casual driving styles. This issue was addressed using the passive LH cooling jacket from a numerical thermo-chemical and electrical model based on varying real-world driving scenarios that can account for varying routes, driving styles, and distances. This study Chapter is in line with the objectives set about in Chapter 1 and seeks to partially fulfil the targets set in milestones 1 and 2. This study is classed as a cellular study, as a single cell was analysed with future work on battery modules to be reviewed to further fulfil milestone 3 targets. The results of this study Chapter have been published in a journal article as seen in the documented Publication section.

[5] **Nicholls**, R.A, Moghimi, M.A., and Griffiths, A.L., Influence of latent heat based passive cooling on the performance of EV battery under automotive drive cycles, *Journal of Energy Storage,* 77, 2024, pp. 109924. https://doi.org/10.1016/j.est.2023.109924

5.1.1 Introduction

Amid the global drive to reduce carbon dioxide (CO_2) emissions, green technologies, especially Electric Vehicles (EVs) and Hybrid Electric Vehicles (HEVs) are at the forefront of the transition away from fossil fuels. This shift has led to a considerable focus on Electrical Energy Storage (EES) technologies, particularly lithium-ion (Li-ion) batteries (LIBs), to enhance energy storage capacities. Several studies stress the urgency of moving from high CO2-emitting Internal Combustion Engine (ICE) vehicles to renewable energy sources (Ghaeminezhad et al., 2022), (Subramanian et al., 2021), (Kumar et al., 2020). Despite the zero-emission nature of EVs and HEVs, some performance limitations persist, such as extended charging periods, driving range, and power output (Tete et al., 2021). Li-ion batteries, with their superior energy density, stability, and extended lifespan, are a preferred choice for major car manufacturers due to their high-quality performance attributes (Yang et al., 2023), (Jaguemont et al., 2016). While battery selection has been researched (Arora et al., 2018), (Kim et al., 2019), improvement in thermal performance and safety for batteries meeting consumer demands and ensuring top-tier product use is crucial for overall performance.

Li-ion batteries are widely favoured for EVs and HEVs, yet they possess certain vulnerabilities, notably their susceptibility to temperature fluctuations. These batteries typically operate within an optimal temperature range of 20 °C to 40 °C (Muenzel et al., 2015), (Landini et al., 2019), (Jilte et al., 2019). Deviating from this range has critical consequences: overheating may result in thermal runaway, leading to battery decomposition, fire, or explosions (Yang et al., 2023), while under-cooling increases internal resistances, causes capacity fading and reduces chemical reactions (Wang et al., 2012), (Ibrahim et al., 2021), (Ostanek et al., 2020), (Raijmakers et al., 2019). A temperature uniformity (Choudhari et al., 2020) greater than 5 °C outside the optimal range significantly affects overall performance. Voltage range also plays a key role, with the power output safety range for single-cell use typically between ~2.5V to 4.2V (Yang et al., 2023). To achieve a positive potential rating or drive relevant devices and vehicles, various batteries need to be connected in series or parallel (Kumar et al., 2020). These safety constraints often affect Li-ion batteries' performance during discharging and recharging.

An effective BTMS, as described in (Raijmakers et al., 2019), plays a crucial role in maintaining the stability of individual battery cells, modules, or packs within their optimal temperature thresholds. When the proposed battery cell or pack generates heat, it can create substantial temperature differences and potentially lead to thermal runaway, an aspect also highlighted in (Raijmakers et al., 2019), (Choudhari et al., 2020), (Wu et al., 2019). Employing active or passive cooling, an efficient BTMS enhances battery efficiency by focusing on crucial factors such as State of Charge (SOC), temperature,

and Power (Yang et al., 2023), which significantly influence battery effectiveness and longevity. SOC represents the battery's capacity balance between 0 and 1. Studies like (Kirad et al., 2021) propose Neural Network (NN) models influenced by time delays, while deep learning, as explored by (Xi et al., 2022), (Guo et al., 2023) offers insights into the advantages and disadvantages of leveraging artificial intelligence (AI), and machine learning (ML) for precise SOC estimations. This research uses numerical computational fluid dynamics (CFD) (Yang et al., 2023) to accurately predict, SOC, Power, and temperature levels.

Research studies often extensively examine the application of BTMS focusing on various designs that utilise active cooling methods like liquid/air cooling (Gulfam et al., 2023), (Worwood et al., 2017) and (Al-Zareer et al., 2018) while passive cooling techniques involve the utilisation of PCMs in applications related to LHS systems (Peng et al., 2022), (Sardari et al., 202020), (Talebizadehsardari et al., 2021). LHS operates on the principle of phase change, where materials transition from solid to liquid and then to gas or vapour, depending on temperature changes and thermal properties. PCMs have increasingly gained popularity in various thermal applications to maintain consistent system temperatures based on specific needs (Rao et al., 2011), (Cao et al., 2020), (Nicholls et al., 2022) and (Du et al., 2018). These material-based energy storage solutions exploit phase change phenomena by absorbing heat energy (Nicholls et al., 2022), (Chen et al., 2019), (Damiano et al., 2015) and (Kollmeyer et al., 2017). Past studies have demonstrated that energy absorbed during battery cycling contributes to sustaining the ideal battery temperature over prolonged periods. To address challenges linked to renewable energy supply and demand, passive cooling methods like PCMs (Nazir et al., 2019), (Alami et al., 2022) and (Huang et al., 2019) have been explored to enhance thermal performance and selection criteria. Additionally, sustainability aspects, particularly in terms of environmental impact, are crucial. An analysis of (Abdulmunem et al., 2023) of bio-based PCM's impact on thermal stability and control for 18650 LIBs, assessed under varying loading conditions, showed promising results with less environmental harm.

Several studies have highlighted the amalgamation of PCMs in designs of BTMS to influence overall thermal performance (Siddique et al., 2018) and (Patel et al., 2020). Investigations into various PCM types (Chacko et al., 2012) and (Patel et al., 2020), have been conducted to evaluate their impact on thermal behaviour. PCM selection criteria rely on factors such as maximum temperature, temperature variation, ambient temperature, and C-rate to determine the most suitable PCM for a given application (Kumar et al., 2020), (Tete et al., 2021) and (Yang et al., 2023). Paraffin-based PCMs have shown effectiveness in managing thermal aspects, and the review (Worwood et al., 2017) outlines the composite nature, functions, and manufacturing details of these materials, providing valuable insights into their potential use in EES systems.

Moreover, previous studies have emphasised examining consecutive charging and discharging, pulsing, and combined heat transfer (CHT) in battery thermal modelling to assess their impact on battery performance. For instance, a study on continuous cycling in EVs (Najafi et al., 2023) explored various setups, including the placement of PCM in the pack around the cells, while also considering the impact of rest time between charging and discharging cycles (ranging from 10 to 20 minutes). Findings revealed that PCM placement around the cells exhibited better results during the initial cycle, whereas PCM in the pack demonstrated limitations in maintaining optimal temperature conditions. Notably, the study suggested that longer rest times led to more consistent temperatures across consecutive cycles.

Similarly, in another investigation (Patel et al., 2020) a 3-dimensional (3D) transient electro-thermal model was employed under drive cycles characterised by high initial ambient temperature and high power demands associated with aggressive driving styles. This study recorded temperature and C-rates, adhering to safety limits during continuous charging and discharging cycles. The findings significantly shed light on the necessity for an effective BTMS to sustain the ideal operating temperature of battery cells when affected by demanding driving cycles.

The precision of battery thermal modelling is critical for effective BTMS, considering heat transfer from the core temperature of batteries. Literature offers diverse, simpler electrochemical models (Jiang et al., 2014) and (Xiaopeng et al., 2014) with drawbacks such as lacking internal state information and side reactions during charging and discharging. However, these models can integrate seamlessly into various BTMS technologies, showing advantages in higher-order modelling (Khamar et al., 2014) over lower-order models (Parvini et al., 2015) and (Zheng et al., 2015). Equivalent circuit models (ECM) (Nicholls et al., 2022) and (Freudiger et al., 2019) have been evaluated under Worldwide Harmonised Light Vehicles Test Procedure (WLTP) conditions (Ghoulam et al., 2022) and (Micari et al., 2022) across different batteries in varied numerical and experimental settings. Various notable drive cycles, like Unified Dynamometer Driving Schedule (LA92) (Khalfi et al., 2021a), Emission test cycle (US06) (Bhavsar et al., 2023), New European Drive Cycle (NEDC) (Shah et al., 2021), Indian drive cycle and Federal Test procedure (FTP-75) (Vikram et al., 2022), have been examined to study battery thermal performance aligned with the behaviour of the drive cycle. These studies have demonstrated the effectiveness of modelling battery systems through experimental and numerical validations, along with the use of PCMs for managing thermal performance during both single and continuous cycling (Yang et al., 2023). Incorporating the modelling of dynamic vehicle driving behaviour in real-life scenarios is crucial for more efficient BTMS designs.

This research work seeks to address the field of battery modelling in which previous studies have shown success in predicting battery behaviour under different driving styles for experimental and

numerical approaches. They have faced challenges in the integration of various loading conditions with BTMS using passive cooling. To bridge the discussed gap in knowledge, this work presents an approach, aiming to model dynamic battery behaviour in the presence of real-world automotive driving for a Panasonic LIB equipped (as a passive cooling approach) with a LH jacket, which, to the author's best knowledge, not explored before. It is noteworthy that, while most existing research primarily analyses battery charging or discharging in single or continuous cycles, this study deals with the impact of unpredictable driving patterns and their associated thermal management. Thus, the novelty of this work lays one investigating the impact of passive cooling under real-world automotive driving cycles at cell level. Consequently, this study shed some light on the haphazard cycling processes and their associated thermal demand in single-cell scenarios. The insights gained from this approach extend beyond individual cells, offering valuable data applicable to module and pack levels while ensuring computational efficiency and early development standardisation. Furthermore, this research assesses BTMS performance, considering SOC, power, and temperature, both with and without LH jackets. Throughout, safety considerations are paramount, with temperature and voltage limits established to prevent thermal runaway and explosions. This research highlights the importance of considering environmental conditions when selecting BTMS configurations for practical EV applications and underscores the need for further exploration of battery modules and packs to fully comprehend and implement innovative thermal management solutions in the field.

The structure of the study follows drive cycle definitions, which describe the nature of drive cycles, numerical methods detailing the models, mathematical approaches, assumptions including thermo-chemical and electrical modelling, safety controls, initial and boundary conditions, and computational model setup. This follows the results and discussion, including verification (special grid, temporal, and mushy zone independency analysis) and validation study, the impact of the LH jacket on the battery performance under automotive drive cycles, and the impact of variation of discharging C-rates and finally suitable conclusions provided.

5.1.2 Drive Cycle Definitions

Drive cycles are known to deal with the variation of the speed of the vehicle versus time. They are normally used to determine fuel consumption and emissions based on a standardised assessment to make a comparison between different vehicles. These tests are focused on the chassis dynamometer to accumulate and assess variation in emissions. Each test is based on real-world driving scenarios depending on travel routes, idle times, driving behaviours (for example speed fluctuations) and distance travelled at a specific time. Figure 5.1 displays the power profile of all the drive cycles used in this

study on the specific battery outlined in Figure 5.2. All drive cycle testing data were collected from the literature (Kollmeyer et al., 2017), (DieselNet, 2022). In the following, a brief explanation of the drive cycles and the physical conditions they are mimicking are provided. It is worth noting that numerical simulations concluded when the data reached the maximum cycle data available, but there was ample data for conducting a thorough numerical analysis and drawing meaningful conclusions. A continuous discharge power result for a single cell is also displayed for comparison purposes of the dynamic behaviour of an aggressive drive cycle compared to continuous discharge regularly seen in the literature.

The figure in this study, Figure 5.1 (A) illustrates the emission test cycle (US06) drive cycle, emphasizing power patterns. This drive cycle represents aggressive and high-speed driving behaviour, featuring rapid speed changes and intense acceleration, typical of real-world conditions. Over 8.01 miles (12.8km), the vehicle maintains an average speed of 48.4 miles per hour (mph) (77.9 kilometres per hour (kph)) and reaches a maximum speed of 80.3 mph (129.2 kph) within 596 seconds. A closer look at the power variations during this phase reveals fluctuations, with the highest power reaching around 25 W and the lowest dropping to approximately -53 W, spanning a total time of 4500 seconds. This cycle is replicated multiple times based on available literature data for the recorded cycles in this study.

The Urban Dynamometer Driving Schedule (UDDS) drive cycle, as depicted in Figure 5.1 (B), illustrates the power profile throughout a specific timeframe. This cycle simulates urban driving conditions, covering a route of 7.5 miles (12.07 km) characterised by frequent stops, with a maximum speed of 56.7 mph (91.25 kph) and an average speed of 19.6 mph (31.5 kph). The UDDS consists of two phases: the first phase lasts 505 seconds (equivalent to 5.78 km at an average speed of 41.2 kph), followed by the second phase, which lasts 867 seconds and begins with a cold start. Weighting factors of 0.43 and 0.53 are applied to the first and second phases, and emissions are expressed in grams per mile (g/mile) or grams per kilometre (g/km). Zooming in on the power fluctuations during a 1500-second interval within this cycle reveals a peak power of around 13 W and a minimum power of approximately -19 W, covering a total period of 22450 seconds. Multiple cycles of this UDDS are considered, and the data is collectively analysed to conclude.

The Highway Fuel Economy Test (HWFT) drive cycle is presented in Figure 5.1 (C) and (D), illustrating the power profile. This test is conducted twice, with a downtime period in between cycles, initially for pre-conditioning and then for the actual conditioning phase. The HWFT simulates vehicle operation to determine the fuel economy of light-duty vehicles' highway fuel economy rating. This cycle involves driving a vehicle over a total distance of 10.26 miles (16.45 km) at an average speed of 48.3 mph (77.7 kph) within 765 seconds. Zooming in on power fluctuations during an 800-second interval within this cycle reveals a peak power of around 18 W and a minimum power of approximately

-16 W, covering a total period of 7500 seconds. Multiple cycles of the HWFT are conducted and analysed to assess performance and draw conclusions regarding fuel economy for light-duty vehicles on highways.

The Unified Dynamometer Driving Schedule (LA92) drive cycle is depicted in Figure 5.1 (E), illustrating the power profile. This cycle is designed for testing Tier 3 vehicles with weights ranging from 10,000 to 14,000 lbs. It involves aggressive driving conditions with high speeds, rapid acceleration and reduced downtime and idling. The LA92 cycle comprises distinct phases:

1. The vehicle covers 11.04 miles (17.7 km) at an average speed of 22.92 mph (36.74 kph) in 1735 seconds.
2. The vehicle travels for 9.8 miles (15.8 km) at an average speed of 24.8 mph (39.6 kph) in 1435 seconds.

Phase 1 includes a 1.2-mile (1.9 km) drive completed in 300 seconds, while phase 2 covers 8.6 miles (13.8 km) in 1135 seconds. Zooming in on power fluctuations over a 1500-second interval within this cycle reveals a peak power of around 35 W and a minimum power of approximately -26 W, spanning a total time of 14,000 seconds. Multiple cycles of the LA92 are conducted and analysed to evaluate the performance of Tier 3 vehicles under these demanding driving conditions.

The Neural Network (NN) drive cycle, depicted in Figure 5.1 (F), presents the power profile over a specific duration. This cycle combines elements from the US06 and LA92 drive cycles, introducing additional dynamics necessary for training neural networks. In a closer examination, a zoomed image reveals power fluctuations over a 600-second interval within this cycle. Within the total captured cycle data, the peak power reaches approximately 28 W, while the minimum power drops to around -38 W. The entire cycle spans about 11,700 seconds. The NN drive cycle is designed to provide diverse driving scenarios used for training neural networks, making it a valuable tool for assessing the performance of various vehicle systems and technologies.

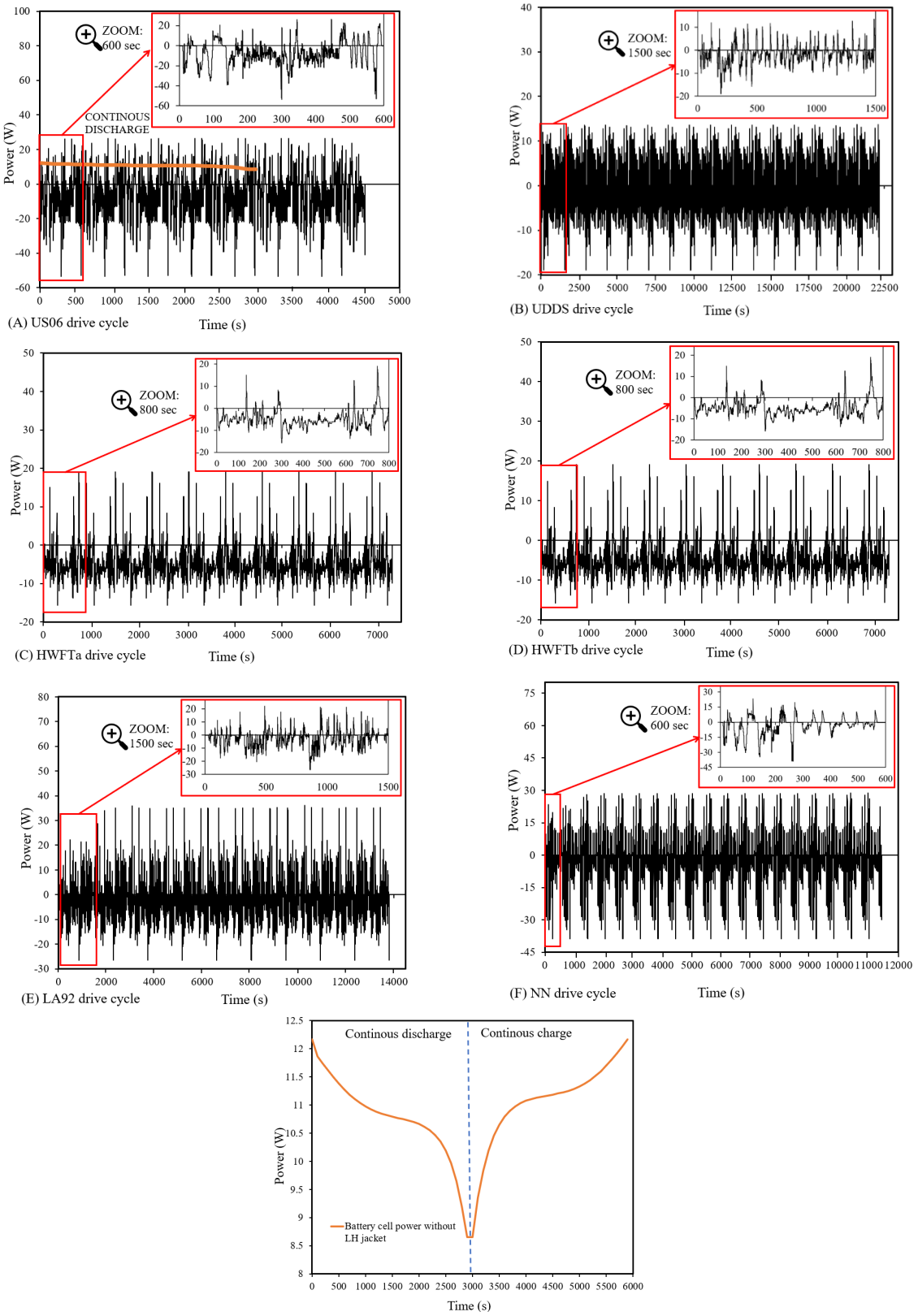

Fig. 5.1 Automotive drive cycles illustrating Power versus time evaluated for a single battery cell under 25 °C at 1 C-rate (A-F) and continuous discharge and recharge comparison.

Furthermore, in Figure 5.1, a plot of power versus time for continuous discharging followed by recharging of a similar cell under the same ambient conditions and C-rate is to distinguish between the haphazard fluctuations seen in the various driving cycles and the more uniform continuous cycles. These continuous cycles are performed as step functions of uniform increments between SOC 0 % to 100 % or specific to the testing applications. This analysis may provide detailed insights into the application of these drive cycles on this specific Panasonic 18650 battery cell. In this case, dynamic behaviour based on driving scenarios including idle time and speed fluctuations have been shown to have different effects on the power required to drive those vehicles which are normally used to decide on fuel consumption as well as emissions in a standardised format. Due to numerical simulation performance, this eliminated potential hazards as well as added costs for experimental setups as well as procurement, labour, and costs to repeat experiments when needed. Moreover, the impact on the LH storage material or LH jacket (PCM) and its capability to reduce the maximum temperature and maintain a more uniform temperature during these rapid fluctuations, as opposed to continuous, uniform cycling, is analysed. The response of the PCM is pivotal and uses its property of low thermal conductivity and slow heat transfer.

5.2 Numerical Method

5.2.1 Models

Figure 5.2 displays the schematic of a Panasonic LIB with an introduced 3 mm LH jacket. In a previous study, (Yang et al., 2023), the impact of PCM circumferential thickness (1 mm, 3 mm, 5 mm, and 7 mm) on the electrical and thermal performance of the battery was investigated. The previous results indicated that a 3mm LH jacket was sufficient to enhance the electrical and thermal performance of the proposed Li-ion battery. It was also concluded that increased thickness could extend the useful life with the penalty of increased weight and less compactness of eventually constructed modules and packs; thus, design engineers should have rational and applied justifications to go beyond 3 mm thickness. In this study, the thermal and electrical performance of the proposed case (battery cell equipped with 3 mm PCM jacket) is compared against the same cell with no LH jacket. It should be noted that in previous studies (Yang et al., 2023) the 3 mm PCM jacket thickness was considered sufficient thickness, which improved the thermal performance during consecutive charging and discharging cycles and was subsequently used in this study based on the results achieved previously. Increasing the volume of PCM can inherently increase the thermal performance of the battery cell for longer but has the disadvantage of imposing additional weight and cost on the system.

Both cells are oriented horizontally and have thermally insulated outer walls to ensure no thermal effect from the ambient will impact the results of these cases. This means that all the heat generated from the battery during the cycling processes would be directly captured by the LH jacket PCM to depict the heat transfer between materials. Horizontal cases were assessed as due to the PCM charging and discharging, these systems are more effective in heat transfer during PCM melting, whereas vertical systems maintain consistent heat transfer (Nicholls et al., 2022), (Gürel et al., 2020), (Adine et al., 2009). Inclination angle reduces the average PCM temperature but affects the PCM melting, since convective heat transfer is dominant (Seddegh et al., 2016), (Kousha et al., 2017). Figure 5.2 shows the active cell zone, the cell tab, and the location of the LH jacket (PCM) around the circumferential area of the battery with horizontal front and side views. Here, the battery cell is an 18650 cylindrical cell type with 18 mm and 65 mm in diameter and length, respectively.

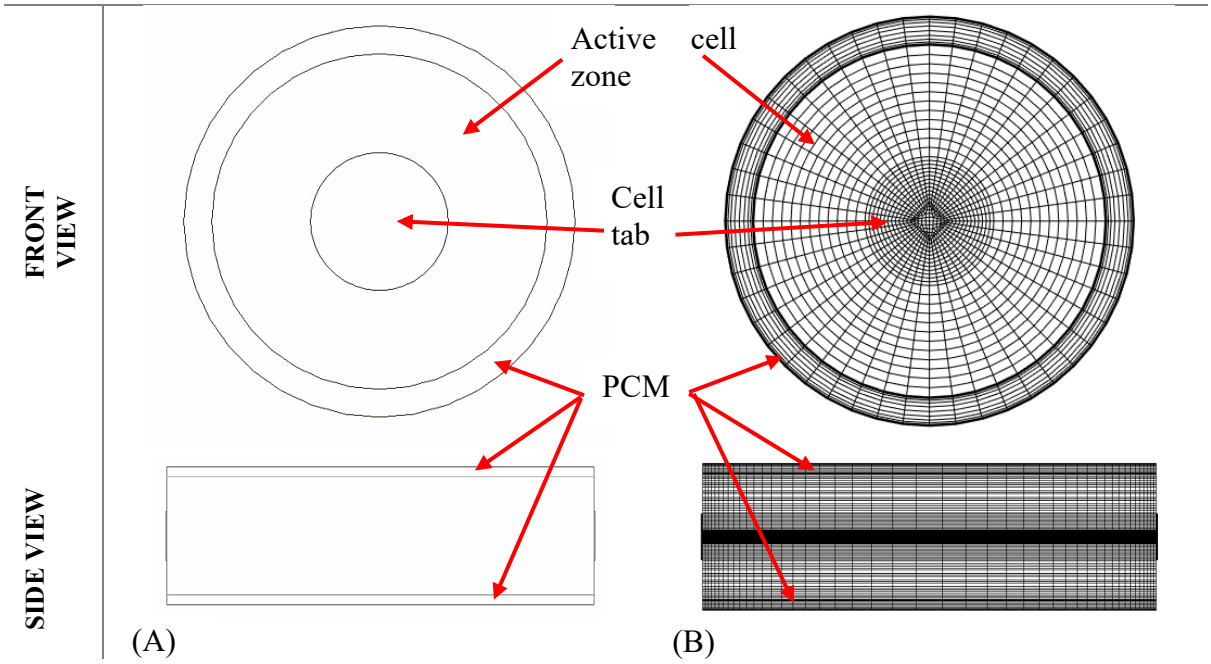

Fig. 5.2 Battery cell with PCM jacket showing front and side views: A) schematic sketch and B) meshed geometry.

5.2.2 Mathematical and numerical model approach

PCM melting engages an enthalpy-porosity formulation. The liquid-solid mushy zone defined as a porous zone is synonymous with the liquid fraction, including sink and momentum zones

appropriately referenced for the drop-in pressure in the solid zones. It is noted that the liquid fraction associates the states of the cell volume defined as either liquid or solid and is included in each domain cell. During every iterative solution, this value is calculated based on the enthalpy balance. To account for the change in the PCM physical state, a boundary region is set between 0 and 1 and signifies where the medium as in fully solid and liquid state, respectively. In this regard, a fully solid medium would have zero velocity and porosity.

The following section accounts for the PCM melting, with the subsequent section detailing the battery model, please check (Yang et al., 2023):

The energy equation follows:

$$\frac{\partial \rho h}{\partial t} + \nabla.(\rho \vec{v} h) = \nabla.(k \nabla T) - \frac{\partial \rho f L}{\partial t} - \nabla.(\rho \vec{v} f L) + S \tag{5.1}$$

The liquid fraction, f, is derived as

$$f = \begin{cases} 0 \\ 1 \\ \frac{T - T_{solidus}}{T_{liquidous} - T_{solidus}} \end{cases} ; \begin{cases} T < T_{solidus} \\ T > T_{liquidous} \\ T_{solidus} < T < T_{liquidous} \end{cases} \tag{5.2}$$

Natural convection flows because of buoyancy flows resulting from the density variation due to temperature. This phenomenon takes place in the molten section of PCM in this study. The flows are encased within a closed boundary so valid Boussinesq Approximation initialises faster convergence at constant density and temperature. The thermal expansion coefficient affects the natural convection flows induced by gravity, which would impact the density variations caused by temperature in the molten PCM region. As long as these are not sizeable differences in the density of the material and temperature differences within the domain are small, then the Boussinesq approximation is accurate. As the temperature of the PCM material increases, the volume is increased per temperature change by the value (0.00091) specified in Table 5.1. This means that there are small changes in volume as the material temperature increases and in melting:

The momentum follows:

$$\frac{\partial \rho_0 \vec{v}}{\partial t} + \nabla.(\rho_0 \vec{v} \vec{v}) = -\nabla P + \nabla.(\mu \nabla \vec{v}) + (\rho - \rho_0) g + \frac{(1-f)^2}{f^3 + \varepsilon} \vec{v} A_{mush} \tag{5.3}$$

Where ε is a number equal set to 0001,

A_{mush} is the mushy zone constant between 10^4 - 10^7. 10^5 was proved to be sufficient for the melting process in this analysis, as discussed in earlier studies (Yang et al., 2023), (Nicholls et al., 2022).

The governing equation for continuity is as follows:

$$\frac{\partial(H)}{\partial\frac{\alpha t}{D^2}} + \nabla.(\vec{v}H) = \nabla.(\nabla \mathrm{T}) \tag{5.4}$$

Where H is derived as the sum of Sensible enthalpy and the Latent heat:

$$H = h_{ref} + \int_{T_{ref}}^{T} C_p\, dT + fL \tag{5.5}$$

ANSYS Fluent 2022 R2 is used to analyse the coupled thermal-electrical result for heat generation rate with the applied Multi-Scale Multi-Domain method (MSMD). This method is primarily based on a multi-domain, multi-physics approach involving atomic Li-ion transport for distributed temperature measured along the battery length. The thermophysical properties of the battery cell, including the active zones, tabs, PCM and insulation, can be found in a previous research study (Yang et al., 2023) in Table 5.1. Various engineering domains use computational fluid dynamics (CFD) software to enhance thermal solutions. This numerical method offers cost and time savings as an alternative to physical experiments, particularly when exploring diverse design variations, along with optimisation tools for enhanced efficiency. Other benefits include parametric exploration for optimal designs and configurations, insights on heat transfer, temperature distribution, and system performance under varying conditions and risk reduction, which mitigates development risks without the necessity of physical prototypes. Although there are drawbacks which can include data dependency for material property for accurate simulations that may not be readily available, aligning simulation results with physical reality often necessitates extensive experimental validations, adding complexity to research and oversimplifications for real-world complexities with disparities between simulated and actual performance. Employing electrochemical and thermal models in computational tools aids in modelling diverse behaviours of batteries for longevity, analysing heat generation, dissipation, and temperature control. Despite existing models' limitations, more detailed models are computationally demanding. SOC and state of health (SOH) estimation methods rely on data processing, and combining different battery models enhances the accuracy, particularly through an electrochemical model based on the electric circuit. In this study, the Equivalent Circuit Model (ECM) model is used to replicate the electrical behaviour of the battery, as seen in a previous study (Yang et al., 2023).

Table 5.1: Thermophysical properties of battery cell (active zone), PCMs and insulation walls (Yang et al., 2023).

	18650 Battery cell (active zone)	Pos Tab	Neg Tab	PCM	Plexiglass (insulation)
Density (kg/m^3)	2092	2719	8978	770	1190
Cp (Specific Heat) ($J/kg-K$)	678	871	381	2196	1470
Thermal Conductivity ($W/m-K$)	18.2	202.4	387.6	0.148	0.19
Viscosity ($kg/m-s$)				0.003	
Thermal Expansion Coefficient ($1/K$)				0.00091	
Pure Solving Melting Heat (J/kg)				243500	
Solidus Temperature (K)				298.15	
Liquidus Temperature (K)				302.15	

In the previous study (Yang et al., 2023), the PCM chosen (N-octadecane) was deemed sufficient to maintain uniform battery temperature at ambient 25 °C due to its solidus and liquidus temperature applicable to the testing scenarios. Different ambient weather conditions were analysed, including extreme winter weather -20 °C, winter weather 0 °C, ambient weather 25 °C, hot summer weather 40 °C, and extreme hot/desert weather 55 °C. It was noted that although at higher temperatures (40 °C and 55 °C) the LH jacket was able to stabilise the battery temperature for longer; the improvement was not significant unless an appropriate PCM (different from N-octadecane) based on extreme weather conditions was introduced in the system. Nevertheless, the study indicated that the chosen PCM (N-octadecane considered in this study as well) at ambient temperature was sufficient to maintain constant/stable temperatures within the optimum temperature (20 °C to 40 °C). The selected PCM also improved the delay effect, increased the useful life of the battery cell and thermal performance enhancement extension for multiple cycles at 20 % and 340 %, respectively. This study does not go into detail on the effectiveness of different PCMs as the main concern of this study was checking the feasibility of utilising PCM as passive cooling under actual drive cycles, but a further study on different PCMs based on the methodology of this work can be considered in the future works of researchers. PCM properties are chosen for their unique attributes, which can include thermal, mechanical, and responsive but must be selected based on the appropriate application and thermal requirements. These might include high latent heat, small phase transition temperatures, and chemically stable and safe for use, as mentioned in the literature in this study.

5.2.3 Assumptions

5.2.3.1 Thermo-chemical and electrical modelling

The following assumptions are applied to the modelled cases:

- The initial SOC of the battery is set to 100 % at the ambient temperature of 25 °C,
- A transient time analysis is used,
- Viscous fluid flow is laminar and incompressible,
- Constant physical properties are applied to the battery cell with conduction heat transfer as the main heat transfer mechanism,
- PCM thermophysical properties remain a constant discounting density due to Boussinesq approximation.

5.2.3.2 Safety controls

To avoid thermal runaway with uncontrolled exothermic chemical reactions from fire and potential explosion due to battery degradation, constraints on the battery temperature and voltage during charging and discharging are maintained in the analysis. These constraints also help to maintain effects from high temperatures, and decomposition of electrolytes, including lithium loss and capacity fade effect and overcharging. The imposed constraints are as follows:

- Minimum and maximum cut-off voltage: 4.2 V and 2.5 V respectively,
- Maximum temperature during charging set to 45 °C and for discharging set to 60 °C.

5.2.3.3 Initial and boundary conditions

The following initial and boundary conditions are applied to the modelled cases:

- Thermophysical properties of the battery cell, PCM and insulation walls in Table 5.1,
- Outer walls insulated,
- Battery tabs set to adiabatic conditions,
- PCM initially at a solid state with liquid fraction as zero.

5.2.4 Computational model setup

The flow model chosen involves laminar viscous flows with an applied pressure-based solver due to the slow movement of the PCM during the melting process This solidification/melting process model is only applicable for a pressure-based solver, as density-based solvers are not available. Transient analysis is preferred to capture changes in the solution with time and to pinpoint changes in phases of the PCM. The pressure Implicit Splitting Operator (PISO) scheme is used for the pressure-velocity coupling for the transient time-based analysis. The solution method for spatial discretisation for pressure is indicated PRESTO! with second-order upwind for momentum and energy equations. Under-relation factors for pressure and momentum are initially set at 0.3 and 0.7 respectively, with density, body forces momentum and energy set to 1. There was no need to vary the liquid fraction update field for under-relaxation factors since suitable convergence was achieved and an appropriate mushy zone constant. The LH model solution convergence is set to 1 microsecond to achieve sufficient convergence. For the electrochemical modelling of the battery, as mentioned in section 5.2.2, the MSMD solution method with ECM E-chemistry model is applied for the battery cell at 2.9 Ah nominal cell capacity. Since a coupled thermal-electrochemical simulation is used, the electro-chemical aspect of the battery would be solved instead of just the heat generation rate, as in other solvers. The model allows for the use of different physics applied to different solution domains in which Li-ion transport occurs at the atomic length scale. The battery is deemed a homogeneous body with the electro-chemical reactions occurring within the active zone. In particular, the ECM model aims to replicate the electric circuit with resistors and capacitors as a function of SOC. The model is deemed suitable for single cell or multi-cell analysis. The solution options specified C-rate at 1, and minimum and maximum cut-off voltages at 2.5 V and 4.2 V, respectively, to match the manufacturer specifications for safe operation. The automotive drive cycle data is implemented as a time-scheduled profile type from Figure 5.1 into the battery model as a profile in the solutions options. This profile provides a time-dependent input based on parameters such as C-rate, current, voltage and power, which can be effectively varied to change the electric load type and the values. It means that the numerical and experimental data captured can then be directly analysed via linear interpolation.

5.3 Results/analysis and discussion

5.3.1 Verification study

Independency analyses were performed involving Mesh, Timestep and Mushy zone (A_{mush}) to ensure the results were of sufficient accuracy. Figure 5.3 (A) displays the analysis of the variation of

grids for both cases with and without the LH jacket, with results of temperature versus time. Three different grid sizes were compared including coarse (24911), selected (84801) and fine (130130) elements and coarse (40128), selected (86877) and fine (116664) elements for the case without and with LH jacket (PCM) respectively. The constructed meshes in the domains were mostly structured grids, where for the sake of brevity only the views of the selected mesh for the battery with LH jacket are displayed in Figure 5.2. As shown in Figure 5.3 (A), the proposed selected meshes (for both cases in the presence and absence of LH jacket) were fine enough to capture the results of this study independent of mesh sizes (less than 1 % divergence recorded for the results of selected mesh versus fine and coarse cases). It is noteworthy that the Orthogonal qualities and skewness for proposed meshes were more than 95 % and less than 25 % respectively, which proves what promising qualities the generated meshes had.

A time-step independency study is shown in Figure 5.3 (B) for a single cell battery discharge at ambient temperature (25 °C) analysing four different time-step sizes (10 s, 50 s, 100 s and 150 s) without LH jacket. Results show that the chosen time-step size at 100 s was sufficient (< 0.1 % deviation) to conduct the study. For the case with LH jacket, a manual adaptive time-step size beginning at 1 microsecond was used until sufficient convergence was seen. The effect on the mushy zone was highlighted in Figure 5.3 (C) with a study between applicable ranges of $1e^4$ to $1e^8$, to realise in the simulation of LH jacket what A_{mush} value (as discussed in Eq. 5.3) was required for accurate results. The study was performed for PCM N-octadecane with an initial solidus temperature at a discharge rate of 1C. Results indicate a minimal effect on the temperature, showing less than 1 % deviation from selected A_{mush} value at $1e^5$. This was elaborated in previous results seen in (Yang et al., 2023) and (Nicholls et al., 2022) where the volume of the circumferential diameter does not show significant change in natural convection heat transfer. This occurs when the PCM starts to melt at the top of the container. For this study, solidification of the PCM was not conducted and only the melting of the PCM during the cycles were recorded.

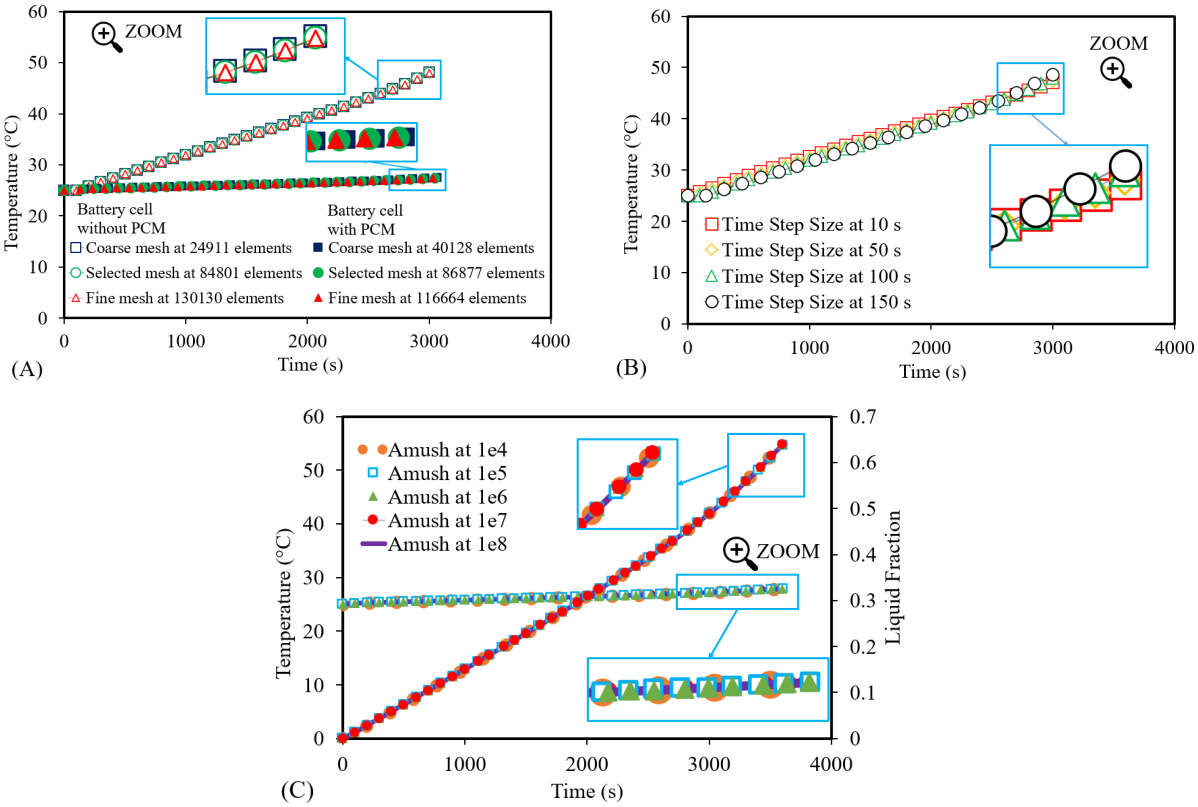

Fig. 5.3 Verification study showing: A) grid independence study, B) temporal independence study and C) mushy zone (A_{mush}) independence study.

5.3.2 Validation study

A numerical validation study shown in Figure 5.4 (A), and (B) presents the battery thermal management validation along with the PCM validation. A battery cell assessed at ambient weather conditions (25 °) for a single discharge at a 1C rate with a heat transfer coefficient set to 7 W/m^{2}K, compared the data from literature with the current study. A deviation of 1 % was seen and deemed sufficient to conduct the variation in drive cycles outlined. In this work, a numerical approach using CFD compounded the use and the advantages, including cost-saving and time-bound, as well as harnessing efficiency, safety, and risk mitigation. The gap between real-world complexity and accuracy in the simulation was closed by combining the experimental data and numerical solutions captured from (Kollmeyer et al., 2017) and (Kirad et al., 2021) to perform parametric studies and provide insights into performance in the presence of a LH jacket. Similar methods were used to show the relationship between the liquid fraction during PCM melting in an enclosed container of constant heat flux. A PCM melting validation shown in Figure 5.4 (B) compares the data for liquid fraction versus Fourier number of captured data from literature (Yang et al., 2023), (Kadivar et al., 2019) and (Darzi et al., 2012) based

on N-eicosane PCM. The study showed less than 1 % deviation and was sufficient to conduct the study based on N-octadecane PCM. In that study, different PCMs were analysed based on the impact of ambient weather conditions on the effectiveness of thermal management, including extreme weather conditions as mentioned in section 5.2.2.

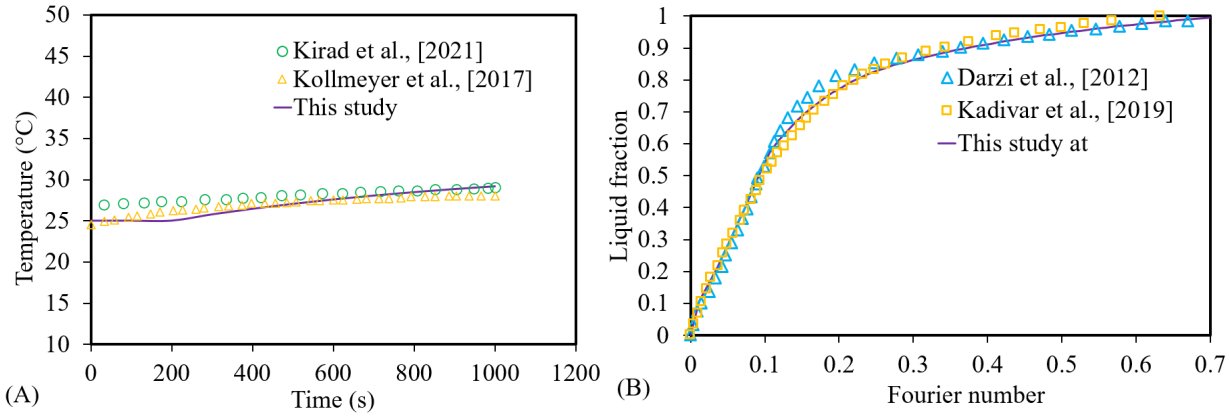

Fig. 5.4 Validation study: A) Single cell battery validation under ambient temperature (25 °C) for a thermal analysis of Temperature vs time (°C) versus Time (s) and B) PCM validation for liquid fraction versus Fourier number compared with literature results.

5.3.3 Impact of LH jacket on battery performance under Automotive drive cycles

In the preceding discussions, an examination of the range of drive cycles studied each with its characterisation behaviours and unique power profiles and applications. The US06 cycle, as seen in Figure 5.1 (A), represents an aggressive driving scenario with rapid speed fluctuations and behaviours following start-up. Meanwhile, the UDDS cycle illustrated in Figure 5.1 (B), mimics an urban route with frequent stops. The HWFT cycle, as displayed in Figure 5.1 (C) and (D), assesses the fuel economy of light-duty vehicles for highway ratings. The LA92 in Figure 5.1 (E) simulates aggressive driving with high speeds and acceleration. Lastly, the NN drive cycle in Figure 5.1 (F) combines features from US06 and LA92 cycles for training neural networks. The drive cycle data captured from (Siddique et al., 2018) and (DieselNet, 2022) serve as valuable tools in various automotive applications. They enable the evaluation of vehicle performance and the effect on battery technologies with emissions and energy efficiency under diverse driving conditions, from aggressive and high-speed scenarios to urban routes. The variation in drive cycles and the effect on thermal performance of battery cells as well as the LH cooling jacket can play a crucial role in advancing automotive technologies and improving vehicle efficiency and sustainability.

The primary objectives of this study were to ascertain the impact of LH jacket (passive cooling) on the thermal and electrical performance of a chosen battery cell under different drive cycles. The results of this investigation are shown in Figure 5.5. The variation of the automotive drive cycles involving US06, UDDS, HWFT, LA92 and NN drive cycles illustrated for Power profiles on an 18650 Panasonic LIB seen in Figure 5.2 and assessed under ambient weather conditions (25 °C) at 1C-rate. The Power profiles shown in Figure 5.5 display the Power output versus time for the combined thermo-chemical and electrical results for a similar battery cell with and without a LH jacket. The full results of the automotive drive cycles seen in Figure 5.1 are implemented numerically as a time-scheduled profile. As seen in the Power profile results, there was an extension in the performance of the battery cell for the cases with the LH jacket. This behaviour is attributed to the fact that the presence of the LH heat jacket can maintain the battery's thermal stability at the optimum range (20 °C to 40 °C) for a longer period, therefore the battery can have better performances as will be discussed in this section. These extensions were significantly seen in the aggressive cycles such as US06, LA92 and NN drive cycles as described in section 5.2.

It is noteworthy that in Figure 5.5 zoomed-in images of the curves are provided to visualise the initial variation in performance as seen in Figure 5.1 between the battery cell Power with and without the LH jacket. For the automotive drive cycles, the initial referenced time was repeated until all the data was completed, and the results of the combined thermo-chemical and electrical results were presented. The provided zoomed images were captured at different time spans depending on the drive cycle nature, as follows: A) US06 – 600 s, B) UDDS – 1500 s, C) HWFTa – 800, D) HWFTb – 800 s, E) LA92 – 1500 s and F) NN – 600 s. In these initial phases, the Power profiles are similar for both cases in the presence and absence of the LH jacket up to and including the full cycles. Each of the different drive cycles has a differing effect on the performance of the battery cell because of their characteristically varied behaviours and therefore has varying effects on the thermal and electrical performance.

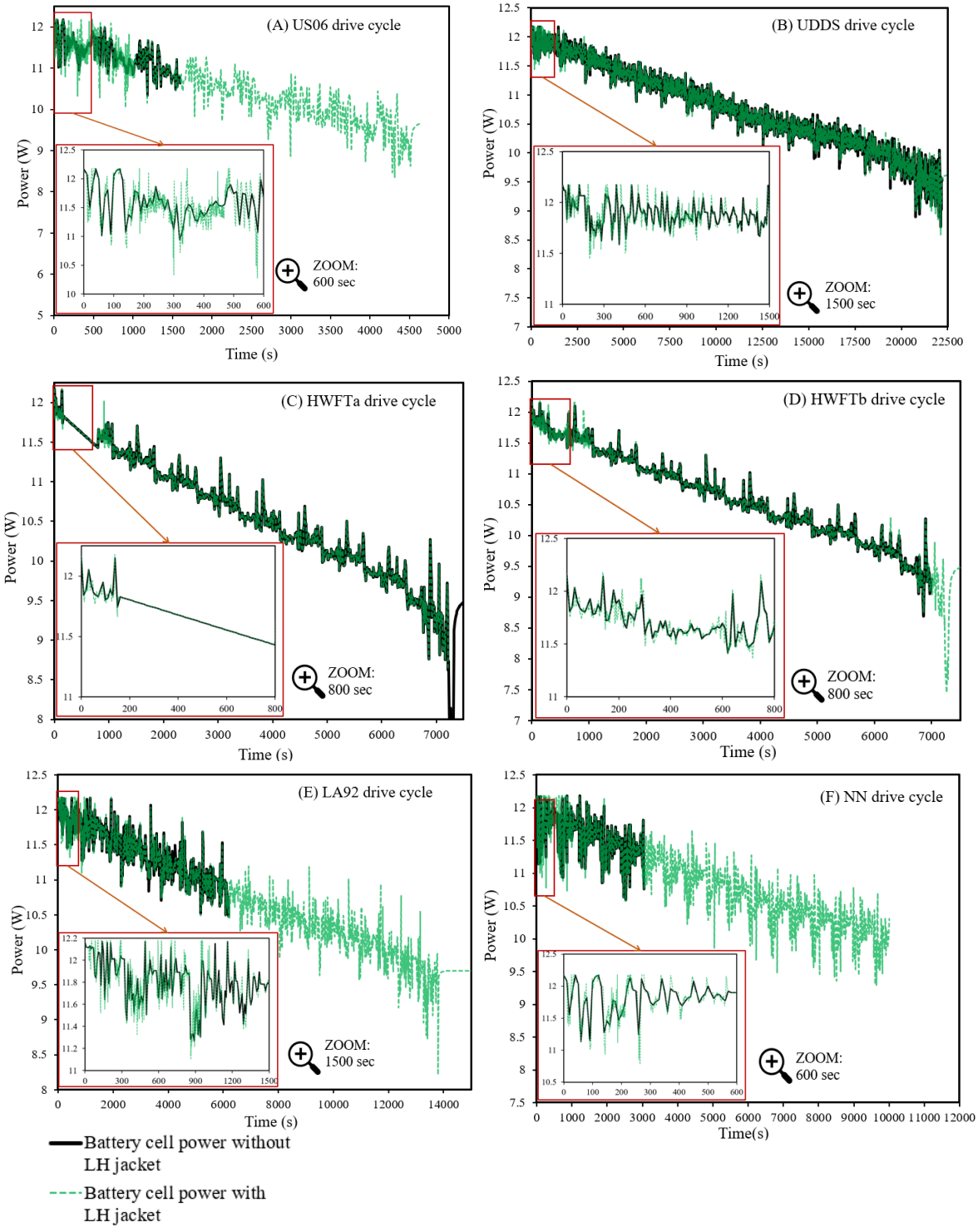

Fig. 5.5 Impact of automotive drive cycles on Power of battery cell with and without LH jacket as seen in legend: A) US06, B) UDDS, C), HWFTa, D) HWFTb, E) LA92 and F) NN.

To investigate the coupled effects of thermo-chemical and electrical performance in this study, temperature, SOC, and liquid fraction for both cases in the presence and absence of LH jacket were recorded. The results for battery temperature distribution and SOC are shown in Figure 5.6 and Figure 5.7, respectively, which were captured when the initial battery state was at 100 % SOC (fully charged battery) at an ambient temperature (25 °C) and C-rate of 1. In both figures, the harsh drive cycle comparison is illustrated in (A), and the casual drive cycle comparison is illustrated in (B).

The varied drive cycles outlined in section 5.1.2 were applied to both cases (with and without LH jacket) with safety measures applied for discharge and charge temperature (60 °C and 45 °C respectively) including cut-off voltage between 2.5 V and 4.2 V. It is noteworthy that under those drive cycles with discussed safety and cut-off considerations, the battery cell is discharged up to ~0 % to 20 % SOC and depends on the drive cycles as will be discussed in this study. It should be noted that when all the LH available from the chosen PCM (N-octadecane) was used, there was a transition to SH, which is shown by a linear rise in battery temperature. This linearised temperature increase during the SH shows a similar gradient pattern during this stage for all cases and is dependent on the battery SOC available at this stage of the drive cycle process. In this case, if the battery SOC was equal to zero or close thereof, then the cycling process would also end. Please note that in this study, as the driving cycles had been recorded over a specific period, the authors could not run the cases to their ultimate limits.

To effectively analyse the thermal performance of the battery cell in the presence and absence of LH jacket (PCM), the results in Figure 5.6 were analysed based on the following criteria:

1st criteria: Comparing the battery temperatures for both cases (with and without LH jacket), at the final instant which the battery without LH jacket case can reach.

2nd criteria: Comparing the time for both cases (with and without LH jacket), at the final temperature that a battery with LH Jacket can reach.

Please note that in those criteria definitions, the batteries undergo the drive cycle until the process is stopped either due to technical or safety considerations or termination of defined drive cycle data.

Indeed, in the definition of 1st criteria as will be discussed later, under different dive cycle loads the battery in the absence of LH jacket cannot undergo the entire defined cycle period (as shown in Figure 5.1) while the case LH jacket can go through a longer period of drive cycle. This is attributed to the fact that, in the absence of LH jacket, the battery either reached the imposed safety threshold or defined cut-off voltage or reached to almost zero SOC (see Figure 5.7). Therefore, in the 1st criteria, the

temperature variation of these two cases at the instant which the battery without LH jacket reaches, are compared.

Notably, there were drive cycles which did not reach the temperature safety limit for either case (with and without LH jacket) (see Figure 5.6) due to either the end of the drive cycles data or the battery SOC ~ 0 (see Figure 5.7). Thus, the 2nd criteria were defined to compare how long takes for both cases to reach the temperature that the battery with LH jacket had at the end of the simulation.

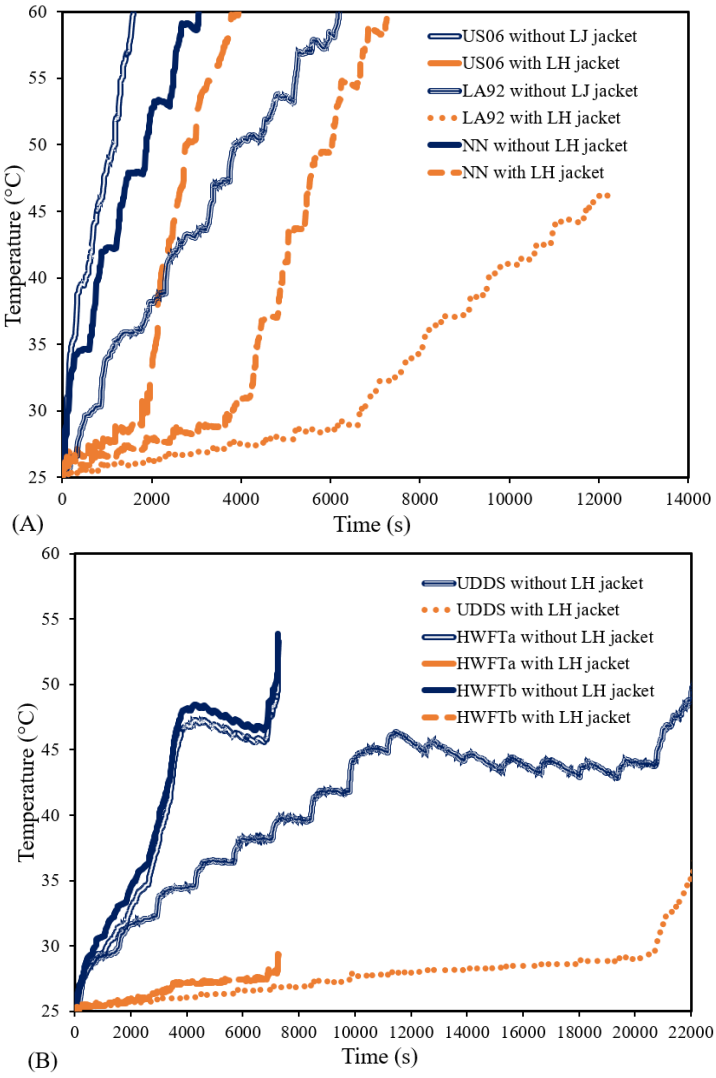

Fig. 5.6 Impact on battery temperature for harsh (A) and casual (B) driving cycles with and without LH jacket.

For the applied drive cycle US06, the case with no LH jacket reached the safety limit temperature at 60 °C as seen in Figure 5.6 (A) within 1,600 s, and subsequently, the further cycling load could not proceed. At this same instance in time, the battery cell in the presence of LH jacket had a temperature of ~ 29 °C (~ 52 % reduction in temperature based on the 1st defined comparison criteria)

and was still well within the optimum temperature range of the battery (20 °C to 40 °C) with the indication that the thermal performance of the cell had been enhanced due to the impact of the LH jacket and the available LH. At around 1,940 s, the liquid fraction of the PCM had reached the upper limit of 1 and all the PCM had been melted and thus SH was the dominant mechanism. During this period (after 1,940 s), the battery cell temperature sharply rose in a linear fashion noted by the cycling effect. This resulted in a rise in temperature to 60 °C in 3,940 seconds at the end of the driving cycle as the safety limit temperature was reached. Thus, the battery ran for a further 1,340 s in the presence of the proposed jacket. I.E. Based on the 2nd defined comparison criteria, the battery with LH jacket lasted ~x2.5 longer period. As seen in Figure 5.7 (A), from the initial state of the battery with the applied drive cycle US06, the SOC of the battery is shown to decrease from 1 to 0.07 at the end of the cycling. This shows that the battery was cycling the Power from 100 % and coinciding with Figure 5.5 (A) as the Power profile was seen to be decreasing over time.

For the applied drive cycle US06, the case with no LH jacket reached the safety limit temperature at 60 °C as seen in Figure 5.6 (A) within 1,600 s, and subsequently, the further cycling load could not proceed. At this same instance in time, the battery cell in the presence of LH jacket had a temperature of ~ 29 °C (~ 52 % reduction in temperature based on the 1st defined comparison criteria) and was still well within the optimum temperature range of the battery (20 °C to 40 °C) with the indication that the thermal performance of the cell had been enhanced due to the impact of the LH jacket and the available LH. At around 1,940 s, the liquid fraction of the PCM had reached the upper limit of 1 and all the PCM had been melted and thus SH was the dominant mechanism. During this period (after 1,940 s), the battery cell temperature sharply rose in a linear fashion noted by the cycling effect. This resulted in a rise in temperature to 60 °C in 3,940 seconds at the end of the driving cycle as the safety limit temperature was reached. Thus, the battery ran for a further 1,340 s in the presence of the proposed jacket. I.E. Based on the 2nd defined comparison criteria, the battery with LH jacket lasted ~x2.5 longer period. As seen in Figure 5.7 (A) from the initial state of the battery with the applied drive cycle US06, the SOC of the battery is shown to decrease from 1 to 0.07 at the end of the cycling. This shows that the battery was cycling the Power from 100 % and coinciding with Figure 5.5 (A) as the Power profile was seen to be decreasing over time.

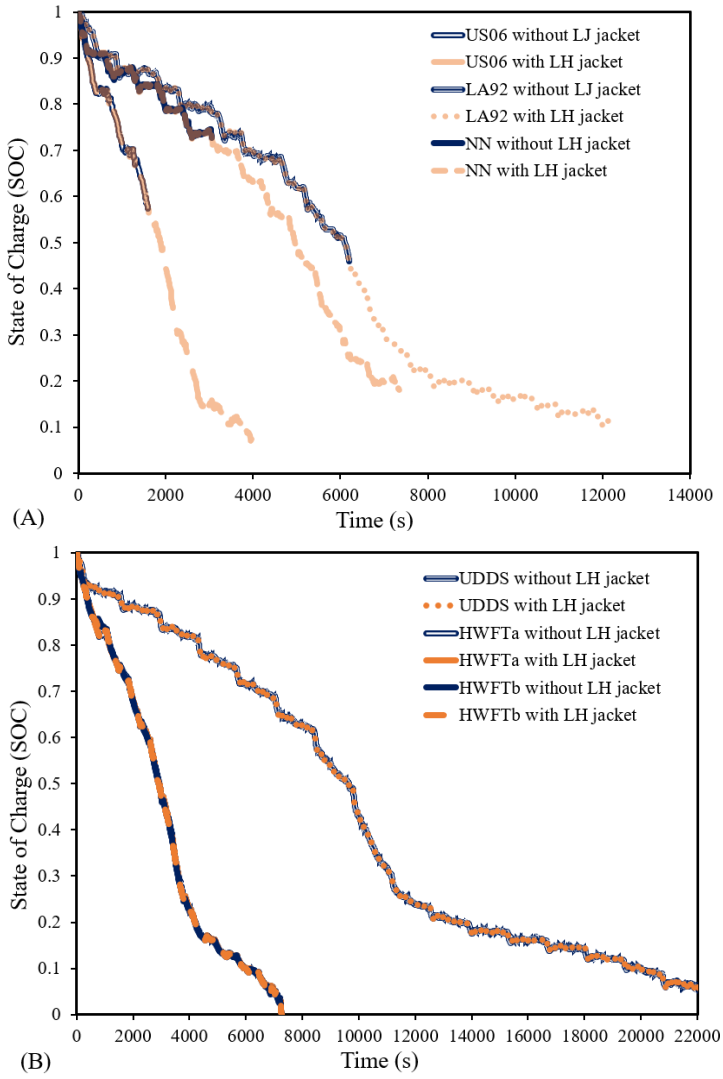

Fig. 5.7 Impact on battery SOC for harsh (A) and casual (B) driving cycles with and without LH jacket.

The impact of LA92 drive cycle on the thermal and electrical performance of both cases (with and without LH jacket) are shown for temperature and SOC in Figure 5.6 (A) and Figure 5.7 (A), respectively. The cycle has an aggressive style behaviour for heavy classes (>10000 lbs) vehicles and so would have a significant impact on the battery thermal performance, as seen in the previous case. For the case without LH jacket, the SOC reduced from 1 to 0.46 (see Figure 5.7 (A)) with the battery temperature reaching the safety limit at 60 °C in 6190 s (see Figure 5.6 (A)) displaying a linear relationship while the battery temperature with LH jacket was at 29 °C (still within the optimum temperature range) at the same instant. This means that the LH jacket led to a ~52 % reduction in temperature based on the first defined comparison criteria. As the case with the LH jacket has not reached its safety limit, it can still undergo the drive cycle. Here, the SOC reduced from 1 to 0.07 in 13710 s at the end of the drive cycle. At this stage, the numerical simulation was concluded as the

battery SOC was ~ 0 Figure 5.7 (A), and no further results were captured. Please note in that case (in the presence of LH jacket), at 6770 s, the PCM liquid fraction reached the maximum at 1 and all the LH was subsequently utilised. Beyond this stage, SH was dominant, and the battery temperature sharply rose to ~53 °C in 13710 s (end of cycle) (see Figure 5.6 (A)). As seen with results from the previous cycles, the battery temperature remained uniform until all the LH was used and SH became active. The change to SH saw a similar linear rise in temperature until the end of the drive cycle. According to 2nd defined comparison criteria, there was a ~2.2x extension in the available usefulness of the battery with LH compared with the battery cell without LH.

Moreover, Figure 5.6 (A) and Figure 5.7 (A) display the results for the NN drive cycle for temperature distribution and SOC, respectively, which represent a combination of the US06 and LA92 drive cycle with supplementary dynamics in the need for training neural networks. With this introduced cycle, for the case without LH jacket, the battery cell temperature rose sharply and linearly to 60 °C in 3050 s Figure 5.6 (A) while the SOC reduced from 1 to 0.73 Figure 5.7 (A) and since the safety limit was reached, no further cycling was performed. When the LH jacket was added, the optimum temperature was maintained for a longer period until all the LH available was used and the liquid fraction reached 1 in 3900 s. As no LH is available, SH becomes the predominant mechanism, and the battery cell temperature rose linearly in a similar fashion as without the LH jacket. The temperature subsequently reached the safety limit at 60 °C in 7340 s with a reduced SOC of ~ 0.18. Therefore, based on the 2nd defined comparison criteria, the introduced LH jacket had prolonged the battery usefulness up to x2.4. also based on the 1st defined comparison criteria, the LH jacket reduces battery temperature by ~52 %.

In the cases for the casual drive cycles, the impact of the UDDS driving cycle cases for temperature and SOC is shown in Figure 5.6 (B) and Figure 5.7 (B), respectively. This cycle had an initial SOC of 1 and ended at 0.07 at the end of the drive cycle. For the case with no Jacket, the battery cell temperature rose steadily until it reached ~ 46 °C at around 11560 s then the temperature gradually declined down to ~ 43 °C at around 19370 s (see Figure 5.6 (B)). The temperature then steadily rose again until the end of the drive cycle, around 22200 s as the battery reached a temperature of ~ 50 °C due to the drive cycle characteristics. However, for the case of which battery cell encapsulated with LH jacket, the temperature variation is more uniform until around 20210 s when all the PCM had been fully melted (LF is equal to 1) and so the temperature rose sharply due to activation of SH. At this stage, the temperature started to rise to ~ 36 °C before the end of the drive cycle (22200 s). In this case, the drive cycle had been completed with both cases lasting the same time (22200 s). Thus, LH jacket reduces the battery temperature by ~28 % based on the 1st defined comparison criteria. In addition, the presence of LH jacket makes the battery temperature rise much more uniformly for a much longer time until the

end of the drive cycle and maintains stability until SH becomes dominant. In other words, based on 2nd defined comparison criteria, the battery with LH jacket lasts ~x5 longer.

Figure 5.6 (B) and Figure 5.7 (B) display similar patterns with the drive cycle HWFT applied with similar thermal performance improvement over both phases. In the absence of LH jacket, the SOC decreased from 1 to 0 within ~7270 s (see Figure 5.7 (B)) as the battery cell temperature rose to ~ 53 °C (see Figure 5.6 (B)). Please note that in this case, the thermal behaviour of the battery is not linear. Indeed, the temperature rose steadily until ~ 48 °C (around 4300 s) before decreasing gradually to ~ 45 °C (around 6800 s) with a sharp rise in temperature to ~ 53 °C at the end of the cycle. In this case, the battery SOC had reached null, and the numerical solution was concluded. In contrast, the case equipped with LH storage maintained uniform battery temperature throughout the entire cycle until the battery SOC was at 0. So, based on the 1st defined comparison criteria, the LH jacket reduces the temperature of the battery by about 45 % and 46 % for HWFTa and HWFTb, respectively. Please note that at the end of the introduced cycle, the liquid fraction of LH storage was around 75 %. This meant that the battery temperature with the LH jacket not only experienced steady temperature throughout the introduced drive cycle with an end temperature of ~ 29 °C but also it still has a 25 % LH jacket which can be used for a longer period of drive cycles. With the LH jacket, the battery temperature was uniform for a significant amount of time until the end of the drive cycle. According to 2nd defined comparison criteria, the battery with the LH jacket lasts more than 10 times (x10) for HWFTa and 16 times (x16) for HWFTb. These cycles were less harsh than the previously noted US06 drive cycle and so the thermal impact on the battery was less severe.

The results of battery performance improvement based on the above-discussed criteria are summarised as follows:

A) Based on the 1st comparison criteria definition, the temperature of the battery in the presence of an LH jacket was reduced by 52 %, 28 %, 45 %, 46 %, 52 %, and 52 % as the battery undergoes the following drive cycles US06, UDDS, HWFTa, HWFTb, LA92, and NN, respectively,
B) Based on the 2nd comparison criteria definition, the battery can last longer in the presence of LH jacket by x2.5 x5, x10, x16, x2.2 and x2.4 as it undergoes the following drive cycles US06, UDDS, HWFTa, HWFTb, LA92, and NN, respectively.

From the highlighted summary, and results shown in Figure 5.6 and Figure 5.7, the most aggressive behaviour drive cycles (US06, LA92, and NN) had significant thermal improvement (over 52 % reduction in battery temperature) with a notable extension in the battery useful life more than 2.2x times and up to 2.4x times. The least reduction in battery temperature was seen for the UDDS drive

cycle due to its characteristic behaviour as discussed in section 5.1.2. In particular, the UDDS drive cycle, even with the lengthiest time out of all the drive cycles in this study, showed the least increase in thermal performance due to the drive cycle behaviour and the least increase in temperature during the cycling process. The most apparent result was the thermal stability that the LH jacket afforded the battery during the cycle. This must be taken into consideration, as indeed with this type of battery cell and for other larger battery cell types, divergent temperature uniformity throughout the battery would be kept to a minimum. Similarly, for the HWFT (a and b) drive cycle, the temperature stability and prolonged battery usefulness were the most apparent improvements, as those cases did manage to stay within the optimum battery temperature during cycling and can significantly increase the range an EV can go through with a single charge.

To further highlight the thermal impact of LH jacket on the battery, isometric temperature contours displayed in Figure 5.8 illustrate the battery cell temperature with and without the LH jacket for all the drive cycles studied. The contours were based on a specified range between 25 °C to the safety limit of 60 °C, as seen by the colour legend. As a quick overview, as seen by the colour legend, the temperature safety limit is from blue up to the green colour band (25 °C to 40 °C). Above the green-coloured band, towards the yellow and red, the battery temperature is beyond the optimum temperature and moving up to the maximum at the safety limit. Each of the drive cycles outlined in this study is shown with the effect on temperature with and without the LH jacket at specific instances in time (0 s, 1000 s, 2000 s, 3000 s, 4000 s and 5000 s) that would effectively capture the changes in temperature during the cycling processes and show the gradual change in temperature as per the colour legend. If the battery temperature reaches the safety limit, no significant change in the coloured contour is seen.

In Figure 5.8, a sample localised temperature contour displays the NN drive cycle at time 5000 s with and without the LH jacket to highlight the difference between the pre-defined global range (25 °C to 60 °C) with the majority of contours in Figure 5.8 captured based on the localised temperature. Since the temperature variation in the local range is small compared with the pre-defined global range, the variation of temperature in a pre-defined global range is not visible (the batteries are displayed in mono-colour format in Figure 5.8). Indeed, the localised battery temperature without the PCM corresponds to the colour bar between 76.7 °C to 77 °C and reveals where the maximum temperature amassed near the centre of the battery with decreasing temperature towards the tabs. Since the highest temperature is near this region, the PCM enveloped in that region captures the heat energy generated and so does not cover the tab region as seen in Figure 5.2. For the same drive cycle (NN) at 5000 s with the specified temperature range, there was no variation in the colour contour beyond the temperature safety limit (60 °C), however, the change seen in the localised temperature range was almost non-detectable (minimal) for a majority period. For this reason, a specified temperature range was useful to

show the variation in battery temperature at different time intervals during the cycling process. With the LH jacket, the battery cell with PCM at the same period shows 41 °C and the highest temperature of the jacketed PCM near the hot zone region and decreasing in temperature towards the tabs, which corresponds to the localised temperature contour.

In Figure 5.8, for all the drive cycles, the initial ambient temperature of 25 °C was seen for the initial time at 0 s corresponding to the colour contour with the lowest temperature. At 1000 s, the temperature rose based on the actions of the drive cycle, with the highest temperature seen for US06, followed by NN and LA92 drive cycles, respectively. The other drive cycles (UDDS, HWFTa and HWFTb) were still within 29 °C to 31 °C, when the temperature rose steadily. At this stage (1000 s), the battery cell with LH jacket maintained low temperatures closer to the ambient, visualised by the temperature contours for all cases.

As noted in Figure 5.6 (A), in the case of the US06 drive cycle, the battery cell temperature reached the temperature safety limit before 2000 s and as shown in Figure 5.8**,** according to the colour legend, the red contour indicates the highest temperature reached and so the contour was majority red from 2000 s. There was no colour change seen beyond this range as the temperature safety limit was reached. However, with the LH jacket, the temperature contour was still in the blue range since the temperature was only ~ 33 °C as compared to without at 60 °C.

As shown in Figure 5.8, at 2000 s, there was an increase in temperature for all cases without LH jacket showing US06 (60 °C) followed by NN (53 °C) and LA92 (38 °C) respectively. The lowest temperature was shown to be the UDDS drive cycle (32 °C) since it was the longest drive cycle out of all and had the lowest impact on the thermal performance at this stage. HWFT (a and b) had similar temperatures, showing 33 °C and 35 °C, respectively. As before, similar temperature contours were seen for the LH jacket case with a noticeable temperature rise seen for the US06 drive cycle as it reached the temperature safety limit at 60 °C. Beyond this temperature range, at 3000 s and 4000 s, the temperature contour did not change as it reached the limit. However, the temperature was at 53 °C and 60 °C at 3000 s and 4000 s, respectively. Albeit it was the harshest drive cycle on the battery, the PCM jacket kept the temperature stable for longer, with the safety limit reached at 4000 s. The cases with the addition of the LH jacket had temperatures below 26 °C (UDDS, HWFTa and b and LA92) with the highest seen for the NN drive cycle (28 °C).

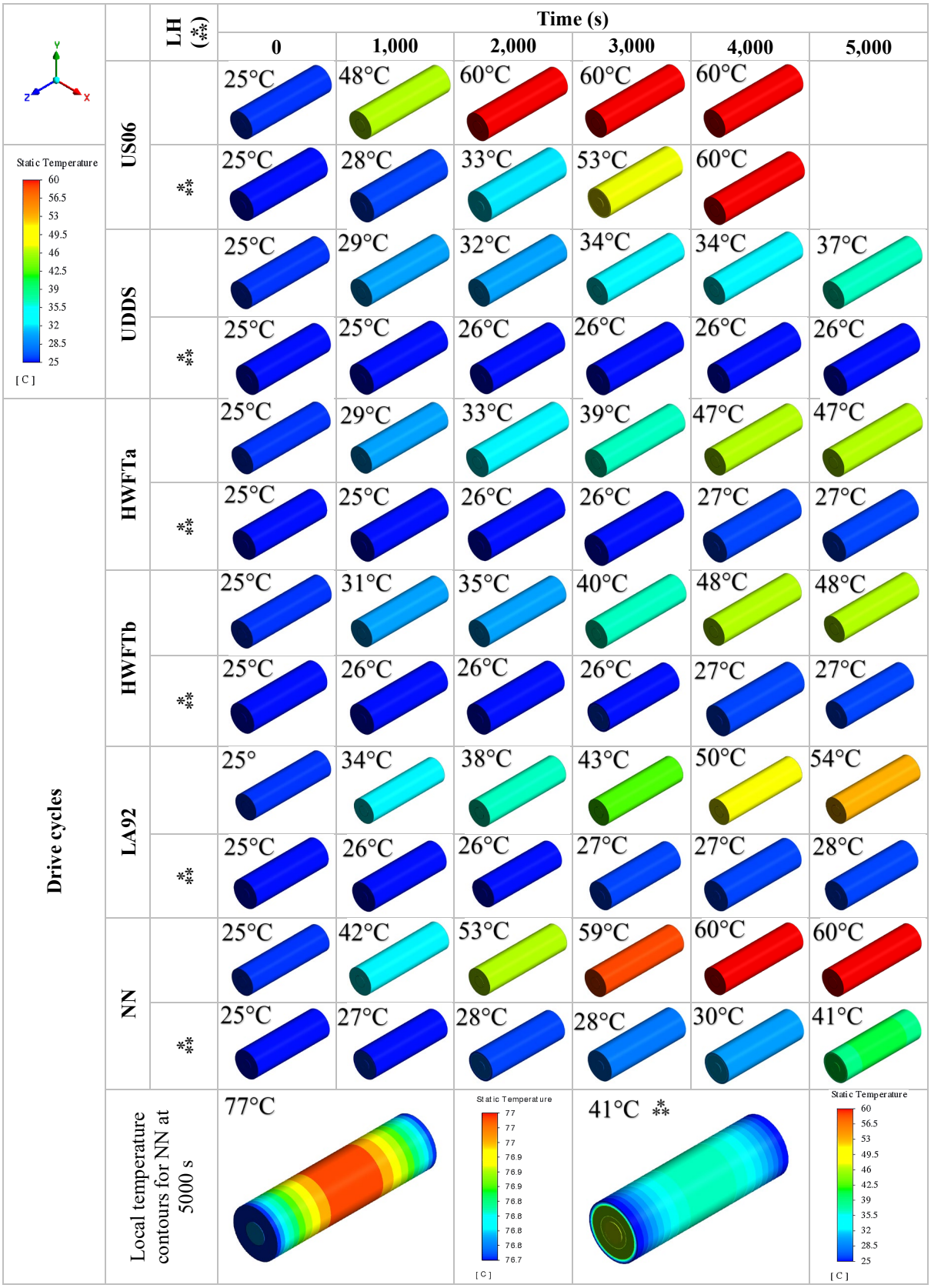

Fig. 5.8 Battery cell temperature contours with (⁂) and without LH jacket as seen in colour legend based on drive cycles: A) US06, B) UDDS, C) HWFTa, D) HWFTb, E) LA92 and F) NN at selected time instances.

Also, at 3,000 s based on Figure 5.8, the most noticeable temperature change was seen for the NN drive cycle, as it too entails harsh driving characteristics with a temperature rise to 59 °C and consequently reaching the temperature safety limit at 4,000 s. The same-coloured contour was shown at 5,000 s since there was no change in the colour at the safety limit. The temperature rose significantly at this point, as seen from the localised temperature contour at 77 °C at 5,000 s. The contour is shown here to make a comparison between the case with the introduced LH jacket. For the case with the LH jacket, the battery temperature was kept at 28 °C, 30 °C, and 41 °C at 3,000 s, 4,000 s and 5,000 s, respectively under the NN drive cycle. For this driving cycle, the battery temperature remained within the optimum temperature shown by the coloured contour.

The UDDS drive cycle at 3,000 s and 4,000 s was the same at 34 °C with the highest temperature shown at 37 °C at 5,000 s and was still within the optimum battery temperature at this time due to the nature of the drive cycle. As seen in this figure (Figure 5.8), the addition of the LH jacket showed a constant temperature at 26 °C at the indicated times which corresponded to Figure 5.6 for being the least harsh cycle in this study. HWFTa and b had similar temperature contours with 1 °C higher seen for the HWFTb cycle. When compared with the case with LH jacket, the temperature remained much more uniform between 26 °C and 27 °C, showing the thermal stability during these drive cycles.

Eventually as shown in Figure 5.8, under the LA92 drive cycle, the battery reached 43 °C at 3,000 s, 50 °C at 4,000 s and 54 °C at 5,000 s showing a steady rise in temperature during these periods shown by the colour contour. With the LH added, the maximum temperature at 5,000 s was at 28 °C showing a more uniform and stable variation in temperature. In all discussed cases, the addition of the LH jacket kept the divergent temperature variation lower than 5 °C except for the US06 and NN drive cycles, which were significantly more severe on the battery thermal condition.

Another important piece of information that can be reported is the liquid fraction. Indeed, as proven in an earlier investigation (Kadivar et al., 2019), the PCM liquid fraction can be almost equal or equal to the thermal energy storage rate ($\eta = Q_s/Q_m$). This thermal energy storage rate is a ratio of the heat energy stored in the PCM jacket, Q_s ,(which is also equivalent to the amount of heat generated in the battery cell to that instance), to the maximum value of the heat energy which can be stored in the PCM jacket, Q_m. It is noteworthy that Q_m can be calculated based on the multiplication of PCM, the density of PCM (given in Table 5.1) and Latent heat of melting for PCM (given in Table 5.1). Thus, liquid fraction is a good representative of both the thermal energy storage rate, and the total amount of thermal energy stored in the process ($Q_s = \eta Q_m$). With this in mind, Figure 5.9 displays a plot of the liquid fraction versus time for a comparison of all the drive cycles assessed. The impact of the drive cycle behaviour on the battery thermal performance is indicated by PCM melting in the least time from

the harshest (US06, NN, and LA92) to casual (HWFTa, HWFTb, and UDDS) drive cycle. The figure also shows that the HWFTa and b drive cycles did not reach the full melting fraction of 1 because it marked the end of the available drive cycle data.

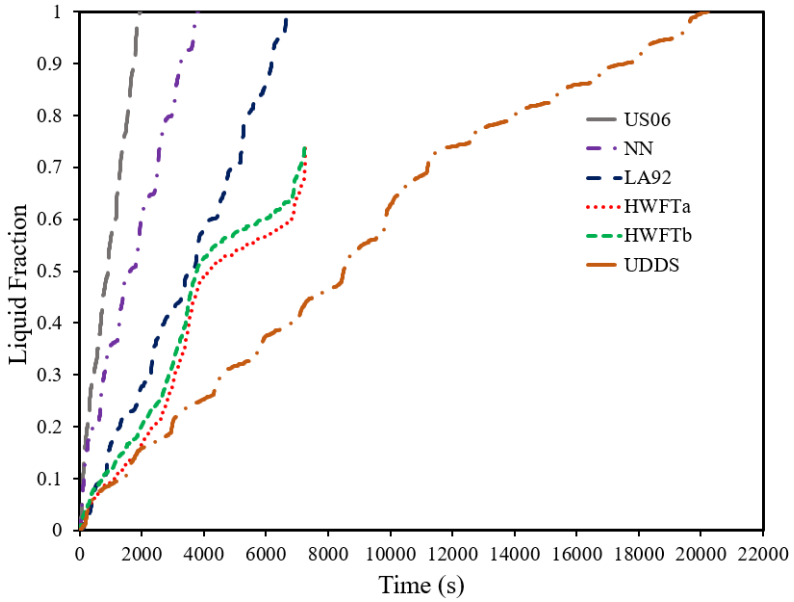

Fig. 5.9 PCM liquid fraction versus time with the applied drive cycles: US06, UDDS, HWFTa, HWFTb, LA92 and NN.

The results show the disparities between the PCM melting performance when compared to the different drive cycles assessed (US06, UDDS, HWFTa, HWFTb, LA92 and NN). It is noted that increased heat generation from the drive cycle behaviour had a significant effect on the battery cell temperature. This was shown in Figure 5.6 (A) for the aggressive driving cycles and Figure 5.7 (A) for the casual driving cycles. Due to the behaviour of the drive cycle and the haphazard nature, particularly for the aggressive driving cycles like US06, the PCM fully melted in the shortest time (1950 s or 3.4x, 1.95x and 10.3x times faster than LA92, NN and UDDS, respectively) as compared to the other aggressive cycles (LA92 – 6710 s and NN – 3810 s) as well as the casual drive cycle which fully melted (UDDS – 20240 s) (see Figure 5.9**)**.

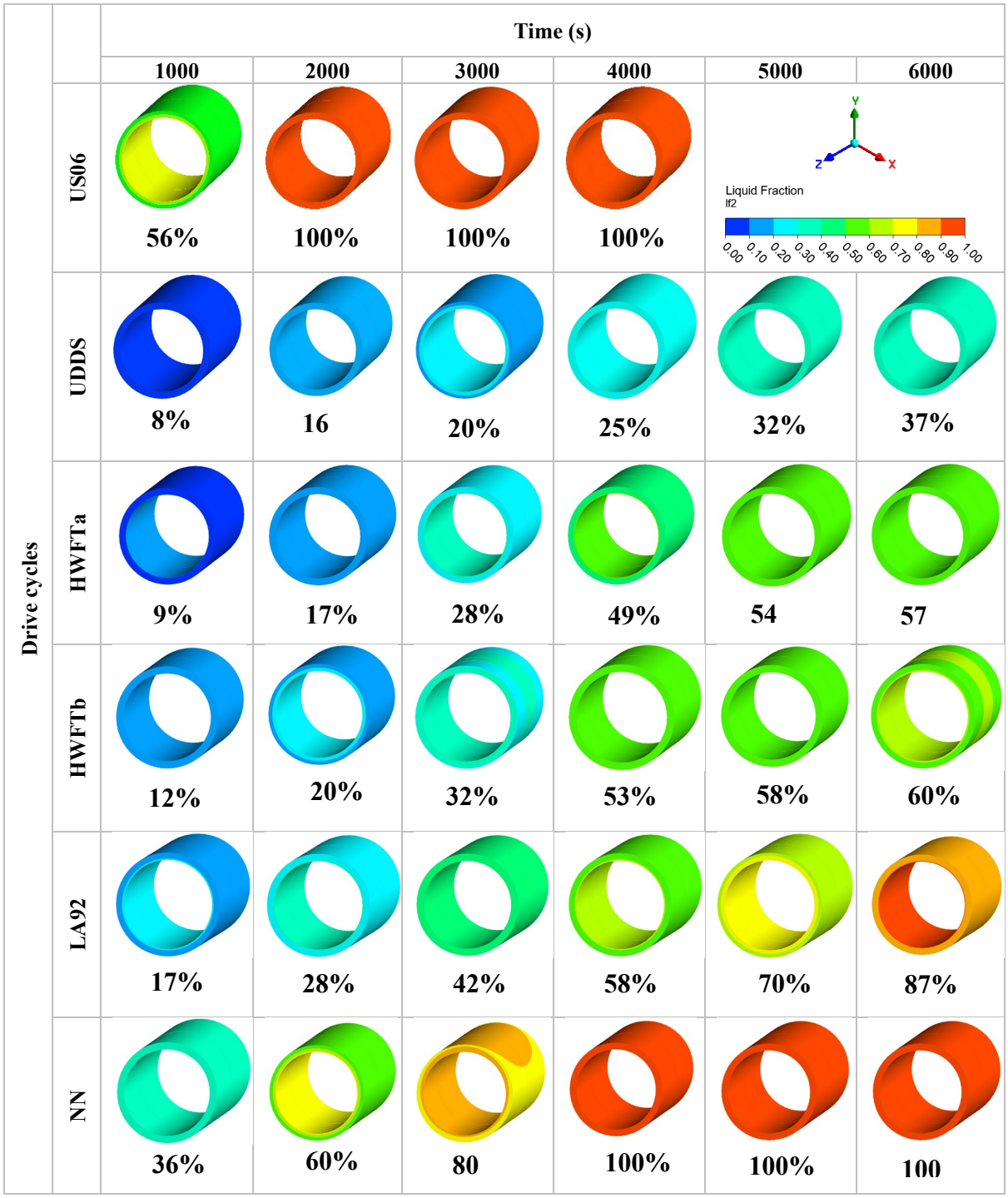

Fig. 5.10 PCM liquid fraction contours showing percentage melted displayed as isometric views as seen in colour legend with the applied drive cycles: A) US06, B) UDDS, C) HWFTa, D) HWFTb, E) LA92 and F) NN at selected time instances.

The circumferential PCM contours with results for liquid fraction are shown in Figure 5.10 for all drive cycles highlighted with isometric views. The contours show the change in liquid fraction between the lower and upper limits of 0 and 1 respectively, as shown by the colour legend. The liquid

fraction contours correspond to the temperature contours as shown in Figure 5.8 with a similar outlook on the results. It should be noted that only a specific range of times were captured as contours for illustration purposes to view the changes in the liquid fraction. The main action of the PCM jacket is to absorb the heat energy generated from the battery during cycling by conduction heat transfer, which increases the internal energy and heat energy of the PCM, raising the temperature above its solidus state (25 °C). Due to the orientation (horizontal) of the battery, the PCM starts to melt from the top section, changing the state from solid to liquid as the liquidus temperature (29 °C) is reached in this region. As the PCM melts, natural convection heat transfer becomes the dominant heat transfer mechanism as the convection currents or vortices are increased. This is attributed to the PCM temperature rise, creating a temperature gradient and subsequent buoyancy forces from the changes in density. This causes the highest temperature fluid regions to rise, creating a circulation effect of Bernard cells. Due to the small circumferential LH jacket thickness and the specified liquid fraction contour range, variation in the mushy region is not highly detailed but the changes can be seen in Figure 5.10.

For all the cycles, an initial condition at 0 s and liquid fraction was at 0 and show the lowest colour contour as per legend. The PCM solidus temperature is the same as the ambient temperature (25 °C) so the liquid fraction would be at 0. As recalled, this value designates that the material is in the solid state at the minimum and 1 for a liquid state at the maximum. As seen in this figure, for the US06 drive cycle and all the other drive cycles assessed, the initial time was shown at 1000 s up to 6000 s with 1000 s increments to illustrate the most dramatic changes in PCM melting. At higher times, with the cycles more evolved and the battery temperature increased, the liquid fraction was closer to maximum or fully melted.

At 1000 s, the liquid fraction was at 56 % for the US06 drive cycle followed by 8 %, 9 %, 12 %, 17 %, and 36 %, for UDDS, HWFTa, HWFTb, LA92 and NN drive cycles, respectively. Since the battery cell was well insulated, it meant that the heat generated from the battery as a direct result of the drive cycle influenced the temperature of the battery, which translated into the LH jacket due to heat conduction. The rate at which the PCM melted was based on the geometry, heat transfer and temperature of the battery cell. These factors were affected by the behaviour of the drive cycles, including the distance travelled and time. In the initial cases, the most severe cycles would cause the highest thermal impact on the battery cell, which was translated into the PCM.

Displayed results in Figure 5.10 showed at 2000 s, the liquid fraction for the US06 drive cycle was at 100 % and thus all the LH was used, displaying a remarkably high-temperature contour. NN drive cycle had the next highest liquid fraction value at 60 % with higher temperature contours shown on the inside of the LH jacket from the heat conduction in the battery cell, but still had LH available to

continue capturing the heat given off by the battery. The other drive cycles UDDS, HWFTa, HWFTb, and LA92 drive cycles had 16 %, 17 %, 20 % and 28 % respectively, which meant they all had a significant amount of accessible LHS to continue to manage the thermal response of the battery.

For the time at 3000 s shown in Figure 5.10, the liquid fraction was at 80 % for NN, 20 %, 28 %, 32 %, and 42 % for UDDS, HWFTa, HWFTb, and LA92 drive cycles, respectively. Even at this time, apart from the US06 drive cycle, there was still accessible LHS and so the temperature remained stable even up to this point. The effect of buoyancy-driven flows is highlighted for the LH jacket liquid fraction for the NN drive cycle and the indication of heat accumulation more to the centre of the cell shows a curved melted feature. A closer look near the tabs shows less PCM melting compared to the inside of the jacket and the at its centre.

At 4000 s, the liquid fraction for the NN drive cycle was at 100 %, so LH turned to SH and the battery temperature started to rise sharply after this stage. The other drive cycles, UDDS, HWFTa, HWFTb, and LA92 drive cycles had 25 %, 49 %, 53 % and 58 % liquid fraction and even at 5000 s they had 32 %, 54 %, 58 % and 70 %, respectively. Results showed that at the times shown for liquid fraction, these drive cycles had remaining LH and kept the battery temperature more uniform and stable to remain within optimum operating temperature for longer comparable to the results shown (see Figure 5.6 and Figure 5.7).

At 6000 s, the liquid fraction of the PCM under the remaining drive cycles which had not been fully melted was at 37 %, 57 %, 60 % and 87 % for UDDS, HWFTa, HWFTb, and LA92, respectively. More of the PCM had become melted within the inner side of the LH jacket as opposed to the outside due to the direct contact from the battery and essential conduction heat transfer. A transition to natural convection heat transfer is either imminent or on track to increase the heat transfer rate as opposed to slower conduction. Results indicate a positive outlook for the PCM under dramatic battery temperature changes, as a direct effect from real-driving cycles displayed the stable nature of PCM melting and low thermal conductivity to transition smoothly from one physical state to another.

5.3.4 Impact of variation of discharging C-rate

Figure 5.11 displays the comparison of the temperature distributions for the battery cell with and without the LH jacket at 0.5C, 1C, 2C, 3C, and 4C discharge rates. For all the discharge rates, the initial battery temperature was at 25 °C. Each test was performed for a single discharge from an initial SOC at 100 % until 0 % with the time taken for the battery cell to fully discharge reduced as the C-rates

were increased. It is seen that the temperature increased to the safety limit at 60 °C faster with increasing C-rates.

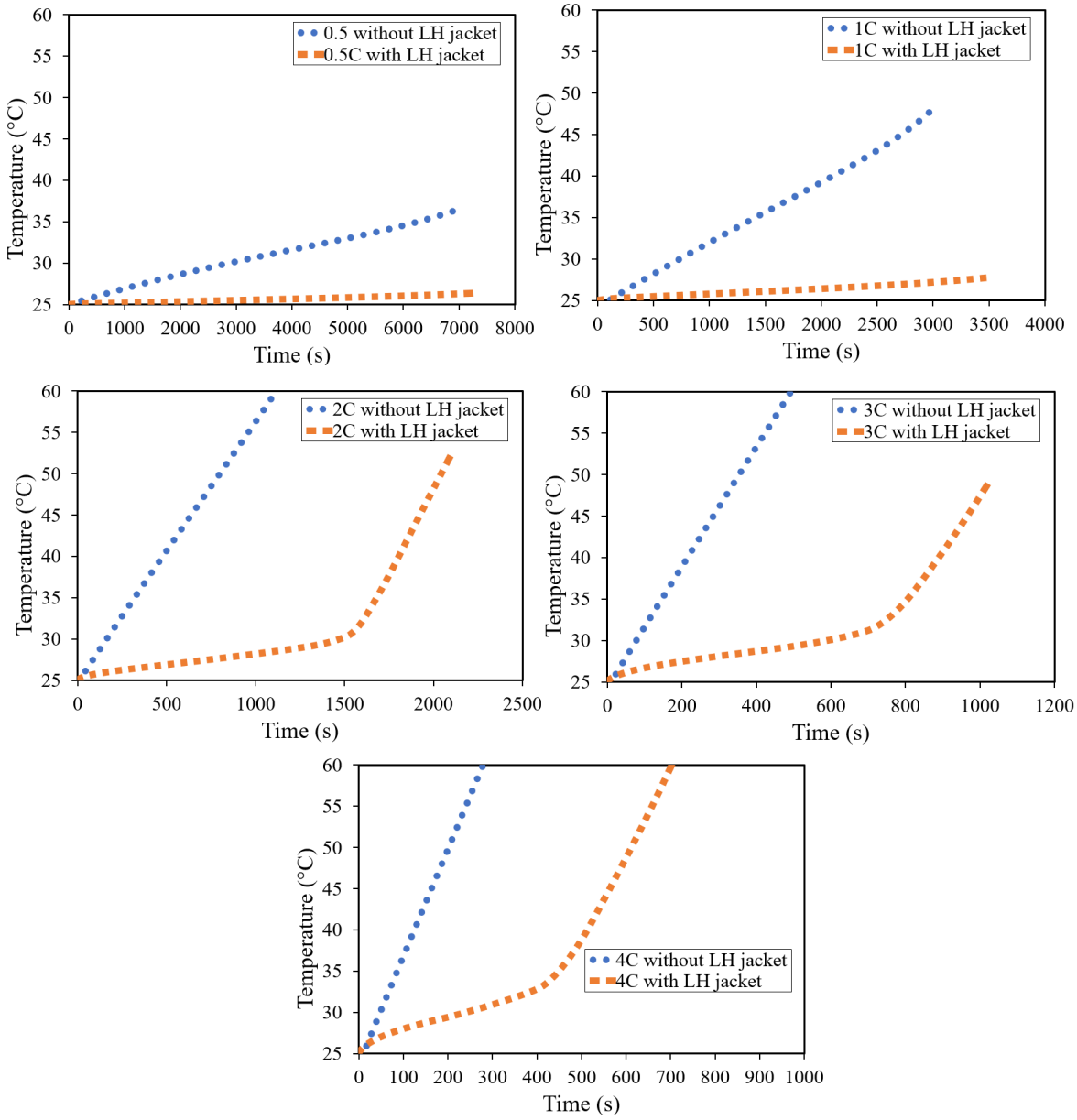

Fig. 5.11 Battery cell temperature distribution with and without LH jacket for discharging rates at 0.5C, 1C, 2C, 3C and 4C.

This increase in temperature can be attributed to the internal heat generation. In comparison, for all the cases where the LH jacket was introduced, the temperature remained within the optimum temperature (20 °C to 40 °C) excluding 0.5C where the limit had not been exceeded in either case. It is also shown that compared to the sharp rise in temperature for the cases without a LH jacket, the ones with LH jacket rose more steadily and uniformly until all the LH was inaccessible. After this stage, a sharp rise can be

seen for all the cases with LH jackets, as SH transfer became dominant. In other words, when the PCM was fully melted, as seen for 2C, 3C, and 4C discharge rates, the system temperature rose in proportion to the cases where no LH was present.

The temperature increased to 11.5 °C and 23.1 °C higher than the ambient temperature for 0.5C and 1C, respectively. For the other cases at 2C, 3C, and 4C there was an increase to 35 °C without a LH jacket, however, there was an increase to 27 °C, 23.8 °C and 35 °C above the ambient temperature, respectively, for the cases with a LH jacket. It is noteworthy that although there was a temperature rise above the optimum working temperatures, there was a delay effect and extension in useful life with the introduced passive cooling. In comparison to the final temperatures at these stages at 2C, 3C, and 4C, there was an extension in useful life by 294 %, 300 % and 250 %, respectively.

5.4 Conclusions

This study explores the impact of varying drive cycles, such as US06, UDDS, HWFTa, HWFTb, LA92 and NN, on the thermal and electrical performance of a single 18650 battery cell, both independently and when equipped with a LH storage PCM jacket. The research harnesses an accurate MSMD ECM model to represent the battery cell's electrical parameters, using real-world automotive drive cycles validated under ambient conditions of 25 °C. The validated model precisely predicts the thermal and electrical performance, complying with the manufacturer's recommended safety limits. Through a combined thermo-chemical and electrical model, it explores power, temperature, SOC, and liquid fraction across different drive cycles, showcasing the need for effective thermal management techniques for aggressive driving scenarios, yielding performance enhancements across all cycles examined. The introduction of the LH jacket significantly extends the battery's optimum operating temperature (20 °C – 40 °C) duration, with notable reductions in temperature (up to 52%) and remarkable increases in battery life (2.2x to 2.4x) during demanding driving cycles (US06, LA92, and NN). It ensures stable and uniform battery temperatures throughout all cycles when LH is accessible, notably beneficial for UDDS and HWFTa and b, where the battery temperature remains within the optimal range, effectively minimising temperature variations, except for the US06 and NN drive cycles, where divergence remains below 5 °C.

5.5 Chapter Summary

This research Chapter investigated an 18650 Lithium-ion cylindrical battery cell jacketed with PCM and assessed under real-world automotive drive cycles. The effectiveness of the LH jacket was analysed under a validated numerical model from electrical parameters of automotive drive cycles ranging from aggressive to casual. The thermal and electrical performance analysed from a combined thermo-chemical and electrical model was analysed for Power, temperature, SOC, and liquid fraction. The results indicated an improvement in the thermal management of the cell across all the drive cycles assessed including an extension in the useful life of the battery when the LH jacket was introduced. In this study, the effect of discharging C-rates was also investigated for the impact of the cell with and without the presence of the LH jacket. Increased C-rates have been attributed to the increased internal heat generation and therefore a required need for an effective thermal management strategy. For the C-rates assessed, the results displayed steady and uniform temperature in the presence of the LH jacket with the addition of a delayed effect that essentially meant that the battery was able to operate longer within the optimum temperature range if LH was available and the discharging time increased until the temperature cut-off was reached. This Chapter evaluated on the integration of the TES with EES as identified as part of the main objectives of this research and acts as a starting point for further research at the modular level. It should be noted that this Chapter was published as seen in the list of publications. The following Chapter 6 discusses the study of TES in greater detail with specifics to the impact of real-world automotive drive cycle data as well as continuous charging/discharging cycles when implemented with passive cooling jackets at the module level for different configurations assessed.

CHAPTER 6: THERMAL PERFORMANCE ANALYSIS OF BATTERY MODULES USING LATENT HEAT COOLING-BASED MANAGEMENT SYSTEM FOR REAL CYCLING MODES IN ELECTRIC VEHICLES [6]

6.1 Chapter Brief

In the previous Chapter, further investigation into the conjugation of TES and EES analysed the impact of an 18650 Li-ion cylindrical battery cell jacketed with PCM. The cell was assessed under various real-world automotive drive cycles as opposed to continuous charging/discharging cycles. The numerical results considered the impact of the LH jacket use under various drive cycle behaviours which included aggressive cycles to casual cycles. The previous Chapter focused on dynamic cycling for automotive drive cycles at the single-cell level. This Chapter analyses the impact of passive cooling for Battery Thermal Management (BTMS) for various battery module configurations under continuous cycles as well as automotive drive cycles. Numerical CFD simulations were used to analyse the effect of LH jackets circumferentially arranged around each cell in a module. Performance indicators such as module temperature, liquid fraction, SOC, and passive potentials for different arrangements of cells were considered. The 3-dimensional (3D) models were analysed based on a specific number of cells on average found in the literature but can be adapted based on the power requirements for any module/pack configuration. In this regard, the focus of the results was based on the effect of busbar connections the heat transfer between cells and the thermal impact from the passive cooling jackets. This Chapter remains in line with the objectives in Chapter 1 and seeks to fulfil the targets set in milestones 2 and 3. The study is classed as a module-level analysis and the results of this Chapter is currently under review for submission to a Journal for publication.

6.1.1 Introduction

The growing concerns over the energy crisis and environmental pollution have navigated the transportation sector into a transition towards the reduction of carbon dioxide (CO_2) emissions by the

[6] **Nicholls**, R.A, Moghimi, M.A., and S. Sehhat, Thermal performance analysis of battery modules with passive cooling under different cycling loads in electric vehicles, *Journal of Energy Storage,* 94, 2024, pp. 112349 https://doi.org/10.1016/j.est.2024.112349.

development of electric vehicles and hybrid electric vehicles (EVs and HEVs). In this regard, applicable renewable energy resources such as electrical energy storage (EES) lithium-ion (Li-ion) (Wen et al., 2020) batteries, have garnered significant attention as a promising source of power for these vehicles. The benefits of using these Li-ion batteries include high specific energy, power, and long cycling life (Malik et al., 2017). However, there have been challenges around overheating in the battery cycling of charging and discharging which can significantly impact on the performance of the battery (Javani et al., 2014). These can include critical failures such as capacity fading and thermal runaway including high-risk safety hazards such as exothermic reactions leading to fire and explosion (Nazir et al., 2019), (Fan et al., 2021). Considering the benefits of using such renewable energy resources (Zhang et al., 2022), mitigation of the risk of overheating such as the use of an effective and reliable battery thermal management system (BTMS) (Kim et al., 2019) is essential for safety and effective operation of Li-ion batteries in EV and HEVs (Liu et al., 2017).

Battery cells usually operate optimally between -20 °C and 60 °C but, are recommended between 25 °C to 40 °C for the best performance and cycle life (Ling et al., 2017), (Yang et al., 2021). Maintenance of the battery temperature within this range as well as reducing the variable temperature difference between individual cells (not more than 5°C) (Perez et al., 2021) in a module or pack, reduces thermal runaway risks whilst preserving operational safety. A variety of cooling methods have been studied and categorised as being either active (Sabbah et al., 2008) or passive (Liu et al., 2017), (Yang et al., 2021) and employed as BTMS to remove or expel unwanted heat generated by the cells and pack. Unfortunately, when operated under abusive conditions, cooling systems that mostly comprise air and liquid cooling (Sabbah et al., 2020), (Safdari et al., 2020) may be insufficient to dissipate the excess heat. Active cooling may provide an enhancement to the thermal management of the battery module/pack; however, it also introduces additional complexities and can reduce the overall efficiency of the supplementary pumps and connections.

Coincidently, the increasing applications of Li-ion batteries in electronic devices (Akula et al., 2022) as well as EVs, can significantly reduce greenhouse gas emissions and pollution. Nevertheless, challenges associated with overheating need to be addressed for the holistic adoption of EVs and the promotion of sustainable transportation solutions. The innovation of BTMS solutions (Menale et al., 2019) has become necessary to manage temperature, improve cycle life as well as safety and the continued growth of clean energy vehicles. This continued research and development in thermal management technologies will play a pivotal role in the seamless integration of Li-ion batteries in electric transportation towards a cleaner and greener future (Qaderi et al., 2022). This study seeks to analyse the combination of passive thermal cooling (Alva et al., 2018), (Gulfam et al., 2019) with EES and provide solutions to battery module/pack overheating.

Adoption of EVs offers significant advantages including reduced fossil fuel consumption and lower emissions. HEVs make use of a combination of battery technology with internal combustion engines (ICE) which only partially reduces the reliance on fossil fuels and can be classed as either full hybrid or recharge from an electric grid source. On the other hand, EVs or battery electric vehicles (BEVs), solely recharge from the grid and benefit from reduced noise pollution, fewer moving parts, and lower maintenance costs, however, battery lifespan and weight require ongoing research to enhance the performance (Alami et al., 2022). An effective BTMS (Ma et al., 2018) plays a pivotal role in ensuring that the Li-ion batteries are operated safely and efficiently, as such, the temperature conditions to which they are exposed have a profound impact on their electrochemical reactions and their materials (Ibrahim et al., 2021). Understanding and controlling the heat generation inside the batteries (Kim et al., 2019) are critical factors in mitigating the effects of temperature. Even at low temperatures, chemical reactions and the rate of electrochemical reactions are affected leading to lower ionic conductivities of the electrodes and electrolytes compounding to lower battery performance. On the other hand, higher temperatures have a more complex effect than lower temperatures. The heat that is generated within the cells is associated with charge transfer and chemical reactions during battery cycling of charging and discharging (Xia et al., 2017). This heat can be reversible (entropic heat) or irreversible from entropy change during electrochemical reactions or polarisation, ohmic heating and leading to unrecoverable heat, respectively.

One of the focal points in managing the thermal effects is to control the temperature within the operating range and actively maintain the temperature within pre-determined safety limits depending on the type of cell. Traditional BTMS require complex and bulky additions (Xia et al., 2017), (Ianniciello et al., 2018) to the vehicle load so passive thermal management solutions can provide the capabilities of absorbing and storing the thermal energy during the rise in temperature and releasing cooling. This makes passive cooling suitable for temperature management in Li-ion batteries. In particular, the use of phase change materials (PCMs) provides a promising approach to improve thermal management (Kizilel et al., 2008). By introducing the batteries with PCMs, a thermal management system with little maintenance requirements is forged. The heat generated from the battery is readily absorbed by the PCM (Nasajpour-Esfahani et al., 2008), (Arora et al., 2018) and stored during the transition from solid to liquid. This aids in maintaining uniform temperature within the pack and reduces abnormalities in temperature which can negatively affect the battery performance (Mohammed et al., 2022). In this regard, PCMs have emerged as a promising solution to store a considerable amount of energy (Tete et al., 2021) as Latent heat, notwithstanding organic, inorganic, or eutectic-based depending on the application. They can reduce the overall maximum temperature and temperature difference (Chen et al., 2019), (Siddique et al., 2018) when combined with batteries to store the heat

depending on the capacity or volume of the PCM. Nevertheless, it is essential to address the challenge of unnecessary temperature increases including local temperature increases, particularly during high-rate charging and discharging (Luo et al., 2022).

In recent studies, the combination of battery cells with PCM has been analysed to evaluate the efficiency and performance of the cells. A study by (Verma et al., 2019) analysed the effects of two ambient conditions as well as PCM thickness on the outer sides of the battery pack with results indicating that 3 mm thickness is sufficient to support the absorption of heat generated from the battery. A study performed by (Yang et al., 2023) analysed the effects of different PCM thicknesses (1 mm, 3 mm, 5 mm, and 7 mm) on the outer circumferential area of an 18650 Panasonic battery. Results indicated that 3 mm PCM circumferential thickness was sufficient for the type of battery cell during consecutive discharge and recharge. (Lamrani et al., 2021) proposed a simplified physical battery model that produces the thermal output of the battery cells with PCM to a reasonable solution. In this case, the temperature and heat generated remained uniform, including convective heat transfer like a lumped thermal model, which was able to predict within reasonable accuracy, the operation of the batteries. This study makes use of the lumped thermal model where individual layers were grouped as a single body to a reasonably accurate solution. In their research, (Talele et al., 2021), they analysed the effect on time-delay for which two different PCMs (paraffin wax and RT-18) were compared for thermal management effectiveness. Their results indicated that the PCM with a lower melting point closer to the ambient temperature of the battery, was more effective as it melted faster and formed a thermally resistive layer in contact with the cell and extended the time to reach the limits set. For this reason, the PCM was chosen based on the ambient temperature assessed. In another study by (Yang et al., 2023), the effect on the performance of a single cell was assessed at different ambient weather conditions (extreme winter, -20 °C; winter weather, 0 °C; regular ambient weather, 25 °C; hot summer weather, 40 °C and desert weather, 55 °C). Results showed that at higher temperatures, the PCM must be chosen closer to the ambient temperature to allow for a delayed effect, allowing the battery to dissipate the heat for longer to the PCM. Other studies have considered a variation in C-rate (Panchal et al., 2018), (Kermani et al., 2023) (Khaboshan et al., 2023), PCM thickness and thermal physical properties for an analytical model to typical cell temperature and heating including natural convection heat transfer (Gan et al., 2020) in the PCM. Results showed that the thickness of PCM is dependent on the melting temperature, as well as the thermal conductivity. Less thickness is required for lower melting temperatures and higher thermal conductivity. The density of the PCM is also important when considering the overall weight of the system.

Cell spacing between cells in a battery pack has been seen in research by (Padalkar et al., 2023) and (Ji et al., 2019) in which the cells in a module were compared for constant spacing with transverse

and longitudinal spacing, contained in an enclosure and enhancement of uniformity with variation in cell to cell spacing, respectively. In this regard, the thermal performance of one cell is directly affected by other cells in the vicinity. For this study, each cells in the module were thermally isolated from one another and so would not be impacted by adjacent cells. With regards to battery modelling, different approaches including the multi-scale multi-domain approach have been studied to perform sufficiently and accurately in measuring the BTMS combined with PCM as seen in their work (Hussain et al., 2023), (Vyroubal et al., 2018), (Li et al., 2023). In this case, the numerical approach for modelling assigns the distributed temperature along the length scale for an equivalent circuit model (ECM) (Kirad et al., 2021), (Chacko et al., 2012) which assigns the model as a circuit that represents the electrical behaviour of the cells. This type of modelling is suitable for battery discharge and recharge as well as sudden fluctuations in electricity that may arise from drive cycling and therefore applicable to this study. Moreover, cycling of continuous discharging or charging or a combination of both analyses the ideal conditions for which the thermal performance is compared through constant modes over time. To fully understand whether passive cooling can control the thermal behaviour of the battery module within acceptable states, dynamic modelling via real-world drive cycles must also be studied on the impact of performance. Studies have analysed the performance of the battery cell as seen in their work (Bhavsar et al., 2023), (Panchal et al., 2018), (Vikram et al., 2022), (Nicholls et al., 2022), indicated significant temperature rise for very harsh conditions and an effective BTMS was mandatory in these cases to prevent the actions of fire and explosions.

To the best author's knowledge, the impact of passive cooling on battery performance under theoretical (continuous charging and discharging) and five actual (real-world drive cycles; from a harsh driving cycle to a casual one) loads at the module level have not been addressed, which shed light on the effectiveness of this approach for BTMS in EV world. Thus, the novelty of this research study lies in evaluating the impact of passive cooling/LH jackets on the thermal management of various configurations of battery modules under different loads (discharging and charging cycling modes as well as drive cycling scenarios, including harsh and casual). In this regard, three configurations were analysed for a total of 24-18650 Panasonic Li-ion cells with 278.4 W of power connected in series and parallel. The arrangement and capacity of the three configurations were as follows: Case 1 (2.9Ah case): 24 series cells (24S), Case 2 (5.9 Ah case): 2 parallel cells with 12 series (2P12S) and Case 3 (8.7 Ah case): 3 parallel cells with 8 series (3P8S). The LH jackets around the individual cells in the module were thermally isolated from neighbouring cells and the heat generated during the operational conditions of either discharging and charging or driving cycles was directly captured by LH jackets. A numerical heat transfer analysis for combined thermo-chemical and electrical modelling was performed using a chosen thickness of PCM. The transient thermal and electrical performance analysis was

conducted to prove concept of using the LH jackets as an effective thermal management system for ambient weather condition.

Understandably, the study outlines the numerical method including models, initial and boundary conditions, assumptions, mathematical and numerical model, and computational model setup. Subsequently, the results and discussion comprise the independency and validation study as well as the outcomes of the study culminating with the conclusions.

6.2 Numerical Method

6.2.1 Models

The battery module characteristics and configurations for the three distinct types of module arrangements are displayed in Figure 6.1. The modules assessed in this study include three different arrangements (24S, 2P12S and 3P8S) consisting of 24 18650 PF Panasonic lithium-ion batteries, with individual 3 mm circumferential LH jackets (for better understanding of module configuration, components were colour-coded in Figure 6.1). The primary aim of this feasibility study was performance assessments of the considered module configuration in the presence and absence of LH jacket for cells, under different cycling loads (continuous cycling as well as dynamic drive cycling), to evaluate the impact of passive cooling (proposed latent heat jacket, as shown in Figure 6.1) at the module level. Please note that in Figure 6.1, only 3 configurations with LH jackets are displayed for the sake of brevity. Therefore, in this study performance of 6 different modules under 2 various cycling loads (continuous and real-world drive cycles) were assessed and compared against each other. The specifications of the considered module in this study against single cell specification were listed in Table 6.1.

Table: 6.1 Single cell and module specifications for 18650PF Panasonic battery.

Specifications	**Battery cell/Module**			
	Single Cell	**Case 1 (24S)**	**Case 2 (2P12S)**	**Case 3 (3P8S)**
Specified C-rate	1	1	1	1
Nominal Cell-capacity (ah)	2.9	2.9	5.8	8.7
Specified system voltage (V)	4	96	48	24
Specified system power (W)	11.6	278.4	278.4	278.4
Maximum cut-off voltage (V)	4.2			
Minimum cut-off voltage (V)	2.5			

The individual cells of the module were regarded as homogenous bodies, in other words, the cathode, anode and current collectors were not solved explicitly. The cells, tabs, and busbars were designed as separate zones for the sake of this study. The outer surface of cells (regardless of being jacketed or not) was insulated to eliminate the effect of the environment. Thus, only the generated heat by the battery was conducted directly to the PCM LH jacket, which better showed the effectiveness of the LH jacket for battery thermal management purposes. The cell-to-cell spacing remained constant at 30 mm between cells (both horizontally in series orientation and vertically in parallel orientation, see Figure 6.1 for further clarification) as they were thermally isolated from one another. All the cells were the same type and format of 18650 Li-ion batteries. As shown in Figure 6.1, busbar connections were assigned accordingly allowing tab-tab connections from the positive tab of one cell to the negative tab of the next battery cell in series arrangement and positive to positive tabs and negative to negative tabs for parallel arrangement to create the different modules. Figure 6.1 also displayed zoomed-in images for a better understanding of the arrangement. The external connectors indicate the areas of the electrical contacts (positive and negative tabs not connected to a busbar). In this regard, the positive phase potential of the first battery was similar to the negative phase potential of the second battery. Subsequently, the same domain was used to resolve both the positive and negative phase potentials of the first and second batteries. The electrochemical reactions occurred within the active zone (battery cell) and both potential equations were computationally solved whereas in the passive zones (tabs/busbar), only a single potential equation was available. The batteries in the modules were connected via real connections (busbars) and were physically resolved including meshed as opposed to virtual connections (absence of busbars) in this study. Such detailed modelling highlighted a visual representation of the heat transfer between tab-busbar connections as well as between different cells in the module, which determined the areas of hot spots (hot temperature zones) concerning additional computational time for the passive zone volumes to be resolved. Each of the cells that made up the battery module consisted of different domains, notable active or e-material zones with positive and negative tabs connected to a busbar. It must be noted that in all cases studied, a horizontal orientation of the cells within the module was adopted for more effective heat transfer as seen in previous studies (Yang et al., 2023), (Nicholls et al., 2024).

Table: 6.2 Value parameters of the thermophysical properties of the PCM and Li-ion cells. (Voller et al., 1987), (Chen et al., 2009).

Parameters	Materials				
	PCM (N-octadecane)	**Battery cell (active zone)**	**Positive Tab**	**Negative Tab**	**Insulation**
Specific heat, Cp (J/kg.K)	2196	678	871	381	1470
Density (kg/m^3)	770	2092	2719	8978	1190
Thermal Conductivity (W/m.K)	0.148	18.2	202.4	387.6	
Solidus Temperature (K)	298.15				
Liquidus Temperature (K)	302.15				
Thermal expansion coefficient (1/K)	0.00091				
Latent heat (J/Kg)	243500				
Dynamic Viscosity (kg/m.s)	0.003				

This study was performed at an ambient temperature of 25 °C for all Cases (24S, 2P12S and 3P8S) to analyse the effect on thermal performance on this single ambient temperature. The selected PCM (N-octadecane) was based upon the optimum operating conditions of the Li-ion 18650 battery cell (20 °C – 40 °C) and as determined in a previous study (Yang et al., 2023), would be sufficient to analyse all tests Cases. The thermal properties of the PCM, module and insulation material can be found in Table 6.2. N-octadecane has a high latent heat, cost-effective and suitable for the temperature range to conduct sufficient analysis on the impact of LHS on the thermal performance of the test Cases. The chosen PCM demonstrated its capability to uphold consistent battery temperatures under the ambient temperature of 25 °C. An extended analysis, shown in the previous study (Yang et al., 2023), analysed the impact of PCMs under various ambient weather conditions from extreme cold (-20 °C) to hot desert conditions (55 °C) for battery performance at cell level.

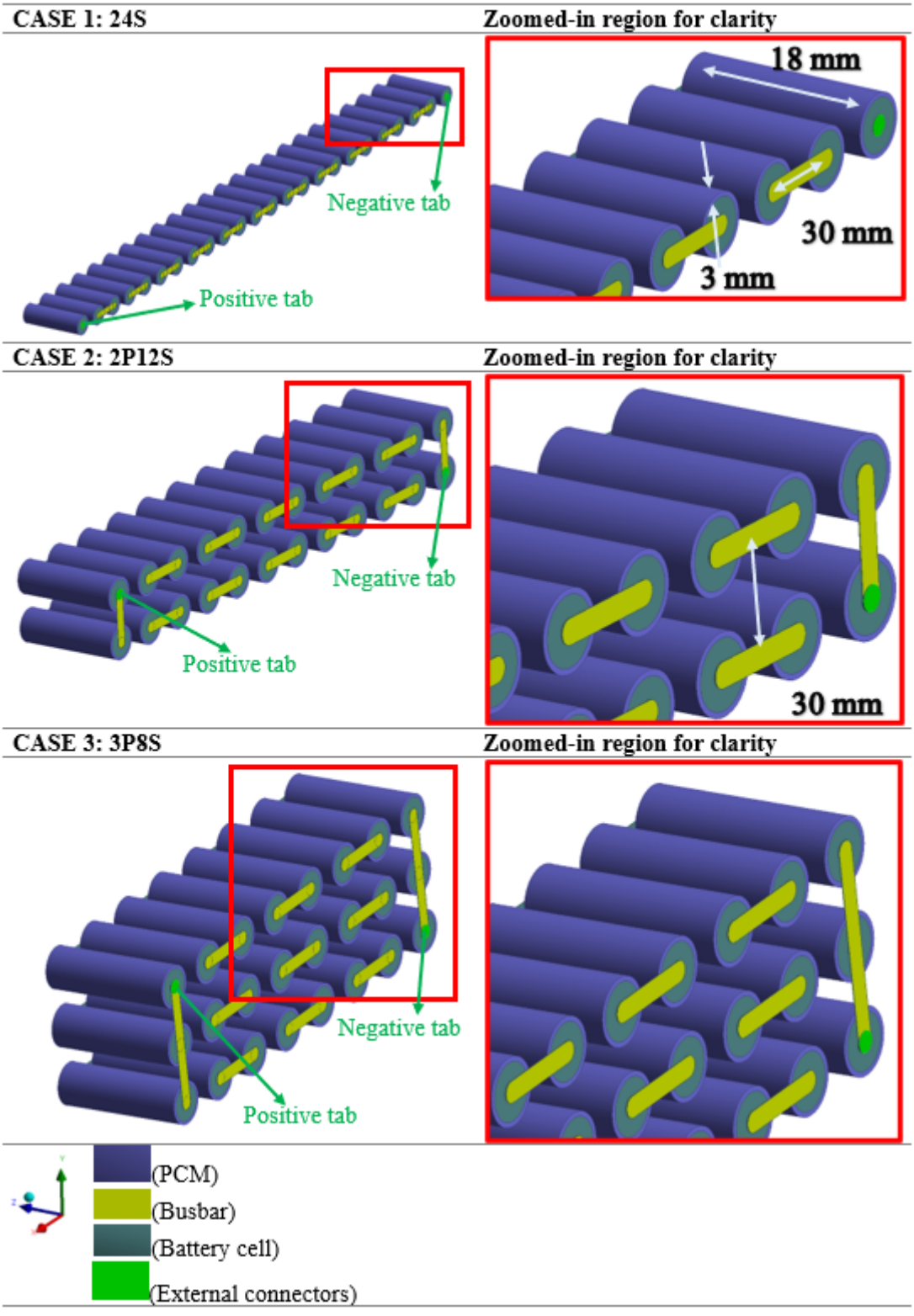

Fig. 6.1 Isometric and zoomed-in view of the considered battery module configurations (Case 1, 2, and 3) in presence of individual PCM jackets.

6.2.2 Initial and boundary conditions

The numerical models depicted in Figure 6.1 were analysed for the following initial and boundary conditions:
For all Cases (1, 2 and 3),

- Insulated outer walls around the LH jackets provided an adiabatic environment independent of adjacent cells and loss of heat to the environment,
- Adiabatic (zero heat flux) walls for battery tabs and coupled walls for busbar connections,
- The solidus temperature represented the PCM's initial state,
- The module temperature was set to ambient 25 °C,
- Conductive battery walls to the PCM and busbar were set to ambient module temperature with heat transfer coefficient set to 7 W/mK.

6.2.3 Assumptions

In the modelling of all Cases (1-3), the following assumptions were considered,

- Battery modules were 100 % charged and ready to be discharged based on a reference capacity equivalent to the nominal module capacity (ah),
- Due to ECM model characteristics at the cell level, homogenous physical battery properties were sustained throughout the analysis with all cells the same in the module and under the same initial conditions,
- Molten PCM was considered compressible and viscous flows laminarly,
- Conduction heat transfer applied and continuous from battery cells to PCM and from tabs to busbars,
- Cells in the module were arranged horizontally (see Figure 6.1) with gravity at 9.81 m/s^2 for LH-based cooling Cases,
- The positive and negative tabs were continuous surfaces,
- Real tabs/busbar conductive volumes formed connections to positive and negative tabs,

- Natural convection heat transfer calculated based on Boussinesq approximation for density approximation in molten PCM.

Essential safety limits were considered for all Cases during charging, discharging and drive cycling as a preventative measure to ensure the system remains within optimum working conditions and free from overheating effects and thermal runaway effects. Beyond these limits were not in the scope of this study and testing was only considered between the recommended manufacturer recommendations.

- For discharging: 60°C,
- For charging: 45 °C,
- For drive cycle modelling: 60°C,
- Between single cells, the minimum and maximum cut-off voltage was at 2.5 V and 4.2 V, respectively.

6.2.4 Mathematical and numerical model

In this study, the combined thermo-chemical and electrical models were used in ANSYS Fluent 2022 R2. An enthalpy-porosity method was used to track the movement of the liquid-solid front or in other words, the "mushy zone" region during phase change. This method eliminates the need to track the movement explicitly. An equal porous zone to the liquid fraction was dedicated to the liquid-solid mushy zone. The liquid fraction in this case was known as the specific cell volumes which were in liquid form corresponding to every cell in the PCM domain. To identify the phase change during melting, the liquid fraction was valued between 0 and 1 which represented lower and upper bounds for solid to liquid. The values were calculated for every iteration corresponding to the enthalpy balance. In the solid state, the null porosity had an equal effect on the velocity. Sink term equations were applied to the momentum equations to represent the pressure drop due to solid regions. These sink terms were also employed in the turbulence equations where there could be reduced porosity indicated by solid regions. For conducting the thermal analysis of the battery model, the heat generated by the system must be accurately performed to fully understand the thermal behaviour during regular operation. There were different methods to perform the coupling, but this study focused on the Multi-Scale Multi Domain (MSMD) solution method which directly solves the electrochemical aspect of the battery. The model addressed the issue with different length scales with distinct physical phenomena and so the distribution of temperature was along the scale of the battery. Based on the assumptions and boundary conditions, the following governing equations were used.

The energy equation for the battery (Kim et al., 2011) is

$$\frac{\partial \rho C_p T}{\partial t} = \nabla.(k\nabla T) + \sigma_+|\nabla \emptyset_+|^2 + \sigma_-|\nabla \emptyset_-|^2 + \dot{q}_{ECh} \quad (6.1)$$

Where $\dot{q}_{ECh} = j_{ech}[V_{OCV} - \mathrm{V} - \mathrm{T}\frac{dU}{dT}$

And $j_{ech} = I\ \frac{Q_{nominal}}{Q_{ref} Vol}$

I is the current and V_{OCV} is the open circuit voltage

In this case, the heat generation for the battery is noted as $\dot{q}_{total} = \dot{q}_{Joule} + \dot{q}_{entropy}$

Where $\dot{q}_{Joule}$ is the irreversible heat and $\dot{q}_{entropy}$ is the reversible heat

The energy equation for the busbar is

$$\frac{\partial \rho C_p T}{\partial t} = \nabla.(k\nabla T) \quad (6.2)$$

The energy equation for the melting is

$$\frac{\partial}{\partial t}(\rho H) = \nabla.(\rho \vec{v} H) + \nabla.(k\nabla T) + S \quad (6.3)$$

$$H = h + \Delta H \quad (6.4)$$

$$h = h_{ref} + \int_{T_{ref}}^{T} C_p\, dT \quad (6.5)$$

$$\Delta H = fL \quad (6.6)$$

$$f = \begin{cases} 0 \\ 1 \\ \frac{T - T_{solidus}}{T_{liquidous} - T_{solidus}} \end{cases} ; \begin{cases} T < T_{solidus} \\ T > T_{liquidous} \\ T_{solidus} < T < T_{liquidous} \end{cases} \quad (6.7)$$

Momentum sink term for reduced porosity in the mushy zone,

$$S = \frac{(1-f)^2}{(f^3 + \varepsilon)} A_{mush} \quad (6.8)$$

The value of the A_{mush} constant is generally between 10^4 - 10^7. For this analysis, 10^5 was proven to be adequate for PCM melting based on the individual PCM volumes around each cell (see Figure 6.1).

The continuity equation for the PCM is

$$\frac{\partial \rho}{\partial t} + \nabla.(\rho \vec{v}) = 0 \quad (6.9)$$

The momentum equation for the PCM is

$$\frac{\partial \rho \vec{v}}{\partial t} + \nabla.(\rho \vec{v}\vec{v}) = -\nabla P + \nabla.(\mu \nabla \vec{v}) + \rho g + \frac{(1-f)^2}{f^3 + \varepsilon} \vec{v} A_{mush} \quad (6.10)$$

$$F_o = \frac{\alpha t}{D^2} \quad (6.11)$$

The Reynold's number is based on laminar fluid flow

$$R_e = \frac{\rho v D}{\mu} \quad (6.12)$$

Furthermore, in the context of the MSMD model, the ECM was used to resolve the electrical behaviour of the module using an electric circuit initially modelled in their study (Kollmeyer et al., 2017), (Kadivar et al., 2019) which involves a six parameter approach comprising three resistors and two capacitors. This model involves the charging and discharging of individuals cells and pack.

Natural convection, driven by buoyancy resulting from density changes due to temperature fluctuations, was observed within the molten phase of the studied PCM. Enclosed within a boundary, the flows adhere to the Boussinesq approximation, facilitating faster convergence under constant density and temperature conditions. As seen in the previous studies (Yang et al., 2023), (Nicholls et al., 2022), the gravity induced natural convection is influenced by the thermal expansion coefficient and directly impacts the density shifts in the molten PCM region, in response to temperature changes. If the temperature fluctuations remained minimal, and the density differences were negligible, then the Boussinesq approximation would be valid. The subtle changes in volume during temperature increases and the melting process was because of the thermal expansion coefficient as mentioned in Table 6.1.

The relationship between the voltage and current is determined by solving the electric circuit equations which are highly dependent on the battery SOC and temperature.

$$V = V_{OC}(SOC) - V_1 - V_2 - R_s(SOC) I(t) \quad (6.13)$$

$$\frac{dV_1}{dt} = -\frac{1}{R_1(SOC) C_1(SOC)} V_1 - \frac{1}{C_1(SOC)} I(t) \quad (6.14)$$

$$\frac{dV_2}{dt} = -\frac{1}{R_2(SOC) C_2(SOC)} V_2 - \frac{1}{C_2(SOC)} I(t) \quad (6.15)$$

$$\frac{d(SOC)}{dt} = I(t)/3600 Q_{ref} \quad (6.16)$$

The fifth order polynomial form for different coefficients of charging and discharging are explicitly resolved as functions based on the following equations:

$$R_s = a_0 + a_1(soc) + a_2(soc)^2 + a_3(soc)^3 + a_4(soc)^4 + a_5(soc)^5 \quad (6.20)$$

$$R_1 = b_0 + b_1(soc) + b_2(soc)^2 + b_3(soc)^3 + b_4(soc)^4 + b_5(soc)^5 \quad (6.21)$$

$$C_1 = c_0 + c_1(soc) + c_2(soc)^2 + c_3(soc)^3 + c_4(soc)^4 + +c_5(soc)^5 \quad (6.22)$$

$$R_2 = d_0 + d_1(soc) + d_2(soc)^2 + d_3(soc)^3 + d_4(soc)^4 + d_5(soc)^5 \quad (6.23)$$

$$C_2 = e_0 + e_1(soc) + e_2(soc)^2 + e_3(soc)^3 + e_4(soc)^4 + e_5(soc)^5 \quad (6.24)$$

$$V_{OCV} = f_0 + f_1(soc) + f_2(soc)^2 + f_3(soc)^3 + f_4(soc)^4 + f_5(soc)^5 \quad (6.25)$$

6.2.5 Computational model setup

A pressure-based solver used for incompressible laminar fluid flow was evaluated in the action of fully discharging and re-charging all Cases for transient time analysis which involves 3D modelling. Fluid flow is viscous with solidification and melting activated for mushy zone values between $10^4 - 10^7$; (Yang et al., 2023), (Nicholls et al., 2022) in which 10^5 was sufficient for the volume of LH jacket around each cell in the module. PRESTO! was used for spatial discretisation under pressure whilst momentum and energy were set to Second Order Upwind. The under-relaxation factors for Pressure, Momentum, Energy, Density, and liquid fraction were as follows: 0.3, 0.7, 1, 1 and 0.9. Convergence criteria is set at 10^{-3} for continuity and momentum and 10^{-6} for energy. This was not checked for the Cases without PCM.

For solution convergence, the transient analysis was set to 100s for time step size during discharging and charging cycling. The LH jacket models' solution convergence was adjusted to 1 microsecond for satisfactory results. The value was adjusted in an adaptive time advancement through to fixed once convergence was achieved and to increase simulation speed. For an MSMD solution method, the ECM E-chemistry model was used to perform the coupled thermal-electrochemical simulation to address the electrochemical aspect of the battery. Minimum and maximum voltage cut-off limits were set to 2.5 V and 4.2 V, respectively. The reduced order method (ROM) under MSMD approach was initialised to reduce computational time after 3 timesteps were first completed. A time-scheduled using profile solution option was selected to input selected drive cycle profiles based on the electric load type. This approach allows for a controlled time-dependent variation of load type and value reliant on requirements including sudden changes in profiles accurately.

6.3 Results/analysis and discussion

6.3.1 Grid and Temporal independence study

A grid independency analysis was performed to analyse the effects on the grid sizes for the solution accuracy. For a single cell approach, the meshing was performed using specific sizing based on edges and bias towards the areas which require higher number of elements to be effectively resolved. In these Cases, three different grid sizes were compared including fine, selected, and coarse with fewer than 1 % deviation for number of elements at 86877 and 84801 without and with the LH jacket, respectively. Orthogonal quality and skewness showed more than 0.95 and less than 0.25 for increased accuracy of results. In the case of the modules, conventional meshing (considered and displayed in earlier studies, (Yang et al., 2023)) was compared with the accuracy of watertight meshing (shown in Figure 6.2) which provides a more robust and high quality meshing. Results compared for single cell 18650 battery with 84801 conventional elements versus 5110 watertight meshing, showed less than 1 % deviation in accuracy of results with and without the LH jacket, resulting in reduced time for meshing. This watertight meshing method was then selected for modelling the modules, which reduced the time taken to mesh each cell, but with similar accuracy of results. In this case a grid independence analysis was performed for the watertight meshing for fine (238557), coarse (144530) and selected (181188) number of elements for the 24S Case. Results showed fewer than 1 % deviation of results, which indicated that the selected number of grids was sufficient to conduct the study. The same meshing controls were used to generate the grids for the other two Cases (Case 2: 185110 and 243874 without and with LH jacket respectively, Case 3: 181397 and 243512 without and with LH jacket respectively). The watertight grid images without LH jackets are therefore illustrated in Figure 6.3 with zoomed-in areas of interest at a different orientation to show the applied watertight meshing.

Additionally, a temporal independency study showed that a fixed 100s time-step size was sufficient for the case without LH jackets as opposed to 10, 50, and 150, with fewer than 0.1 % deviation. In the other Cases with LH jackets, an adaptive type of time-step size was used to achieve accurate results with an indication of convergence. This was also significant due to the slow melting of the PCM and to accurately capture the transition from solid to liquid during the initial stages of conduction heat transfer and the onset of buoyancy driven convection flows in tracking of the melting front. Moreover, a mushy zone constant study as seen in their work (Yang et al., 2023), (Nicholls et al., 2022) showed that A_{mush} values between 10^4 and 10^9 was less significant during the conduction phase in the initial PCM melting and increased in the natural convection phase where buoyancy driven flows and Bernard cells formation were more prevalent. It was also noted that the volume of PCM had a direct impact on the convection phase, as greater sized vortices can be fully developed. Due to the small

circumferential diameter (3 mm) surrounding each of the cells in the module, the variation of the A_{mush} values did not have a substantial impact on the solution results and so $A_{mush} = 10^5$ was chosen.

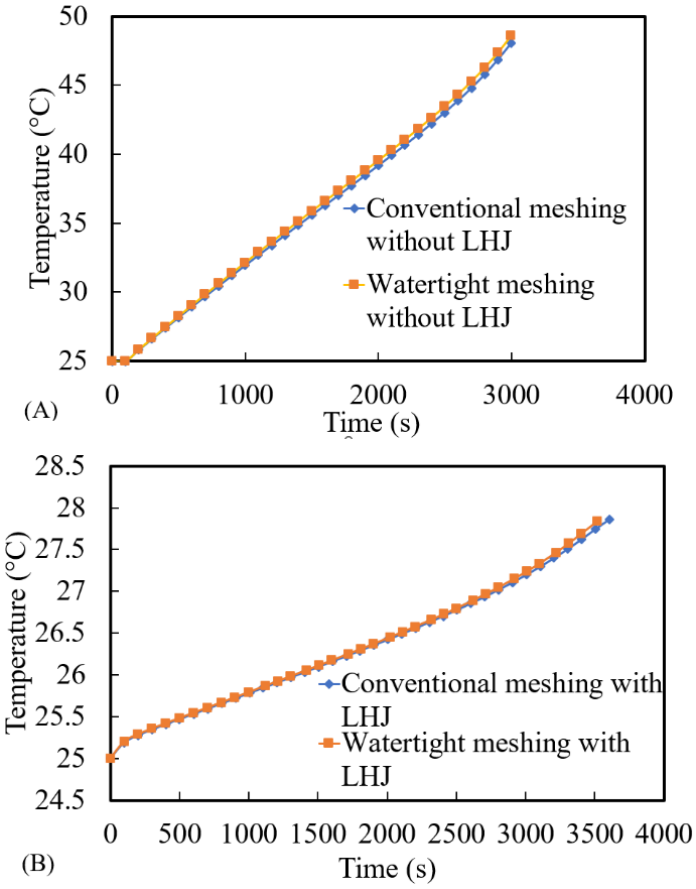

Fig. 6.2 Comparison of Temperature (°C) vs Time (s) for conventional meshing approach vs watertight automated meshing for a single 18650 Li-ion cell: A) without LH jacket and B) with LH jacket.

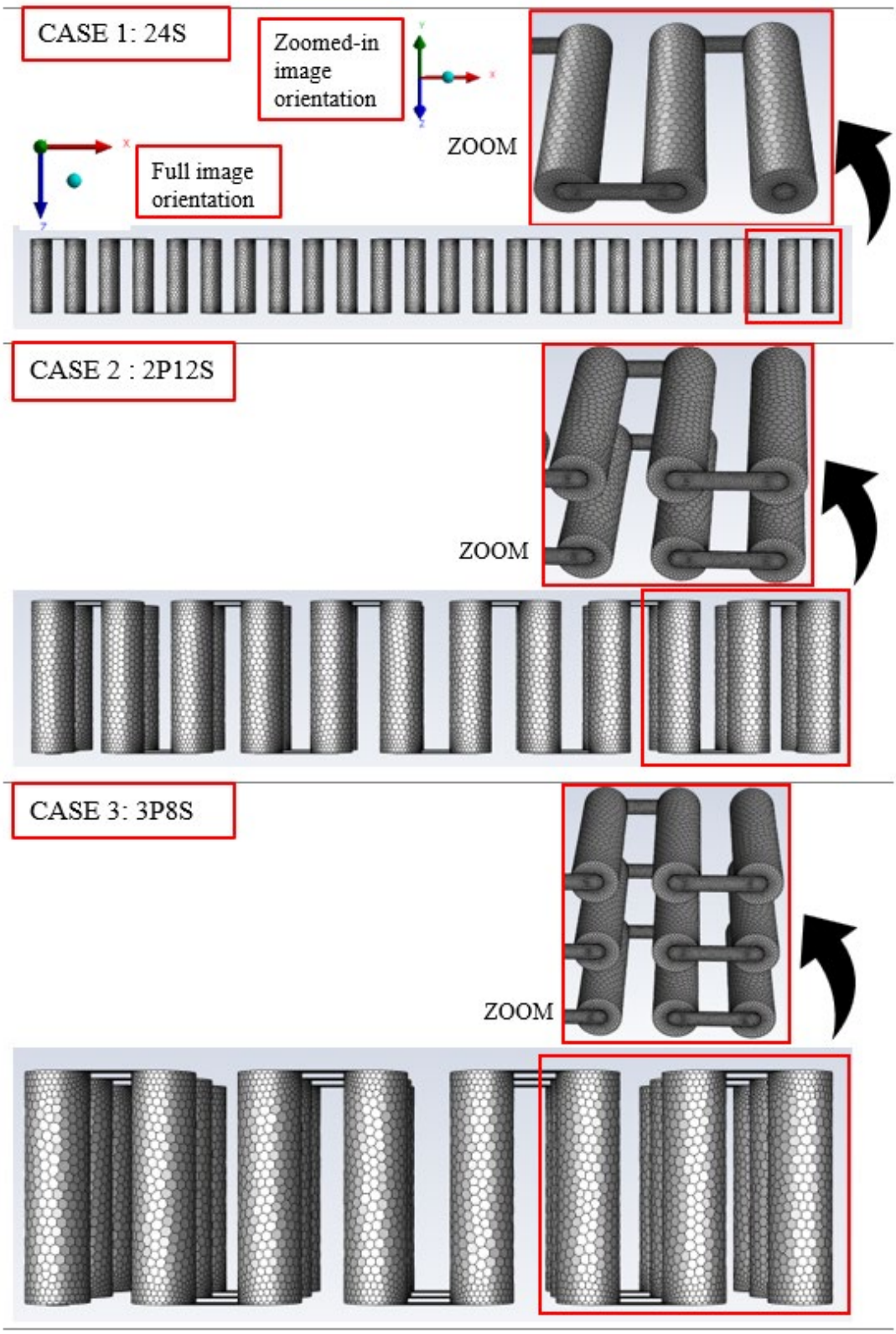

Fig. 6.3 Watertight grid images of all three Cases without LH jackets with zoomed-in partial images at selected areas.

6.3.2 Validation study

In a previous study (Yang et al., 2023), a battery cell thermal performance analysis was compared with literature (Kirad et al., 2021), (Kollmeyer et al., 2017) for numerical and experimental data for an 18650 Li-ion Panasonic battery cell at ambient 25 °C for 1C-rate. The heat transfer coefficient at the walls was at 7 W/mK, with fewer than 1 % difference in results for a single discharge as seen in Figure 6.4 (A). Additionally, a validation study (Darzi et al., 2012), (Kadivar et al., 2019) on sub-cooled PCM (N-eicosane) melting for a double pipe heat exchanger within the cylindrical annulus, at $A_{mush} = 10^5$ with inner cylinder set to 329.15 K and thermal conductivity at 400 W/mK, was analysed for the effects of charging and discharging. Results shown in Figure 6.4 (B) indicate less than 1 % difference from the study to numerical data.

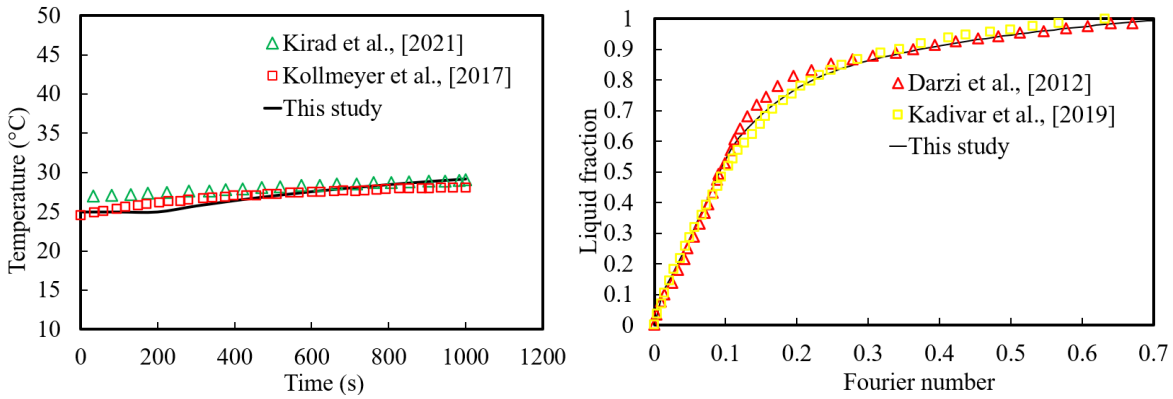

Fig. 6.4 Validation study: A) Cell thermal study for Temperature (°C) versus Time (s) data from literature (Kirad et al., 2021), (Kollmeyer et al., 2017) compared with present study at 25 °C B) study of liquid fraction versus Fourier Number (FO) data from literature compared with the present study (Darzi et al., 2012), (Kadivar et al., 2019).

6.3.3 Technical Discussion

Before analysing the effects of the proposed passive cooling system under different cycling loads, there are few technical points need to be discussed for further clarification of the technical stuff for readers.

1. The choice of PCM is important with high LH capacity and selected based on the ambient and operating conditions of the system/battery module. The solid-to-liquid phase change reduces the volume change and highly manageable as opposed to liquid-to-gas type PCMs and deemed more appropriate to this study. In this study the selected solid PCM N-octadecane (Table 6.1) was jacketed around each individual cell and in

direct contact with the circumferential diameter along the battery length (Shown in Figure 6.1) and eventually a module was constructed with the proposed battery configuration.

2. As the battery temperature rose due to discharging, the solidified PCM (LH source) absorbs the heat as the conduction heat transfer mechanism was dominant until the PCM was melted and natural convection heat transfer became dominant in molten PCM. This process continued until the entire the PCM volume was liquified, then the available LH would be expired and there was a transition to Sensible Heat (SH), where the temperature of the system did not remain constant and start to rise sharply.

3. The heat generated from the battery module was absorbed by the PCM making use of the LH capacity of phase change at liquidous temperature acting as a cooling agent with the capacity to store a large volume of LH, whilst maintaining a constant temperature. It was therefore essential that the volume of PCM used should be of sufficient amount to be able to absorb the amount of heat generated. Generally, seen in literature (Alami et al., 2022), (Kizilel et al., 2008), (Mohammed et al., 2022), (Talele et al., 2021), the PCM surrounds the cells in a container by which neighbouring cell temperatures influences each other and so cell spacing was integral to improve the design. The module Cases seen in Figure 6.1, can be treated as individual systems with no thermal impact since each cell is thermally isolated. This forgoes the need of design with cell-to-cell spacing and a reduction of SH. Moreover, all the volume of available PCM would be accessible, which would not be the case if the cells were far apart and dependant on the container design, if not cylindrical. In those Cases, a percentage of PCM would not be integral to the cooling process and would then be less efficient for additional weight not used. Although adding PCM volume around each cell can be advantageous to absorb additional heat and increase the delay time for PCM melting, the energy consumed will not out-weigh the benefits since increased weight will reduce the overall EV thermal performance. In this instance, the 3 mm jackets proved sufficient to evaluate the effect on the performance.

4. In this study, various drive cycle characteristics and parametrisation were assessed for the same proposed module Cases (24S, 2P12S and 3P8S). They were implemented based on voltage profiles. These dynamic profiles were specifically used in section 6.3.4.2 where the real-world drive cycles were assessed. All the test cycles were based

on validation study (Vikram et al., 2022) for a single cell and then scaled up based on the number of cells in the module. In the literature study, the battery pack was initially scaled down from 3680 cells to a single cell to reduce computational time. Each of the drive cycles would present a unique dynamic change and therefore erratic changes in temperature was expected but still follows a distinguishable pattern which was identified.

5. As seen in literature (Ling et al., 2014), (Yang et al., 2021), (Yang et al., 2023), the battery optimal working temperature range is between 20 °C to 40 °C and manufacture specifications states that the safety limits for use are bounded between -20 °C to 60 °C during discharging mode and not greater than 45 °C during charging mode. Beyond these ranges, the battery safety critical conditions were met, whereby thermal runaway and potentially severe degradation of the battery can occur. Thus, in these simulations to prevent undercooling and overcharging, the following restrictions were imposed; voltage cut-off limits at cell level (2.5 V to 4.2 V), SOC limits (between 0 to 1), and module temperature restricted to below the safety limits. This will present the desired outcome where the safety and risk assessments were managed accordingly. Disastrous effects can occur from the operation of the cells outside of these limits and so these stop conditions were initialised. This approach was seen in the cycling phases, where an accurate estimation of the predicted time it would take to reach just before the maximum and/or minimum SOC value and voltages, was achieved. Homogeneous temperature between cells was also analysed to ensure the disparity of temperature between cells in the module was kept to a minimum. In this regard, individual LH jackets were modelled around the cells which were placed at an equal distance from one another for an effective comparison.

6.3.4 Discussion on the effectiveness of the proposed passive cooling system

To analysis the effectiveness of the proposed passive cooling system, three different arrangements of modules (24S, 2P12S and 3P8S) are made up of 24 series and/or parallel 18650 Li-ion Panasonic cells discharged at constant 1 C-rate, until the SOC was approximately 0 or the temperature/voltage safety limits were reached. The proposed arrangements, have different voltage/passive zone potential and current which can better assess the effectiveness of the proposed passive cooling design. Indeed, the specified system power for all the Cases (24S, 2P12S and 3P8S)

remained the same at 278.4 W, and the capacities (between 2900 Ah to 8700 Ah) of each of the modules varied based on the cell arrangements comprising of series and parallel cells. The test of arrangements also provides an insight into the thermal uniformity between cells in the module, whereas the C-rate gives an indication of the current value, which would be dissipated within 1 hour if the cells were to be discharged from the fully charged position.

In addition to better check the effectiveness of the proposed cooling system, the discussed modules were assessed in presence and absence of the LH jackets which gave an insight of effectiveness of the proposed system. Thus, for this study in combined 6 modules were considered which three of those Cases (24S, 2P12S and 3P8S) equipped with LH jackets and 3 of them (24S, 2P12S and 3P8S) without jackets. Finally, in this study all those 6 cases were imposed to two different loads: 1- A theoretical scenario (a continuous cycling), and 2- haphazard variations of electrical boundary conditions (five actual driving loads). These scenarios were imposed on the proposed battery modules to capture following results: the module temperature, SOC, passive zone potential/voltage and the liquid fraction of the PCM. The following subsection of the articles, report the results of those loads on the 6 discussed modules.

6.3.4.1 Study on the impact of theoretical load scenario (a continuous cycling)

In this section the impact of the proposed passive cooling system on thermal management for three discussed modules (24S, 2P12S and 3P8S) in presence and absence of LH jackets under continuous 1C cycling is discussed. This work builds upon a previous study (Nicholls et al., 2024), in which an investigation was conducted using a passive cooling LH jacket with PCM to manage the thermal performance of a single Panasonic Li-on 18650 battery cell under real-world drive cycles. The study addressed the impact of driving behaviours on a single cell model validated from literature (Kirad et al., 2021), (Kollmeyer et al., 2017) when compared to continuous battery cycling. In continuous cycling, the cell was discharged and then recharged without resting phases between the different cycling modes. Thus, the impact from heat dissipation on maximum temperature, SOC, power, and liquid fraction was effectively analysed. The conjugated models based on distinct driving scenarios, demonstrated that LH jackets significantly enhance battery performance by 50 %, especially in aggressive driving cycles. This becomes necessary for validation including detailed electrochemical modelling that must be verified to simulate and understand these complex processes under varying stress/loading levels. This allows for crucial benchmarking and calibrating models to ensure alignment with real-world cell behaviour and at the same time, save on computational time for more complex

models with higher grid element sizes in those cases of modules/pack level. The validation of the material used permits understanding of combining individual cells arranged together to investigate how they interact with one another. The thermal management including electrical connectors, busbars and overall system integration provides insights on scaling effects where factors like heat dissipation and electrical connection become more pronounced. In this scaling, management of the cells become crucial with additional challenges arising including uniform performance across cells in a module and to manage the energy distribution.

In that regard, contours of battery temperature in presence and absence of the LH jackets for Case 1 (24S) are shown in Figure 6.5. Figure 6.5 (A) displays a 2D top view comparison of these two cases at 6 instances within 1 hour and Figure 6.5 (B) displays 3D Isometric views of those cases at only one instance (3500s) which were picked for the sake of brevity. The global temperature of the cells as well as temperature differences can be seen in Figure 6.5 (B) at the same time as 3500s, to clearly show the temperature differences within a closer colour bar range. Zoomed-in areas of the cells provide more apparent contours as well as PCM temperature. For clarity, in this figure, the zoomed-in areas show the cells (4 different snapshots) at the ends of the module case (24S) including the locations of the positive (Tab_p) and negative (Tab_n) tab connection cells (far ends). These snapshots will provide a better picture of understanding the temperature variation in the ending cells and corresponding busbar connections as opposed to the cells within the middle of the module

As shown in Figure 6.5 (A), in the presence of LH, the temperature of the module was low at all the selected different time instances (depicted by the dark blue contours) and only varied within 3.5K (the temperature range of 298.15K to 301.65K). However, in the absence of LH jacket, for Case 1 (24S), the temperature rise was more obvious with increased temperature illustrated by the colour bar legend, especially when Figure 6.5 (B) is considered as well, where global temperature contours are displayed. These global temperature contours show a closer range of temperature (the minimum, 303.2K to the maximum, 322.5K) to include both cases with and without LH jackets. They definitively indicate the temperature differences within various connections of the domain (module) including busbar, cells, and tabs. In the absence of LH jackets for 24S case, the temperature rose from initial ambient (25 °C) to the safety limit temperature (60 °C) (coloured contours from blue, 298.15K, to red, 333.15K) for Figure 6.5 (A) and between coloured contours from blue, 303.2K, to red, 322.5K in Figure 6.5 (B). It is noteworthy that in this case (24S - without LH jacket), the higher temperature cells captured at the far ends of the module displays where the negative and positive tab external connections are located. These cells (far end cells) were within the temperature range of 322.65K to 326.15K as shown in Figure 6.5 (A) in the colour bar, whereas the central cells in the module ranged between 319.15K to 322.65K at 3500s. The colour band in Figure 6.5 (B) has a maximum temperature range up to 322.5K as this shows the global temperature range to indicate more vividly the high temperatures as opposed to the user

specified case for minimum and maximum temperature limits in kelvin (298.15K to 333.15K). A much clearer depiction of the comparison between the case with and without LH jackets is therefore shown. Compared to the case with LH jackets at 3500s, the temperature of the module remained within 298.15K to 301.65K, which represents a decrease in maximum temperature by 24.5K with the proposed passive cooling approach.

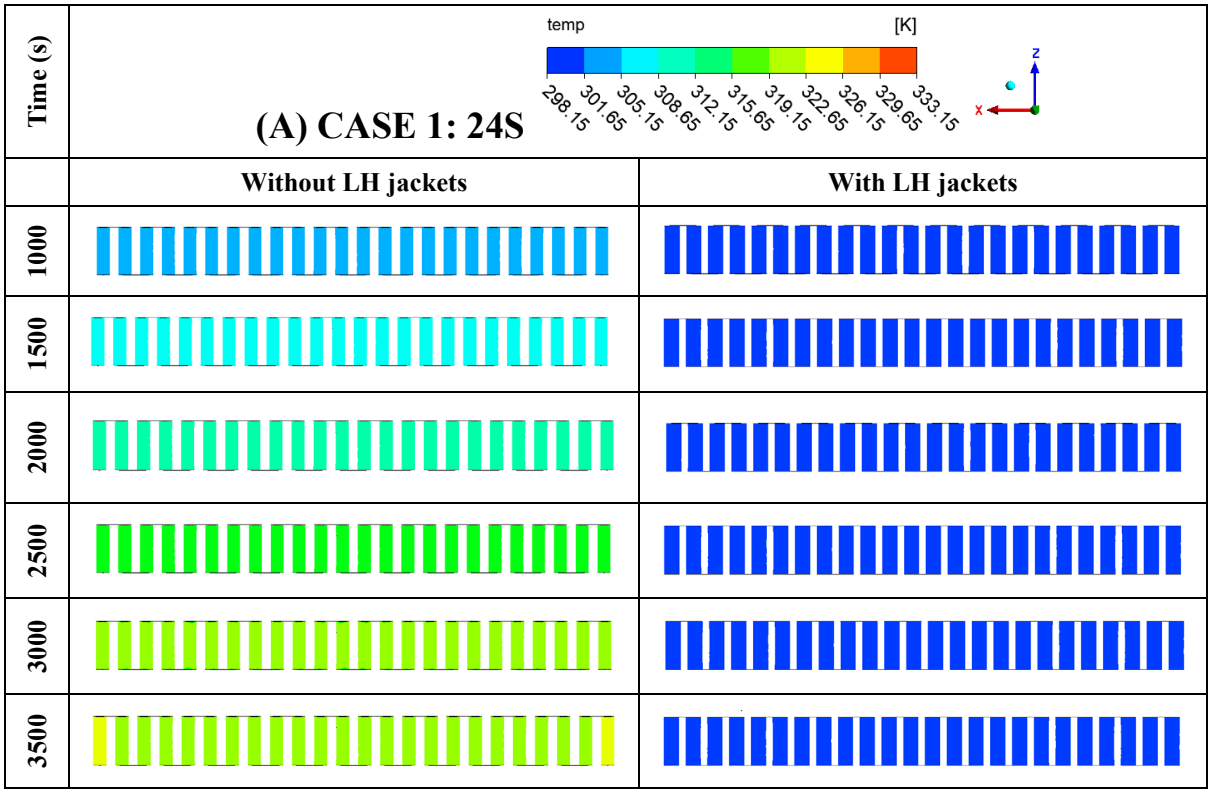

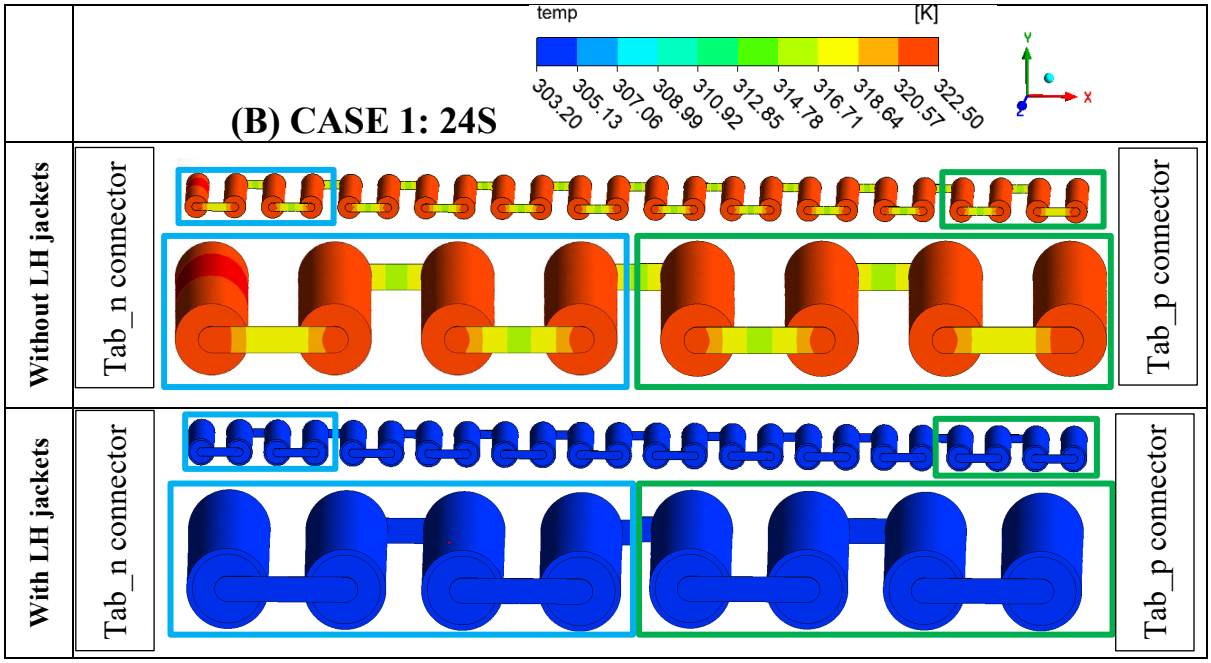

Fig. 6.5 Case 1 (24S) Temperature contours at indicated times for module discharging: A) 2D midplane top view at indicated timeframes and B) 3D Isometric view with zoomed-in images of the external connected cells showing higher temperatures at 3500s.

Therefore, in this case one can conclude that higher temperatures are seen for the ending cells and corresponding busbar connections as opposed to the cells within the middle of the module, which was better depicted in Figure 6.6. Indeed, in Figure 6.6 the 3D isometric view of the case without LH jacket was displayed with different localised temperature approach to better illustrate the busbar temperature variations and temperature at the ending cells. As shown in this picture, during the module discharge at 3500s in absence of LH jacket, the module localised temperature range was between 316.41K to 322.52K and represents a significant temperature difference (~6.11K) for continuous discharging, resulting in a clear need of heat dissipation from the module to reduce the effects of overheating. This could be achieved by using passive cooling LH jackets as its impact was clearly shown in Figure 6.5 (B) even with the busbar connections.

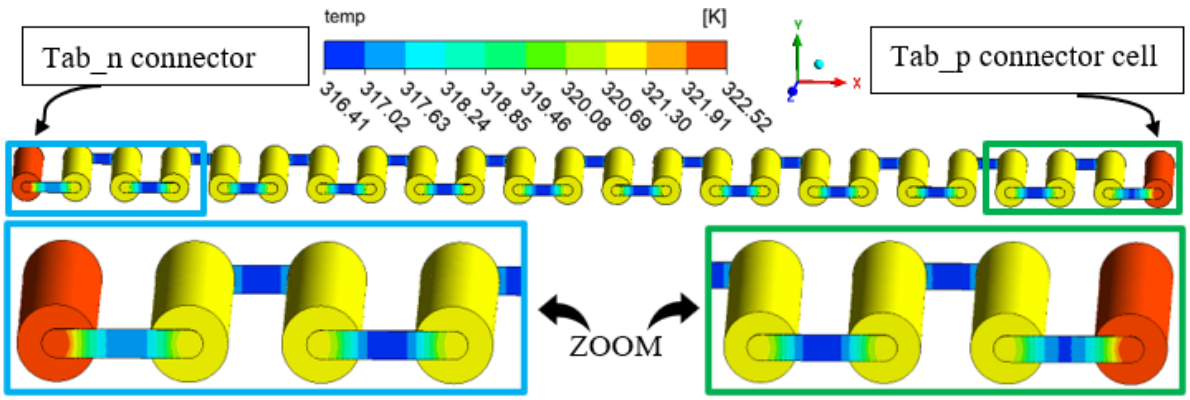

Fig. 6.6 Isometric view with zoomed-in images of the external connected cells (far ends), for Case 1 (24S) without LH jackets at 3500s with Localised Temperature contours.

Figure 6.7 (A) displayed the temperature contours at selected instances during discharge for Case 2 (2P12S) in presence and absence of passive cooling. Similarly, in Figure 6.7 (A), a 2D top view comparison of the two cases for the module (with and without LH jackets) showed 12 cells in series at 6 instances in time within 1 hour. Figure 6.7 (B) displayed a 3D Isometric view at one instance (3500s) to maintain conciseness. As seen in Figure 6.7 (A), with the introduced LH jackets, the module temperature remained low at selected time instances as seen similarly with the first case (see Figure 6.5 (A)). The coloured contours remained dark blue and within the temperature range displayed by the colour band (298.15K to 301.65K) and still within 3.5K. Contrastingly, without the introduced LH jackets, for Case 2 (2P12S), the module temperature, and indeed individual cell temperature increase shown by the colour bar legend, was more distinct, particularly when considering the contours shown in Figure 6.7 (B). The contours shown in Figure 6.7 (B) illustrate a global temperature legend with colour band between 303.2K (minimum) and 322.5K (maximum) for both with and without LH jackets. Similarly, the temperature rise shown in Figure 6.7 (A) was between 298.15K to 333.15K and represents the initial temperature (25 °C) and safety temperature limit (60 °C), respectively. The temperature of the cells without LH jackets at 3500s lie within the range of 319.15K to 322.65K as displayed by the colour band. The contours indicated uniform temperature between them and did not clearly show the variation in hot temperature at the external connector cells due to the top view displayed, as well as all the cells were not shown in that view. However, Figure 6.7 (B) clearly shows the higher temperature cells near the external connectors, in particular, the positive tab connector (Tab_p). These cells were within the range of 318.64K to 320.57K without LH jackets indicated by the colour band (see Figure 6.7 (B)). All the other cells in the module were between 316.71K to 318.64K at 3500s. When analysed for the case with LH jackets at 3500s, Figure 6.7 (A) shows the module temperature within the range

of 298.15K to 301.65K and a reduction in maximum temperature by 21K. Figure 6.7 (B) clearly indicates that the introduction of the LH jackets can maintain thermal stability between all the cells in the module whilst reducing the maximum temperature limit achieved within the time.

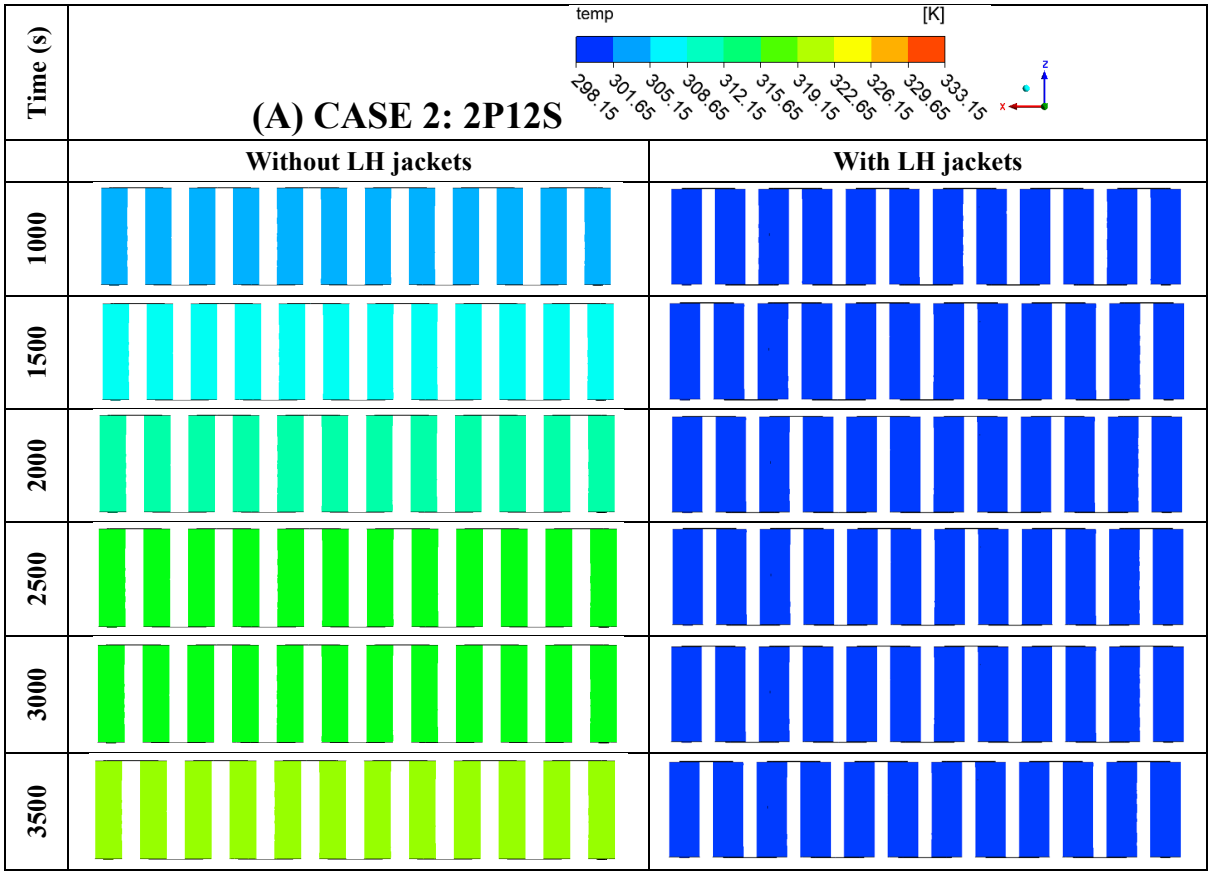

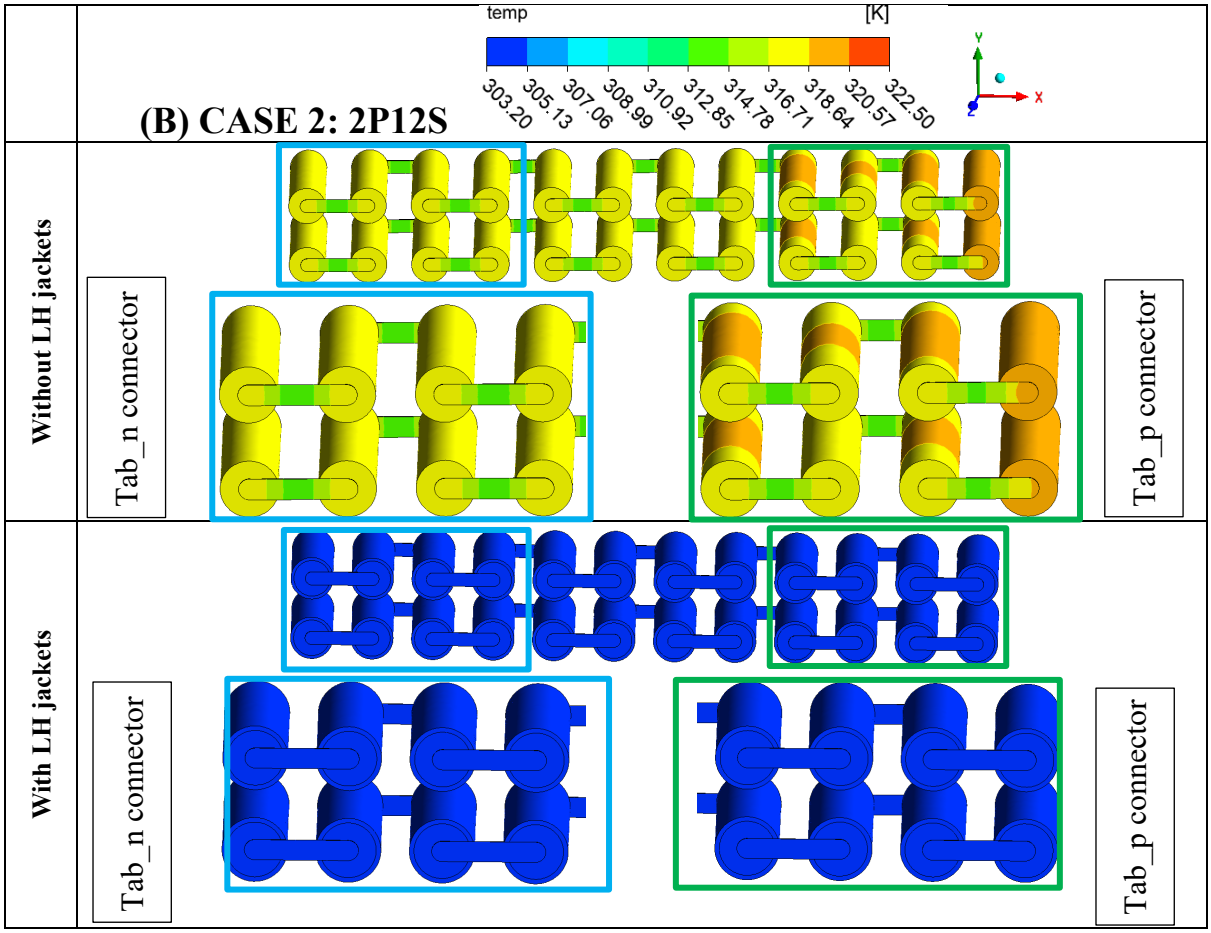

Fig. 6.7 Case 2 (2P12S) Temperature contours at indicated times for module discharging: A) 2D midplane top view at indicated times B) 3D Isometric view with zoomed-in images of the external connected cells showing higher temperatures at 3500s.

Figure 6.8 displays the Isometric view of localised temperature contours for Case 2 (2P12S) without LH jackets at 3500s to further illustrate the differences in temperature between the external connector cells as well as all the cells in the module arrangement including busbar temperature. The temperature range had been further reduced to indicate the locations of lowest temperature (blue) to the highest temperature (red). It was quite clear that the highest temperature cells were in the vicinity of the positive tab external connector cell and then propagated throughout the rest of the module. It was interesting that the negative tab external connector cell in this case, had one of the lowest temperature regions as seen by the colour bar legend, with the lowest temperature cell being the furthest away from the positive external connector (Tab_p). In this case, during the discharging cycle, the module temperature ranged between a minimum and maximum temperature at 314.10K to 319.22K, respectively, with a temperature difference of 5.12K at 3500s. This meant that an appropriate BTMS

strategy was required to prevent overheating which can be achieved with the proposed passive cooling as shown in Figure 6.7.

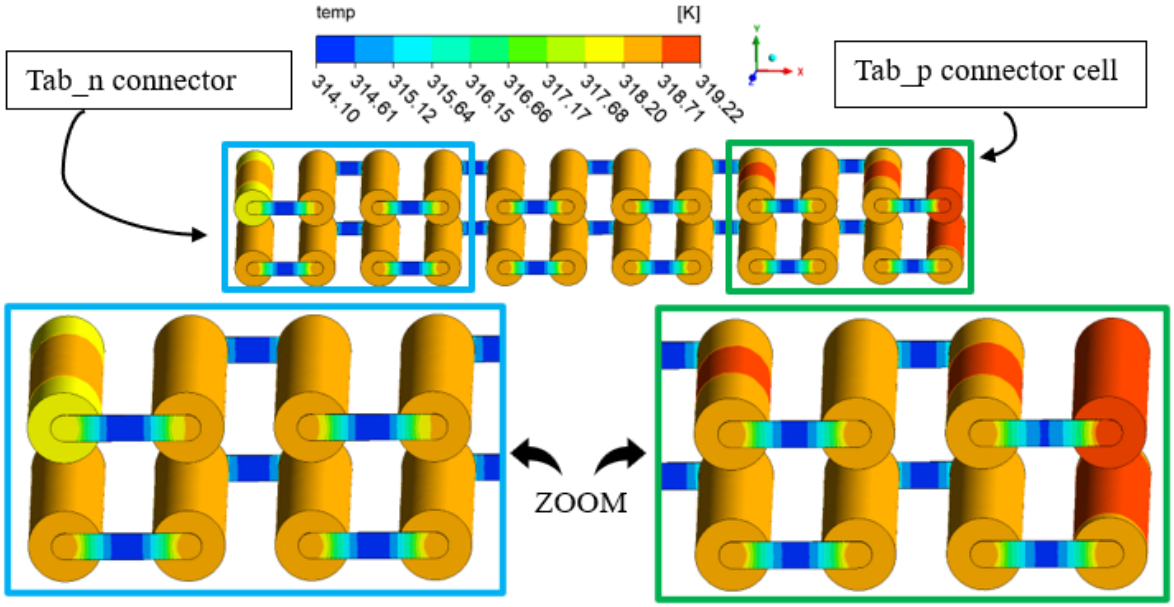

Fig. 6.8 3D Isometric view with zoomed-in images of the external connected cells (far ends), for Case 2 (2P12S) without LH jackets at 3500s with Localised Temperature contour.

Furthermore, Figure 6.9 shows the temperature contours for Case 3 (3P8S) at 6 different time intervals during discharge in presence and absence of LH jackets. Figure 6.9 (A) displays the top view in 2D for 8 cells in series within 6 time intervals from 1000s to 3500s with 500s increments. The passive cooling LH based BTMS displayed low temperatures even up to the 3500s period within 1 hour as indicated by the colour contours which showed dark blue. This behaviour was similar to previous cases (Case 1: 24S and Case 2: 2P12S) which demonstrates the effectiveness of passive cooling in reducing maximum battery temperature during continuous discharging/charging (a continuous cycling load). This was confirmed in Figure 6.9 (B) for an Isometric 3D view showing global temperature contours with and without LH jackets at 3500s. In the previous 2 Cases (Case 1: 24S and Case 2: 2P12S), when passive cooling was available, the temperature of the cells remained within a low temperature range of 298.15K to 301.65K, likewise, Case 3: 3P8S, also remained within that temperature range even for all the times shown. Due to this low temperature range well below the temperature safety limit, suggested that the heat was readily absorbed even in this arrangement of cells and certainly as seen for the other two Cases studied. The temperature difference was still within 3.5K as seen by the colour band (see Figure 6.9 (A)).

However, compared to the case without LH jackets, the rise in temperature was more apparent, as indeed, there was a definitive change in the colour contour even from the initial time at 1000s, with a maximum temperature range between 305.15K to 308.65K. This certainly indicated that an increase in current/nominal capacity (Case 1: 2.9Ah to Case 3: 8.7Ah) influenced the thermal performance of the module, impacting on the heat dissipated within the cells in the module. The higher temperature cell was at the positive external connector (Tab_p), with distributed heat throughout the module decreasing as it moves towards the other cells during the cycling process. This was displayed (see Figure 6.9 (A)) as the time was increased from 1000s to 3500s. The highest temperature at 3500s for the case without LH jackets was shown to be the positive external connector tab cell which ranged between 322.65K to 326.15K. This meant that there was a drop in maximum temperature of 24.5K when the LH jackets were introduced, and passive cooling was available. The downside of the presented view in Figure 6.9 (A) is only the top level row of 8 cells in the module are visible and does not clearly show the heat transfer within all the cells. Thus Figure 6.9 (B) presented to show an Isometric view for a global and more narrow temperature range. The highest temperature (range between 320.57K to 322.50K) cell was seen to be the positive tab external connector cell (Tab_p) and the heat was dissipated throughout the rest of the module via the connecting busbars. Even the busbar connections near the Tab_p for the external connector cell has a higher temperature distribution than the other busbars as seen by the colour legend. These cells exhibit higher temperature than the rest of the cells because of the higher voltage as opposed to the anode (negative tab external connector Tab_n). This behaviour was seen for all the time intervals showing higher temperature cells on the left and decreased as it moved to the right because of the orientation of the module (see Figure 6.9 (A)).

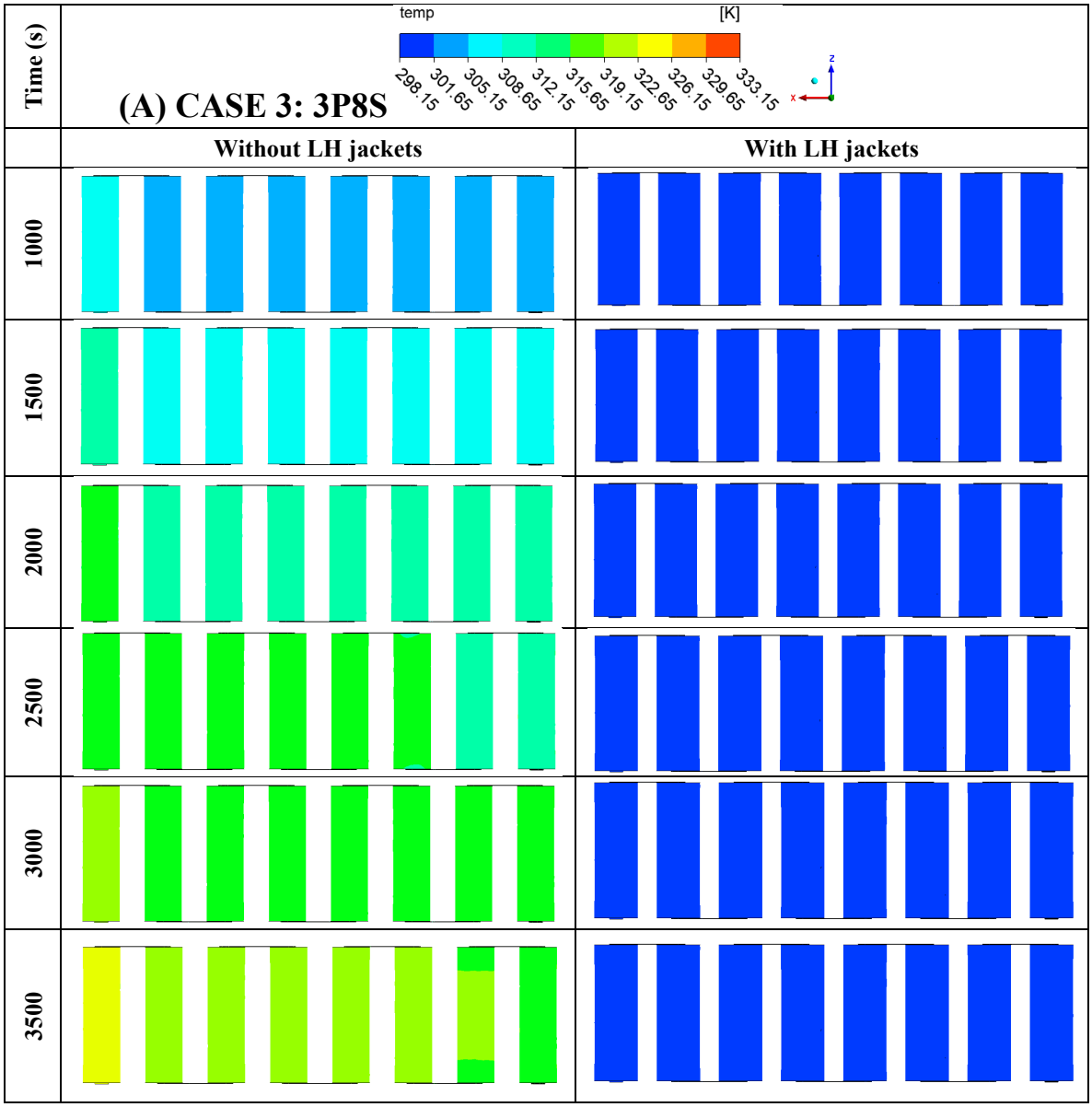
Time (s)
temp
[K]
298.15
301.65
305.15
308.65
312.15
315.65
319.15
322.65
326.15
329.65
333.15
(A) CASE 3: 3P8S
Without LH jackets
With LH jackets
1000
1500
2000
2500
3000
3500

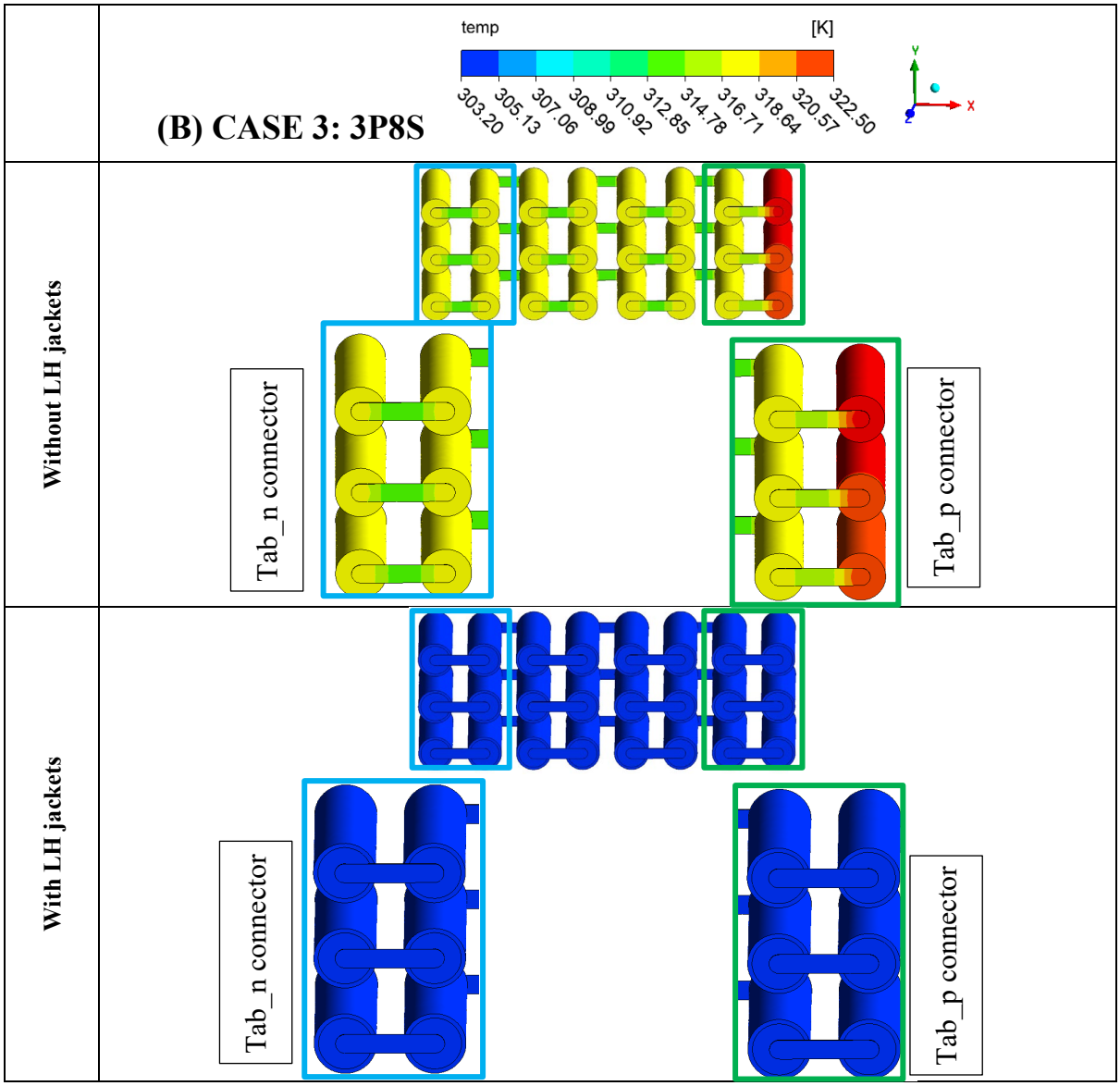

Fig. 6.9 Case 3 (3P8S) Temperature contours at indicated times for module discharging: A) 2D midplane top view at indicated times and B) 3D Isometric view with zoomed-in images of the external connected cells showing higher temperatures at 3500s.

To further illustrate the variation in temperature differences as described similarly with the two Cases before (Case 1 and 2), Figure 6.10 illustrates an Isometric view of localised temperatures without LH jackets at 3500s showing a minimum to maximum temperature range between 313.26K to 325.15K, respectively. The positive external connecter (Tab_p) showed the highest temperature (range between 322.77K to 323.96K) and followed the cells in the busbar connections nearby. The other cells in the middle of the module showed similar temperature ranges as the heat was propagated throughout the rest of the module. During the discharging cycle, the module temperature ranged between 313.26K to

325.15K as per the localised temperature colour band at 3500s, representing a temperature difference of 11.89K. Thus, an effective BTMS was required to prevent large temperature differences and eventually overheating which can be fulfilled with the proposed passive cooling design.

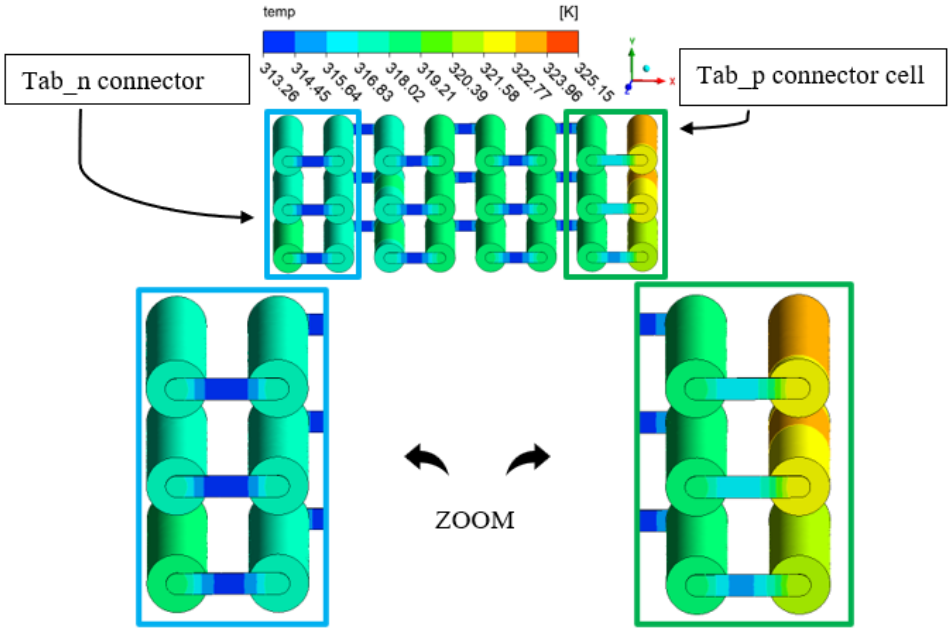

Fig. 6.10 3D Isometric view with zoomed-in images of the externally connected cells (far ends), for Case 2 (3P8S) without LH jackets at 3500s with Localised Temperature contour.

Eventually, the effectiveness of the proposed passive cooling for all the modules under continuous cycling load was assessed in Figure 6.11. Figure 6.11 displayed the plots of continuous cycling of temperature and SOC versus time as well as the passive zone potential and PCM liquid fraction versus time for all the aforementioned cases. In all cases, the results were reported until whichever of the following criteria was met earlier: 1) the battery temperature reached to safety limit, or 2) the module had been completely discharged. It is worth noting that the total time for continuous discharging varied between the different Cases as indeed this attributed to the configuration and specification of the considered module arrangements. Due to this variation, the nominal cell capacity (Ah) and the voltages (V) were different in each Case, however, as discussed earlier, for accurate modelling and comparison, the number and type of cells in each module remained the same. The Power (W) was the same across all modules assessed (see Table 6.1). When the nominal cell capacity was amplified from the change in series to parallel configurations, the time for complete discharge was also increased. The full results were displayed in Figure 6.11 for all cases as opposed to certain time intervals for the contours which were chosen for brevity.

Figure 6.11 (A) presents results for Case 1 (24S). As seen in the graph of temperature versus time, the introduced LH jackets allowed a more uniform, slow, and steady rise from an initial ambient at 25 °C as opposed to the sharp increase in temperature in the absence of LH jackets for the same discharge period. At the end of the discharging cycle, the module temperature was approximately 28 °C with the LH jackets when compared to (~) 48 °C without the LH jackets. This represented a drop in maximum temperature by 42 % (20 °C in about 48 °C). The results demonstrated that if there was available LH, the heat dissipated by the module would be readily absorbed by the PCM jacket and increase the useful life or delay time. The passive zone potential was as expected with a smooth decrease followed by a sharp decrease in voltage when more than 95 % of the SOC was released, and the PCM was approximately 80 % liquified. This meant that there was still available LH to follow consecutive charging for the case with LH jackets since the module temperature was below the charging safety limit (45 °C).

Figure 6.11 (B) shows the results of Case 2 (2P12S). As shown in this figure, introducing LH jackets led to a marginal increase in temperature (reaching 29 °C) in the 5500s, right before all the PCM had been melted as observed from the liquid fraction curve. Due to unavailable LH after this time, the module temperature rose sharply as SH became active until the module had less than 10 % SOC. At this time (6600s), the module temperature with LH jackets had reached its maximum at 42 °C. In contrast, the module case without LH jackets in the same period had reached close to the discharging safety limit at 60 °C. This meant passive cooling could effectively control the maximum temperature of the module in this case as well (equates to an 18 °C drop in maximum temperature in 6600s). Importantly, the presence of the available LH maintained stable and uniform temperature up to around 5500s as iterated previously while the module without LH jackets had reached ~ 54 °C in 5500s. In addition, the proposed passive cooling could effectively control the maximum temperature of the module without reaching to safety limit of the module. This result highlighted the impact and effectiveness of the proposed passive thermal management strategy for this module.

The results of Case 3 (3P8S) are shown in Figure 6.11 (C). As shown for this case, the temperature curve rose sharply at the beginning during the first 100s, which was attributed to initial SH storage before equilibrium of heat caused a slow rise until the LH storage was activated and finally consumed at 31 °C in 5900s. This (consumption of LH) was displayed in the liquid fraction curve which reached its maximum of 1 or 100 % at 5900s. Beyond this time, for the module in the presence of the LH jackets, the temperature started to rise similarly to without the LH jackets until the safety limit temperature was reached (10780s). When compared to the case without LH jackets, the module temperature reached 60 °C at 5270s. In this case, the numerical analysis was stopped due to the temperature safety limit reached and so the other results of SOC and passive zone potential (V) were

also stopped. When both cases (with and without LH jackets) were compared right before all PCM was melted, there was a drop in temperature of 29 °C by the introduction of the proposed system. Also, due to the delay effect, there was a significant extension in useful time resulting in ~200 % module useful life before the temperature safety limit was reached. It was also worth noting that the temperature difference between cells was kept below 5K for all Cases with LH cooling jackets and indicated improved thermal equilibrium between cells as compared without LH cooling. As mentioned previously, an even greater increase in the capacity (8.7 Ah) from Case 1 (2.9Ah) was displayed and did cause an increase in the delay time for the module to reach the safety limit of 60 °C but less than Case 2. This was attributed to distinct factors including differences in voltage and current distribution but was a clear indication that the arrangement of cells in a module has a differing effect on the capacity and temperature disseminated.

Regardless of the arrangement, these studies showed that the proposed thermal management system was effective for various modules under theoretical cycling load.

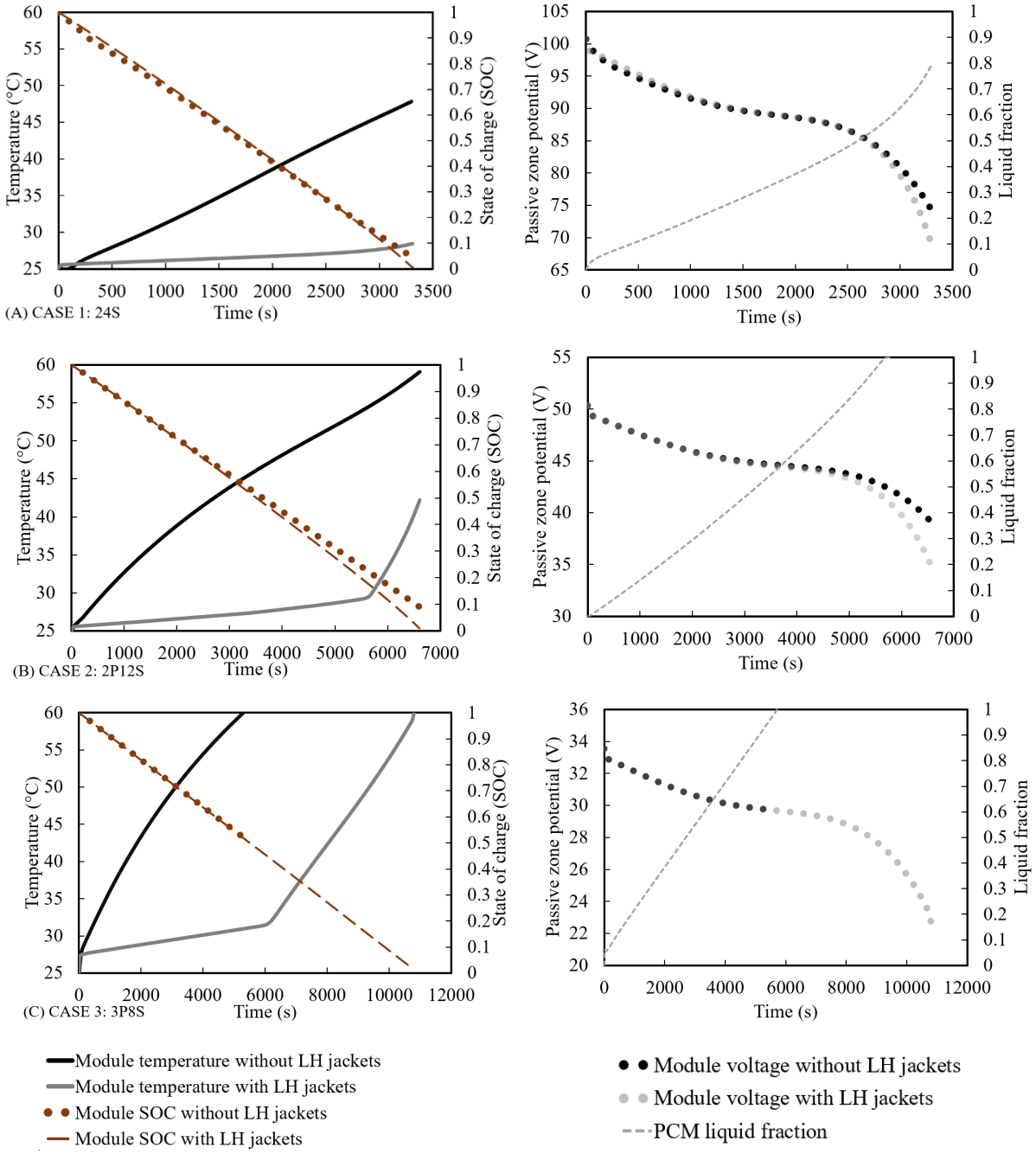

Fig. 6.11 Continuous cycling (Discharging) results of all Cases (24S, 2P12S and 3P85).

6.3.4.2 Study on the impact of real-world drive cycling

The previous analysis 6.3.4.1 was conducted as the researchers wanted to investigate fundamentally how the battery would behave under an ideal environment for profiles such as the voltage, power, and SOC during discharging/charging cycling. In those scenarios, the modules were discharged continuously at a constant C-rate with the option of continuous charging afterwards without resting if the safety limits were not breached. This testing assessed the system's durability and reliability for continuous cycling, but a more dynamic approach is necessary where idealistic conditions are not likely. Therefore, in this section, 6.3.4.2, a shift from continuous cycling (discharging/charging) to more dynamic battery modelling was considered to assess the effect of the proposed passive thermal management system on battery module temperature, SOC, passive zone potential and liquid fraction under realistic loads.

Thus, the following five different driving cycles were considered, Supplemental Federal Test Procedure (SFTP) (US06), Unified Cycle Driving Schedule or Unified LA92 (LA92), Neural Network (NN) combination cycle, Urban Dynamometer Driving Schedule (UDDS) and Highway Fuel Economy Test (HWFTa). These dynamic drive cycling replicated conditions on which vehicles are driven on different roads and environmental terrains which drivers may encounter and can include hills, flat roads, winding, or straight roads and of differing pitch that may include a variety of appropriate driving styles. In particular, the US06 (highest power requirement), LA92 and NN drive cycles consist of more harsh or aggressive driving. These include light vehicles driven at rapid velocity and acceleration with reduced stopping and idling within a 10-mile distance. On the other hand, the UDDS and HWFTa, for light-duty vehicles, represent more casual driving in Urban areas which can include very frequent idling and stopping as well as long distances. A full description of the drive cycle definitions used in the previous study (Nicholls et al., 2024) was outlined in more detail including power fluctuations within a specified time extracted from previous literary work published (Kirad et al., 2021), (Kollmeyer et al., 2017).

The results of the effects of the drive cycles on the proposed module configurations are presented in Figures 6.12 to 6.14 for Case 1 (24S), Case 2 (2P12S) and Case 3 (3P8S), respectively. All the captured results for the dynamic cycle loads on the proposed modules displayed rapid serrations from the power variation in contrast with smooth lines and curves from continuous cycling (results of section 6.3.4.1) captured at constant C-rate (1C), power (278.4 W), and ambient temperature (25 °C). Please note that for these drive cycle cases, only a specific range of time was available for reference and so the analysis was concluded when the limits of the available data were reached, or the temperature/voltage limits were hit. This was also reliant on the SOC available which would have been fully expired or near the end of the module capacity.

Results of Case 1 (24S) are shown in Figure 6.12, for all the considered cycles. As presented, the presence of LH jackets improved the thermal performance of the module for all the drive cycles with either expansion in useful life or maintenance of stable temperature. For the aggressive cycle US06 module (shown in Figure 6.12 (A)), the thermal performance improved by 223 % with more than a 2000s extension in the useful life of the module until the temperature safety limit was reached. This behaviour was displayed in the temperature curves of the cases without and with LH jackets reaching the temperature safety limit (60 °C) at the 1640s and 3710s, respectively. In addition, the SOC, initially set at 1 or 100 %, was reduced to ~50 % without LH jackets and more than ~90 % of the module discharged in the presence of the LH jackets before reaching to safety limit. The passive zone potentials displayed in Figure 6.12 (A) (US06), the sporadic changes from the dynamic drive cycle behaviour and vary between ~70 V to 100 V, with a clear distinction shown between the cases in the presence and absence of LH jackets. For the cases with introduced LH jackets, there was an increase in the voltage profile corresponding to the temperature curves. Even though there was available SOC for the case without LH jackets, due to the temperature limit hit, all the other results were stopped and captured accordingly.

Similar improvements in thermal performance can be seen with the other harsh drive cycles. LA92 drive cycle on the thermal performance of the module (24S) is shown in Figure 6.12 (B) and represents another aggressive driving cycle with improved thermal performance at 186 % when compared at the end of the cycle. For the case without LH jackets, the temperature was close to 58.7 °C (7060s) while the case with LH jackets was around 49 °C (13130s). At these end levels, the SOC had reached ~30 % and ~14 %, in the absence and presence of the proposed passive cooling approach, respectively from an initial state of 100 %. At the same time, the passive zone potential varied between 75 V to 100 V with the results showing almost double the life for the case with LH jackets as opposed to without the LH jackets.

The third aggressive cycle (NN drive cycle) is displayed in Figure 6.12 (C). In this case, there was also a reduction in temperature for the introduced passive cooling case with 184 % extended time to reach the temperature safety limit (60 °C) in the 6760s as opposed to 3670s for the case without the LH jackets. The SOC was reduced to 20 % and 70 % for the 24S module with and without the LH jackets, respectively. Due to the specific safety limits as identified previously, the study was concluded at these indicators. It was noted that the range for this drive cycle for Case 1 cycled between maximum 100 V and minimum 80 V, with the liquid fraction for the harsh cycles also following the same gradient as the modules without the LH jackets, to illustrate that the heat energy was absorbed.

For the casual Cases UDDS and HWFTa shown in Figure 6.12 (D) and E, more than 90 % of the module state was discharged but the battery module temperature did not rise above 45 °C.

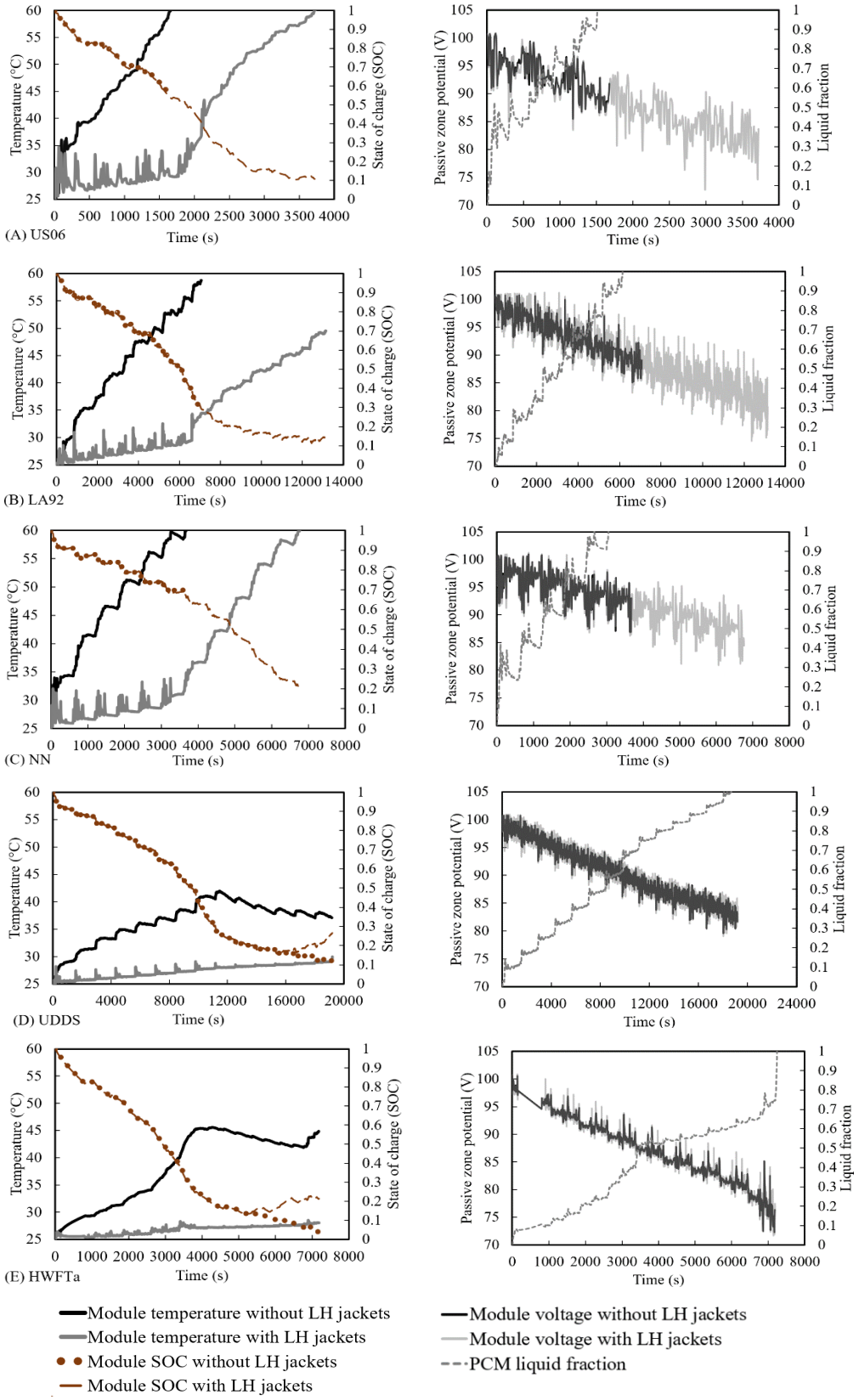

Fig. 6.12 Case 1 (24S) Temperature (°C) versus Time (s) analysis of Cases without LH jackets compared with LH jackets during different drive cycling modes.

Furthermore, the battery module temperature with the proposed LH jackets was kept well below 30 °C throughout the cycling and was deemed sufficient to maintain the thermal performance for longer. Compared to the more aggressive drive cycles, however, the liquid fraction continued to rise towards the end of the cycling. This meant that the volume of LH was just enough to support the data before the temperature rise would be seen in the case without LH jackets. As seen for all the cases with LH jackets, before the liquid fraction was at 1, the module temperature did not rise higher than 35 °C and represents an optimum working temperature for the modules assessed. Only when the LH was consumed and SH was prevalent, did the temperature increase follow the same characteristics as in the cases without passive cooling.

Moreover, Figure 6.13 shows the results of different drive cycles on the performance of Case 2 (2P12S). As can be concluded from this figure, regardless of the change in the arrangement of the cells, which would have a different capacity and voltage (see Table 6.1), the LH jackets enhanced the battery module thermal performance and the efficiency of the system. The same results were captured in the previous section 6.3.4.1 as well.

Concerning the most aggressive driving cycle, US06 (shown in Figure 6.13 (A)), there was approximately 200 % improvement in the useful life with the remaining 80 % of the SOC in the presence of the LH jackets as opposed to the lack of those jackets. Indeed, the Cases with and without LH jackets reached the temperature safety limit within the 1970s and 990s, respectively. When compared with Case 1 (24S), the time to reach 60 °C was shortened by 165 % (Case 1: 1640s; Case 2: 990s) which was attributed to the change in arrangement of the module to include parallel cells with double the nominal capacity (see Table 6.1). This meant that increased current was discharged from the module during the same total time to discharge (within 1 hour) and hence, an increase in overall module temperature was seen. The passive zone potential saw an increase in cycling time as seen in the passive zone potential curves with the liquid fraction shown at 1 in 1500s. Beyond this point (1500s), the module temperature rose in the same gradient as with the case with LH jackets like the case without LH jackets.

Comparable results were captured for the harsh drive cycles LA92 (shown in Figure 6.13 (B)) and NN (shown in Figure 6.13 (C)) as well, where under those drive cycles approximately 200 % extension in useful life of the module with introduced passive cooling (LA92: 12197s at 55 °C and NN: 5513s at 60 °C) compared to the module without LH jackets (LA92: 6170s at 60 °C and NN: 2580s at 60 °C). For Case 2, the maximum and minimum voltages for passive zone potentials were between maximum 50 V and minimum 30 V, respectively. Likewise, the liquid fraction followed the same gradient as the modules without the LH jackets.

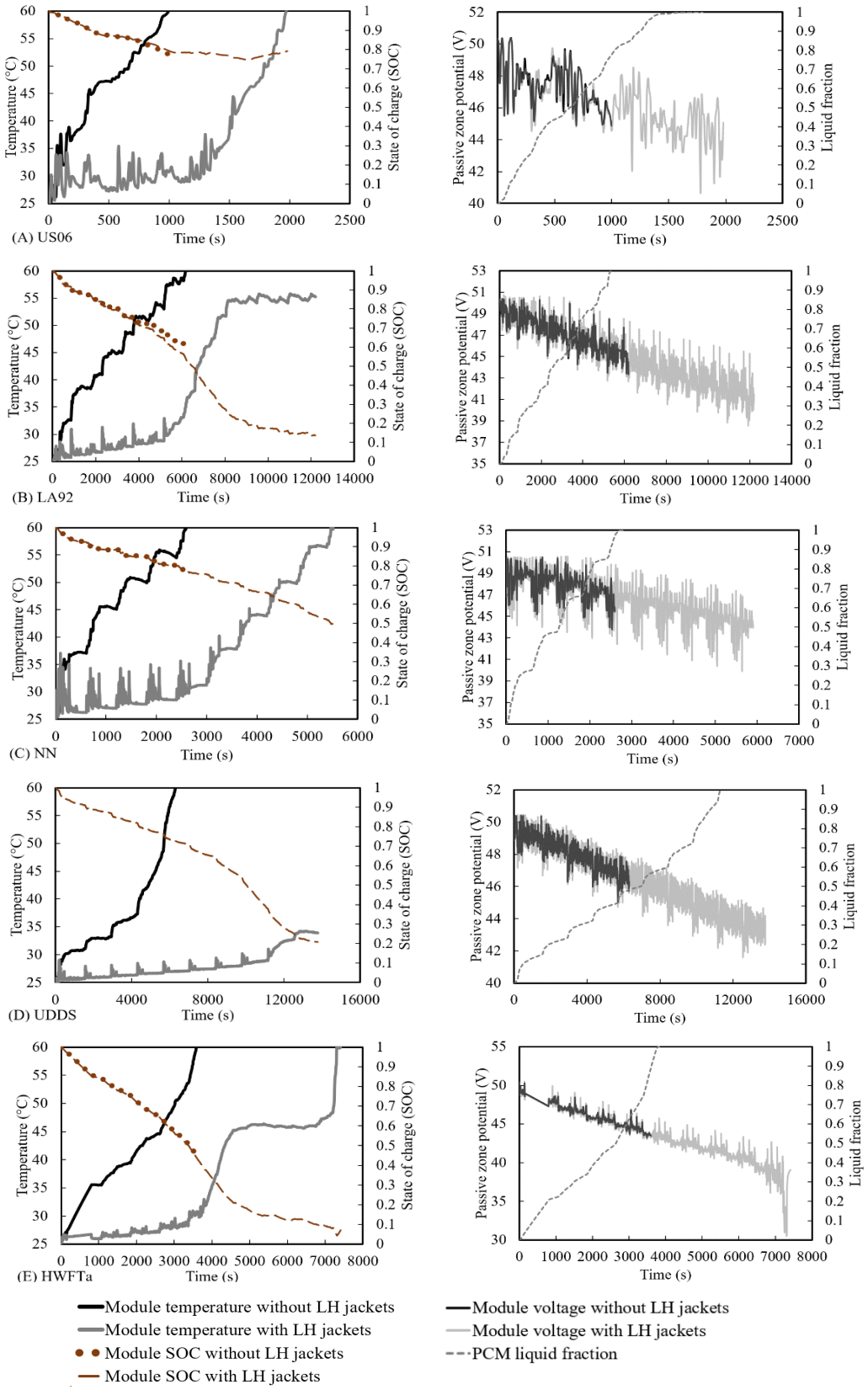

Fig. 6.13 Performance behaviour of Case 2 (2P12S module) in the presence and absence of LH jacket under different drive cycles.

Results illustrated, that compared to the casual drive cycles, UDDS (shown in Figure 6.13 (D)) and HWFTa (shown in Figure 6.13 (E)), displayed 218 % and 203 % extension in useful life, respectively, when the LH jackets were introduced (UDDS: 13752s at 34 °C and HWFTa: 7300s at 60 °C) as opposed to without (UDDS: 6270s at 60 °C and HWFTa: 3580s at 60 °C). At the completion of the cycle or the safety limit reached, shown by the SOC and the passive zone potential, indeed, only the UDDS drive cycle with LH jackets remained below 35 °C. For both Case 1 and Case 2, while LH was still available, the battery modules were maintained below 35 °C - 40 °C and only rose sharply when the LH was depleted.

Finally, the performance results of the third Case (3P8S) under various drive loads are displayed in Figure 6.14. As shown in this figure, the LH jackets improved the thermal performance of the module for all drive cycles which were displayed in the temperature profiles. Distinctly, the battery module temperature without LH jackets were discharged to the safety limit of 60 °C in less time than it took for Case 2, and then Case 1. This was because of the increased current in the module due to the parallel arrangement of cells. This was also conferred from the lowered passive zone potentials, which cycled between the maximum of 34 V to minimum of 27 V. In this test Case as well, there was an intensification in the haphazard nature of the module temperature rise compared to the other Cases (24S and 2P12S), but when the LH jackets were employed, greater thermal stability was also attained by the module.

The most aggressive drive cycle, US06 (shown in Figure 6.14 (A)) had a significant effect on Case 3, with up to 580 % increase in battery useful life in presence of LH jackets compared to their absences. The corresponding time as shown by the temperature profiles were 310s without LH jackets and 1820s with LH jackets at 60 °C. Correspondingly, results from the other aggressive cycles, LA92 (shown in Figure 6.14 (B)) and NN (shown in Figure 6.14 (C)) had 146 % and 400 % increase in thermal performance enhancements with LH jacket cooling (LA92: 3370s at 60 °C and NN: 5230s at 58 °C) in contrast without (LA92: 2310s at 60 °C and NN: 1280s at 58 °C). The life extension was illustrated similarly for the passive zone potential profiles. The liquid fraction increased in a comparable way to the battery module temperature without LH jackets and the absorption of heat was directly captured and illustrated. Beyond consumption of the LH, the temperature sharply increased by SH.

For the casual drive cycles, UDDS (shown in Figure 6.14 (D)) and HWFTa (shown in Figure 6.14 (E)), improvements in thermal performance of 289 % and 197 %, respectively in the presence of LH jackets were illustrated in contrast to the cases without LH jackets. The time shown in the results of the temperature profiles at 60 °C were at 2960s and 8570s without and with LH jackets, respectively for UDDS drive cycle, whilst for the HWFTa drive cycle, it was presented as 1870s without LH jackets and 3690s with LH jackets, respectively. The SOC for the modules were all above 50 % but safe

discharge of battery cells was the main priority, so the cycling was ceased once the temperature safety limit was reached. It was found that the effect of different intensities of drive cycles has had a significant effect on the module thermal performance depending on the arrangement of cells. The increased current and lowered voltage including locomotive behaviour can cause an intensification of module temperature to reach safety limits much faster as seen in the results. In comparison of the harshest drive cycle US06 applied to Case 1 without LH jackets, Case 3 module temperature reached the safety temperature limit (60 °C) in 1/5th of the time even though it had 3x the capacity in Ah (see Table 6.1). This was also seen for the transition to the casual drive cycles where the temperature safety limit was not reached in Case 1 but hit in Case 2 and Case 3. This meant that low current modules under causal drive cycles were not severely impacted thermally, however, the opposite was true for high current modules under both aggressive and even casual drive cycles based on the test Cases in this study.

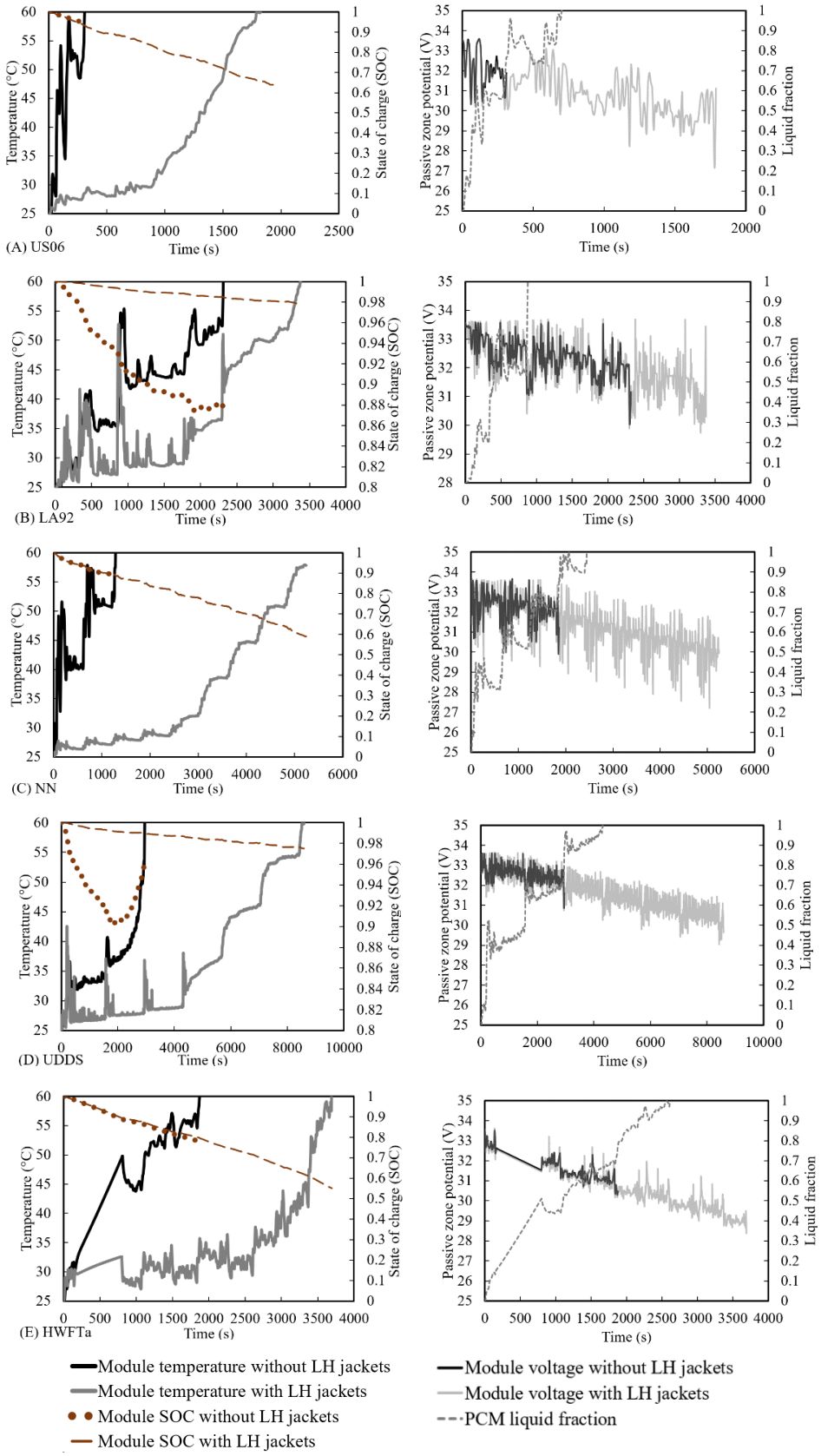

Fig. 6.14 Case 3 (3P8S) Temperature (°C) versus Time (s) analysis of Cases without LH jackets compared with LH jackets during different drive cycling modes.

6.4 Conclusions

In the present study, battery modules with natural cooling LH jackets function as thermal heat sinks to form a BTMS. The 3D thermo-chemical and electrical modelling using the MSMD ECM approach presents energy equations for combined models including PCM and busbars with all the heat energy absorbed by the PCM. Modelling of phase change takes into consideration the mushy zone parameters which are dependent on the temperature. The models for liquid fraction melting and battery cycling were validated from literature results which included numerically and experimentally assessed data with less than 1 % variation in errors. This validated model underwent verification in grid and temporal dependency tests with a 1 % relative error. Scaled models were used to assess different parameters and the effect of thermal performance including ambient temperature, SOC, passive zone potential and liquid fraction. Three models were analysed which involved different arrangements of 24 cells, Li-ion battery modules, which included Case 1 (24S), Case 2 (2P12S) and Case 3 (3P8S) at a constant discharging C-rate of 1 for both continuous battery cycling and under the impact of real-world drive cycles which varied from aggressive to casual. The main conclusions were as follows:

- Regardless of arrangement the module requires a cooling method to be able to disperse the generated heat and reduce overheating from multiple cycling,
- The sharp increase in cell temperature mimicked by the liquid fraction indicated that the heat had been sufficiently absorbed by the LH cooling jackets and successfully functioned as thermal heat sinks and managed the battery module temperature for different arrangements and capacities,
- Introduced natural convection cooling to maintain uniform and stable temperature based on indicated circumferential diameter during continuous and even under drive cycle scenarios,
- During continuous cycling, the BTMS based on LH jackets reduced the maximum module temperature by 20 °C for all Cases assessed,
- The temperature difference between cells was kept below 5 °C for all Cases with LH cooling jackets and indicates improved thermal equilibrium between cells as compared without LH cooling,
- Under all the test drive cycles, the thermal performance was improved with introduced LH jackets resulting on average over 200 % extension in useful battery life.

6.5 Chapter Summary

This research Chapter investigated the impact of passive cooling for BTMS for various configurations of module levels under continuous discharging/charging cycles as well as haphazard variations of real-world automotive drive cycles. The thermal and electrical performance of the modules for different configurations were analysed based on results of Power, temperature, SOC, and liquid fraction. The results of introduced LH jackets around each cell in the modules showed an increase in thermal efficiency regardless of the configurations. These configurations can be adapted based on the power requirements for the module/pack so selected scaled models were chosen for a specific number of cells analysed. It was shown that the configurations with the LH jackets maintained stable and uniform temperature distribution for longer even minimising the temperature difference between cells in the module under both continuous charging/discharging and under real-world automotive drive cycling. This Chapter evaluated the module level analysis for battery thermal management using passive cooling as part of the objectives of this research. It should be noted that this Chapter is currently under review as it was submitted for publication. The following Chapter 7 provides the conclusions and recommendations derived from each of the study chapters including the key points covered as well as potential research particular to this thesis and beyond.

CHAPTER 7: CONCLUSION and RECOMMENDATIONS

7.1 Conclusions

In this doctoral research, the impact of corrugated fins on a longitudinally and transversally arranged horizontal DPHX was thoroughly analysed in **Chapter 3**. The study involved numerical exploration across five different cases involving charging and discharging processes with N-eicosane PCM in the concentric LHS system. The results demonstrated notable similarities between the observed data and predicted numerical information from literature, indicating minor deviations for total melting time. Conduction was the primary mode of heat transfer during melting, succeeded by convection after a specific duration of PCM liquefaction. Notably, heat transfer occurred more readily in the top half of the PCM during charging while melting occurred at a slower pace at the bottom. The research observed that the transversal corrugated fins displayed the fastest melting rate, exhibiting an 88 % reduction in overall melting time compared to the unfinned case, thus presenting a substantial enhancement in heat transfer. While there was no significant improvement in heat transfer for the longitudinal fin cases, the transversal corrugated fin illustrated a 27 % improvement due to the same cross-sectional area.

Moreover, **Chapter 4** analysed the effects of the Li-ion cylindrical battery cell coupled with LHS PCM, extensively analysed across diverse ambient weather conditions, including extreme temperature ranging from -20 °C to 55 °C. Variations in circumferential PCM thickness, mesh, time-step, and mushy zone analyses were performed. The outcomes indicated excellent agreement, with minimal deviation from literature and effective battery thermal performance enhancement with the introduced PCM. Under regular ambient weather (25 °C), the PCM showcased a 20 % extension of thermal performance after a single discharge, maintaining stable temperature for multiple cycles, achieving a total extension of 3.4x times. However, variations in ambient temperature above 25 °C unveiled limitations in the effectiveness of the chosen PCM. Temperatures exceeding the PCM melting point resulted in a shift from LHS to SHS, with temperature linearly increasing beyond the defined limits. For higher temperature of 40 °C and 55 °C, appropriate PCMs initially sustained constant battery temperature within optimal values, but extreme conditions such as 55 °C led to a single discharge cycle from reaching the cut-off limit. Nonetheless, a substantial 80 % improvement in thermal performance was observed. Additionally, lower temperature (0 °C and -20 °C) with PCM showcased consistent thermal stability across multiple discharge cycles. These findings underscored the critical importance of selecting the most suitable PCM based on the thermal properties and environmental conditions. Once identified, this combined PCM-battery model could sustain optimum operating conditions for prolonged periods, holding promise for applications requiring robust and stable battery performance. In conclusion, this comprehensive investigation provides an in-depth understanding of the Li-ion

cylindrical battery cell coupled with LHS PCM under varying environmental conditions. While the chosen PCM demonstrated substantial enhancement in thermal performance under standard ambient temperatures, limitations were evident in extreme weather scenarios, particularly above the 25 °C melting point of the PCM. However, judicious selection of appropriate PCM types for varying weather conditions enabled the model to maintain constant battery temperature within optimal ranges for numerous cycles. This offers valuable insights into enhancing battery thermal management systems for diverse weather conditions.

Furthermore, the research **Chapter 5** extensively investigated the influence of a PCM-jacketed 18650 Li-ion cylindrical battery cell under real-world automotive drive cycles. Using a validated numerical model, the study assessed the effectiveness of a Latent Heat (LH) jacket in regulating the cell's thermal and electrical performance across various driving conditions. Employing a combined thermo-chemical and electrical model, the study analysed power, temperature, State of Charge (SOC), and liquid fraction. Results consistently demonstrated improved thermal management and extended battery life when the LH jacket was employed across all the drive cycles assessed. Moreover, the research delved into the impact of different cycle such as US06, UDDS, HWFTa and b, LA92 and NN, on the performance of a single 18650 battery cell, with and without the LH jacket. Leveraging on accurate multi-scale, multi-domain (MSMD) electrochemical model (ECM), the study accurately portrayed the battery cell's electrical parameters under real-world driving cycles at an ambient temperature of 25 °C. The model's validation aligned precisely with safety limits recommended by manufacturers. The combined thermo-chemical and electrical model highlighted the necessity for effective thermal management strategies, particularly in demanding driving scenarios. Integration of the LH jacket notably extended the battery's optimal operating temperature range, reducing temperature by up to 52 % and significantly increasing battery life during intense driving cycles. The jacket ensured stable and uniform battery temperature across most cycles, especially for UDDS and HWFTa and b, effectively minimising temperature variations. However, in US06, LA92 and NN drive cycles, minor temperature divergence below 5 °C persisted. This research chapter serves as an essential starting point for future exploration, especially at modular level, aiming to integrate Thermal Energy Storage (TES) with Electrical Energy Storage (EES), offering critical insights into thermal management techniques for varying automotive drive cycles.

Finally, research **Chapter 6** explored the influence of passive cooling on BTMS by analysing various module configurations under continuous charging and discharging cycles, along with diverse real-world automotive drive cycles as described in Chapter 5. The investigation focussed on assessing the thermal and electrical performance of these modules, considering power output, temperature regulation, SOC, and liquid fraction. The addition of LH jackets around the cells consistently displayed

enhanced thermal efficiency across the different module configurations, catering to diverse power demands by scaling the models for specific cell quantities. The LH jackets effectively maintained stable and uniform temperature distribution, reducing temperature variations between cells during continuous cycling and real-world driving scenarios. This research evaluated the BTMS using passive natural convection cooling LH jackets as efficient thermal heat sinks. The methodology includes the comprehensive 3D thermo-chemical and electrical model MSMD ECM validated through literature comparisons with minimal errors. Several key findings showed the following:

- regardless of the module configurations, effective cooling methods are crucial to disperse the heat and prevent overheating during repeated cycling,
- rise in cell temperature, illustrated with liquid fraction , indicated successful heat absorption by LH cooling jackets, effectively managing temperature across varied arrangements and capacities,
- natural convection cooling maintained stable temperature, ensuring thermal equilibrium during continuous cycling and various drive cycle simulations,
- the LH jackets reduced the module temperature by 20 °C for all configurations during continuous cycling,
- the temperature difference between the cells was consistently under 5 °C when LH cooling was employed, signifying improved thermal balance among cells,
- under all tested drive cycles, the utilisation of the LH jackets led to a substantial increase in the battery's useful life by over 200 °C.

In conclusion, this research demonstrates the efficacy of LH cooling jackets in mitigating overheating and stabilising the temperature within battery modules under continuous cycling and diverse real-world drive conditions.

7.2 Recommendations for future work

From Chapter 3:

1. **Exploration of fin configurations**: Further studies could experiment with increased number of transversal corrugated fins within battery modules, this exploration can examine how variations in fin quantity impact the heat transfer efficiency within the battery system. Analysing diverse fin quantities and configurations, particularly in transversal orientations, can unveil optimal structures that improve thermal regulation. This may not be limited to the type of fin used in this work, but new designs can be explored including materials, shape, and optimisation for reduced melting time in passive cooling applications.
2. **Optimisation of fin angles**: Investigating the impact of fin angles on heat dissipation within the battery system could offer valuable insights. By varying the angles of the fins in the study, the research could discern the optimal fin configuration that can maximise the convective heat transfer and enhance the overall thermal performance of the system.
3. **PCM selection and fin materials**: Examining the suitability of different PCMs and fin materials, with exploration into new PCM material specific to the most suitable characteristics and thermo-physical properties can be a way forward for effective battery thermal management. Exploring a range of PCM properties and varied enhanced conductive materials, with a consideration towards heat storage and dissipation characteristics, can determine the most effective combinations for improved thermal performance.
4. **Study on PCM conduction and convective heat transfer**: Conducting in-depth investigations into PCM's conductive and convective heat transfer processes can provide essential understanding for renewable energy storage devices that necessitate fast charging and extended discharging. Detailed studies on how PCMs manage heat conduction and convection during charge and discharge cycles would be instrumental in refining the performance of BTMS, ensuring optimal energy storage under different operating conditions.

From Chapter 4:

1. **PCM material development**: Investigating novel PCM formulations or composite materials which can exhibit adaptive phase change properties can be an area of exploration. By developing PCMs capable of transitioning through phase changes at specific temperature

thresholds while accommodating a broader temperature range, can be a viable option to tailor passive cooling effectiveness to the application.

2. **Temperature-specific PCM formulations**: Research into phase transition temperature thresholds by designing/formulating materials that can facilitate gradual transition through multiple phases over a wide range of temperatures can be crucial in adapting to various environmental conditions without losing the efficacy of thermal regulation.
3. **Modular and tailored PCM solutions**: Research focusing on modular PCM systems can present adaptable solutions for customised container shapes even specific to temperature conditions in different environments. Circular jackets were studied but an adaption to this shape based on application can be explored, especially for different battery geometries.
4. **Thermal stability and longevity**: Investigating the long-term stability and durability of these PCMs is fundamental. Ensuring that they can maintain their thermal characteristics and phase transition over numerous charging and discharging cycles, along with exposure to extreme conditions can be valuable to real-world applications.
5. **Environmental and cost considerations**: Analysing the environmental impact and cost-effectiveness of passive cooling technology compared to other methods including active cooling and hybrid systems is essential for scalability and practicality. The environmental footprint, recyclability, and cost-effectiveness ensure their feasibility for widespread deployment across battery technologies.

From Chapter 5:

1. **Refining PCMs/passive cooling methods and battery systems**: Exploring various PCM configurations, compositions, and their interaction with battery systems including different types of battery types based on applications. Different passive cooling methods including hybrids, altering the PCM materials for improvement or reduction in thermal conductivity, structural designs, and placement around the battery cells can be studied to maximise heat absorption capacity and thermal performance.
2. **Thermal variations in drive cycle dynamics**: Research can be used to address a more comprehensive understanding of drive cycle dynamics on battery temperature fluctuations even at different ambient weather conditions. Optimisation of PCM volume and size can also be an area of research.
3. **Intelligent thermal management systems**: The development of intelligent thermal management systems which can dynamically adjust based on the specific drive cycle conditions can be studied and implemented. This can include even variations of PCM for a combined PCM

system with use of smart control systems. This can involve real-time adjustments to enhance the battery's thermal conditions during diverse driving scenarios, improving performance and longevity.

From Chapter 6:

1. **Refinement in PCM integration**: Fine-tuning the integration with battery module/pack systems with passive cooling PCMs can include refinement into enhancing distribution, volume, or type of PCM used to ensure that it effectively maintains temperature under various conditions. Additionally, studies on the efficiency of different PCM materials or combinations can enhance the adaptability and heat absorption capabilities of these systems.
2. **Exploration of varied environmental conditions**: Investigation of wider environmental and drive cycle conditions would be beneficial. Analysing different extreme weather conditions, variable drive cycles, and unexpected temperature changes can provide a more comprehensive understanding of how the battery system equipped with LH cooling jackets behaves in different scenarios.
3. **Development of adaptive thermal management strategies**: The creation of intelligent thermal management systems capable of adapting to changing conditions can significantly improve battery efficiency. A focus on designing systems which can adjust to PCM configurations, circulation, or heat absorption levels in response to real-time environmental or operational changes. Adaptive strategies which can self-optimise in diverse scenarios will be pivotal for robust battery performance.
4. **Real-time monitoring and control:** Research which integrates smart monitoring and control systems into the thermal management of batteries could further enhance performance. Investigating sensor technologies and feedback mechanisms that enable real-time monitoring and adjustment of PCM systems would contribute to proactive and precise thermal management, preventing overheating and maximising the battery life span.
5. **Integration with AI and Machine Learning:** Exploring the integration of artificial intelligence (AI) and machine learning (ML) algorithms in thermal management systems can pave the way for more intelligent, predictive, and self-learning battery management. Developing algorithms that learn from past behaviours and make proactive adjustments to enhance thermal performance under varying conditions could be a remarkable direction for future studies.

REFERENCES

A.R., Anbumalar, S., A.F. and , P.K. (2015) *Computational Fluid Analysis of Lithium-Ion Battery Using ANSYS Fluent*.

Abada, S., Marlair, G., Lecocq, A., Petit, M., Sauvant-Moynot, V. and Huet, F. (2016) 'Safety focused modelling of lithium-ion batteries: A review', *Journal of Power Sources,* 306, pp. 178-192 Available at: 10.1016/j.jpowsour.2015.11.100.

Abbas, S., Ramadan, Z., and Park, C.W. (2021) 'Thermal performance analysis of compact-type simulative battery module with paraffin as phase-change material and flat plate heat pipe', *International journal of heat and mass transfer,* 173, pp. 1 Available at: 10.1016/j.ijheatmasstransfer.2021.121269.

Abdulateef, A.M., Abdulateef, J., Al-Abidi, A.A., Sopian, K., Mat, S. and Mahdi, M.S. (2019) 'A combination of fins-nanoparticle for enhancing the discharging of phase-change material used for liquid desiccant air conditioning unite', *Journal of energy storage,* 24, pp. 100784 Available at: 10.1016/j.est.2019.100784.

Abdulateef, A.M., Abdulateef, J., Sopian, K., Mat, S. and Ibrahim, A. (2019) 'Optimal fin parameters used for enhancing the melting and solidification of phase-change material in a heat exchanger unite', *Case studies in thermal engineering,* 14, pp. 100487 Available at: 10.1016/j.csite.2019.100487.

Abdulateef, A.M., Jaszczur, M., Hassan, Q., Anish, R., Niyas, H., Sopian, K. and Abdulateef, J. (2021) 'Enhancing the melting of phase change material using a fins–nanoparticle combination in a triplex tube heat exchanger', *Journal of energy storage,* 35, pp. 102227 Available at: 10.1016/j.est.2020.102227.

Abdulateef, A.M., Mat, S., Sopian, K., Abdulateef, J. and Gitan, A.A. (2017) 'Experimental and computational study of melting phase-change material in a triplex tube heat exchanger with longitudinal/triangular fins', *Solar energy,* 155, pp. 142-153 Available at: 10.1016/j.solener.2017.06.024.

Abourabia, A. and Moneim, S. (2019) 'Analytical solution of sea water steady magneto-hydrodynamic equations subjected to stretching sheet under induced magnetic field and heat transfer', *Mathematical Modelling of Engineering Problems,* 6(1), pp. 141-151 Available at: 10.18280/mmep.060119.

Abreha, B.G., Mahanta, P. and Trivedi, G. (2020) 'Thermal performance evaluation of multi-tube cylindrical LHS system', *Applied thermal engineering,* 179, pp. 115743 Available at: 10.1016/j.applthermaleng.2020.115743.

Adeniran, A. and Park, S. (2023) 'Optimized cooling and thermal analysis of lithium-ion pouch cell under fast charging cycles for electric vehicles', *Journal of Energy Storage,* 68, pp. 107580 Available at: 10.1016/j.est.2023.107580.

Ahmad, S., Liu, Y., Khan, S.A., Hao, M. and Huang, X. (2023) 'Hybrid battery thermal management by coupling fin intensified phase change material with air cooling', *Journal of Energy Storage,* 64, pp. 107167 Available at: 10.1016/j.est.2023.107167.

Ahmadi, R., Hosseini, M.J., Ranjbar, A.A. and Bahrampoury, R. (2018) 'Phase change in spiral coil heat storage systems', *Sustainable cities and society,* 38, pp. 145-157 Available at: 10.1016/j.scs.2017.12.026.

Akbari, H., Browne, M.C., Ortega, A., Huang, M.J., Hewitt, N.J., Norton, B., and McCormack, S.J. (2019) 'Efficient energy storage technologies for photovoltaic systems', *Solar energy,* 192, pp. 144-168 Available at: 10.1016/j.solener.2018.03.052.

Akula, R. and Balaji, C. (2022) 'Thermal management of 18650 Li-ion battery using novel fins–PCM–EG composite heat sinks', *Applied Energy,* 316, pp. 119048 Available at: 10.1016/j.apenergy.2022.119048.

Al Siyabi, I., Khanna, S., Mallick, T. and Sundaram, S. (2019) 'An experimental and numerical study on the effect of inclination angle of phase change materials thermal energy storage system', *Journal of energy storage,* 23, pp. 57-68 Available at: 10.1016/j.est.2019.03.010.

Al-abidi, A.A., Bin Mat, S., Sopian, K., Sulaiman, M.Y. and Mohammed, A.T. (2013) 'CFD applications for Latent heat thermal energy storage: a review', *Renewable & sustainable energy reviews,* 20, pp. 353-363 Available at: 10.1016/j.rser.2012.11.079.

Al-Abidi, A.A., Mat, S., Sopian, K., Sulaiman, M.Y. and Mohammad, A.T. (2013a) 'Internal and external fin heat transfer enhancement technique for Latent heat thermal energy storage in triplex tube heat exchangers', *Applied thermal engineering,* 53(1), pp. 147-156 Available at: 10.1016/j.applthermaleng.2013.01.011.

Al-Abidi, A.A., Mat, S., Sopian, K., Sulaiman, M.Y. and Mohammad, A.T. (2013b) 'Numerical study of PCM solidification in a triplex tube heat exchanger with internal and external fins', *International journal of heat and mass transfer,* 61, pp. 684-695 Available at: 10.1016/j.ijheatmasstransfer.2013.02.030.

Alami, A.H., Maghrabie, H.M., Abdelkareem, M.A., Sayed, E.T., Yasser, Z., Salameh, T., Rahman, S.M.A., Rezk, H. and Olabi, A.G. (2022) 'Potential applications of phase change materials for batteries' thermal management systems in electric vehicles', *Journal of energy storage,* 54, pp. 105204 Available at: 10.1016/j.est.2022.105204.

Al-Hallaj, S., and Selman, J.R. (2002) 'Thermal modeling of secondary lithium batteries for electric vehicle/hybrid electric vehicle applications', *Journal of Power Sources,* 110(2), pp. 341-348 Available at: https://doi.org/10.1016/S0378-7753(02)00196-9.

Ali, H.M., Ashraf, M.J., Giovannelli, A., Irfan, M., Irshad, T.B., Hamid, H.M., Hassan, F. and Arshad, A. (2018) 'Thermal management of electronics: An experimental analysis of triangular, rectangular and circular pin-fin heat sinks for various PCMs', *International journal of heat and mass transfer,* 123, pp. 272-284 Available at: 10.1016/j.ijheatmasstransfer.2018.02.044.

Alrashdan, A., Mayyas, A.T. and Al-Hallaj, S. (2010) 'Thermo-mechanical behaviors of the expanded graphite-phase change material matrix used for thermal management of Li-ion battery packs', *Journal of Materials Processing Technology,* 210(1), pp. 174-179 Available at: https://doi.org/10.1016/j.jmatprotec.2009.07.011.

Alva, G., Lin, Y. and Fang, G. (2018) 'An overview of thermal energy storage systems', *Energy (Oxford),* 144, pp. 341-378 Available at: 10.1016/j.energy.2017.12.037.

Aly, K.A., El-Lathy, A.R. and Fouad, M.A. (2019) 'Enhancement of solidification rate of Latent heat thermal energy storage using corrugated fins', *Journal of energy storage,* 24, pp. 100785 Available at: 10.1016/j.est.2019.100785.

Al-Zareer, M., Dincer, I. and Rosen, M.A. (2020) 'A thermal performance management system for lithium-ion battery packs', *Applied Thermal Engineering,* 165, pp. 114378 Available at: https://doi.org/10.1016/j.applthermaleng.2019.114378.

Al-Zareer, M., Dincer, I. and Rosen, M.A. (2019) 'Comparative assessment of new liquid-to-vapor type battery cooling systems', *Energy,* 188, pp. 116010 Available at: https://doi.org/10.1016/j.energy.2019.116010.

Al-Zareer, M., Dincer, I. and Rosen, M.A. (2018a) 'Development and evaluation of a new ammonia boiling based battery thermal management system', *Electrochimica Acta,* 280, pp. 340-352 Available at: https://doi.org/10.1016/j.electacta.2018.05.093.

Al-Zareer, M., Dincer, I. and Rosen, M.A. (2018b) 'Heat and mass transfer modeling and assessment of a new battery cooling system', *International Journal of Heat and Mass Transfer,* 126, pp. 765-778 Available at: https://doi.org/10.1016/j.ijheatmasstransfer.2018.04.157.

Al-Zareer, M., Dincer, I. and Rosen, M.A. (2018c) 'A novel phase change based cooling system for prismatic lithium ion batteries', *International Journal of Refrigeration,* 86, pp. 203-217 Available at: https://doi.org/10.1016/j.ijrefrig.2017.12.005.

Al-Zareer, M., Dincer, I. and Rosen, M.A. (2018d) 'Performance assessment of a new hydrogen cooled prismatic battery pack arrangement for hydrogen hybrid electric vehicles', *Energy Conversion and Management,* 173, pp. 303-319 Available at: https://doi.org/10.1016/j.enconman.2018.07.072.

Al-Zareer, M., Dincer, I. and Rosen, M.A. (2017a) 'Electrochemical modeling and performance evaluation of a new ammonia-based battery thermal management system for electric and hybrid electric vehicles', *Electrochimica Acta,* 247, pp. 171-182 Available at: https://doi.org/10.1016/j.electacta.2017.06.162.

Al-Zareer, M., Dincer, I. and Rosen, M.A. (2017b) 'Novel thermal management system using boiling cooling for high-powered lithium-ion battery packs for hybrid electric vehicles', *Journal of Power Sources,* 363, pp. 291-303 Available at: https://doi.org/10.1016/j.jpowsour.2017.07.067.

Amagour, M.E.H., Rachek, A., Bennajah, M. and Ebn Touhami, M. (2018) 'Experimental investigation and comparative performance analysis of a compact finned-tube heat exchanger uniformly filled with a phase change material for thermal energy storage', *Energy conversion and management,* 165, pp. 137-151 Available at: 10.1016/j.enconman.2018.03.041.

Anish, R., Mariappan, V., Hitha, P.S. and Arun, B.S. (2020) 'Accelerated charging of PCM in a horizontal shell and multi-finned tube energy storage system', *Materials today : proceedings,* Available at: 10.1016/j.matpr.2020.08.461.

Arena, S., Casti, E., Gasia, J., Cabeza, L.F. and Cau, G. (2017) 'Numerical simulation of a finned-tube LHTES system: influence of the mushy zone constant on the phase change behaviour', *Energy procedia,* 126, pp. 517-524 Available at: 10.1016/j.egypro.2017.08.237.

Arıcı, M., Tütüncü, E., Yıldız, Ç and Li, D. (2020) 'Enhancement of PCM melting rate via internal fin and nanoparticles', *International journal of heat and mass transfer,* 156, pp. 119845 Available at: 10.1016/j.ijheatmasstransfer.2020.119845.

Arora, S. (2018) 'Selection of thermal management system for modular battery packs of electric vehicles: A review of existing and emerging technologies', *Journal of Power Sources,* 400, pp. 621-640 Available at: https://doi.org/10.1016/j.jpowsour.2018.08.020.

Arun, A., Gupta, C. and Howe, R. (2015) 'Polyether Ether Ketone (PEEK) Fluidic Cell to Study Electrochemistry of Microelectrodes on Silicon Substrate', *ECS solid state letters,* 4(10), pp. P67-P71 Available at: 10.1149/2.0021510ssl.

Baby, R. and Balaji, C. (2014) 'Thermal performance of a PCM heat sink under different heat loads: An experimental study', *International journal of thermal sciences,* 79(79), pp. 240-249 Available at: 10.1016/j.ijthermalsci.2013.12.018.

Bai, F., Chen, M., Song, W., Li, Y., Feng, Z. and Li, Y. (2019) 'Thermal performance of pouch Lithium-ion battery module cooled by phase change materials', *Energy Procedia,* 158, pp. 3682-3689 Available at: 10.1016/j.egypro.2019.01.891.

Bais, A.R., Subhedar, D.G. and Panchal, S. (2022) 'Critical thickness of nano-enhanced RT-42 paraffin based battery thermal management system for electric vehicles: A numerical study', *Journal of Energy Storage,* 52, pp. 104757 Available at: 10.1016/j.est.2022.104757.

Balakrishnan, P.G., Ramesh, R. and Prem Kumar, T. (2006) 'Safety mechanisms in lithium-ion batteries', *Journal of Power Sources,* 155(2), pp. 401-414 Available at: https://doi.org/10.1016/j.jpowsour.2005.12.002.

Bamdezh, M.A. and Molaeimanesh, G.R. (2020) 'Impact of system structure on the performance of a hybrid thermal management system for a Li-ion battery module', *Journal of Power Sources,* 457, pp. 227993 Available at: https://doi.org/10.1016/j.jpowsour.2020.227993.

Bamdezh, M.A., Molaeimanesh, G.R. and Zanganeh, S. (2020) 'Role of foam anisotropy used in the phase-change composite material for the hybrid thermal management system of lithium-ion battery', *Journal of Energy Storage,* 32, pp. 101778 Available at: https://doi.org/10.1016/j.est.2020.101778.

Barai, A., Chouchelamane, G.H., Guo, Y., McGordon, A. and Jennings, P. (2015) 'A study on the impact of lithium-ion cell relaxation on electrochemical impedance spectroscopy', *Journal of Power Sources,* 280, pp. 74-80 Available at: https://doi.org/10.1016/j.jpowsour.2015.01.097.

Bazai, H., Moghimi, M.A., Mohammed, H.I., Babaei-Mahani, R. and Talebizadehsardari, P. (2020) 'Numerical study of circular-elliptical double-pipe thermal energy storage systems', *Journal of energy storage,* 30, pp. 101440 Available at: 10.1016/j.est.2020.101440.

Behi, H., Karimi, D., Behi, M., Ghanbarpour, M., Jaguemont, J., Sokkeh, M.A., Gandoman, F.H., Berecibar, M. and Van Mierlo, J. (2020) 'A new concept of thermal management system in Li-ion battery using air cooling and heat pipe for electric vehicles', *Applied Thermal Engineering,* 174, pp. 115280 Available at: https://doi.org/10.1016/j.applthermaleng.2020.115280.

Bernagozzi, M., Georgoulas, A., Miché, N. and Marengo, M. (2023) 'Heat pipes in battery thermal management systems for electric vehicles: A critical review', *Applied Thermal Engineering,* 219, pp. 119495 Available at: 10.1016/j.applthermaleng.2022.119495.

Bhavsar, S., Kant, K. and Pitchumani, R. (2023) 'Robust model-predictive thermal control of lithium-ion batteries under drive cycle uncertainty', *Journal of power sources,* 557, pp. 232496 Available at: 10.1016/j.jpowsour.2022.232496.

Biswas, J., Malzone, P.Q. and Rößler, F. (2021) 'Energy storage selection and operation for night-time survival of small lunar surface systems', *Acta Astronautica,* 185, pp. 308-318 Available at: https://doi.org/10.1016/j.actaastro.2021.04.042.

Biwole, P.H., Groulx, D., Souayfane, F. and Chiu, T. (2018) 'Influence of fin size and distribution on solid-liquid phase change in a rectangular enclosure', *International journal of thermal sciences,* 124, pp. 433-446 Available at: 10.1016/j.ijthermalsci.2017.10.038.

Bohacek, J., Raudensky, M. and Karimi-Sibaki, E. (2019) 'Polymeric hollow fibers: Uniform temperature of Li-ion cells in battery modules', *Applied Thermal Engineering,* 159, pp. 113940 Available at: https://doi.org/10.1016/j.applthermaleng.2019.113940.

Bohacek, J., Raudensky, M., Kroulikova, T. and Karimi-Sibaki, E. (2019) 'Polymeric hollow fibers: A supercompact cooling of Li-ion cells', *International Journal of Thermal Sciences,* 146, pp. 106060 Available at: https://doi.org/10.1016/j.ijthermalsci.2019.106060.

Broatch, A., Olmeda, P., Margot, X. and Agizza, L. (2022) 'A generalized methodology for lithium-ion cells characterization and lumped electro-thermal modelling', *Applied Thermal Engineering,* 217, pp. 119174 Available at: 10.1016/j.applthermaleng.2022.119174.

Browne, M.C., Norton, B., and McCormack, S.J. (2015) 'Phase change materials for photovoltaic thermal management', *Renewable & sustainable energy reviews,* 47, pp. 762-782 Available at: 10.1016/j.rser.2015.03.050.

Browne, M.C., Quigley, D., Hard, H.R., Gilligan, S., Ribeiro, N.C.C., Almeida, N., and McCormack, S.J. (2016) 'Assessing the Thermal Performance of Phase Change Material in a Photovoltaic/Thermal System', *Energy procedia,* 91, pp. 113-121 Available at: 10.1016/j.egypro.2016.06.184.

Budiman, A.C., Kaleg, S., Sudirja, Amin and Hapid, a. (2021) 'Passive thermal management of battery module using paraffin-filled tubes: An experimental investigation', *Engineering Science and Technology, an International Journal,* Available at: https://doi.org/10.1016/j.jestch.2021.06.011.

Cao, J., Ling, Z., Fang, X. and Zhang, Z. (2020a) 'Delayed liquid cooling strategy with phase change material to achieve high temperature uniformity of Li-ion battery under high-rate discharge', *Journal of Power Sources,* 450, pp. 227673 Available at: https://doi.org/10.1016/j.jpowsour.2019.227673.

Cao, J., Ling, Z., Lin, S., He, Y., Fang, X. and Zhang, Z. (2021) 'Thermochemical heat storage system for preventing battery thermal runaway propagation using sodium acetate trihydrate/expanded graphite', *Chemical Engineering Journal,* , pp. 133536 Available at: https://doi.org/10.1016/j.cej.2021.133536.

Cao, J., Luo, M., Fang, X., Ling, Z. and Zhang, Z. (2020b) 'Liquid cooling with phase change materials for cylindrical Li-ion batteries: An experimental and numerical study', *Energy,* 191, pp. 116565 Available at: https://doi.org/10.1016/j.energy.2019.116565.

Cao, X., Yuan, Y., Xiang, B. and Haghighat, F. (2018a) 'Effect of natural convection on melting performance of eccentric horizontal shell and tube Latent heat storage unit', *Sustainable cities and society,* 38, pp. 571-581 Available at: 10.1016/j.scs.2018.01.025.

Cao, X., Yuan, Y., Xiang, B., Sun, L. and Xingxing, Z. (2018b) 'Numerical investigation on optimal number of longitudinal fins in horizontal annular phase change unit at different wall temperatures', *Energy and buildings,* 158, pp. 384-392 Available at: 10.1016/j.enbuild.2017.10.029.

Cen, J. and Jiang, F. (2020) 'Li-ion power battery temperature control by a battery thermal management and vehicle cabin air conditioning integrated system', *Energy for Sustainable Development,* 57, pp. 141-148 Available at: https://doi.org/10.1016/j.esd.2020.06.004.

Cen, J., Li, Z. and Jiang, F. (2018) 'Experimental investigation on using the electric vehicle air conditioning system for lithium-ion battery thermal management', *Energy for Sustainable Development,* 45, pp. 88-95 Available at: https://doi.org/10.1016/j.esd.2018.05.005.

Chacko, S., and Chung, Y.M. (2012) 'Thermal modelling of Li-ion polymer battery for electric vehicle drive cycles', *Journal of Power Sources,* 213, pp. 296-303 Available at: 10.1016/j.jpowsour.2012.04.015.

Chavan, S., Liu, J., Venkateswarlu, B., Joo, S.W. and Kim, S.C. (2023) 'Numerical simulation of lithium-ion battery thermal management systems: A comparison of fluid flow channels and cooling fluids', *Journal of Energy Storage,* 73, pp. 108940 Available at: 10.1016/j.est.2023.108940.

Chen, G., Sun, G., Jiang, D. and Su, Y. (2020) 'Experimental and numerical investigation of the Latent heat thermal storage unit with PCM packing at the inner side of a tube', *International journal of heat and mass transfer,* 152, pp. 119480 Available at: 10.1016/j.ijheatmasstransfer.2020.119480.

Chen, H., Cong, T.N., Yang, W., Tan, C., Li, Y. and Ding, Y. (2009) 'Progress in electrical energy storage system: A critical review', *Progress in Natural Science,* 19(3), pp. 291-312 Available at: 10.1016/j.pnsc.2008.07.014.

Chen, J., Kang, S., E, J., Huang, Z., Wei, K., Zhang, B., Zhu, H., Deng, Y., Zhang, F. and Liao, G. (2019) 'Effects of different phase change material thermal management strategies on the cooling performance of the power lithium ion batteries: A review', *Journal of Power Sources,* 442, pp. 227228 Available at: https://doi.org/10.1016/j.jpowsour.2019.227228.

Chen, K., Chen, Y., She, Y., Song, M., Wang, S. and Chen, L. (2020) 'Construction of effective symmetrical air-cooled system for battery thermal management', *Applied thermal engineering,* 166, pp. 114679 Available at: 10.1016/j.applthermaleng.2019.114679.

Chen, M., and Rincon-Mora, G.A. (2006) 'Accurate electrical battery model capable of predicting runtime and I-V performance', *IEEE transactions on energy conversion,* 21(2), pp. 504-511 Available at: 10.1109/TEC.2006.874229.

Chen, M., Dongxu, O., Liu, J. and Wang, J. (2019) 'Investigation on thermal and fire propagation behaviors of multiple lithium-ion batteries within the package', *Applied Thermal Engineering,* 157, pp. 113750 Available at: https://doi.org/10.1016/j.applthermaleng.2019.113750.

Chen, M., Ouyang, D., Weng, J., Liu, J. and Wang, J. (2019) 'Environmental pressure effects on thermal runaway and fire behaviors of lithium-ion battery with different cathodes and state of charge', *Process Safety and Environmental Protection,* 130, pp. 250-256 Available at: https://doi.org/10.1016/j.psep.2019.08.023.

Chen, X., Yang, W., Shen, J., Xu, X. and Zhou, F. (2023) 'Thermal performance of hybrid battery thermal management system with air cooling and phase change material embedding biomimetic variable section fins', *Applied Thermal Engineering,* 231, pp. 120985 Available at: 10.1016/j.applthermaleng.2023.120985.

Chen, X., Zhou, F., Yang, W., Gui, Y. and Zhang, Y. (2022) 'A hybrid thermal management system with liquid cooling and composite phase change materials containing various expanded graphite contents for cylindrical lithium-ion batteries', *Applied Thermal Engineering,* 200, pp. 117702 Available at: https://doi.org/10.1016/j.applthermaleng.2021.117702.

Chitta, S.D., Akkaldevi, C., Jaidi, J., Panchal, S., Fowler, M. and Fraser, R. (2021) 'Comparison of lumped and 1D electrochemical models for prismatic 20Ah LiFePO4 battery sandwiched between minichannel cold-plates', *Applied Thermal Engineering,* 199, pp. 117586 Available at: https://doi.org/10.1016/j.applthermaleng.2021.117586.

Cho, J., Jeong, S. and Kim, Y. (2015) 'Commercial and research battery technologies for electrical energy storage applications', *Progress in energy and combustion science,* 48, pp. 84-101 Available at: 10.1016/j.pecs.2015.01.002.

Choi, D.H., Lee, J., Hong, H., and Kang, Y.T. (2014) 'Thermal conductivity and heat transfer performance enhancement of phase change materials (PCM) containing carbon additives for heat storage application', *International journal of refrigeration,* 42, pp. 112-120 Available at: 10.1016/j.ijrefrig.2014.02.004.

Choi, D., Shamim, N., Crawford, A., Huang, Q., Vartanian, C.K., Viswanathan, V.V., Paiss, M.D., Alam, M.J.E., Reed, D.M. and Sprenkle, V.L. (2021) 'Li-ion battery technology for grid application', *Journal of Power Sources,* 511, pp. 230419 Available at: https://doi.org/10.1016/j.jpowsour.2021.230419.

Choudhari, V.G., Dhoble, D.A.S. and Sathe, T.M. (2020) 'A review on effect of heat generation and various thermal management systems for lithium ion battery used for electric vehicle', *Journal of Energy Storage,* 32, pp. 101729 Available at: https://doi.org/10.1016/j.est.2020.101729.

Choudhari, V.G., Dhoble, A.S. and Panchal, S. (2020) 'Numerical analysis of different fin structures in phase change material module for battery thermal management system and its optimization', *International journal of heat and mass transfer,* 163, pp. 120434 Available at: 10.1016/j.ijheatmasstransfer.2020.120434.

Cicconi, P., Kumar, P. and Varshney, P. (2020) 'A support approach for the modular design of Li-ion batteries: A test case with PCM', *Journal of energy storage,* 31, pp. 101684 Available at: 10.1016/j.est.2020.101684.

Coman, P.T., Darcy, E.C., Veje, C.T. and White, R.E. (2017) 'Numerical analysis of heat propagation in a battery pack using a novel technology for triggering thermal runaway', *Applied Energy,* 203, pp. 189-200 Available at: https://doi.org/10.1016/j.apenergy.2017.06.033.

Cook, K.A. and Sastry, A.M. (2005) 'An algorithm for selection and design of hybrid power supplies for MEMS with a case study of a micro-gas chromatograph system', *Journal of Power Sources,* 140(1), pp. 181-202 Available at: https://doi.org/10.1016/j.jpowsour.2004.06.071.

Cozzolino, R., Chiappini, D. and Bella, G. (2019) 'Experimental characterisation of a novel thermal energy storage based on open-cell copper foams immersed in organic phase change material', *Energy conversion and management,* 200, pp. 112101 Available at: 10.1016/j.enconman.2019.112101.

Dai, W. and Lai, H. (2024) 'Comparative study of flow-channel layout schemes in liquid cooling plates of a prismatic battery module', *Applied Thermal Engineering,* 236, pp. 121501 Available at: 10.1016/j.applthermaleng.2023.121501.

Dai, X., Kong, D., Du, J., Zhang, Y. and Ping, P. (2021) 'Investigation on effect of phase change material on the thermal runaway of lithium-ion battery and exploration of flame retardancy improvement', *Process Safety and Environmental Protection,* Available at: https://doi.org/10.1016/j.psep.2021.12.051.

Darzi, A.R., Farhadi, M. and Sedighi, K. (2012) 'Numerical study of melting inside concentric and eccentric horizontal annulus', *Applied mathematical modelling,* 36(9), pp. 4080-4086 Available at: 10.1016/j.apm.2011.11.033.

De Césaro Oliveski, R., Becker, F., Rocha, L.A.O., Biserni, C. and Eberhardt, G.E.S. (2021) 'Design of fin structures for phase change material (PCM) melting process in rectangular cavities', *Journal of energy storage,* 35 Available at: 10.1016/j.est.2021.102337.

Debich, B., El Hami, A., Yaich, A., Gafsi, W., Walha, L. and Haddar, M. (2020) 'Design optimization of PCM-based finned heat sinks for mechatronic components: A numerical investigation and parametric study', *Journal of energy storage,* 32, pp. 101960 Available at: 10.1016/j.est.2020.101960.

Delgado, J.M.P.Q., Martinho, J.C., Vaz Sá, A., Guimarães, A.S. and Abrantes, V. (2018) *Thermal Energy Storage with Phase Change Materials.* Cham: Springer International Publishing AG.

Deng, S., Nie, C., Wei, G. and Ye, W. (2019) 'Improving the melting performance of a horizontal shell-tube Latent-heat thermal energy storage unit using local enhanced finned tube', *Energy and buildings,* 183, pp. 161-173 Available at: 10.1016/j.enbuild.2018.11.018.

Dhaidan, N.S., Khodadadi, J.M., Al-Hattab, T.A. and Al-Mashat, S.M. (2013) 'Experimental and numerical investigation of melting of NePCM inside an annular container under a constant heat flux including the effect of eccentricity', *International journal of heat and mass transfer,* 67, pp. 455-468 Available at: 10.1016/j.ijheatmasstransfer.2013.08.002.

Dhumane, R., Ling, J., Aute, V. and Radermacher, R. (2017) 'Portable personal conditioning systems: Transient modeling and system analysis', *Applied Energy,* 208, pp. 390-401 Available at: https://doi.org/10.1016/j.apenergy.2017.10.023.

Diao, Y.H., Liang, L., Zhao, Y.H., Wang, Z.Y. and Bai, F.W. (2019) 'Numerical investigation of the thermal performance enhancement of Latent heat thermal energy storage using longitudinal rectangular fins and flat micro-heat pipe arrays', *Applied energy,* 233-234, pp. 894-905 Available at: 10.1016/j.apenergy.2018.10.024.

Drake, S.J., Martin, M., Wetz, D.A., Ostanek, J.K., Miller, S.P., Heinzel, J.M. and Jain, A. (2015) 'Heat generation rate measurement in a Li-ion cell at large C-rates through temperature and heat flux measurements', *Journal of power sources,* 285, pp. 266-273 Available at: 10.1016/j.jpowsour.2015.03.008.

Du, K., Calautit, J.K., Wang, Z., Wu, Y. and Liu, H. (2018) 'A review of the applications of phase change materials in cooling, heating and power generation in different temperature ranges', *Applied Energy,* 220 Available at: 10.1016/j.apenergy.2018.03.005.

Du, S., Lai, Y., Ai, L., Ai, L., Cheng, Y., Tang, Y. and Jia, M. (2017) 'An investigation of irreversible heat generation in lithium-ion batteries based on a thermo-electrochemical coupling method', *Applied Thermal Engineering,* 121, pp. 501-510 Available at: 10.1016/j.applthermaleng.2017.04.077.

Duan, J., Xiong, Y. and Yang, D. (2020) 'Study on the effect of multiple spiral fins for improved phase change process', *Applied thermal engineering,* 169, pp. 114966 Available at: 10.1016/j.applthermaleng.2020.114966.

E, J., Yi, F., Li, W., Zhang, B., Zuo, H., Wei, K., Chen, J., Zhu, H., Zhu, H. and Deng, Y. (2021) 'Effect analysis on heat dissipation performance enhancement of a lithium-ion-battery pack with heat pipe for central and southern regions in China', *Energy (Oxford),* 226, pp. 120336 Available at: 10.1016/j.energy.2021.120336.

El Idi, M.M., Karkri, M. and Abdou Tankari, M. (2021) 'A passive thermal management system of Li-ion batteries using PCM composites: Experimental and numerical investigations', *International Journal of Heat and Mass Transfer,* 169, pp. 120894 Available at: https://doi.org/10.1016/j.ijheatmasstransfer.2020.120894.

El idi, M., Karkri, M., Abdou Tankari, M. And Vincent, S. (2021) 'Hybrid cooling based battery thermal management using composite phase change materials and forced convection', *Journal of Energy Storage,* 41, pp. 102946 Available at: https://doi.org/10.1016/j.est.2021.102946.

Elsanusi, O.S. and Nsofor, E.C. (2021) 'Melting of multiple PCMs with different arrangements inside a heat exchanger for energy storage', *Applied thermal engineering,* 185 Available at: 10.1016/j.applthermaleng.2020.116046.

Elsayed, A.O. (2018) 'Numerical investigation on PCM melting in triangular cylinders', *Alexandria engineering journal,* 57(4), pp. 2819-2828 Available at: 10.1016/j.aej.2018.01.005.

Elsewify, O., Souri, M., Esfahani, M.N., Hosseinzadeh, E. and Jabbari, M. (2021) 'A new method for internal cooling of a large format lithium-ion battery pouch cell', *Energy,* 225, pp. 120139 Available at: https://doi.org/10.1016/j.energy.2021.120139.

Esapour, M., Hamzehnezhad, A., Rabienataj Darzi, A.A. and Jourabian, M. (2018) 'Melting and solidification of PCM embedded in porous metal foam in horizontal multi-tube heat storage system', *Energy conversion and management,* 171, pp. 398-410 Available at: 10.1016/j.enconman.2018.05.086.

Fadl, M. and Eames, P.C. (2019) 'Numerical investigation of the influence of mushy zone parameter Amush on heat transfer characteristics in vertically and horizontally oriented thermal energy storage systems', *Applied thermal engineering,* 151, pp. 90-99 Available at: 10.1016/j.applthermaleng.2019.01.102.

Fallahi, A., Guldentops, G., Tao, M., Granados-Focil, S. and Van Dessel, S. (2017) 'Review on solid-solid phase change materials for thermal energy storage: Molecular structure and thermal properties', *Applied Thermal Engineering,* 127, pp. 1427-1441 Available at: 10.1016/j.applthermaleng.2017.08.161.

Fan, L., Xiao, Y., Zeng, Y., Fang, X., Wang, X., Xu, X., Yu, Z., Hong, R., Hu, Y. and Cen, K. (2013) 'Effects of melting temperature and the presence of internal fins on the performance of a phase change material (PCM)-based heat sink', *International journal of thermal sciences,* 70, pp. 114-126 Available at: 10.1016/j.ijthermalsci.2013.03.015.

Fan, R., Zheng, N. and Sun, Z. (2021) 'Evaluation of fin intensified phase change material systems for thermal management of Li-ion battery modules', *International journal of heat and mass transfer,* 166, pp. 120753 Available at: 10.1016/j.ijheatmasstransfer.2020.120753.

Fan, X., Meng, C., Yang, Y., Lin, J., Li, W., Zhao, Y., Xie, S. and Jiang, C. (2023) 'Numerical optimization of the cooling effect of a bionic fishbone channel liquid cooling plate for a large prismatic lithium-ion battery pack with high discharge rate', *Journal of Energy Storage,* 72, pp. 108239 Available at: 10.1016/j.est.2023.108239.

Feng, T., Yang, L., Zhao, X., Zhang, H. and Qiang, J. (2015) 'Online identification of lithium-ion battery parameters based on an improved equivalent-circuit model and its implementation on battery state-of-power prediction', *Journal of power sources,* 281, pp. 192-203 Available at: 10.1016/j.jpowsour.2015.01.154.

Fernández Pulido, Y., Blanco, C., Anseán, D., García, V.M., Ferrero, F. and Valledor, M. (2017) 'Determination of suitable parameters for battery analysis by Electrochemical Impedance Spectroscopy', *Measurement: journal of the International Measurement Confederation,* 106, pp. 1-11 Available at: 10.1016/j.measurement.2017.04.022.

Ferreira, H.L., Garde, R., Fulli, G., Kling, W. and Lopes, J.P. (2013) 'Characterisation of electrical energy storage technologies', *Energy (Oxford),* 53, pp. 288-298 Available at: 10.1016/j.energy.2013.02.037.

Galazutdinova, Y., Ushak, S., Farid, M., Al-Hallaj, S. and Grágeda, M. (2021) 'Development of the inorganic composite phase change materials for passive thermal management of Li-ion batteries: Application', *Journal of Power Sources,* 491, pp. 229624 Available at: https://doi.org/10.1016/j.jpowsour.2021.229624.

Gan, Y., He, L., Liang, J., Tan, M., Xiong, T. and Li, Y. (2020) 'A numerical study on the performance of a thermal management system for a battery pack with cylindrical cells based on heat pipes', *Applied Thermal Engineering,* 179, pp. 115740 Available at: https://doi.org/10.1016/j.applthermaleng.2020.115740.

Gan, Y., Wang, J., Liang, J., Huang, Z. and Hu, M. (2020) 'Development of thermal equivalent circuit model of heat pipe-based thermal management system for a battery module with cylindrical cells', *Applied Thermal Engineering,* 164, pp. 114523 Available at: https://doi.org/10.1016/j.applthermaleng.2019.114523.

Gan, Y., Wang, J., Liang, J., Huang, Z. and Hu, M. (2020) 'Development of thermal equivalent circuit model of heat pipe-based thermal management system for a battery module with cylindrical cells', *Applied thermal engineering,* 164, pp. 114523 Available at: 10.1016/j.applthermaleng.2019.114523.

Ganesan, N., Basu, S., Hariharan, K.S., Kolake, S.M., Song, T., Yeo, T., Sohn, D.K. and Doo, S. (2016) 'Physics based modeling of a series parallel battery pack for asymmetry analysis, predictive control and life extension', *Journal of Power Sources,* 322, pp. 57-67 Available at: https://doi.org/10.1016/j.jpowsour.2016.05.005.

Ghadbeigi, L., Day, B., Lundgren, K., and Sparks, T.D. (2018) 'Cold temperature performance of phase change material based battery thermal management systems', *Energy Reports,* 4, pp. 303-307 Available at: https://doi.org/10.1016/j.egyr.2018.04.001.

G-H. Kim (2011) 'Multi-Domain Modeling of Lithium-Ion Batteries Encompassing Multi-Physics in Varied Length Scales. *J. of Electrochemical Soc*. 158 (8). A955-A969.

González, B. and Prieto, M.M. (2021) 'Radiant heating floors with PCM bands for thermal energy storage: A numerical analysis', *International journal of thermal sciences,* 162 Available at: 10.1016/j.ijthermalsci.2020.106803.

Gou, J., Liu, W. and Luo, Y. (2019) 'The thermal performance of a novel internal cooling method for the electric vehicle battery: An experimental study', *Applied thermal engineering,* 161, pp. 114102 Available at: 10.1016/j.applthermaleng.2019.114102.

Goussian, A., LeBel, F., Trovão, J.P. and Boulon, L. (2019) 'Passive hybrid energy storage system based on lithium-ion capacitor for an electric motorcycle', *Journal of Energy Storage,* 25, pp. 100884 Available at: https://doi.org/10.1016/j.est.2019.100884.

Goutam, S., Nikolian, A., Jaguemont, J., Smekens, J., Omar, N., Van Dan Bossche, P. and Van Mierlo, J. (2017) 'Three-dimensional electro-thermal model of Li-ion pouch cell: Analysis and comparison of cell design factors and model assumptions', *Applied thermal engineering,* 126, pp. 796-808 Available at: 10.1016/j.applthermaleng.2017.07.206.

Gozdur, R., Guzowski, B., Dimitrova, Z., Noury, A., Mitukiewicz, G. and Batory, D. (2021) 'An energy balance evaluation in lithium-ion battery module under high temperature operation', *Energy Conversion and Management,* 227, pp. 113565 Available at: https://doi.org/10.1016/j.enconman.2020.113565.

Greco, A., Jiang, X. and Cao, D. (2015) 'An investigation of lithium-ion battery thermal management using paraffin/porous-graphite-matrix composite', *Journal of Power Sources,* 278, pp. 50-68 Available at: 10.1016/j.jpowsour.2014.12.027.

Gulfam, R., Zhang, P. and Meng, Z. (2019) 'Advanced thermal systems driven by paraffin-based phase change materials – A review', *Applied Energy,* 238, pp. 582-611 Available at: 10.1016/j.apenergy.2019.01.114.

Guo, M., Kim, G. and White, R.E. (2013) 'A three-dimensional multi-physics model for a Li-ion battery', *Journal of Power Sources,* 240(15 October 2013), pp. 80-94 Available at: 10.1016/j.jpowsour.2013.03.170.

Guo, R. and Shen, W. (2022) 'A Review of Equivalent Circuit Model Based Online State of Power Estimation for Lithium-Ion Batteries in Electric Vehicles', *Vehicles,* 4(1), pp. 1-31 Available at: 10.3390/vehicles4010001.

Guo, Y., Qiu, Y., Lei, B., Wu, Y., Shi, Y., Cao, W., Liu, H. and Jiang, F. (2023) 'Modeling and analysis of liquid-cooling thermal management of an in-house developed 100 kW/500 kWh energy storage container consisting of lithium-ion batteries retired from electric vehicles', *Applied Thermal Engineering,* 232, pp. 121111 Available at: 10.1016/j.applthermaleng.2023.121111.

Gürtürk, M. and Kok, B. (2020) 'A new approach in the design of heat transfer fin for melting and solidification of PCM', *International journal of heat and mass transfer,* 153, pp. 119671 Available at: 10.1016/j.ijheatmasstransfer.2020.119671.

Hajighafoori Boukani, N., Dadvand, A. and Chamkha, A.J. (2018) 'Melting of a Nano-enhanced Phase Change Material (NePCM) in partially-filled horizontal elliptical capsules with different aspect ratios', *International journal of mechanical sciences,* 149, pp. 164-177 Available at: 10.1016/j.ijmecsci.2018.09.056.

Hajizadeh, M.R., Selimefendigil, F., Muhammad, T., Ramzan, M., Babazadeh, H. and Li, Z. (2020) 'Solidification of PCM with nano powders inside a heat exchanger', *Journal of molecular liquids,* 306, pp. 112892 Available at: 10.1016/j.molliq.2020.112892.

Hajjar, A., Jamesahar, E., Shirivand, H., Ghalambaz, M. and Babaei Mahani, R. (2020) 'Transient phase change heat transfer in a metal foam-phase change material heatsink subject to a pulse heat flux', *Journal of Energy Storage,* 31, pp. 101701 Available at: https://doi.org/10.1016/j.est.2020.101701.

Hameer, S., and van Niekerk, J.L. (2015) 'A review of large-scale electrical energy storage', *International journal of energy research,* 39(9), pp. 1179-1195 Available at: 10.1002/er.3294.

Han, G., Kwon, Y., Kim, J.B., Lee, S., Bae, J., Cho, E., Lee, B.J., Cho, S. and Park, J. (2020) 'Development of a high-energy-density portable/mobile hydrogen energy storage system incorporating an electrolyzer, a metal hydride and a fuel cell', *Applied Energy,* 259, pp. 114175 Available at: https://doi.org/10.1016/j.apenergy.2019.114175.

Hashemzadeh, P., Désilets, M., Lacroix, M. and Jokar, A. (2022) 'Investigation of the P2D and of the modified single-particle models for predicting the nonlinear behavior of Li-ion batteries', *Journal of energy storage,* 52, pp. 104909 Available at: 10.1016/j.est.2022.104909.

He, J., Sazzad Hosen, M., Youssef, R., Kalogiannis, T., Van Mierlo, J. and Berecibar, M. (2023) 'A lumped electro-thermal model for a battery module with a novel hybrid cooling system', *Applied Thermal Engineering,* 221, pp. 119874 Available at: 10.1016/j.applthermaleng.2022.119874.

He, L., Tang, X., Luo, Q., Liao, Y., Luo, X., Liu, J., Ma, L., Dong, D., Gan, Y. and Li, Y. (2022) 'Structure optimization of a heat pipe-cooling battery thermal management system based on fuzzy grey relational analysis', *International Journal of Heat and Mass Transfer,* 182, pp. 121924 Available at: https://doi.org/10.1016/j.ijheatmasstransfer.2021.121924.

Hémery, C., Pra, F., Robin, J. and Marty, P. (2014) 'Experimental performances of a battery thermal management system using a phase change material', *Journal of power sources,* 270, pp. 349-358 Available at: 10.1016/j.jpowsour.2014.07.147.

Heyhat, M.M., Mousavi, S. and Siavashi, M. (2020) 'Battery thermal management with thermal energy storage composites of PCM, metal foam, fin and nanoparticle', *Journal of energy storage,* 28, pp. 101235 Available at: 10.1016/j.est.2020.101235.

Ho, V., Chang, K., Lee, S.W., and Kim, S.H. (2020) 'Transient thermal analysis of a Li-ion battery module for electric cars based on various cooling fan arrangements', *Energies,* 13(9), pp. 2387.

Hofmann, M.H., Czyrka, K., Brand, M.J., Steinhardt, M., Noel, A., Spingler, F.B. and Jossen, A. (2018) 'Dynamics of current distribution within battery cells connected in parallel', *Journal of Energy Storage,* 20, pp. 120-133 Available at: https://doi.org/10.1016/j.est.2018.08.013.

Hosseini, M.J., Ranjbar, A.A., Rahimi, M. and Bahrampoury, R. (2015) 'Experimental and numerical evaluation of longitudinally finned Latent heat thermal storage systems', *Energy and buildings,* 99, pp. 263-272 Available at: 10.1016/j.enbuild.2015.04.045.

Hosseini, M.J., Ranjbar, A.A., Sedighi, K. and Rahimi, M. (2012) 'A combined experimental and computational study on the melting behavior of a medium temperature phase change storage material inside shell and tube heat exchanger', *International communications in heat and mass transfer,* 39(9), pp. 1416-1424 Available at: 10.1016/j.icheatmasstransfer.2012.07.028.

Hosseinizadeh, S.F., Tan, F.L. and Moosania, S.M. (2011) 'Experimental and numerical studies on performance of PCM-based heat sink with different configurations of internal fins', *Applied thermal engineering,* 31(17), pp. 3827-3838 Available at: 10.1016/j.applthermaleng.2011.07.031.

Hosseinzadeh, E., Genieser, R., Worwood, D., Barai, A., Marco, J. and Jennings, P. (2018) 'A systematic approach for electrochemical-thermal modelling of a large format lithium-ion battery for electric vehicle application', *Journal of Power Sources,* 382, pp. 77-94 Available at: 10.1016/j.jpowsour.2018.02.027.

Hosseinzadeh, E., Marco, J. and Jennings, P. (2019) 'Combined electrical and electrochemical-thermal model of parallel connected large format pouch cells', *Journal of Energy Storage,* 22, pp. 194-207 Available at: 10.1016/j.est.2019.02.004.

Hu, C., Li, H., Wang, Y., Hu, X. and Tang, D. (2022) 'Experimental and numerical investigations of lithium-ion battery thermal management using flat heat pipe and phase change material', *Journal of Energy Storage,* 55, pp. 105743 Available at: 10.1016/j.est.2022.105743.

Hu, X., Zheng, Y., Howey, D.A., Perez, H., Foley, A. and Pecht, M. (2020) 'Battery warm-up methodologies at subzero temperatures for automotive applications: Recent advances and perspectives', *Progress in Energy and Combustion Science,* 77, pp. 100806 Available at: https://doi.org/10.1016/j.pecs.2019.100806.

Huang, D., Zhang, H., Wang, X., Huang, X. and Dai, H. (2021) 'Experimental investigations on the performance of mini-channel evaporator refrigeration system for thermal management of power batteries', *International Journal of Refrigeration,* 130, pp. 117-127 Available at: https://doi.org/10.1016/j.ijrefrig.2021.05.038.

Huang, R., Li, Z., Hong, W., Wu, Q. and Yu, X. (2020) 'Experimental and numerical study of PCM thermophysical parameters on lithium-ion battery thermal management', *Energy Reports,* 6, pp. 8-19 Available at: https://doi.org/10.1016/j.egyr.2019.09.060.

Huang, Y., Cheng, W. and Zhao, R. (2019) 'Thermal management of Li-ion battery pack with the application of flexible form-stable composite phase change materials', *Energy Conversion and Management,* 182, pp. 9-20 Available at: https://doi.org/10.1016/j.enconman.2018.12.064.

Huang, Y., Wei, C. and Fang, Y. (2022) 'Numerical investigation on optimal design of battery cooling plate for uneven heat generation conditions in electric vehicles', *Applied thermal engineering,* 211, pp. 118476 Available at: 10.1016/j.applthermaleng.2022.118476.

Hussain, A., Abidi, I.H., Tso, C.Y., Chan, K.C., Luo, Z., and Chao, C.Y.H. (2018) 'Thermal management of lithium ion batteries using graphene coated nickel foam saturated with phase change materials', *International journal of thermal sciences,* 124, pp. 23-35 Available at: 10.1016/j.ijthermalsci.2017.09.019.

Hussain, A., Tso, C.Y. and Chao, C.Y.H. (2016) 'Experimental investigation of a passive thermal management system for high-powered lithium ion batteries using nickel foam-paraffin composite', *Energy (Oxford),* 115, pp. 209-218 Available at: 10.1016/j.energy.2016.09.008.

Hussain, M., Khan, M.K. and Pathak, M. (2023) 'Thermal analysis of phase change material encapsulated Li-ion battery pack using multi-scale multi-dimensional framework', *Journal of Energy Storage,* 65, pp. 107290 Available at: 10.1016/j.est.2023.107290.

Ianniciello, L., Biwolé, P.H. and Achard, P. (2018) 'Electric vehicles batteries thermal management systems employing phase change materials', *Journal of Power Sources,* 378, pp. 383-403 Available at: https://doi.org/10.1016/j.jpowsour.2017.12.071.

Ibrahim, A. and Jiang, F. (2021) 'The electric vehicle energy management: An overview of the energy system and related modeling and simulation', *Renewable and Sustainable Energy Reviews,* 144, pp. 111049 Available at: https://doi.org/10.1016/j.rser.2021.111049.

Ioan Sarbu and Calin Sebarchievici (2018) 'A Comprehensive Review of Thermal Energy Storage', *Sustainability (Basel, Switzerland),* 10(2), pp. 191 Available at: 10.3390/su10010191.

Jaguemont, J., Boulon, L. and Dubé, Y. (2016) 'A comprehensive review of lithium-ion batteries used in hybrid and electric vehicles at cold temperatures', *Applied Energy,* 164, pp. 99-114 Available at: https://doi.org/10.1016/j.apenergy.2015.11.034.

Jaguemont, J. and Van Mierlo, J. (2020) 'A comprehensive review of future thermal management systems for battery-electrified vehicles', *Journal of energy storage,* 31, pp. 101551 Available at: 10.1016/j.est.2020.101551.

Javani, N., Dincer, I., Naterer, G.F. and Yilbas, B.S. (2014a) 'Heat transfer and thermal management with PCMs in a Li-ion battery cell for electric vehicles', *International journal of heat and mass transfer,* 72, pp. 690-703 Available at: 10.1016/j.ijheatmasstransfer.2013.12.076.

Javani, N., Dincer, I., Naterer, G.F. and Rohrauer, G.L. (2014b) 'Modeling of passive thermal management for electric vehicle battery packs with PCM between cells', *Applied thermal engineering,* 73(1), pp. 307-316 Available at: 10.1016/j.applthermaleng.2014.07.037.

Jeon, D.H. (2014) 'Numerical modeling of lithium ion battery for predicting thermal behavior in a cylindrical cell', *Current applied physics,* 14(2), pp. 196-205 Available at: 10.1016/j.cap.2013.11.006.

Ji, C., Wang, B., Wang, S., Pan, S., Wang, D., Qi, P. and Zhang, K. (2019) 'Optimization on uniformity of lithium-ion cylindrical battery module by different arrangement strategy', *Applied Thermal Engineering,* 157, pp. 113683 Available at: https://doi.org/10.1016/j.applthermaleng.2019.04.093.

Jia, X., Zhai, X. and Cheng, X. (2019) 'Thermal performance analysis and optimization of a spherical PCM capsule with pin-fins for cold storage', *Applied thermal engineering,* 148, pp. 929-938 Available at: 10.1016/j.applthermaleng.2018.11.105.

Jiang, D., Liao, Z., Li, P., Yu, G. and Xu, C. (2019) 'The evolution of the mushy zone during the melting process of a binary nitrate salt', *International journal of heat and mass transfer,* 142, pp. 118456 Available at: 10.1016/j.ijheatmasstransfer.2019.118456.

Jiang, J., Li, D. and Dou, R. (2019) 'A lattice Boltzmann modeling and analysis of the thermal convection in a lithium-ion battery', *Computers & Mathematics with Applications,* 77(10), pp. 2695-2706 Available at: https://doi.org/10.1016/j.camwa.2019.01.002.

Jiang, J., Liu, Q., Zhang, C. and Zhang, W. (2014) 'Evaluation of Acceptable Charging Current of Power Li-ion Batteries Based on Polarization Characteristics', *IEEE transactions on industrial electronics (1982),* 61(12), pp. 6844-6851 Available at: 10.1109/TIE.2014.2320219.

Jiang, K., Liao, G., E, J., Zhang, F., Chen, J. and Leng, E. (2020) 'Thermal management technology of power lithium-ion batteries based on the phase transition of materials: A review', *Journal of Energy Storage,* 32, pp. 101816 Available at: 10.1016/j.est.2020.101816.

Jiang, L., Zhang, H., Li, J. and Xia, P. (2019) 'Thermal performance of a cylindrical battery module impregnated with PCM composite based on thermoelectric cooling', *Energy (Oxford),* 188, pp. 116048 Available at: 10.1016/j.energy.2019.116048.

Jilte, R.D., Kumar, R., Ahmadi, M.H. and Chen, L. (2019) 'Battery thermal management system employing phase change material with cell-to-cell air cooling', *Applied Thermal Engineering,* 161, pp. 114199 Available at: https://doi.org/10.1016/j.applthermaleng.2019.114199.

Jilte, R., Afzal, A. and Panchal, S. (2021) 'A novel battery thermal management system using nano-enhanced phase change materials', *Energy (Oxford),* 219 Available at: 10.1016/j.energy.2020.119564.

Jindal, P., Kumar, B.S. and Bhattacharya, J. (2021) 'Coupled electrochemical-abuse-heat-transfer model to predict thermal runaway propagation and mitigation strategy for an EV battery module', *Journal of Energy Storage,* 39, pp. 102619 Available at: https://doi.org/10.1016/j.est.2021.102619.

Jmal, I. and Baccar, M. (2015) 'Numerical study of PCM solidification in a finned tube thermal storage including natural convection', *Applied thermal engineering,* 84, pp. 320-330 Available at: 10.1016/j.applthermaleng.2015.03.065.

Joress, H., Green, M.L., Takeuchi, I., and Hattrick-Simpers, J.R. (2022) 'Applications of High Throughput (Combinatorial) Methodologies to Electronic, Magnetic, Structural, and Energy-Related Materials☆', in Caballero, F.G. (ed.) *Encyclopedia of Materials: Metals and Alloys* Oxford: Elsevier, pp. 353-371.

Joshi, V. and Rathod, M.K. (2019) 'Constructal enhancement of thermal transport in Latent heat storage systems assisted with fins', *International journal of thermal sciences,* 145, pp. 105984 Available at: 10.1016/j.ijthermalsci.2019.105984.

Joshy, N., Hajiyan, M., Siddique, A.R.M., Tasnim, S., Simha, H. and Mahmud, S. (2020) 'Experimental investigation of the effect of vibration on phase change material (PCM) based battery thermal management system', *Journal of Power Sources,* 450, pp. 227717 Available at: https://doi.org/10.1016/j.jpowsour.2020.227717.

Jouhara, H., Żabnieńska-Góra, A., Khordehgah, N., Ahmad, D. and Lipinski, T. (2020) 'Latent thermal energy storage technologies and applications: A review', *International Journal of Thermofluids,* 5-6, pp. 100039 Available at: 10.1016/j.ijft.2020.100039.

Joybari, M.M., Haghighat, F. and Seddegh, S. (2017) 'Natural convection characterization during melting of phase change materials: Development of a simplified front tracking method', *Solar energy,* 158, pp. 711-720 Available at: 10.1016/j.solener.2017.10.031.

Joybari, M.M., Haghighat, F., Seddegh, S. and Yuan, Y. (2019) 'Simultaneous charging and discharging of phase change materials: Development of correlation for liquid fraction', *Solar energy,* 188, pp. 788-798 Available at: 10.1016/j.solener.2019.06.051.

Kadivar, M.R., Moghimi, M.A., Sapin, P. and Markides, C.N. (2019) 'Annulus eccentricity optimisation of a phase-change material (PCM) horizontal double-pipe thermal energy store', *Journal of energy storage,* 26, pp. 101030 Available at: 10.1016/j.est.2019.101030.

Kalapala, L. and Devanuri, J.K. (2021) 'Effect of orientation on thermal performance of a Latent heat storage system equipped with annular fins – An experimental and numerical investigation', *Applied thermal engineering,* 183 Available at: 10.1016/j.applthermaleng.2020.116244.

Kamkari, B. and Shokouhmand, H. (2014) 'Experimental investigation of phase change material melting in rectangular enclosures with horizontal partial fins', *International journal of heat and mass transfer,* 78, pp. 839-851 Available at: 10.1016/j.ijheatmasstransfer.2014.07.056.

Kandukuru, S. and Vohra, M. (2023) *An in-depth review of the battery thermal management system for electric vehicles and evaluation strategies* AIP Publishing.

Kannan, V., Fisher, A. and Birgersson, E. (2021) 'Monte Carlo assisted sensitivity analysis of a Li-ion battery with a phase change material', *Journal of Energy Storage,* 35, pp. 102269 Available at: https://doi.org/10.1016/j.est.2021.102269.

Kansara, K., Singh, V.K., Patel, R., Bhavsar, R.R. and Vora, A.P. (2021) 'Numerical investigations of phase change material under the influence of low gravity environment', *International journal of heat and mass transfer,* 167 Available at: 10.1016/j.ijheatmasstransfer.2020.120811.

Kausthubharam, Koorata, P.K. and Chandrasekaran, N. (2021) 'Numerical investigation of cooling performance of a novel air-cooled thermal management system for cylindrical Li-ion battery module', *Applied Thermal Engineering,* 193, pp. 116961 Available at: 10.1016/j.applthermaleng.2021.116961.

Kazemi, M., Hosseini, M.J., Ranjbar, A.A. and Bahrampoury, R. (2018) 'Improvement of longitudinal fins configuration in Latent heat storage systems', *Renewable energy,* 116, pp. 447-457 Available at: 10.1016/j.renene.2017.10.006.

Kenisarin, M.M., Mahkamov, K., Costa, S.C. and Makhkamova, I. (2020) 'Melting and solidification of PCMs inside a spherical capsule: A critical review', *Journal of energy storage,* 27, pp. 101082 Available at: 10.1016/j.est.2019.101082.

Keshteli, A.N. and Sheikholeslami, M. (2020) 'Influence of Al2O3 nanoparticle and Y-shaped fins on melting and solidification of paraffin', *Journal of molecular liquids,* 314, pp. 113798 Available at: 10.1016/j.molliq.2020.113798.

Khamar, M. and Askari, J. (May 2014) *A charging method for Lithium-ion battery using Min-max optimal control.* IEEE, pp. 1239.

Khan, L.A. and Khan, M.M. (2020) 'Role of orientation of fins in performance enhancement of a Latent thermal energy storage unit', *Applied thermal engineering,* 175, pp. 115408 Available at: 10.1016/j.applthermaleng.2020.115408.

Khateeb, S.A., Farid, M.M., Selman, J.R. and Al-Hallaj, S. (2006) 'Mechanical–electrochemical modeling of Li-ion battery designed for an electric scooter', *Journal of Power Sources,* 158(1), pp. 673-678 Available at: https://doi.org/10.1016/j.jpowsour.2005.09.059.

Khateeb, S.A., Farid, M.M., Selman, J.R. and Al-Hallaj, S. (2004) 'Design and simulation of a lithium-ion battery with a phase change material thermal management system for an electric scooter', *Journal of Power Sources,* 128(2), pp. 292-307 Available at: https://doi.org/10.1016/j.jpowsour.2003.09.070.

Khateeb, S.A., Amiruddin, S., Farid, M., Selman, J.R. and Al-Hallaj, S. (2005) 'Thermal management of Li-ion battery with phase change material for electric scooters: experimental validation', *Journal of power sources,* 142(1), pp. 345-353 Available at: 10.1016/j.jpowsour.2004.09.033.

Khatibi, M., Nemati-Farouji, R., Taheri, A., Kazemian, A., Ma, T. and Niazmand, H. (2021) 'Optimization and performance investigation of the solidification behaviour of nano-enhanced phase change materials in triplex-tube and shell-and-tube energy storage units', *Journal of energy storage,* 33 Available at: 10.1016/j.est.2020.102055.

Kiani, M., Omiddezyani, S., Houshfar, E., Miremadi, S.R., Ashjaee, M. and Mahdavi Nejad, A. (2020) 'Lithium-ion battery thermal management system with Al2O3/AgO/CuO nanofluids and phase change material', *Applied Thermal Engineering,* 180, pp. 115840 Available at: https://doi.org/10.1016/j.applthermaleng.2020.115840.

Kim, J., Oh, J. and Lee, H. (2019) 'Review on battery thermal management system for electric vehicles', *Applied thermal engineering,* 149, pp. 192-212 Available at: 10.1016/j.applthermaleng.2018.12.020.

Kim, U.S., Yi, J., Shin, C.B., Han, T. and Park, S. (2011) 'Modelling the thermal behaviour of a lithium-ion battery during charge', *Journal of Power Sources,* 196(11), pp. 5115-5121 Available at: 10.1016/j.jpowsour.2011.01.103.

Kirad, K. and Chaudhari, M. (2021) 'Design of cell spacing in lithium-ion battery module for improvement in cooling performance of the battery thermal management system', *Journal of Power Sources,* 481, pp. 229016 Available at: https://doi.org/10.1016/j.jpowsour.2020.229016.

Kizilel, R., Lateef, A., Sabbah, R., Farid, M.M., Selman, J.R. and Al-Hallaj, S. (2008) 'Passive control of temperature excursion and uniformity in high-energy Li-ion battery packs at high current and ambient temperature', *Journal of Power Sources,* 183(1), pp. 370-375 Available at: https://doi.org/10.1016/j.jpowsour.2008.04.050.

Klimeš, L., Charvát, P., Mastani Joybari, M., Zálešák, M., Haghighat, F., Panchabikesan, K., El Mankibi, M. and Yuan, Y. (2020) 'Computer modelling and experimental investigation of phase change hysteresis of PCMs: The state-of-the-art review', *Applied Energy,* 263, pp. 114572 Available at: 10.1016/j.apenergy.2020.114572.

KÖK, C. and ALKAYA, A. (2020) 'Investigation of Thermal Behavior of Lithium-Ion Batteries under Different Loads', *European Mechanical Science,* 4(3), pp. 96-102 Available at: 10.26701/ems.635707.

Kollmeyer, P., Hackl, A. and Emadi, A. (Jun 2017) *Li-ion battery model performance for automotive drive cycles with current pulse and EIS parameterization.* IEEE, pp. 486.

Kousha, N., Hosseini, M.J., Aligoodarz, M.R., Pakrouh, R. and Bahrampoury, R. (2017) 'Effect of inclination angle on the performance of a shell and tube heat storage unit – An experimental study', *Applied thermal engineering,* 112, pp. 1497-1509 Available at: 10.1016/j.applthermaleng.2016.10.203.

Kousksou, T., Bruel, P., Jamil, A., El Rhafiki, T. and Zeraouli, Y. (2014) 'Energy storage: Applications and challenges', *Solar energy materials and solar cells,* 120(Part. A), pp. 59-80 Available at: 10.1016/j.solmat.2013.08.015.

Kozak, Y., Abramzon, B. and Ziskind, G. (2013) 'Experimental and numerical investigation of a hybrid PCM–air heat sink', *Applied thermal engineering,* 59(1-2), pp. 142-152 Available at: 10.1016/j.applthermaleng.2013.05.021.

Kshetrimayum, K.S., Yoon, Y., Gye, H. and Lee, C. (2019) 'Preventing heat propagation and thermal runaway in electric vehicle battery modules using integrated PCM and micro-channel plate cooling system', *Applied Thermal Engineering,* 159, pp. 113797 Available at: 10.1016/j.applthermaleng.2019.113797.

Kumar, M., and Krishna, D.J. (2017) 'Influence of Mushy Zone Constant on Thermohydraulics of a PCM', *Energy procedia,* 109, pp. 314-321 Available at: 10.1016/j.egypro.2017.03.074.

Kumar, P., Chaudhary, D., Varshney, P., Varshney, U., Yahya, S.M. and Rafat, Y. (2020) 'Critical review on battery thermal management and role of nanomaterial in heat transfer enhancement for electrical vehicle application', *Journal of Energy Storage,* 32, pp. 102003 Available at: https://doi.org/10.1016/j.est.2020.102003.

Kumaresan, G., Santosh, R., Revanth, H., Raju, G. and Bhattacharyya, S. (2019) 'CFD and Experimental Analysis of Phase Change Material Behaviour Encapsulated in Internally Finned Spherical Capsule', *E3S web of conferences,* 128, pp. 1002 Available at: 10.1051/e3sconf/201912801002.

Kwon, K.H., Shin, C.B., Kang, T.H. and Kim, C. (2006) 'A two-dimensional modelling of a lithium-polymer battery', *Journal of Power Sources,* 163(1), pp. 151-157 Available at: 10.1016/j.jpowsour.2006.03.012.

Lai, Y., Du, S., Ai, L., Ai, L., Cheng, Y., Tang, Y. and Jia, M. (2015) 'Insight into heat generation of lithium-ion batteries based on the electrochemical-thermal model at high discharge rates', *International journal of hydrogen energy,* 40(38), pp. 13039-13049 Available at: 10.1016/j.ijhydene.2015.07.079.

Lamrani, B., Lebrouhi, B.E., Khattari, Y. and Kousksou, T. (2021) 'A simplified thermal model for a lithium-ion battery pack with phase change material thermal management system', *Journal of energy storage,* 44, pp. 103377 Available at: 10.1016/j.est.2021.103377.

Landini, S., Leworthy, J. and O'Donovan, T.S. (2019) 'A Review of Phase Change Materials for the Thermal Management and Isothermalisation of Lithium-Ion Cells', *Journal of Energy Storage,* 25, pp. 100887 Available at: https://doi.org/10.1016/j.est.2019.100887.

Lee, W., Hong, J., Song, J., Yang, W. and Kim, J. (2023) 'Fabrication of high-performance thermally conductive phase change material composites with porous ceramic filler network for efficient thermal management', *Composites Science and Technology,* 240, pp. 110092 Available at: 10.1016/j.compscitech.2023.110092.

Lei, Z., Zhang, Y. and Lei, X. (2018) 'Improving temperature uniformity of a lithium-ion battery by intermittent heating method in cold climate', *International Journal of Heat and Mass Transfer,* 121, pp. 275-281 Available at: https://doi.org/10.1016/j.ijheatmasstransfer.2017.12.159.

Li, C., Ding, Y., Zhou, Z., Jin, Y., Ren, X., Cao, C. and Hu, H. (2023) 'Parameter optimization and sensitivity analysis of a Lithium-ion battery thermal management system integrated with composite phase change material', *Applied thermal engineering,* 228, pp. 120530 Available at: 10.1016/j.applthermaleng.2023.120530.

Li, H., Saini, A., Liu, C., Yang, J., Wang, Y., Yang, T., Pan, C., Chen, L. and Jiang, H. (2021) 'Electrochemical and thermal characteristics of prismatic lithium-ion battery based on a three-dimensional electrochemical-thermal coupled model', *Journal of energy storage,* 42, pp. 102976 Available at: 10.1016/j.est.2021.102976.

Li, J., Cheng, Y., Ai, L., Jia, M., Du, S., Yin, B., Woo, S. and Zhang, H. (2015) '3D simulation on the internal distributed properties of lithium-ion battery with planar tabbed configuration', *Journal of Power Sources,* 293, pp. 993-1005 Available at: 10.1016/j.jpowsour.2015.06.034.

c

Li, T.X., Wu, S., Yan, T., Xu, J.X. and Wang, R.Z. (2016) 'A novel solid–gas thermochemical multilevel sorption thermal battery for cascaded solar thermal energy storage', *Applied Energy,* 161, pp. 1-10 Available at: 10.1016/j.apenergy.2015.09.084.

Li, W.Q., Qu, Z.G., He, Y.L. and Tao, Y.B. (2014) 'Experimental study of a passive thermal management system for high-powered lithium-ion batteries using porous metal foam saturated with phase change materials', *Journal of power sources,* 255, pp. 9-15 Available at: 10.1016/j.jpowsour.2014.01.006.

Li, Z., Niu, H. and Jiang, X. (2017) 'Simulation of electrical abuse of high-power lithium-ion batteries', *Energy Procedia,* 142, pp. 3468-3473 Available at: https://doi.org/10.1016/j.egypro.2017.12.231.

Liang, Z., Wang, R., Malt, A.H., Souri, M., Esfahani, M.N. and Jabbari, M. (2021) 'Systematic evaluation of a flat-heat-pipe-based thermal management: Cell-to-cell variations and battery ageing', *Applied Thermal Engineering,* 192, pp. 116934 Available at: 10.1016/j.applthermaleng.2021.116934.

Lin, C., Xu, S., Chang, G. and Liu, J. (2015) 'Experiment and simulation of a LiFePO4 battery pack with a passive thermal management system using composite phase change material and graphite sheets', *Journal of Power Sources,* 275, pp. 742-749 Available at: https://doi.org/10.1016/j.jpowsour.2014.11.068.

Lin, J., Liu, X., Li, S., Zhang, C. and Yang, S. (2021) 'A review on recent progress, challenges and perspective of battery thermal management system', *International Journal of Heat and Mass Transfer,* 167, pp. 120834 Available at: 10.1016/j.ijheatmasstransfer.2020.120834.

Lin, X., Zhang, X., Ji, J., Liu, L., Wu, Y., Yang, M., Lu, D. and Zheng, H. (2021) 'Development of flexible form-stable phase change material with enhanced electrical resistance for thermal management', *Journal of Cleaner Production,* 311, pp. 127517 Available at: https://doi.org/10.1016/j.jclepro.2021.127517.

Lin, X., Zhang, X., Ji, J., Liu, L., Yang, M. and Zou, L. (2022) 'Experimental investigation of form-stable phase change material with enhanced thermal conductivity and thermal-induced flexibility for thermal management', *Applied Thermal Engineering,* 201, pp. 117762 Available at: https://doi.org/10.1016/j.applthermaleng.2021.117762.

Ling, Z., Cao, J., Zhang, W., Zhang, Z., Fang, X. and Gao, X. (2018) 'Compact liquid cooling strategy with phase change materials for Li-ion batteries optimized using response surface methodology', *Applied Energy,* 228, pp. 777-788 Available at: https://doi.org/10.1016/j.apenergy.2018.06.143.

Ling, Z., Chen, J., Fang, X., Zhang, Z., Xu, T., Gao, X. and Wang, S. (2014) 'Experimental and numerical investigation of the application of phase change materials in a simulative power batteries thermal management system', *Applied Energy,* 121, pp. 104-113 Available at: 10.1016/j.apenergy.2014.01.075.

Ling, Z., Wang, F., Fang, X., Gao, X. and Zhang, Z. (2015) 'A hybrid thermal management system for lithium ion batteries combining phase change materials with forced-air cooling', *Applied Energy,* 148, pp. 403-409 Available at: 10.1016/j.apenergy.2015.03.080.

Ling, Z., Wen, X., Zhang, Z., Fang, X. and Gao, X. (2018) 'Thermal management performance of phase change materials with different thermal conductivities for Li-ion battery packs operated at low temperatures', *Energy,* 144, pp. 977-983 Available at: https://doi.org/10.1016/j.energy.2017.12.098.

Ling, Z., Zhang, Z., Shi, G., Fang, X., Wang, L., Gao, X., Fang, Y., Xu, T., Wang, S. and Liu, X. (2014) 'Review on thermal management systems using phase change materials for electronic components, Li-ion batteries and photovoltaic modules', *Renewable and Sustainable Energy Reviews,* 31, pp. 427-438 Available at: https://doi.org/10.1016/j.rser.2013.12.017.

Liu, H., Sun, K., Shi, X., Yang, H., Dong, H., Kou, Y., Das, P., Wu, Z. and Shi, Q. (2021) 'Two-dimensional materials and their derivatives for high performance phase change materials: emerging trends and challenges', *Energy Storage Materials,* 42, pp. 845-870 Available at: https://doi.org/10.1016/j.ensm.2021.08.022.

Liu, H., Wei, Z., He, W. and Zhao, J. (2017) 'Thermal issues about Li-ion batteries and recent progress in battery thermal management systems: A review', *Energy Conversion and Management,* 150, pp. 304-330 Available at: https://doi.org/10.1016/j.enconman.2017.08.016.

Liu, K., Hu, X., Yang, Z., Xie, Y. and Feng, S. (2019) 'Lithium-ion battery charging management considering economic costs of electrical energy loss and battery degradation', *Energy Conversion and Management,* 195, pp. 167-179 Available at: 10.1016/j.enconman.2019.04.065.

Liu, L., Su, D., Tang, Y. and Fang, G. (2016) 'Thermal conductivity enhancement of phase change materials for thermal energy storage: A review', *Renewable & sustainable energy reviews,* 62, pp. 305-317 Available at: 10.1016/j.rser.2016.04.057.

Liu, M., Saman, W. and Bruno, F. (2012) 'Review on storage materials and thermal performance enhancement techniques for high temperature phase change thermal storage systems', *Renewable & sustainable energy reviews,* 16(4), pp. 2118-2132 Available at: 10.1016/j.rser.2012.01.020.

Liu, S., Peng, H., Hu, Z., Ling, X. and Huang, J. (2019) 'Solidification performance of a Latent heat storage unit with innovative longitudinal triangular fins', *International journal of heat and mass transfer,* 138, pp. 667-676 Available at: 10.1016/j.ijheatmasstransfer.2019.04.121.

Liu, Y., Liao, Y.G. and Lai, M. (Sep 2019) *Temperature Distribution on Lithium-Ion Polymer Battery Cell: Experiment and Modeling.* Piscataway: IEEE, pp. 1.

Liu, Z., Yao, Y. and Wu, H. (2013) 'Numerical modeling for solid–liquid phase change phenomena in porous media: Shell-and-tube type Latent heat thermal energy storage', *Applied energy,* 112, pp. 1222-1232 Available at: 10.1016/j.apenergy.2013.02.022.

Liu, Z., Huang, J., Cao, M., Jiang, G., Yan, Q. and Hu, J. (2021) 'Experimental study on the thermal management of batteries based on the coupling of composite phase change materials and liquid cooling', *Applied thermal engineering,* 185 Available at: 10.1016/j.applthermaleng.2020.116415.

Lu, Z., Yu, X., Wei, L., Qiu, Y., Zhang, L., Meng, X. and Jin, L. (2018) 'Parametric study of forced air cooling strategy for lithium-ion battery pack with staggered arrangement', *Applied Thermal Engineering,* 136, pp. 28-40 Available at: https://doi.org/10.1016/j.applthermaleng.2018.02.080.

Luan, C., Ma, C., Wang, C., Chang, L., Xiao, L., Yu, Z. and Li, H. (2021) 'Influence of the connection topology on the performance of lithium-ion battery pack under cell-to-cell parameters variations', *Journal of Energy Storage,* 41, pp. 102896 Available at: https://doi.org/10.1016/j.est.2021.102896.

Luo, J., Zou, D., Wang, Y., Wang, S. and Huang, L. (2022) 'Battery thermal management systems (BTMs) based on phase change material (PCM): A comprehensive review', *Chemical engineering journal (Lausanne, Switzerland : 1996),* 430, pp. 132741 Available at: 10.1016/j.cej.2021.132741.

Luo, L., Liu, Y., Liao, Z. and Zhong, J. (2023) 'Optimal structure design and heat transfer characteristic analysis of X-type air-cooled battery thermal management system', *Journal of Energy Storage,* 67, pp. 107681 Available at: 10.1016/j.est.2023.107681.

Luo, M., Song, J., Ling, Z., Zhang, Z. and Fang, X. (2021) 'Phase change material coat for battery thermal management with integrated rapid heating and cooling functions from −40 °C to 50 °C', *Materials Today Energy,* 20, pp. 100652 Available at: https://doi.org/10.1016/j.mtener.2021.100652.

Luo, X., Guo, Q., Li, X., Tao, Z., Lei, S., Liu, J., Kang, L., Zheng, D. and Liu, Z. (2020) 'Experimental investigation on a novel phase change material composites coupled with graphite film used for thermal management of lithium-ion batteries', *Renewable Energy,* 145, pp. 2046-2055 Available at: https://doi.org/10.1016/j.renene.2019.07.112.

Luo, X., Wang, J., Dooner, M. and Clarke, J. (2015) 'Overview of current development in electrical energy storage technologies and the application potential in power system operation', *Applied energy,* 137, pp. 511-536 Available at: 10.1016/j.apenergy.2014.09.081.

Lv, Y., Yang, X., Zhang, G. and Li, X. (2019) 'Experimental research on the effective heating strategies for a phase change material based power battery module', *International Journal of Heat and Mass Transfer,* 128, pp. 392-400 Available at: https://doi.org/10.1016/j.ijheatmasstransfer.2018.07.037.

Lyu, C., Song, Y., Yang, D., Wang, W., Zhu, S., Ge, Y. and Wang, L. (2022) 'Surrogate model of liquid cooling system for lithium-ion battery using extreme gradient boosting', *Applied Thermal Engineering,* 213, pp. 118675 Available at: 10.1016/j.applthermaleng.2022.118675.

Ma, S., Jiang, M., Tao, P., Song, C., Wu, J., Wang, J., Deng, T. and Shang, W. (2018) 'Temperature effect and thermal impact in lithium-ion batteries: A review', *Progress in Natural Science: Materials International,* 28(6), pp. 653-666 Available at: https://doi.org/10.1016/j.pnsc.2018.11.002.

Madani, S.S., Ziebert, C. and Marzband, M. (2023) 'Thermal Behavior Modeling of Lithium-Ion Batteries: A Comprehensive Review', *Symmetry (Basel),* 15(8), pp. 1597 Available at: 10.3390/sym15081597.

Maghrabie, H.M., Olabi, A.G., Alami, A.H., Radi, M.A., Zwayyed, F., salamah, T., Wilberforce, T. and Abdelkareem, M.A. (2022) 'Numerical simulation of heat pipes in different applications', *International Journal of Thermofluids,* 16, pp. 100199 Available at: 10.1016/j.ijft.2022.100199.

Magri, L., Sequino, L. and Ferrari, C. (2023) 'Simulating the Electrochemical-Thermal Behavior of a Prismatic Lithium-Ion Battery on the Market under Various Discharge Cycles', *Batteries (Basel),* 9(8), pp. 397 Available at: 10.3390/batteries9080397.

Mahdi, J.M., Lohrasbi, S., Ganji, D.D. and Nsofor, E.C. (2018) 'Accelerated melting of PCM in energy storage systems via novel configuration of fins in the triplex-tube heat exchanger', *International journal of heat and mass transfer,* 124, pp. 663-676 Available at: 10.1016/j.ijheatmasstransfer.2018.03.095.

Mahdi, J.M., Mohammed, H.I., Hashim, E.T., Talebizadehsardari, P. and Nsofor, E.C. (2020) 'Solidification enhancement with multiple PCMs, cascaded metal foam and nanoparticles in the shell-and-tube energy storage system', *Applied energy,* 257, pp. 113993 Available at: 10.1016/j.apenergy.2019.113993.

Mahdi, J.M. and Nsofor, E.C. (2016) 'Solidification of a PCM with nanoparticles in triplex-tube thermal energy storage system', *Applied thermal engineering,* 108, pp. 596-604 Available at: 10.1016/j.applthermaleng.2016.07.130.

Mahdi, M.S., Hasan, A.F., Mahood, H.B., Campbell, A.N., Khadom, A.A., Karim, A.M.A. and Sharif, A.O. (2019) 'Numerical study and experimental validation of the effects of orientation and configuration on melting in a Latent heat thermal storage unit', *Journal of energy storage,* 23, pp. 456-468 Available at: 10.1016/j.est.2019.04.013.

Mahdi, M.S., Mahood, H.B., Mahdi, J.M., Khadom, A.A. and Campbell, A.N. (2020) 'Improved PCM melting in a thermal energy storage system of double-pipe helical-coil tube', *Energy conversion and management,* 203, pp. 112238 Available at: 10.1016/j.enconman.2019.112238.

Mahek, M.K., Alkhedher, M., Ghazal, M., Abdelkareem, M.A., Ramadan, M. and Olabi, A. (2023) 'Effects of control volume outlet variation on axial air cooling of lithium-ion batteries', *International Journal of Thermofluids,* 19, pp. 100373 Available at: 10.1016/j.ijft.2023.100373.

Mahmoud, S., Tang, A., Toh, C., AL-Dadah, R. and Soo, S.L. (2013) 'Experimental investigation of inserts configurations and PCM type on the thermal performance of PCM based heat sinks', *Applied energy,* 112, pp. 1349-1356 Available at: 10.1016/j.apenergy.2013.04.059.

Malik, M., Dincer, I., Rosen, M. and Fowler, M. (2017) 'Experimental Investigation of a New Passive Thermal Management System for a Li-ion Battery Pack Using Phase Change Composite Material', *Electrochimica acta,* 257, pp. 345-355 Available at: 10.1016/j.electacta.2017.10.051.

Malik, M., Dincer, I. and Rosen, M.A. (2016) 'Review on use of phase change materials in battery thermal management for electric and hybrid electric vehicles', *International journal of energy research,* 40(8), pp. 1011-1031 Available at: 10.1002/er.3496.

Mallya, N. and Haussener, S. (2021) 'Buoyancy-driven melting and solidification heat transfer analysis in encapsulated phase change materials', *International journal of heat and mass transfer,* 164 Available at: 10.1016/j.ijheatmasstransfer.2020.120525.

Mao, B., Chen, H., Cui, Z., Wu, T. and Wang, Q. (2018) 'Failure mechanism of the lithium ion battery during nail penetration', *International Journal of Heat and Mass Transfer,* 122, pp. 1103-1115 Available at: https://doi.org/10.1016/j.ijheatmasstransfer.2018.02.036.

Maqbool, Z., Hanief, M. and Parveez, M. (2023) 'Review on performance enhancement of phase change material based heat sinks in conjugation with thermal conductivity enhancers for electronic cooling', *Journal of Energy Storage,* 60, pp. 106591 Available at: 10.1016/j.est.2022.106591.

Marri, G.K., Srikanth, R. and Balaji, C. (2020) 'Effect of phase change and ambient temperatures on the thermal performance of a solid-liquid phase change material based heat sinks', *Journal of energy storage,* 30, pp. 101327 Available at: 10.1016/j.est.2020.101327.

Martínez-Rosas, E., Vasquez-Medrano, R. and Flores-Tlacuahuac, A. (2011) 'Modeling and simulation of lithium-ion batteries', *Computers & chemical engineering,* 35(9), pp. 1937-1948 Available at: 10.1016/j.compchemeng.2011.05.007.

Mashayekhi, M., Houshfar, E. and Ashjaee, M. (2020) 'Development of hybrid cooling method with PCM and Al2O3 nanofluid in aluminium minichannels using heat source model of Li-ion batteries', *Applied Thermal Engineering,* 178, pp. 115543 Available at: https://doi.org/10.1016/j.applthermaleng.2020.115543.

Mastali Majdabadi, M., Farhad, S., Farkhondeh, M., Fraser, R.A. and Fowler, M. (2015) 'Simplified electrochemical multi-particle model for LiFePO4 cathodes in lithium-ion batteries', *Journal of power sources,* 275, pp. 633-643 Available at: 10.1016/j.jpowsour.2014.11.066.

Mastani Joybari, M., Haghighat, F. and Seddegh, S. (2017) 'Numerical investigation of a triplex tube heat exchanger with phase change material: Simultaneous charging and discharging', *Energy and buildings,* 139, pp. 426-438 Available at: 10.1016/j.enbuild.2017.01.034.

Mat, S., Al-Abidi, A.A., Sopian, K., Sulaiman, M.Y. and Mohammad, A.T. (2013) 'Enhance heat transfer for PCM melting in triplex tube with internal–external fins', *Energy conversion and management,* 74, pp. 223-236 Available at: 10.1016/j.enconman.2013.05.003.

Mekrisuh, K.u., Singh, D., and Udayraj (2020) 'Performance analysis of a vertically oriented concentric-tube PCM based thermal energy storage system: Parametric study and correlation development', *Renewable energy,* 149, pp. 902-916 Available at: 10.1016/j.renene.2019.10.074.

Memon, A., Mishra, G., and Gupta, A.K. (2020) 'Buoyancy-driven melting and heat transfer around a horizontal cylinder in square enclosure filled with phase change material', *Applied thermal engineering,* 181, pp. 115990 Available at: 10.1016/j.applthermaleng.2020.115990.

Menale, C., D'Annibale, F., Mazzarotta, B. and Bubbico, R. (2019) 'Thermal management of lithium-ion batteries: An experimental investigation', *Energy (Oxford),* 182, pp. 57-71 Available at: 10.1016/j.energy.2019.06.017.

Mills, A., Farid, M., Selman, J.R. and Al-Hallaj, S. (2006) 'Thermal conductivity enhancement of phase change materials using a graphite matrix', *Applied Thermal Engineering,* 26(14), pp. 1652-1661 Available at: https://doi.org/10.1016/j.applthermaleng.2005.11.022.

Mohaghegh, M.R., Alomair, Y., Alomair, M., Tasnim, S.H., Mahmud, S. and Abdullah, H. (2021) 'Melting of PCM inside a novel encapsulation design for thermal energy storage system', *Energy conversion and management. X,* 11, pp. 100098 Available at: 10.1016/j.ecmx.2021.100098.

Mohamed, S.A., Al-Sulaiman, F.A., Ibrahim, N.I., Zahir, M.H., Al-Ahmed, A., Saidur, R., Yılbaş, B.S. and Sahin, A.Z. (2017) 'A review on current status and challenges of inorganic phase change materials for thermal energy storage systems', *Renewable & sustainable energy reviews,* 70, pp. 1072-1089 Available at: 10.1016/j.rser.2016.12.012.

Mohammed, A.G., Elfeky, K.E. and Wang, Q. (2022a) 'Recent advancement and enhanced battery performance using phase change materials based hybrid battery thermal management for electric vehicles', *Renewable and Sustainable Energy Reviews,* 154, pp. 111759 Available at: 10.1016/j.rser.2021.111759.

Mohammed, A.G., Elfeky, K.E. and Wang, Q. (2022b) 'Recent advancement and enhanced battery performance using phase change materials based hybrid battery thermal management for electric vehicles', *Renewable & sustainable energy reviews,* 154, pp. 111759 Available at: 10.1016/j.rser.2021.111759.

Mokashi, I., Afzal, A., Al-Mdallal, Q., Syam Sundar, L., Khan, S.A., Abdullah, N.A., Azami, M.H. and Saleel, C.A. (2022) 'Effect of non-conjugate and conjugate condition on heat transfer from battery pack', *Alexandria Engineering Journal,* 61(4), pp. 3131-3145 Available at: https://doi.org/10.1016/j.aej.2021.08.042.

Molaeimanesh, G.R., Mousavi-Khoshdel, S.M. and Nemati, A.B. (2020) *Investigation of Temperature Distribution During Dynamic Stress Test on the Surface of Lithium-ion Battery used in an Electric Hybrid Vehicle*.

Mondal, B., Lopez, C.F., Verma, A. and Mukherjee, P.P. (2018) 'Vortex generators for active thermal management in lithium-ion battery systems', *International Journal of Heat and Mass Transfer,* 124, pp. 800-815 Available at: https://doi.org/10.1016/j.ijheatmasstransfer.2018.04.015.

Moradi, R., Kianifar, A. and Wongwises, S. (2017) 'Optimization of a solar air heater with phase change materials: Experimental and numerical study', *Experimental thermal and fluid science,* 89, pp. 41-49 Available at: 10.1016/j.expthermflusci.2017.07.011.

Mousavi G., S.M. and Nikdel, M. (2014) 'Various battery models for various simulation studies and applications', *Renewable and Sustainable Energy Reviews,* 32, pp. 477-485 Available at: 10.1016/j.rser.2014.01.048.

Muenzel, V., Hollenkamp, A.F., Bhatt, A.I., de Hoog, J., Brazil, M., Thomas, D.A. and Mareels, I. (2015) 'A Comparative Testing Study of Commercial 18650-Format Lithium-Ion Battery Cells', *Journal of the Electrochemical Society,* 162(8), pp. A1592-A1600 Available at: 10.1149/2.0721508jes.

Murali, G., Sravya, G.S.N., Jaya, J. and Naga Vamsi, V. (2021) 'A review on hybrid thermal management of battery packs and it's cooling performance by enhanced PCM', *Renewable and Sustainable Energy Reviews,* 150, pp. 111513 Available at: https://doi.org/10.1016/j.rser.2021.111513.

Murugan, M., Saravanan, A., Elumalai, P.V., Murali, G., Dhineshbabu, N.R., Kumar, P. and Afzal, A. (2022) 'Thermal management system of lithium-ion battery packs for electric vehicles: An insight based on bibliometric study', *Journal of Energy Storage,* 52, pp. 104723 Available at: 10.1016/j.est.2022.104723.

Najafi Khaboshan, H., Jaliliantabar, F., Adam Abdullah, A. and Panchal, S. (2023) 'Improving the cooling performance of cylindrical lithium-ion battery using three passive methods in a battery thermal management system', *Applied thermal engineering,* 227, pp. 120320 Available at: 10.1016/j.applthermaleng.2023.120320.

Nasajpour-Esfahani, N., Garmestani, H., Rozati, M. and Smaisim, G.F. (2023) 'The role of phase change materials in lithium-ion batteries: A brief review on current materials, thermal management systems, numerical methods, and experimental models', *Journal of energy storage,* 63, pp. 107061 Available at: 10.1016/j.est.2023.107061.

Nazir, H., Batool, M., Bolivar Osorio, F.J., Isaza-Ruiz, M., Xu, X., Vignarooban, K., Phelan, P., Inamuddin and Kannan, A.M. (2019) 'Recent developments in phase change materials for energy storage applications: A review', *International journal of heat and mass transfer,* 129, pp. 491-523 Available at: 10.1016/j.ijheatmasstransfer.2018.09.126.

Nazzi Ehms, J.H., De Césaro Oliveski, R., Oliveira Rocha, L.A. and Biserni, C. (2018) 'Theoretical and numerical analysis on phase change materials (PCM): A case study of the solidification process of erythritol in spheres', *International journal of heat and mass transfer,* 119, pp. 523-532 Available at: 10.1016/j.ijheatmasstransfer.2017.11.124.

Nemati, H., Moradaghay, M., Moghimi, M.A. and Meyer, J.P. (2020) 'Natural convection heat transfer over horizontal annular elliptical finned tubes', *International communications in heat and mass transfer,* 118, pp. 104823 Available at: 10.1016/j.icheatmasstransfer.2020.104823.

Nemati, H., Moradaghay, M., Shekoohi, S.A., Moghimi, M.A. and Meyer, J.P. (2020) 'Natural convection heat transfer from horizontal annular finned tubes based on modified Rayleigh Number', *International communications in heat and mass transfer,* 110, pp. 104370 Available at: 10.1016/j.icheatmasstransfer.2019.104370.

Nemes, R., Ciornei, S., Ruba, M., Hedesiu, H. and Martis, C. (May 2019) *Modeling and simulation of first-order Li-ion battery cell with experimental validation.* IEEE, pp. 1.

Nicholls, R.A, Moghimi, M.A., and Griffiths, A.L., Can passive cooling be a practical solution for the thermal management of battery in electric vehicles, *Proceedings of the 16th International Conference on Heat Transfer, Fluid Mechanics and Thermodynamics and Editorial Board of Applied Thermal Engineering*, Amsterdam, Netherlands, Accepted, August 2022.

Nicholls, R.A, Moghimi, M.A., and Griffiths, A.L., A comparative study of corrugated fins during melting of phase change material in a double pipe heat exchanger, *Proceedings of the 17th UK International Heat Transfer Conference*, Manchester, United Kingdom, Paper number 116, April 2022. http://cfd.mace.manchester.ac.uk/ukhtc21-proc/papers/O-12-5.pdf.

Nicholls, R.A, Moghimi, M.A., and Griffiths, A.L., Impact of fin type and orientation on performance of phase change material-based double pipe thermal energy storage, *Journal of Energy storage*, 50, 2022, pp 104671. https://doi.org/10.1016/j.est.2022.104671.

Nicholls, R.A., Moghimi, M.A., and Griffiths, A.L. (2024) 'Influence of latent heat based passive cooling on the performance of EV battery under automotive drive cycles', *Journal of Energy Storage,* 77, pp. 109924 https://doi.org/.1016/j.est.2023.109924.

Nie, C., Deng, S. and Liu, J. (2020) 'Effects of fins arrangement and parameters on the consecutive melting and solidification of PCM in a Latent heat storage unit', *Journal of energy storage,* 29, pp. 101319 Available at: 10.1016/j.est.2020.101319.

Nie, P., Zhang, S., Ran, A., Yang, C., Chen, S., Li, Z., Zhang, X., Deng, W., Liu, T., Kang, F. and Wei, G. (2021) 'Full-cycle electrochemical-thermal coupling analysis for commercial lithium-ion batteries', *Applied Thermal Engineering,* 184, pp. 116258 Available at: 10.1016/j.applthermaleng.2020.116258.

Niu, J., Xie, N., Zhong, Y., gao, X., Fang, Y. and Zhang, Z. (2021) 'Numerical analysis of battery thermal management system coupling with low-thermal-conductive phase change material and liquid cooling', *Journal of energy storage,* 39, pp. 102605 Available at: 10.1016/j.est.2021.102605.

Oh, S., Lee, J., Lee, H., Shin, D., Thalluri, T. and Shin, K. (Oct 2019) *Design of Battery Thermal Management Unit with PCM for Electrical Vehicle: Part I: Modelling and Analysis of Pouch Type Battery Cell.* IEEE, pp. 82.

Olabi, A.G., Maghrabie, H.M., Adhari, O.H.K., Sayed, E.T., Yousef, B.A.A., Salameh, T., Kamil, M. and Abdelkareem, M.A. (2022) 'Battery thermal management systems: Recent progress and challenges', *International Journal of Thermofluids,* 15, pp. 100171 Available at: 10.1016/j.ijft.2022.100171.

Olfian, H., Ajarostaghi, S.S.M., Farhadi, M. and Ramiar, A. (2021) 'Melting and solidification processes of phase change material in evacuated tube solar collector with U-shaped spirally corrugated tube', *Applied thermal engineering,* 182 Available at: 10.1016/j.applthermaleng.2020.116149.

Osmani, K., Alkhedher, M., Ramadan, M., Choi, D.S., Li, L.K.B., Doranehgard, M.H. and Olabi, A. (2023) 'Recent progress in the thermal management of lithium-ion batteries', *Journal of Cleaner Production,* 389, pp. 136024 Available at: 10.1016/j.jclepro.2023.136024.

Özdemir, T., Ekici, Ö and Köksal, M. (2021) 'Numerical and experimental investigation of the thermal and electrical characteristics of a lithium ion cell', *E3S Web of Conferences,* 321, pp. 3007 Available at: 10.1051/e3sconf/202132103007.

Padalkar, A.B., Chaudhari, M.B. and Funde, A.M. (2023) 'Computational investigation for reduction in auxiliary energy consumption with different cell spacing in battery pack', *Journal of energy storage,* 65, pp. 107265 Available at: 10.1016/j.est.2023.107265.

Pan, M. and Lai, W. (2017) 'Cutting copper fiber/paraffin composite phase change material discharging experimental study based on heat dissipation capability of Li-ion battery', *Renewable Energy,* 114, pp. 408-422 Available at: https://doi.org/10.1016/j.renene.2017.07.004.

Pan, M. and Zhong, Y. (2018) 'Experimental and numerical investigation of a thermal management system for a Li-ion battery pack using cutting copper fiber sintered skeleton/paraffin composite phase change materials', *International journal of heat and mass transfer,* 126, pp. 531-543 Available at: 10.1016/j.ijheatmasstransfer.2018.06.014.

Panchal, S., Khasow, R., Dincer, I., Agelin-Chaab, M., Fraser, R. and Fowler, M. (2017) 'Thermal design and simulation of mini-channel cold plate for water cooled large sized prismatic lithium-ion battery', *Applied thermal engineering,* 122, pp. 80-90 Available at: 10.1016/j.applthermaleng.2017.05.010.

Panchal, S., Mathew, M., Fraser, R. and Fowler, M. (2018) 'Electrochemical thermal modeling and experimental measurements of 18650 cylindrical lithium-ion battery during discharge cycle for an EV', *Applied thermal engineering,* 135, pp. 123-132 Available at: 10.1016/j.applthermaleng.2018.02.046.

Pandey, A.K., Hossain, M.S., Tyagi, V.V., Abd Rahim, N., Selvaraj, J.A./. and Sari, A. (2018) 'Novel approaches and recent developments on potential applications of phase change materials in solar energy', *Renewable & sustainable energy reviews,* 82, pp. 281-323 Available at: 10.1016/j.rser.2017.09.043.

Pandey, B., Banerjee, R. and Sharma, A. (2021) 'Coupled EnergyPlus and CFD analysis of PCM for thermal management of buildings', *Energy and buildings,* 231 Available at: 10.1016/j.enbuild.2020.110598.

Parsa, S.M., Norozpour, F., Shoeibi, S., Shahsavar, A., Aberoumand, S., Afrand, M., Said, Z. and Karimi, N. (2023) 'Lithium-ion battery thermal management via advanced cooling parameters: State-of-the-art review on

application of machine learning with exergy, economic and environmental analysis', *Journal of the Taiwan Institute of Chemical Engineers,* 148, pp. 104854 Available at: 10.1016/j.jtice.2023.104854.

Parsazadeh, M. and Duan, X. (2018) 'Numerical study on the effects of fins and nanoparticles in a shell and tube phase change thermal energy storage unit', *Applied energy,* 216, pp. 142-156 Available at: 10.1016/j.apenergy.2018.02.052.

Parvini, Y. and Vahidi, A. (Jul 01, 2015) *Maximizing charging efficiency of lithium-ion and lead-acid batteries using optimal control theory.* American Automatic Control Council, pp. 317.

Patel, J.R. and Rathod, M.K. (2020) 'Recent developments in the passive and hybrid thermal management techniques of lithium-ion batteries', *Journal of Power Sources,* 480, pp. 228820 Available at: 10.1016/j.jpowsour.2020.228820.

Patel, J.R., Joshi, V. and Rathod, M.K. (2020) 'Thermal performance investigations of the melting and solidification in differently shaped macro-capsules saturated with phase change material', *Journal of energy storage,* 31, pp. 101635 Available at: 10.1016/j.est.2020.101635.

Patil, S.R., Lokavarapu, B.R. and Thaliyanveedu, H.K. (2023) 'Optimization of battery cooling system used in electric vehicles', *Journal of Energy Storage,* 58, pp. 106299 Available at: 10.1016/j.est.2022.106299.

Peng, P. and Jiang, F. (2016) 'Thermal safety of lithium-ion batteries with various cathode materials: A numerical study', *International journal of heat and mass transfer,* 103, pp. 1008-1016 Available at: 10.1016/j.ijheatmasstransfer.2016.07.088.

Perez Estevez, M.A., Calligaro, S., Bottesi, O., Caligiuri, C. and Renzi, M. (2021) 'An electro-thermal model and its electrical parameters estimation procedure in a lithium-ion battery cell', *Energy (Oxford),* 234, pp. 121296 Available at: 10.1016/j.energy.2021.121296.

Piao, N., Gao, X., Yang, H., Guo, Z., Hu, G., Cheng, H. and Li, F. (2022) 'Challenges and development of lithium-ion batteries for low temperature environments', *eTransportation,* 11, pp. 100145 Available at: https://doi.org/10.1016/j.etran.2021.100145.

PIELICHOWSKA, K. and PIELICHOWSKI, K. (2014) 'Phase change materials for thermal energy storage', *Progress in materials science,* 65, pp. 67-123 Available at: 10.1016/j.pmatsci.2014.03.005.

Ping, P., Peng, R., Kong, D., Chen, G. and Wen, J. (2018) 'Investigation on thermal management performance of PCM-fin structure for Li-ion battery module in high-temperature environment', *Energy Conversion and Management,* 176, pp. 131-146 Available at: 10.1016/j.enconman.2018.09.025.

Ping, P., Zhang, Y., Kong, D. and Du, J. (2021) 'Investigation on battery thermal management system combining phase changed material and liquid cooling considering non-uniform heat generation of battery', *Journal of energy storage,* 36, pp. 102448 Available at: 10.1016/j.est.2021.102448.

Plunkett, S.T., Chen, C., Rojaee, R., Doherty, P., Sik Oh, Y., Galazutdinova, Y., Krishnamurthy, M. and Al-Hallaj, S. (2021) 'Enhancing thermal safety in lithium-ion battery packs through parallel cell 'current dumping' mitigation', *Applied Energy,* 286, pp. 116495 Available at: https://doi.org/10.1016/j.apenergy.2021.116495.

Prakash, S.A., Hariharan, C., Arivazhagan, R., Sheeja, R., Raj, V.A.A. and Velraj, R. (2021) 'Review on numerical algorithms for melting and solidification studies and their implementation in general purpose computational fluid dynamic software', *Journal of energy storage,* 36, pp. 102341 Available at: 10.1016/j.est.2021.102341.

Pu, L., Zhang, S., Xu, L. and Li, Y. (2020) 'Thermal performance optimization and evaluation of a radial finned shell-and-tube Latent heat thermal energy storage unit', *Applied thermal engineering,* 166, pp. 114753 Available at: 10.1016/j.applthermaleng.2019.114753.

Qaderi, A. and Veysi, F. (2021) 'Investigation of a water-NEPCM cooling thermal management system for cylindrical 18650 Li-ion batteries', *Energy,* , pp. 122570 Available at: https://doi.org/10.1016/j.energy.2021.122570.

Qaiser, R., Khan, M.M., Khan, L.A. and Irfan, M. (2021) 'Melting performance enhancement of PCM based thermal energy storage system using multiple tubes and modified shell designs', *Journal of energy storage,* 33 Available at: 10.1016/j.est.2020.102161.

Qian, X., Xuan, D., Zhao, X. and Shi, Z. (2019) 'Heat dissipation optimization of lithium-ion battery pack based on neural networks', *Applied thermal engineering,* 162, pp. 114289 Available at: 10.1016/j.applthermaleng.2019.114289.

Qin, P., Jia, Z., Jin, K., Duan, Q., Sun, J. and Wang, Q. (2021) 'The experimental study on a novel integrated system with thermal management and rapid cooling for battery pack based on C6F12O spray cooling in a closed-loop', *Journal of Power Sources,* 516, pp. 230659 Available at: https://doi.org/10.1016/j.jpowsour.2021.230659.

Qin, P., Liao, M., Zhang, D., Liu, Y., Sun, J. and Wang, Q. (2019) 'Experimental and numerical study on a novel hybrid battery thermal management system integrated forced-air convection and phase change material', *Energy Conversion and Management,* 195, pp. 1371-1381 Available at: https://doi.org/10.1016/j.enconman.2019.05.084.

Qin, Z., Ji, C., Low, Z., Dubey, S., Hoong Choo, F. and Duan, F. (2017) 'Effect of Fin Location on the Latent Heat Storage: A Numerical Study', *Energy procedia,* 143, pp. 320-326 Available at: 10.1016/j.egypro.2017.12.691.

Qu, Z.G., Li, W.Q. and Tao, W.Q. (2014) 'Numerical model of the passive thermal management system for high-power lithium ion battery by using porous metal foam saturated with phase change material', *International journal of hydrogen energy,* 39(8), pp. 3904-3913 Available at: 10.1016/j.ijhydene.2013.12.136.

Rabienataj Darzi, A.A., Jourabian, M. and Farhadi, M. (2016) 'Melting and solidification of PCM enhanced by radial conductive fins and nanoparticles in cylindrical annulus', *Energy conversion and management,* 118, pp. 253-263 Available at: 10.1016/j.enconman.2016.04.016.

Raizah, Z. and Aly, A.M. (2021) 'Double-diffusive convection of a rotating circular cylinder in a porous cavity suspended by nano-encapsulated phase change materials', *Case studies in thermal engineering,* Available at: 10.1016/j.csite.2021.100864.

Ran, Y., Su, Y., Yan, K., Jiang, X., Zhao, Y., Shen, X., Liu, X., Yang, X., Chen, L. and Wu, F. (2023) 'Electrical–thermal–fluidic coupling Li-ion battery pack consistency study', *Journal of Energy Storage,* 70, pp. 108031 Available at: 10.1016/j.est.2023.108031.

Ranjbar Kermani, J., Mahlouji Taheri, M., Shafii, M.B. and Moosavi, A. (2023) 'Analytical solution, optimization and design of a phase change cooling pack for cylindrical lithium-ion batteries', *Applied thermal engineering,* 232, pp. 120963 Available at: 10.1016/j.applthermaleng.2023.120963.

Ranjbaran, Y.S., Shojaeefard, M.H. and Molaeimanesh, G.R. (2023) 'Thermal performance enhancement of a passive battery thermal management system based on phase change material using cold air passageways for lithium batteries', *Journal of Energy Storage,* 68, pp. 107744 Available at: 10.1016/j.est.2023.107744.

Rao, Z. and Wang, S. (2011) 'A review of power battery thermal energy management', *Renewable and Sustainable Energy Reviews,* 15(9), pp. 4554-4571 Available at: https://doi.org/10.1016/j.rser.2011.07.096.

Rao, Z., Wang, S. and Zhang, G. (2011) 'Simulation and experiment of thermal energy management with phase change material for ageing LiFePO4 power battery', *Energy Conversion and Management,* 52(12), pp. 3408-3414 Available at: https://doi.org/10.1016/j.enconman.2011.07.009.

Rathod, M.K. and Banerjee, J. (2015) 'Thermal performance enhancement of shell and tube Latent Heat Storage Unit using longitudinal fins', *Applied thermal engineering,* 75, pp. 1084-1092 Available at: 10.1016/j.applthermaleng.2014.10.074.

Rathore, P.K.S. and Shukla, S.K. (2019) 'Potential of macroencapsulated PCM for thermal energy storage in buildings: A comprehensive review', *Construction & building materials,* 225, pp. 723-744 Available at: 10.1016/j.conbuildmat.2019.07.221.

Reji Kumar, R., Samykano, M., Pandey, A.K., Kadirgama, K. and Tyagi, V.V. (2020) 'Phase change materials and nano-enhanced phase change materials for thermal energy storage in photovoltaic thermal systems: A

futuristic approach and its technical challenges', *Renewable & sustainable energy reviews,* 133, pp. 110341 Available at: 10.1016/j.rser.2020.110341.

Ren, H., Jia, L., Dang, C. and Qi, Z. (2022) 'An electrochemical-thermal coupling model for heat generation analysis of prismatic lithium battery', *Journal of Energy Storage,* 50, pp. 104277 Available at: 10.1016/j.est.2022.104277.

Ren, Q., Xu, H. and Luo, Z. (2019) 'PCM charging process accelerated with combination of optimized triangle fins and nanoparticles', *International journal of thermal sciences,* 140, pp. 466-479 Available at: 10.1016/j.ijthermalsci.2019.03.005.

Reuben Raj, C., Suresh, S., Vasudevan, S., Chandrasekar, M., Kumar Singh, V. and Bhavsar, R.R. (2020) 'Thermal performance of nano-enriched form-stable PCM implanted in a pin finned wall-less heat sink for thermal management application', *Energy Conversion and Management,* 226, pp. 113466 Available at: 10.1016/j.enconman.2020.113466.

Riahi, S., Saman, W.Y., Bruno, F., Belusko, M., and Tay, N.H.S. (2018) 'Performance comparison of Latent heat storage systems comprising plate fins with different shell and tube configurations', *Applied energy,* 212, pp. 1095-1106 Available at: 10.1016/j.apenergy.2017.12.109.

Rostami, S., Afrand, M., Shahsavar, A., Sheikholeslami, M., Kalbasi, R., Aghakhani, S., Shadloo, M.S. and Oztop, H.F. (2020) 'A review of melting and freezing processes of PCM/nano-PCM and their application in energy storage', *Energy (Oxford),* 211, pp. 118698 Available at: 10.1016/j.energy.2020.118698.

Sabbah, R., Kizilel, R., Selman, J.R. and Al-Hallaj, S. (2008) 'Active (air-cooled) vs. passive (phase change material) thermal management of high power lithium-ion packs: Limitation of temperature rise and uniformity of temperature distribution', *Journal of Power Sources,* 182(2), pp. 630-638 Available at: https://doi.org/10.1016/j.jpowsour.2008.03.082.

Safdari, M., Ahmadi, R. and Sadeghzadeh, S. (2020) 'Numerical investigation on PCM encapsulation shape used in the passive-active battery thermal management', *Energy,* 193, pp. 116840 Available at: https://doi.org/10.1016/j.energy.2019.116840.

Salunkhe, P.B. and Shembekar, P.S. (2012) 'A review on effect of phase change material encapsulation on the thermal performance of a system', *Renewable & sustainable energy reviews,* 16(8), pp. 5603-5616 Available at: 10.1016/j.rser.2012.05.037.

Samanta, A. and Chowdhuri, S. (2021) 'Active Cell Balancing of Lithium-ion Battery Pack Using Dual DC-DC Converter and Auxiliary Lead-acid Battery', *Journal of Energy Storage,* 33, pp. 102109 Available at: https://doi.org/10.1016/j.est.2020.102109.

Samba, A., Omar, N., Gualous, H., Firouz, Y., Van den Bossche, P., Van Mierlo, J. and Boubekeur, T.I. (2014) 'Development of an Advanced Two-Dimensional Thermal Model for Large size Lithium-ion Pouch Cells', *Electrochimica acta,* 117, pp. 246-254 Available at: 10.1016/j.electacta.2013.11.113.

Santhanagopalan, S., Guo, Q., Ramadass, P. and White, R.E. (2006) 'Review of models for predicting the cycling performance of lithium ion batteries', *Journal of Power Sources,* 156(2), pp. 620-628 Available at: 10.1016/j.jpowsour.2005.05.070.

Saqli, K., Bouchareb, H., M'sirdi, K.N., Naamane, A. and Oudghiri, M. (Jun 2020) *Electric and Thermal Model of Li-ion battery pack with cylindrical components.* IEEE, pp. 1.

Sarani, I., Payan, S., Nada, S.A. and Payan, A. (2020) 'Numerical investigation of an innovative discontinuous distribution of fins for solidification rate enhancement in PCM with and without nanoparticles', *Applied thermal engineering,* 176, pp. 115017 Available at: 10.1016/j.applthermaleng.2020.115017.

Sarani, I., Payan, S., Payan, A. and Nada, S.A. (2020) 'Enhancement of energy storage capability in RT82 phase change material using strips fins and metal-oxide based nanoparticles', *Journal of energy storage,* 32 Available at: 10.1016/j.est.2020.102009.

Sarchami, A., Najafi, M., Imam, A. and Houshfar, E. (2022) 'Experimental study of thermal management system for cylindrical Li-ion battery pack based on nanofluid cooling and copper sheath', *International Journal of Thermal Sciences,* 171, pp. 107244 Available at: https://doi.org/10.1016/j.ijthermalsci.2021.107244.

Sardari, P.T., Babaei-Mahani, R., Giddings, D., Yasseri, S., Moghimi, M.A. and Bahai, H. (2020) 'Energy recovery from domestic radiators using a compact composite metal Foam/PCM Latent heat storage', *Journal of cleaner production,* 257, pp. 120504 Available at: 10.1016/j.jclepro.2020.120504.

Sardari, P.T., Giddings, D., Grant, D., Gillott, M., and Walker, G.S. (2020) 'Discharge of a composite metal foam/phase change material to air heat exchanger for a domestic thermal storage unit', *Renewable energy,* 148, pp. 987-1001 Available at: 10.1016/j.renene.2019.10.084.

Sardari, P.T., Mohammed, H.I., Giddings, D., walker, G.S., Gillott, M. and Grant, D. (2019) 'Numerical study of a multiple-segment metal foam-PCM Latent heat storage unit: Effect of porosity, pore density and location of heat source', *Energy,* 189 Available at: 10.1016/j.energy.2019.116108.

Sattari, H., Mohebbi, A., Afsahi, M.M. and Azimi Yancheshme, A. (2017) 'CFD simulation of melting process of phase change materials (PCMs) in a spherical capsule', *International journal of refrigeration,* 73, pp. 209-218 Available at: 10.1016/j.ijrefrig.2016.09.007.

Saw, L.H., Somasundaram, K., Ye, Y. and Tay, A.A.O. (2014) 'Electro-thermal analysis of Lithium Iron Phosphate battery for electric vehicles', *Journal of Power Sources,* 249, pp. 231-238 Available at: https://doi.org/10.1016/j.jpowsour.2013.10.052.

Saw, L.H., Ye, Y. and Tay, A.A.O. (2016) 'Integration issues of lithium-ion battery into electric vehicles battery pack', *Journal of Cleaner Production,* 113, pp. 1032-1045 Available at: https://doi.org/10.1016/j.jclepro.2015.11.011.

Seaman, A., Dao, T. and McPhee, J. (2014) 'A survey of mathematics-based equivalent-circuit and electrochemical battery models for hybrid and electric vehicle simulation', *Journal of Power Sources,* 256, pp. 410-423 Available at: 10.1016/j.jpowsour.2014.01.057.

Seddegh, S., Wang, X. and Henderson, A.D. (2016) 'A comparative study of thermal behaviour of a horizontal and vertical shell-and-tube energy storage using phase change materials', *Applied thermal engineering,* 93, pp. 348-358 Available at: 10.1016/j.applthermaleng.2015.09.107.

Seddegh, S., Wang, X. and Henderson, A.D. (2015) 'Numerical investigation of heat transfer mechanism in a vertical shell and tube Latent heat energy storage system', *Applied thermal engineering,* 87, pp. 698-706 Available at: 10.1016/j.applthermaleng.2015.05.067.

Sefidan, A.M., Sojoudi, A. and Saha, S.C. (2017) 'Nanofluid-based cooling of cylindrical lithium-ion battery packs employing forced air flow', *International Journal of Thermal Sciences,* 117, pp. 44-58 Available at: https://doi.org/10.1016/j.ijthermalsci.2017.03.006.

Sefidan, A.M., Sojoudi, A., Saha, S.C. and Cholette, M. (2017) 'Multi-layer PCM solidification in a finned triplex tube considering natural convection', *Applied thermal engineering,* 123, pp. 901-916 Available at: 10.1016/j.applthermaleng.2017.05.156.

Selokar, U., Qiao, Q. and Lu, H. (May 2019) *PCM and the thermal model in battery design.* IEEE, pp. 596.

Septiadi, W.N., Alim, M. and Adi, M.N.P. (2022) 'The application of battery thermal management system based on heat pipes and phase change materials in the electric bike', *Journal of Energy Storage,* 56, pp. 106014 Available at: 10.1016/j.est.2022.106014.

Shahid, S. and Agelin-Chaab, M. (2021) 'Development of hybrid thermal management techniques for battery packs', *Applied Thermal Engineering,* 186, pp. 116542 Available at: https://doi.org/10.1016/j.applthermaleng.2020.116542.

Shahid, S. and Agelin-Chaab, M. (2018) 'Development and analysis of a technique to improve air-cooling and temperature uniformity in a battery pack for cylindrical batteries', *Thermal Science and Engineering Progress,* 5, pp. 351-363 Available at: https://doi.org/10.1016/j.tsep.2018.01.003.

Shahjalal, M., Shams, T., Islam, M.E., Alam, W., Modak, M., Hossain, S.B., Ramadesigan, V., Ahmed, M.R., Ahmed, H. and Iqbal, A. (2021) 'A review of thermal management for Li-ion batteries: Prospects, challenges, and issues', *Journal of Energy Storage,* 39, pp. 102518 Available at: https://doi.org/10.1016/j.est.2021.102518.

Shahsavar, A., Al-Rashed, A.A.A.A., Entezari, S. and Sardari, P.T. (2019) 'Melting and solidification characteristics of a double-pipe Latent heat storage system with sinusoidal wavy channels embedded in a porous medium', *Energy (Oxford),* 171, pp. 751-769 Available at: 10.1016/j.energy.2019.01.045.

Shahsavar, A., Goodarzi, A., Mohammed, H.I., Shirneshan, A. and Talebizadehsardari, P. (2020) 'Thermal performance evaluation of non-uniform fin array in a finned double-pipe Latent heat storage system', *Energy (Oxford),* 193, pp. 116800 Available at: 10.1016/j.energy.2019.116800.

Shahsavar, A., Khosravi, J., Mohammed, H.I. and Talebizadehsardari, P. (2020) 'Performance evaluation of melting/solidification mechanism in a variable wave-length wavy channel double-tube Latent heat storage system', *Journal of energy storage,* 27, pp. 101063 Available at: 10.1016/j.est.2019.101063.

Shahsavar, A., Majidzadeh, A.H., Mahani, R.B. and Talebizadehsardari, P. (2021) 'Entropy and thermal performance analysis of PCM melting and solidification mechanisms in a wavy channel triplex-tube heat exchanger', *Renewable energy,* 165, pp. 52-72 Available at: 10.1016/j.renene.2020.11.074.

Sharifi, N., Bergman, T.L. and Faghri, A. (2011) 'Enhancement of PCM melting in enclosures with horizontally-finned internal surfaces', *International journal of heat and mass transfer,* 54(19), pp. 4182-4192 Available at: 10.1016/j.ijheatmasstransfer.2011.05.027.

Sharma, A., Tyagi, V.V., Chen, C.R. and Buddhi, D. (2009) 'Review on thermal energy storage with phase change materials and applications', *Renewable & sustainable energy reviews,* 13(2), pp. 318-345 Available at: 10.1016/j.rser.2007.10.005.

Sharma, R.K., Ganesan, P., Tyagi, V.V., Metselaar, H.S.C. and Sandaran, S.C. (2015a) 'Developments in organic solid–liquid phase change materials and their applications in thermal energy storage', *Energy Conversion and Management,* 95, pp. 193-228 Available at: 10.1016/j.enconman.2015.01.084.

Sharma, R.K., Ganesan, P., Tyagi, V.V., Metselaar, H.S.C. and Sandaran, S.C. (2015b) 'Developments in organic solid–liquid phase change materials and their applications in thermal energy storage', *Energy conversion and management,* 95, pp. 193-228 Available at: 10.1016/j.enconman.2015.01.084.

Sheikholeslami, M., Lohrasbi, S. and Ganji, D.D. (2016) 'Numerical analysis of discharging process acceleration in LHTESS by immersing innovative fin configuration using finite element method', *Applied thermal engineering,* 107, pp. 154-166 Available at: 10.1016/j.applthermaleng.2016.06.158.

Shen, M. and Gao, Q. (2019) *A review on battery management system from the modeling efforts to its multiapplication and integration* Hindawi Limited.

Shen, Z., Chen, S., Liu, X. and Chen, B. (2021) 'A review on thermal management performance enhancement of phase change materials for vehicle lithium-ion batteries', *Renewable and Sustainable Energy Reviews,* 148, pp. 111301 Available at: 10.1016/j.rser.2021.111301.

Sheng, L., Zhang, H., Su, L., Zhang, Z., Zhang, H., Li, K., Fang, Y. and Ye, W. (2021) 'Effect analysis on thermal profile management of a cylindrical lithium-ion battery utilizing a cellular liquid cooling jacket', *Energy,* 220, pp. 119725 Available at: https://doi.org/10.1016/j.energy.2020.119725.

Sheng, L., Zhang, H., Zhang, H., Su, L. and Zhang, Z. (2021) 'Lightweight liquid cooling based thermal management to a prismatic hard-cased lithium-ion battery', *International Journal of Heat and Mass Transfer,* 170, pp. 120998 Available at: https://doi.org/10.1016/j.ijheatmasstransfer.2021.120998.

Shi, S., Xie, Y., Li, M., Yuan, Y., Yu, J., Wu, H., Liu, B. and Liu, N. (2017) 'Non-steady experimental investigation on an integrated thermal management system for power battery with phase change materials', *Energy conversion and management,* 138, pp. 84-96 Available at: 10.1016/j.enconman.2017.01.069.

Shi, Y., Ahmad, S., Liu, H., Lau, K.T. and Zhao, J. (2021) 'Optimization of air-cooling technology for LiFePO4 battery pack based on deep learning', *Journal of Power Sources,* 497, pp. 229894 Available at: https://doi.org/10.1016/j.jpowsour.2021.229894.

Shokouhmand, H. and Kamkari, B. (2013) 'Experimental investigation on melting heat transfer characteristics of lauric acid in a rectangular thermal storage unit', *Experimental thermal and fluid science,* 50, pp. 201-212 Available at: 10.1016/j.expthermflusci.2013.06.010.

Siddique, A.R.M., Mahmud, S. and Heyst, B.V. (2018) 'A comprehensive review on a passive (phase change materials) and an active (thermoelectric cooler) battery thermal management system and their limitations', *Journal of Power Sources,* 401, pp. 224-237 Available at: https://doi.org/10.1016/j.jpowsour.2018.08.094.

Sinaga, R., Darkwa, J., Omer, S.A. and Worral, M. (2022) 'The microencapsulation, thermal enhancement, and applications of medium and high-melting temperature phase change materials: A review', *International Journal of Energy Research,* Available at: 10.1002/er.7860.

Situ, W., Zhang, G., Li, X., Yang, X., Wei, C., Rao, M., Wang, Z., Wang, C. and Wu, W. (2017) 'A thermal management system for rectangular LiFePO4 battery module using novel double copper mesh-enhanced phase change material plates', *Energy,* 141, pp. 613-623 Available at: https://doi.org/10.1016/j.energy.2017.09.083.

Soliman, A.S., Zhu, S., Xu, L., Dong, J. and Cheng, P. (2021) 'Numerical simulation and experimental verification of constrained melting of phase change material in cylindrical enclosure subjected to a constant heat flux', *Journal of energy storage,* 35 Available at: 10.1016/j.est.2021.102312.

Somasundaram, K., Birgersson, E. and Mujumdar, A.S. (2012) 'Thermal–electrochemical model for passive thermal management of a spiral-wound lithium-ion battery', *Journal of Power Sources,* 203, pp. 84-96 Available at: https://doi.org/10.1016/j.jpowsour.2011.11.075.

Stefanopoulou, A.G. and Kim, Y. (2015) '10 - System-level management of rechargeable lithium-ion batteries', in Franco, A.A. (ed.) *Rechargeable Lithium Batteries* Woodhead Publishing, pp. 281-302.

Sturm, J., Ludwig, S., Zwirner, J., Ramirez-Garcia, C., Heinrich, B., Horsche, M.F. and Jossen, A. (2019) 'Suitability of physicochemical models for embedded systems regarding a nickel-rich, silicon-graphite lithium-ion battery', *Journal of Power Sources,* 436, pp. 226834 Available at: https://doi.org/10.1016/j.jpowsour.2019.226834.

Sun, J., Mao, B. and Wang, Q. (2021) 'Progress on the research of fire behavior and fire protection of lithium ion battery', *Fire Safety Journal,* 120, pp. 103119 Available at: https://doi.org/10.1016/j.firesaf.2020.103119.

Sun, Z., Fan, R., Yan, F., Zhou, T. and Zheng, N. (2019) 'Thermal management of the lithium-ion battery by the composite PCM-Fin structures', *International journal of heat and mass transfer,* 145, pp. 118739 Available at: 10.1016/j.ijheatmasstransfer.2019.118739.

Suresh Patil, M., Seo, J. and Lee, M. (2021) 'A novel dielectric fluid immersion cooling technology for Li-ion battery thermal management', *Energy Conversion and Management,* 229, pp. 113715 Available at: 10.1016/j.enconman.2020.113715.

Talebizadehsardari, P., Mahdi, J.M., Mohammed, H.I., Moghimi, M.A., Hossein Eisapour, A. and Ghalambaz, M. (2021) 'Consecutive charging and discharging of a PCM-based plate heat exchanger with zigzag configuration', *Applied thermal engineering,* 193, pp. 116970 Available at: 10.1016/j.applthermaleng.2021.116970.

Talele, V., Thorat, P., Gokhale, Y.P. and VK, M. (2021) 'Phase change material based passive battery thermal management system to predict delay effect', *Journal of Energy Storage,* 44, pp. 103482 Available at: 10.1016/j.est.2021.103482.

Tan, S. and Zhang, X. (2023) 'Progress of research on phase change energy storage materials in their thermal conductivity', *Journal of Energy Storage,* 61, pp. 106772 Available at: 10.1016/j.est.2023.106772.

Tan, W.C., Saw, L.H., Thiam, H.S., Xuan, J., Cai, Z. and Yew, M.C. (2018) 'Overview of porous media/metal foam application in fuel cells and solar power systems', *Renewable & sustainable energy reviews,* 96, pp. 181-197 Available at: 10.1016/j.rser.2018.07.032.

Tang, S., Tian, H., Zhou, J. and Li, H. (2021) 'Evaluation and optimization of melting performance in a horizontal thermal energy storage unit with non-uniform fins', *Journal of energy storage,* 33, pp. 102124 Available at: 10.1016/j.est.2020.102124.

Tang, Z., Wang, S., Liu, Z. and Cheng, J. (2020) 'Numerical analysis of temperature uniformity of a liquid cooling battery module composed of heat-conducting blocks with gradient contact surface angles', *Applied Thermal Engineering,* 178, pp. 115509 Available at: https://doi.org/10.1016/j.applthermaleng.2020.115509.

Tete, P.R., Gupta, M.M. and Joshi, S.S. (2021) 'Developments in battery thermal management systems for electric vehicles: A technical review', *Journal of Energy Storage,* 35, pp. 102255 Available at: 10.1016/j.est.2021.102255.

Thakur, A.K., Prabakaran, R., Elkadeem, M.R., Sharshir, S.W., Arıcı, M., Wang, C., Zhao, W., Hwang, J. and Saidur, R. (2020) 'A state of art review and future viewpoint on advance cooling techniques for Lithium–ion battery system of electric vehicles', *Journal of Energy Storage,* 32, pp. 101771 Available at: https://doi.org/10.1016/j.est.2020.101771.

Tian, L., Liu, X., Chen, S. and Shen, Z. (2020) 'Effect of fin material on PCM melting in a rectangular enclosure', *Applied thermal engineering,* 167, pp. 114764 Available at: 10.1016/j.applthermaleng.2019.114764.

Tian, W., Dang, S., Liu, G., Guo, Z. and Yang, X. (2021) 'Thermal transport in phase change materials embedded in metal foam: evaluation on inclination configuration', *Journal of Energy Storage,* 33, pp. 102166 Available at: https://doi.org/10.1016/j.est.2020.102166.

Tian, Y., and Zhao, C.Y. (2011) 'A numerical investigation of heat transfer in phase change materials (PCMs) embedded in porous metals', *Energy (Oxford),* 36(9), pp. 5539-5546 Available at: 10.1016/j.energy.2011.07.019.

Tomaszewska, A., Chu, Z., Feng, X., O'Kane, S., Liu, X., Chen, J., Ji, C., Endler, E., Li, R., Liu, L., Li, Y., Zheng, S., Vetterlein, S., Gao, M., Du, J., Parkes, M., Ouyang, M., Marinescu, M., Offer, G. and Wu, B. (2019) 'Lithium-ion battery fast charging: A review', *eTransportation,* 1, pp. 100011 Available at: 10.1016/j.etran.2019.100011.

Tousi, M., Sarchami, A., Kiani, M., Najafi, M. and Houshfar, E. (2021) 'Numerical study of novel liquid-cooled thermal management system for cylindrical Li-ion battery packs under high discharge rate based on AgO nanofluid and copper sheath', *Journal of Energy Storage,* 41, pp. 102910 Available at: https://doi.org/10.1016/j.est.2021.102910.

Tran, M., DaCosta, A., Mevawalla, A., Panchal, S. and Fowler, M. (2021) 'Comparative Study of Equivalent Circuit Models Performance in Four Common Lithium-Ion Batteries: LFP, NMC, LMO, NCA', *Batteries (Basel),* 7(3), pp. 51 Available at: 10.3390/batteries7030051.

Tran, M., Mevawala, A., Panchal, S., Raahemifar, K., Fowler, M. and Fraser, R. (2020) 'Effect of integrating the hysteresis component to the equivalent circuit model of Lithium-ion battery for dynamic and non-dynamic applications', *Journal of energy storage,* 32, pp. 101785 Available at: 10.1016/j.est.2020.101785.

Ungurean, L., Cârstoiu, G., Micea, M.V. and Groza, V. (2017) 'Battery state of health estimation: a structured review of models, methods and commercial devices', *International Journal of energy research,* 41(2), pp. 151-181 Available at: 10.1002/er.3598.

Velumani, D. and Bansal, A. (2022) 'Thermal Behavior of Lithium- and Sodium-Ion Batteries: A Review on Heat Generation, Battery Degradation, Thermal Runway – Perspective and Future Directions', *Energy & fuels,* 36(23), pp. 14000-14029 Available at: 10.1021/acs.energyfuels.2c02889.

Verma, A., Shashidhara, S. and Rakshit, D. (2019) 'A comparative study on battery thermal management using phase change material (PCM)', *Thermal Science and Engineering Progress,* 11, pp. 74-83 Available at: 10.1016/j.tsep.2019.03.003.

Verma, S.P. and Saraswati, S. (2023) 'Numerical and experimental analysis of air-cooled Lithium-ion battery pack for the evaluation of the thermal performance enhancement', *Journal of Energy Storage,* 73, pp. 108983 Available at: 10.1016/j.est.2023.108983.

Vikas, Yadav, A. and Soni, S.K. (2017) *Simulation of Melting Process of a Phase Change Material (PCM) using ANSYS (Fluent)*.

Vikram, S., Vashisht, S. and Rakshit, D. (2022) 'Performance analysis of liquid-based battery thermal management system for Electric Vehicles during discharge under drive cycles', *Journal of energy storage,* 55, pp. 105737 Available at: 10.1016/j.est.2022.105737.

Vyroubal, P. and Kazda, T. (2018) 'Equivalent circuit model parameters extraction for lithium-ion batteries using electrochemical impedance spectroscopy', *Journal of energy storage,* 15, pp. 23-31 Available at: 10.1016/j.est.2017.10.019.

Wang, F., Nasajpour-Esfahani, N., Alizadeh, A., Fadhil Smaisim, G., Abed, A.M., Hadrawi, S.K., Aminian, S., Sabetvand, R. and Toghraie, D. (2023) 'Thermal performance of a phase change material (PCM) microcapsules containing Au nanoparticles in a nanochannel: A molecular dynamics approach', *Journal of Molecular Liquids,* 373, pp. 121128 Available at: 10.1016/j.molliq.2022.121128.

Wang, N., Li, C., Li, W., Chen, X., Li, Y. and Qi, D. (2021a) 'Heat dissipation optimization for a serpentine liquid cooling battery thermal management system: An application of surrogate assisted approach', *Journal of Energy Storage,* 40, pp. 102771 Available at: https://doi.org/10.1016/j.est.2021.102771.

Wang, N., Li, C., Li, W., Huang, M. and Qi, D. (2021b) 'Effect analysis on performance enhancement of a novel air cooling battery thermal management system with spoilers', *Applied Thermal Engineering,* 192, pp. 116932 Available at: https://doi.org/10.1016/j.applthermaleng.2021.116932.

Wang, Q., Jiang, B., Li, B. and Yan, Y. (2016) 'A critical review of thermal management models and solutions of lithium-ion batteries for the development of pure electric vehicles', *Renewable and Sustainable Energy Reviews,* 64, pp. 106-128 Available at: https://doi.org/10.1016/j.rser.2016.05.033.

Wang, Q., Mao, B., Stoliarov, S.I. and Sun, J. (2019) 'A review of lithium-ion battery failure mechanisms and fire prevention strategies', *Progress in Energy and Combustion Science,* 73, pp. 95-131 Available at: https://doi.org/10.1016/j.pecs.2019.03.002.

Wang, Q., Ping, P., Zhao, X., Chu, G., Sun, J. and Chen, C. (2012) 'Thermal runaway caused fire and explosion of lithium-ion battery', *Journal of Power Sources,* 208, pp. 210-224 Available at: https://doi.org/10.1016/j.jpowsour.2012.02.038.

Wang, R., Liang, Z., Souri, M., Esfahani, M.N. and Jabbari, M. (2022) 'Numerical analysis of lithium-ion battery thermal management system using phase change material assisted by liquid cooling method', *International Journal of Heat and Mass Transfer,* 183, pp. 122095 Available at: 10.1016/j.ijheatmasstransfer.2021.122095.

Wang, T., Tseng, K.J. and Zhao, J. (2015) 'Development of efficient air-cooling strategies for lithium-ion battery module based on empirical heat source model', *Applied Thermal Engineering,* 90, pp. 521-529 Available at: https://doi.org/10.1016/j.applthermaleng.2015.07.033.

Wang, T., Tseng, K.J., Zhao, J. and Wei, Z. (2014) 'Thermal investigation of lithium-ion battery module with different cell arrangement structures and forced air-cooling strategies', *Applied Energy,* 134, pp. 229-238 Available at: https://doi.org/10.1016/j.apenergy.2014.08.013.

Wang, W., Zhang, X., Xin, C. and Rao, Z. (2018) 'An experimental study on thermal management of lithium-ion battery packs using an improved passive method', *Applied Thermal Engineering,* 134, pp. 163-170 Available at: https://doi.org/10.1016/j.applthermaleng.2018.02.011.

Wang, Y. and Wu, J. (2019) 'Performance improvement of the thermal management system of lithium-ion battery module on purely electric AUVs', *Applied Thermal Engineering,* 146, pp. 74-84 Available at: https://doi.org/10.1016/j.applthermaleng.2018.09.108.

Wang, Y., Yu, Y., Jing, Z., Wang, C., Zhou, G. and Zhao, W. (2021) 'Thermal performance of lithium-ion batteries applying forced air cooling with an improved aluminium foam heat sink design', *International Journal of Heat and Mass Transfer,* 167, pp. 120827 Available at: https://doi.org/10.1016/j.ijheatmasstransfer.2020.120827.

Wang, Z., Zhang, H. and Xia, X. (2017) 'Experimental investigation on the thermal behaviour of cylindrical battery with composite paraffin and fin structure', *International journal of heat and mass transfer,* 109, pp. 958-970 Available at: 10.1016/j.ijheatmasstransfer.2017.02.057.

Wang, Z., Zhang, Z., Jia, L. and Yang, L. (2015) 'Paraffin and paraffin/aluminium foam composite phase change material heat storage experimental study based on thermal management of Li-ion battery', *Applied thermal engineering,* 78, pp. 428-436 Available at: 10.1016/j.applthermaleng.2015.01.009.

Wazeer, A., Das, A., Abeykoon, C., Sinha, A. and Karmakar, A. (2022) 'Phase change materials for battery thermal management of electric and hybrid vehicles: A review', *Energy Nexus,* 7, pp. 100131 Available at: 10.1016/j.nexus.2022.100131.

Wen, J., Zhao, D. and Zhang, C. (2020) 'An overview of electricity powered vehicles: Lithium-ion battery energy storage density and energy conversion efficiency', *Renewable Energy,* 162, pp. 1629-1648 Available at: https://doi.org/10.1016/j.renene.2020.09.055.

Weng, J., He, Y., Ouyang, D., Yang, X., Chen, M., Cui, S., Zhang, G., Yuen, R.K.K. and Wang, J. (2021) 'Honeycomb-inspired design of a thermal management module and its mitigation effect on thermal runaway propagation', *Applied Thermal Engineering,* 195, pp. 117147 Available at: https://doi.org/10.1016/j.applthermaleng.2021.117147.

Weng, J., He, Y., Ouyang, D., Yang, X., Zhang, G. and Wang, J. (2019) 'Thermal performance of PCM and branch-structured fins for cylindrical power battery in a high-temperature environment', *Energy Conversion and Management,* 200, pp. 112106 Available at: https://doi.org/10.1016/j.enconman.2019.112106.

Weng, J., Ouyang, D., Liu, Y., Chen, M., Li, Y., Huang, X. and Wang, J. (2021) 'Alleviation on battery thermal runaway propagation: Effects of oxygen level and dilution gas', *Journal of Power Sources,* 509, pp. 230340 Available at: https://doi.org/10.1016/j.jpowsour.2021.230340.

Weng, J., Ouyang, D., Yang, X., Chen, M., Zhang, G. and Wang, J. (2021) 'Experimental study on thermal behavior of PCM-module coupled with various cooling strategies under different temperatures and protocols', *Applied Thermal Engineering,* 197, pp. 117376 Available at: https://doi.org/10.1016/j.applthermaleng.2021.117376.

Weng, J., Ouyang, D., Yang, X., Chen, M., Zhang, G. and Wang, J. (2020) 'Optimization of the internal fin in a phase-change-material module for battery thermal management', *Applied Thermal Engineering,* 167, pp. 114698 Available at: https://doi.org/10.1016/j.applthermaleng.2019.114698.

Weng, J., Xiao, C., Ouyang, D., Yang, X., Chen, M., Zhang, G., Yuen, R.K.K. and Wang, J. (2022) 'Mitigation effects on thermal runaway propagation of structure-enhanced phase change material modules with flame retardant additives', *Energy,* 239, pp. 122087 Available at: https://doi.org/10.1016/j.energy.2021.122087.

Weng, J., Yang, X., Ouyang, D., Chen, M., Zhang, G. and Wang, J. (2019) 'Comparative study on the transversal/lengthwise thermal failure propagation and heating position effect of lithium-ion batteries', *Applied Energy,* 255, pp. 113761 Available at: https://doi.org/10.1016/j.apenergy.2019.113761.

Weragoda, D.M., Tian, G., Burkitbayev, A., Lo, K. and Zhang, T. (2023) 'A comprehensive review on heat pipe based battery thermal management systems', *Applied Thermal Engineering,* 224, pp. 120070 Available at: 10.1016/j.applthermaleng.2023.120070.

Williford, R.E., Viswanathan, V.V. and Zhang, J. (2009) 'Effects of entropy changes in anodes and cathodes on the thermal behavior of lithium ion batteries', *Journal of power sources,* 189(1), pp. 101-107 Available at: 10.1016/j.jpowsour.2008.10.078.

Wiriyasart, S., Hommalee, C., Sirikasemsuk, S., Prurapark, R. and Naphon, P. (2020) 'Thermal management system with nanofluids for electric vehicle battery cooling modules', *Case Studies in Thermal Engineering,* 18, pp. 100583 Available at: https://doi.org/10.1016/j.csite.2020.100583.

Wu, L., Zhang, X. and Liu, X. (2020) 'Numerical analysis and improvement of the thermal performance in a Latent heat thermal energy storage device with spiderweb-like fins', *Journal of energy storage,* 32, pp. 101768 Available at: 10.1016/j.est.2020.101768.

Wu, P., Shao, G., Guo, C., Lu, Y., Dong, X., Zhong, Y. and Liu, A. (2019) 'Long cycle life, low self-discharge carbon anode for Li-ion batteries with pores and dual-doping', *Journal of Alloys and Compounds,* 802, pp. 620-627 Available at: 10.1016/j.jallcom.2019.06.233.

Wu, S., Xiong, R., Li, H., Nian, V. and Ma, S. (2020) 'The state of the art on preheating lithium-ion batteries in cold weather', *Journal of Energy Storage,* 27, pp. 101059 Available at: https://doi.org/10.1016/j.est.2019.101059.

Wu, W., Ye, G., Zhang, G. and Yang, X. (2022) 'Composite phase change material with room-temperature-flexibility for battery thermal management', *Chemical Engineering Journal,* 428, pp. 131116 Available at: https://doi.org/10.1016/j.cej.2021.131116.

Wu, W., Wang, S., Wu, W., Chen, K., Hong, S. and Lai, Y. (2019a) 'A critical review of battery thermal performance and liquid based battery thermal management', *Energy Conversion and Management,* 182, pp. 262-281 Available at: https://doi.org/10.1016/j.enconman.2018.12.051.

Wu, W., Wang, S., Wu, W., Chen, K., Hong, S. and Lai, Y. (2019b) 'A critical review of battery thermal performance and liquid based battery thermal management', *Energy Conversion and Management,* 182, pp. 262-281 Available at: 10.1016/j.enconman.2018.12.051.

Wu, W., Yang, X., Zhang, G., Ke, X., Wang, Z., Situ, W., Li, X. and Zhang, J. (2016) 'An experimental study of thermal management system using copper mesh-enhanced composite phase change materials for power battery pack', *Energy (Oxford),* 113, pp. 909-916 Available at: 10.1016/j.energy.2016.07.119.

Wu, W., Zhang, G., Ke, X., Yang, X., Wang, Z. and Liu, C. (2015) 'Preparation and thermal conductivity enhancement of composite phase change materials for electronic thermal management', *Energy conversion and management,* 101, pp. 278-284 Available at: 10.1016/j.enconman.2015.05.050.

Xia, G., Cao, L. and Bi, G. (2017) 'A review on battery thermal management in electric vehicle application', *Journal of Power Sources,* 367, pp. 90-105 Available at: https://doi.org/10.1016/j.jpowsour.2017.09.046.

Xia, Q., Wang, Z., Ren, Y., Yang, D., Sun, B., Feng, Q. and Qian, C. (2021) 'Performance reliability analysis and optimization of lithium-ion battery packs based on multiphysics simulation and response surface methodology', *Journal of Power Sources,* 490, pp. 229567 Available at: https://doi.org/10.1016/j.jpowsour.2021.229567.

Xiao, C., Li, S., Zhu, S., Zhang, G. and Yang, X. (2021) 'Series of solid-solid phase change materials with ultra-high thermal stability and controllable phase change temperature: kilogram-leveled preparation and application investigation', *Journal of Energy Storage,* 36, pp. 102405 Available at: https://doi.org/10.1016/j.est.2021.102405.

Xiaopeng Chen, Weixiang Shen, Zhenwei Cao And Kapoor, A. (2014) 'Adaptive gain sliding mode observer for state of charge estimation based on combined battery equivalent circuit model', *Computers & chemical engineering,* 64, pp. 114-123 Available at: 10.1016/j.compchemeng.2014.02.015.

Xie, N., Zhang, Y., Liu, X., Luo, R., Liu, Y. and Ma, C. (2023) 'Thermal performance and structural optimization of a hybrid thermal management system based on MHPA/PCM/liquid cooling for lithium-ion battery', *Applied Thermal Engineering,* 235, pp. 121341 Available at: 10.1016/j.applthermaleng.2023.121341.

Xu, B., Lee, J., Kwon, D., Kong, L. and Pecht, M. (2021) 'Mitigation strategies for Li-ion battery thermal runaway: A review', *Renewable and Sustainable Energy Reviews,* 150, pp. 111437 Available at: https://doi.org/10.1016/j.rser.2021.111437.

Xu, H., Zhang, X., Xiang, G. and Li, H. (2021) 'Optimization of liquid cooling and heat dissipation system of lithium-ion battery packs of automobile', *Case Studies in Thermal Engineering,* 26, pp. 101012 Available at: https://doi.org/10.1016/j.csite.2021.101012.

Xu, J., Duan, Q., Zhang, L., Liu, Y., Zhao, C. and Wang, Q. (2022) 'Experimental study of the cooling effect of water mist on 18650 lithium-ion battery at different initial temperatures', *Process Safety and Environmental Protection,* 157, pp. 156-166 Available at: https://doi.org/10.1016/j.psep.2021.10.034.

Xu, J., Lan, C., Qiao, Y. and Ma, Y. (2017) 'Prevent thermal runaway of lithium-ion batteries with minichannel cooling', *Applied Thermal Engineering,* 110, pp. 883-890 Available at: https://doi.org/10.1016/j.applthermaleng.2016.08.151.

Xu, J., Guo, Z., Xu, Z., Zhou, X. and Mei, X. (2023) 'A systematic review and comparison of liquid-based cooling system for lithium-ion batteries', *eTransportation,* 17, pp. 100242 Available at: 10.1016/j.etran.2023.100242.

Xu, M., Zhang, Z., Wang, X., Jia, L. and Yang, L. (2015) 'A pseudo three-dimensional electrochemical–thermal model of a prismatic LiFePO4 battery during discharge process', *Energy,* 80, pp. 303-317 Available at: 10.1016/j.energy.2014.11.073.

Xu, X., Tong, G. and Li, R. (2020) 'Numerical study and optimizing on cold plate splitter for lithium battery thermal management system', *Applied thermal engineering,* 167, pp. 114787 Available at: 10.1016/j.applthermaleng.2019.114787.

Xu, Y., Zhang, H., Xu, X. and Wang, X. (2021) 'Numerical analysis and surrogate model optimization of air-cooled battery modules using double-layer heat spreading plates', *International Journal of Heat and Mass Transfer,* 176, pp. 121380 Available at: https://doi.org/10.1016/j.ijheatmasstransfer.2021.121380.

Xu, Z., Wang, J., Lund, P.D. and Zhang, Y. (2022) 'Co-estimating the state of charge and health of lithium batteries through combining a minimalist electrochemical model and an equivalent circuit model', *Energy (Oxford),* 240, pp. 122815 Available at: 10.1016/j.energy.2021.122815.

Yadav, A.K., Donepudi, T. and Siddani, B.S. (2020) 'Numerical and experimental investigation of melting characteristics of phase change material-RT58', *Thermal Science and Engineering Progress,* 17, pp. 100378 Available at: 10.1016/j.tsep.2019.100378.

Yagci, O.K., Avci, M. and Aydin, O. (2019) 'Melting and solidification of PCM in a tube-in-shell unit: Effect of fin edge lengths' ratio', *Journal of energy storage,* 24, pp. 100802 Available at: 10.1016/j.est.2019.100802.

Yan, H., Marr, K.C. and Ezekoye, O.A. (2022) 'Thermal runaway behavior of nickel–manganese–cobalt 18650 lithium-ion cells induced by internal and external heating failures', *Journal of Energy Storage,* 45, pp. 103640 Available at: https://doi.org/10.1016/j.est.2021.103640.

Yan, J., Li, K., Chen, H., Wang, Q. and Sun, J. (2016) 'Experimental study on the application of phase change material in the dynamic cycling of battery pack system', *Energy Conversion and Management,* 128, pp. 12-19 Available at: https://doi.org/10.1016/j.enconman.2016.09.058.

Yang, B., Wang, J., Cao, P., Zhu, T., Shu, H., Chen, J., Zhang, J. and Zhu, J. (2021) 'Classification, summarization and perspectives on state-of-charge estimation of lithium-ion batteries used in electric vehicles: A critical comprehensive survey', *Journal of energy storage,* 39, pp. 102572 Available at: 10.1016/j.est.2021.102572.

Yang, M., Nicholls, R.A., Moghimi, M.A., and Griffiths, A.L. (2023) 'Performance management of EV battery coupled with Latent heat jacket at cell level', *Journal of Power Sources,* 558, pp. 232618 Available at: 10.1016/j.jpowsour.2022.232618.

Yang, R., Wang, M. and Xi, H. (2023) 'Thermal investigation and forced air-cooling strategy of battery thermal management system considering temperature non-uniformity of battery pack', *Applied Thermal Engineering,* 219, pp. 119566 Available at: 10.1016/j.applthermaleng.2022.119566.

Yang, W., Zhou, F., Chen, X., Li, K. and Shen, J. (2023) 'Thermal performance of honeycomb-type cylindrical lithium-ion battery pack with air distribution plate and bionic heat sinks', *Applied Thermal Engineering,* 218, pp. 119299 Available at: 10.1016/j.applthermaleng.2022.119299.

Yang, X., Guo, J., Yang, B., Cheng, H., Wei, P. and He, Y. (2020) 'Design of non-uniformly distributed annular fins for a shell-and-tube thermal energy storage unit', *Applied energy,* 279, pp. 115772 Available at: 10.1016/j.apenergy.2020.115772.

Yang, Y., Chen, L., Tong, K., Yang, L., Jiang, K., Kong, Y. and Du, X. (2022) 'Thermal-electrical characteristics of lithium-ion battery module in series connection with a hybrid cooling', *International Journal of Heat and Mass Transfer,* 184, pp. 122309 Available at: https://doi.org/10.1016/j.ijheatmasstransfer.2021.122309.

Yang, Y., Chen, L., Yang, L. and Du, X. (2021) 'Numerical study of combined air and phase change cooling for lithium-ion battery during dynamic cycles', *International Journal of Thermal Sciences,* 165, pp. 106968 Available at: https://doi.org/10.1016/j.ijthermalsci.2021.106968.

Yao, L., Yang, B., Cui, H., Zhuang, J., Ye, J. And Xue, J. (2016) 'Challenges and progresses of energy storage technology and its application in power systems', *Journal of modern power systems and clean energy,* 4(4), pp. 519-528 Available at: 10.1007/s40565-016-0248-x.

Yarbrough, D.W. and Kuan, C. (1983) *The Thermal Conductivity of Solid N-Eicosane, N-Octadecane, N-Heptadecane, N-Pentadecane, and N-Tetradecane* Springer US.

Ye, J., Aldaher, A.Y.M. and Tan, G. (2023) 'Thermal performance analysis of 18,650 battery thermal management system integrated with liquid-cooling and air-cooling', *Journal of Energy Storage,* 72, pp. 108766 Available at: 10.1016/j.est.2023.108766.

Ye, W., Guo, H., Huang, S. and Hong, Y. (2018) 'Research on melting and solidification processes for enhanced double tubes with constant wall temperature/wall heat flux', *Heat transfer, Asian research,* 47(3), pp. 583-599 Available at: 10.1002/htj.21328.

Yetik, O. and Karakoc, T.H. (2021) 'Estimation of thermal effect of different busbars materials on prismatic Li-ion batteries based on artificial neural networks', *Journal of Energy Storage,* 38, pp. 102543 Available at: https://doi.org/10.1016/j.est.2021.102543.

Yin, H., Zadshir, M. and Pao, F. (2022) '10 - Perspectives of the current, emerging, and future BIPVT technologies', in Yin, H., Zadshir, M. and Pao, F. (eds.) *Building Integrated Photovoltaic Thermal Systems* Academic Press, pp. 503-572.

Yoo, K. and Kim, J. (2019) 'Thermal behavior of full-scale battery pack based on comprehensive heat-generation model', *Journal of power sources,* 433, pp. 226715 Available at: 10.1016/j.jpowsour.2019.226715.

Youssef, R., Hosen, M.S., He, J., Jaguemont, J., De Sutter, L., Van Mierlo, J. and Berecibar, M. (2021) 'Effect analysis on performance enhancement of a novel and environmental evaporative cooling system for lithium-ion battery applications', *Journal of Energy Storage,* 37, pp. 102475 Available at: https://doi.org/10.1016/j.est.2021.102475.

Youssef, W., Ge, Y.T. and Tassou, S.A. (2018) 'CFD modelling development and experimental validation of a phase change material (PCM) heat exchanger with spiral-wired tubes', *Energy conversion and management,* 157, pp. 498-510 Available at: 10.1016/j.enconman.2017.12.036.

Yu, C., Zhang, X., Chen, X., Zhang, C. and Chen, Y. (2020) 'Melting performance enhancement of a Latent heat storage unit using gradient fins', *International journal of heat and mass transfer,* 150, pp. 119330 Available at: 10.1016/j.ijheatmasstransfer.2020.119330.

Yuan, Y., Cao, X., Xiang, B. and Du, Y. (2016) 'Effect of installation angle of fins on melting characteristics of annular unit for Latent heat thermal energy storage', *Solar energy,* 136, pp. 365-378 Available at: 10.1016/j.solener.2016.07.014.

Yue, Q.L., He, C.X., Jiang, H.R., Wu, M.C. and Zhao, T.S. (2021) 'A hybrid battery thermal management system for electric vehicles under dynamic working conditions', *International Journal of Heat and Mass Transfer,* 164, pp. 120528 Available at: https://doi.org/10.1016/j.ijheatmasstransfer.2020.120528.

Zadeh, P.G., Gholamalizadeh, E., Wang, Y. and Chung, J.D. (2022) 'Electrochemical modeling of a thermal management system for cylindrical lithium-ion battery pack considering battery capacity fade', *Case studies in thermal engineering,* 32, pp. 101878 Available at: 10.1016/j.csite.2022.101878.

Zakeri, B. and Syri, S. (2015) 'Electrical energy storage systems: A comparative life cycle cost analysis', *Renewable & sustainable energy reviews,* 42, pp. 569-596 Available at: 10.1016/j.rser.2014.10.011.

Zayed, M.E., Zhao, J., Li, W., Elsheikh, A.H., Elbanna, A.M., Jing, L. and Geweda, A.E. (2020) 'Recent progress in phase change materials storage containers: Geometries, design considerations and heat transfer improvement methods', *Journal of energy storage,* 30, pp. 101341 Available at: 10.1016/j.est.2020.101341.

Zhang, C., Allafi, W., Dinh, Q., Ascencio, P. and Marco, J. (2018) 'Online estimation of battery equivalent circuit model parameters and state of charge using decoupled least squares technique', *Energy (Oxford),* 142, pp. 678-688 Available at: 10.1016/j.energy.2017.10.043.

Zhang, F., Lu, F., Liang, B., Zhu, Y., Gou, H., Xiao, K. and He, Y. (2023) 'Thermal performance analysis of a new type of branch-fin enhanced battery thermal management PCM module', *Renewable Energy,* 206, pp. 1049-1063 Available at: 10.1016/j.renene.2023.02.083.

Zhang, H., Wu, X., Wu, Q. and Xu, S. (2019) 'Experimental investigation of thermal performance of large-sized battery module using hybrid PCM and bottom liquid cooling configuration', *Applied Thermal Engineering,* 159, pp. 113968 Available at: https://doi.org/10.1016/j.applthermaleng.2019.113968.

Zhang, H., Li, C., Zhang, R., Lin, Y. and Fang, H. (2020) 'Thermal analysis of a 6s4p Lithium-ion battery pack cooled by cold plates based on a multi-domain modeling framework', *Applied Thermal Engineering,* 173, pp. 115216 Available at: 10.1016/j.applthermaleng.2020.115216.

Zhang, H., Baeyens, J., Cáceres, G., Degrève, J. and Lv, Y. (2016) 'Thermal energy storage: Recent developments and practical aspects', *Progress in energy and combustion science,* 53, pp. 1-40 Available at: 10.1016/j.pecs.2015.10.003.

Zhang, J., Cao, Z., Huang, S., Huang, X., Han, Y., Wen, C., Honoré Walther, J. and Yang, Y. (2023) 'Solidification performance improvement of phase change materials for Latent heat thermal energy storage using novel branch-structured fins and nanoparticles', *Applied Energy,* 342, pp. 121158 Available at: 10.1016/j.apenergy.2023.121158.

Zhang, J., Li, X., Zhang, G., Wang, Y., Guo, J., Wang, Y., Huang, Q., Xiao, C. and Zhong, Z. (2020) 'Characterization and experimental investigation of aluminum nitride-based composite phase change materials for battery thermal management', *Energy conversion and management,* 204, pp. 112319 Available at: 10.1016/j.enconman.2019.112319.

Zhang, J., Liu, H., Zheng, M., Chen, M., Zhao, L. and Du, D. (2022) 'Numerical study on a preheating method for lithium-ion batteries under cold weather conditions using phase change materials coupled with heat films', *Journal of Energy Storage,* 47, pp. 103651 Available at: 10.1016/j.est.2021.103651.

Zhang, S., Nie, F., Cheng, J., Yang, H. and Gao, Q. (2024) 'Optimizing the air flow pattern to improve the performance of the air-cooling lithium-ion battery pack', *Applied Thermal Engineering,* 236, pp. 121486 Available at: 10.1016/j.applthermaleng.2023.121486.

Zhang, T., Gao, C., Gao, Q., Wang, G., Liu, M., Guo, Y., Xiao, C. and Yan, Y.Y. (2015) 'Status and development of electric vehicle integrated thermal management from BTM to HVAC', *Applied Thermal Engineering,* 88, pp. 398-409 Available at: https://doi.org/10.1016/j.applthermaleng.2015.02.001.

Zhang, W., Liang, Z., Ling, G. and Huang, L. (2021) 'Influence of phase change material dosage on the heat dissipation performance of the battery thermal management system', *Journal of Energy Storage,* 41, pp. 102849 Available at: 10.1016/j.est.2021.102849.

Zhang, X., Lu, J., Yuan, S., Yang, J. and Zhou, X. (2017) 'A novel method for identification of lithium-ion battery equivalent circuit model parameters considering electrochemical properties', *Journal of Power Sources,* 345, pp. 21-29 Available at: 10.1016/j.jpowsour.2017.01.126.

Zhang, X., Li, Z., Luo, L., Fan, Y. and Du, Z. (2022) 'A review on thermal management of lithium-ion batteries for electric vehicles', *Energy (Oxford),* 238, pp. 121652 Available at: 10.1016/j.energy.2021.121652.

Zhang, Y., Huang, J., Cao, M., Du, G., Liu, Z. and wang, L. (2021) 'A novel sandwich structured phase change material with well impact energy absorption performance for Li-ion battery application', *Journal of Energy Storage,* 40, pp. 102769 Available at: https://doi.org/10.1016/j.est.2021.102769.

Zhang, Y., Song, X., Ma, C., Hao, D. and Chen, Y. (2020) 'Effects of the structure arrangement and spacing on the thermal characteristics of Li-ion battery pack at various discharge rates', *Applied Thermal Engineering,* 165, pp. 114610 Available at: https://doi.org/10.1016/j.applthermaleng.2019.114610.

Zhang, Z., Zhang, L., Schlueter, J.A., Redfern, P.C., Curtiss, L. and Amine, K. (2010) 'Understanding the redox shuttle stability of 3,5-di-tert-butyl-1,2-dimethoxybenzene for overcharge protection of lithium-ion batteries', *Journal of Power Sources,* 195(15), pp. 4957-4962 Available at: https://doi.org/10.1016/j.jpowsour.2010.02.075.

Zhang, Z. and Wei, K. (2020) 'Experimental and numerical study of a passive thermal management system using flat heat pipes for lithium-ion batteries', *Applied Thermal Engineering,* 166, pp. 114660 Available at: 10.1016/j.applthermaleng.2019.114660.

Zhao, C.Y., Lu, W. and Tian, Y. (2010) 'Heat transfer enhancement for thermal energy storage using metal foams embedded within phase change materials (PCMs)', *Solar energy,* 84(8), pp. 1402-1412 Available at: 10.1016/j.solener.2010.04.022.

Zhao, C., Cao, W., Dong, T. and Jiang, F. (2018) 'Thermal behavior study of discharging/charging cylindrical lithium-ion battery module cooled by channeled liquid flow', *International Journal of Heat and Mass Transfer,* 120, pp. 751-762 Available at: https://doi.org/10.1016/j.ijheatmasstransfer.2017.12.083.

Zhao, C., Opolot, M., Liu, M., Bruno, F., Mancin, S., Flewell-Smith, R. and Hooman, K. (2021) 'Simulations of melting performance enhancement for a PCM embedded in metal periodic structures', *International journal of heat and mass transfer,* 168, pp. 120853 Available at: 10.1016/j.ijheatmasstransfer.2020.120853.

Zhao, J., Rao, Z., Huo, Y., Liu, X. and Li, Y. (2015) 'Thermal management of cylindrical power battery module for extending the life of new energy electric vehicles', *Applied Thermal Engineering,* 85, pp. 33-43 Available at: https://doi.org/10.1016/j.applthermaleng.2015.04.012.

Zhao, J., Zhao, Y., An, J., Yuan, C., Zhao, Y., Xiang, Y. and Yang, J. (2021) 'Thermally conductive silicone composites modified by graphene-oxide aerogel beads loaded with phase change materials as efficient heat sinks', *Applied Thermal Engineering,* 189, pp. 116713 Available at: https://doi.org/10.1016/j.applthermaleng.2021.116713.

Zhao, R., Gu, J. and Liu, J. (2017) 'Optimization of a phase change material based internal cooling system for cylindrical Li-ion battery pack and a hybrid cooling design', *Energy,* 135, pp. 811-822 Available at: https://doi.org/10.1016/j.energy.2017.06.168.

Zhao, R., Zhang, S., Gu, J., Liu, J., Carkner, S. and Lanoue, E. (2014) 'An experimental study of lithium ion battery thermal management using flexible hydrogel films', *Journal of Power Sources,* 255, pp. 29-36 Available at: https://doi.org/10.1016/j.jpowsour.2013.12.138.

Zhao, R., Zhang, S., Liu, J. and Gu, J. (2015) 'A review of thermal performance improving methods of lithium ion battery: Electrode modification and thermal management system', *Journal of power sources,* 299, pp. 557-577 Available at: 10.1016/j.jpowsour.2015.09.001.

Zhao, Y., Zou, B., Li, C. and Ding, Y. (2019) 'Active cooling based battery thermal management using composite phase change materials', *Energy Procedia,* 158, pp. 4933-4940 Available at: https://doi.org/10.1016/j.egypro.2019.01.697.

Zheng Chen, Bing Xia, Mi, C.C., and Rui Xiong (2015) 'Loss-Minimization-Based Charging Strategy for Lithium-Ion Battery', *IEEE transactions on industry applications,* 51(5), pp. 4121-4129 Available at: 10.1109/TIA.2015.2417118.

Zheng, Y., Gao, W., Han, X., Ouyang, M., Lu, L. and Guo, D. (2019) 'An accurate parameters extraction method for a novel on-board battery model considering electrochemical properties', *Journal of Energy Storage,* 24, pp. 100745 Available at: 10.1016/j.est.2019.04.019.

Zhou, H., Dai, C., Liu, Y., Fu, X. and Du, Y. (2020) 'Experimental investigation of battery thermal management and safety with heat pipe and immersion phase change liquid', *Journal of Power Sources,* 473, pp. 228545 Available at: https://doi.org/10.1016/j.jpowsour.2020.228545.

Zhou, H., Zhou, F., Zhang, Q., Wang, Q. and Song, Z. (2019) 'Thermal management of cylindrical lithium-ion battery based on a liquid cooling method with half-helical duct', *Applied Thermal Engineering,* 162, pp. 114257 Available at: https://doi.org/10.1016/j.applthermaleng.2019.114257.

Zhou, Z., Chen, S., Luo, M., Du, W., Wu, Y. and Yu, Y. (2023) 'Effect of mechanical vibration on phase change material based thermal management system for a cylindrical lithium-ion battery at high ambient temperature and high discharge rate', *International Journal of Heat and Mass Transfer,* 211, pp. 124255 Available at: 10.1016/j.ijheatmasstransfer.2023.124255.

Zhu, Y., Xiao, J., Chen, T., Chen, A., Zhou, S., Liu, Z. and Xia, Z. (2019) 'Experimental and numerical investigation on composite phase change material (PCM) based heat exchanger for breathing air cooling', *Applied thermal engineering,* 155, pp. 631-636 Available at: 10.1016/j.applthermaleng.2019.04.014.

Zhu, Z., Huang, Y., Hu, N., Zeng, Y. and Fan, L. (2018) 'Transient performance of a PCM-based heat sink with a partially filled metal foam: Effects of the filling height ratio', *Applied thermal engineering,* 128, pp. 966-972 Available at: 10.1016/j.applthermaleng.2017.09.047.

Zhuang, Y., Chen, T., Chen, J., Li, J., Guan, M. and Chen, Y. (2021) 'Thermal uniformity performance of a hybrid battery thermal management system using phase change material and cooling plates arrayed in the manner of honeycomb', *Thermal Science and Engineering Progress,* 26, pp. 101094 Available at: https://doi.org/10.1016/j.tsep.2021.101094.

Zichen, W. and Changqing, D. (2021) 'A comprehensive review on thermal management systems for power lithium-ion batteries', *Renewable and Sustainable Energy Reviews,* 139, pp. 110685 Available at: 10.1016/j.rser.2020.110685.

Ziye Ling, Jiajie Chen, Xiaoming Fang, Zhengguo Zhang, Tao Xu, Xuenong Gao and Shuangfeng Wang (2014) 'Experimental and numerical investigation of the application of phase change materials in a simulative power batteries thermal management system', *Applied energy,* 121, pp. 104-113 Available at: 10.1016/j.apenergy.2014.01.075.

Żygadło, M., Kotowski, J. and Oko, J. (2018) 'Green computing and energy storage systems', *E3S web of conferences,* 44, pp. 202 Available at: 10.1051/e3sconf/20184400202.

BIBLIOGRAPHY

Allen, K. (2005) *Study Skills: a student survival guide*. Chichester: Wiley.

Bennet, M., and Ho, D. (2014) *Project management for engineers.* New Jersey: World Scientific.

Branson, S., (2011) *Heat exchangers: types, designs, and applications.* Hauppauge, N.Y.: Nova Science Publishers.

Cengel, Y., Cimbala, J., and Turner, R. (2012) *Fundamentals of thermal-fluid sciences.* 4th Edition. London: McGraw-Hill.

Davidson, P., (2015) *Turbulence: an introduction for scientists and engineers.* 2nd Edition. Oxford: Oxford University Press.

Kakac, S., Liu, H., and Pramuanjaroenkij, A. (2012) *Heat exchangers: selection, rating, and thermal design.* London: CRC.

Leong, E., Heah, C., and Ong, K. (2016) *Guide to research projects for engineering students: planning, writing, and presenting*. Boca Raton: CRC Press.

Maier, P., Barney, A., and Price, G. (2009) *Study Skills for science, engineering, and technology students*. Essex: Pearson Education Limited.

McMillan, K., and Weyers, J. (2013) *How to research and write a successful Ph.D.* Harlow: Pearson.

Murray, R. (2017) *How to write a thesis.* London: Open University Press.

Sorensen, B., (2015) *Solar energy storage.* Amsterdam: Academic Press.

Thulukkanam, K., (2013) *Heat exchanger design handbook.* 2nd Edition. Boca Raton: CRC Press.